325 p.

**N63 22054**

CODE-1

NASA CR 51242

OTS PRICE

XEROX $ 19.75 ph

MICROFILM $ 9.95 mf.

SQT

1138

# LUNAR ORBITER CAPSULE
# FINAL PHASE-OUT REPORT

Contract 950340

Prepared for

JET PROPULSION LABORATORIES
CALIFORNIA INSTITUTE OF TECHNOLOGY
Pasadena, California

Prepared by

ASTRO-ELECTRONICS DIVISION
DEFENSE ELECTRONIC PRODUCTS
RADIO CORPORATION OF AMERICA
Princeton, New Jersey

AED 1762

December 31, 1962

RE-ORDER No. 62-489

# FOREWORD

This report presents the results of RCA effort on Phase II of the Lunar Orbiter Capsule Study, JPL Contract No. 950340, for the phase-out period preceding contract termination on 10 October 1962.

The Phase II study effort was divided into two parts. The first part was concerned with system integration for a specific lunar orbiter capsule configuration. The various trade-offs to be considered had been initially studied during Phase I of the contract. The effects of these trade-offs were to be evaluated during Phase II, and a specific system was to be recommended. Functional specifications for the recommended system were to be prepared. The trade-off evaluation effort and system recommendation were completed and reported to JPL in RCA Report No. AED-1616, "Lunar Orbiter Preliminary Configuration Report," dated 25 September 1962. Contract termination prevented completion of the functional specifications for the recommended system. The detailed analysis accomplished as part of that effort up to the time of termination is presented as Part I of this report.

The second part of the Phase II study effort was to consider general system problems in the areas of data interpretation and system growth potential. This part of the effort also was terminated before many of the initial objectives were fulfilled. Meaningful results were obtained in some areas, however, and these are presented as Part II of this report.

RCA gratefully acknowledges the assistance provided by the several JPL groups and staff personnel who participated actively in this study.

RE-ORDER No. 62-489

# PART I.

RE-ORDER No. 62-4F9

# TABLE OF CONTENTS

Section Page

1 SUMMARY . . . . . . . . . . . . . . . . . . . . . . . . . . . . . . I. 1-1

A. Introduction . . . . . . . . . . . . . . . . . . . . . . . . . . I. 1-1
B. Summary of Results . . . . . . . . . . . . . . . . . . . . . . I. 1-1

2 SYSTEM ANALYSIS . . . . . . . . . . . . . . . . . . . . . . . . . I. 2-1

A. Mission Objectives . . . . . . . . . . . . . . . . . . . . . . . I. 2-1
B. Design Criteria . . . . . . . . . . . . . . . . . . . . . . . . . I. 2-1
C. Trajectory Considerations . . . . . . . . . . . . . . . . . . . I. 2-3
D. In-Orbit Considerations . . . . . . . . . . . . . . . . . . . . I. 2-7
E. Operational Sequence of Events . . . . . . . . . . . . . . . . I. 2-36

3 PRELIMINARY SYSTEM DESIGN ANALYSIS . . . . . . . . . . . . . I. 3-1

A. Retropropulsion . . . . . . . . . . . . . . . . . . . . . . . . . I. 3-1
B. Attitude Control Subsystem . . . . . . . . . . . . . . . . . . I. 3-7
C. Telecommunications . . . . . . . . . . . . . . . . . . . . . . I. 3-34
D. Video Subsystem . . . . . . . . . . . . . . . . . . . . . . . . I. 3-58
E. Power Supply . . . . . . . . . . . . . . . . . . . . . . . . . . I. 3-76
F. Mechanical Design of Lunar Orbiter Capsule . . . . . . . . . I. 3-89
G. Thermal Control . . . . . . . . . . . . . . . . . . . . . . . . I. 3-97
H. Quality Control . . . . . . . . . . . . . . . . . . . . . . . . . I. 3-110
I. Master Program Plan . . . . . . . . . . . . . . . . . . . . . . I. 3-120

4 FAILURE MODE AND RELIABILITY ANALYSIS . . . . . . . . . . . I. 4-1

A. Scope of Analysis . . . . . . . . . . . . . . . . . . . . . . . . I. 4-1
B. Mathematical Model . . . . . . . . . . . . . . . . . . . . . . . I. 4-1
C. Reliability Analysis and Prediction . . . . . . . . . . . . . . I. 4-5
D. Failure Effects Analysis . . . . . . . . . . . . . . . . . . . . I. 4-5
E. Reliability Program for LOC Design and Development . . . . . . . . . . . . . . . . . . . . . . . . . . I. 4-16

# LIST OF ILLUSTRATIONS

Figure | | Page
I. 1. B-1 Directional Antenna Inertia Configuration . . . . . . . . . . . . . I. 1-2

I. 2. C-1 Probability and Aim Point Altitude vs. Velocity Increment . . . . . . . . . . . . . . . . . . . . . . . . . . . . . . . . . I. 2-5
I. 2. D-1 Nominal Injection Orbit at First Quarter . . . . . . . . . . . . . I. 2-9
I. 2. D-2 Nominal Injection Orbit with Illumination at Half-Quarter . . . . . . . . . . . . . . . . . . . . . . . . . . . . . . I. 2-11
I. 2. D-3 Nominal Injection Orbit with Illumination at 1.5 Quarter . . . . . . . . . . . . . . . . . . . . . . . . . . . . . . . . I. 2-15
I. 2. D-4 A Non-Nominal Injection Orbit at Half-Quarter . . . . . . . . . I. 2-17
I. 2. D-5 A Non-Nominal Injection Orbit at First Quarter . . . . . . . . I. 2-19
I. 2. D-6 Useful Illumination Per Orbit for Initial Sun Position of 90° East Longitude . . . . . . . . . . . . . . . . . . . . . . . . I. 2-21
I. 2. D-7 Useful Illumination Per Orbit for Initial Sun Position of 45° East Longitude . . . . . . . . . . . . . . . . . . . . . . . . I. 2-22
I. 2. D-8 Useful Illumination Per Orbit for Initial Sun Position of 135° East Longitude . . . . . . . . . . . . . . . . . . . . . . . I. 2-22
I. 2. D-9 TV Camera f-Number Relations Nomograph . . . . . . . . . . . I. 2-31
I. 2. D-10 Lunar Orbit Altitude, Endlap, Frame Size, and Resolution Relations Nomograph . . . . . . . . . . . . . . . . . . I. 2-33
I. 2. D-11 Lunar Orbit Altitude, Resolution and Smear Relations Nomograph . . . . . . . . . . . . . . . . . . . . . . . . I. 2-37
I. 2. D-12 TV Camera Resolution and Readout Time Relations Nomograph . . . . . . . . . . . . . . . . . . . . . . . . . . . . . . . I. 2-39

I. 3. A-1 LOC Solid Propellant Retromotor, Preliminary Design Configuration . . . . . . . . . . . . . . . . . . . . . . . . . I. 3-4
I. 3. B-1 Block Diagram of an Alternate Attitude Control Subsystem . . . . . . . . . . . . . . . . . . . . . . . . . . . . . . . I. 3-8
I. 3. B-2 Limit Cycle Phase-Plane Diagram . . . . . . . . . . . . . . . . . . I. 3-12
I. 3. B-3 Analog Program for Roll-Yaw Analysis . . . . . . . . . . . . . . . I. 3-14
I. 3. B-4 Programming for Vehicle Response and Gas Consumption . . . . . . . . . . . . . . . . . . . . . . . . . . . . . . . I. 3-15
I. 3. B-5 Torquing Circuitry Block Diagram . . . . . . . . . . . . . . . . . . I. 3-16
I. 3. B-6 Block Diagram of the Low-Pass Filter . . . . . . . . . . . . . . . I. 3-17
I. 3. B-7 Block Diagram of the Roll and Yaw Channel of the Horizon Scanner Back-up System . . . . . . . . . . . . . . . . . I. 3-20
I. 3. B-8 Vehicle-Moon Relationship at Minimum Altitude . . . . . . . . I. 3-26
I. 3. B-9 Vehicle-Moon Relationship at Maximum Altitude . . . . . . . . I. 3-27
I. 3. B-10 Mosaic Arrangement of Visible-Light Sensor . . . . . . . . . . I. 3-28

# LIST OF ILLUSTRATIONS (Continued)

| Figure | | Page |
|---|---|---|
| I. 3. B-11 | Geometry of Barnes Engineering Horizon Scanner | I. 3-29 |
| I. 3. B-12 | Geometry of ATL Horizon Tracker | I. 3-31 |
| I. 3. C-1 | Block Diagram of the Video Transmission Subassembly | I. 3-40 |
| I. 3. C-2 | Block Diagram of the Tracking Transponder Subassembly | I. 3-40 |
| I. 3. C-3 | Block Diagram of the Ranger 6 through 9 Command Subassembly | I. 3-41 |
| I. 3. C-4 | Block Diagram of the Encoder Subassembly for a 3-watt Telemetry Link with Five Subcarrier Channels | I. 3-43 |
| I. 3. C-5 | Design of the L-Band Directional Antenna | I. 3-50 |
| I. 3. C-6 | Directional Antenna Feed Dipole Disk, Linearly Polarized | I. 3-51 |
| I. 3. C-7 | Directional Antenna Feed Double-Dipole, Linearly Polarized | I. 3-51 |
| I. 3. C-8 | L-Band Cavity Backed Slot, Linearly Polarized | I. 3-52 |
| I. 3. C-9 | Equivalent Circuit of the Transponder Antenna Slot-Cavity | I. 3-54 |
| I. 3. C-10 | Techniques Considered for Achieving Circularly Polarized Radiation from a Cavity | I. 3-54 |
| I. 3. D-1 | Block Diagram of the Television Subsystem | I. 3-58 |
| I. 3. D-2 | Block Diagram of the Generator Counter Circuits | I. 3-60 |
| I. 3. D-3 | Basic Camera Timing Diagrams | I. 3-62 |
| I. 3. D-4 | Block Diagram of the TV Camera | I. 3-63 |
| I. 3. D-5 | Block Diagram of the Combiner Unit | I. 3-65 |
| I. 3. D-6 | Optical Schematic of a Catadioptric Anastigmat | I. 3-67 |
| I. 3. D-7 | Block Diagram of the TV Recording and Display Equipment | I. 3-69 |
| I. 3. D-8 | Block Diagram of Ground Receivers and Demodulators | I. 3-70 |
| I. 3. D-9 | Block Diagram of Power Distribution Cabinet | I. 3-71 |
| I. 3. D-10 | Block Diagram of the Monitor and Control Cabinet | I. 3-71 |
| I. 3. D-11 | Block Diagram of the Sync and Video Simulator | I. 3-72 |
| I. 3. D-12 | Block Diagram of the Film Recorder | I. 3-73 |
| I. 3. E-1 | LOC Power Profile Less Continuous Load $P_C$ for the First 40 Days in Orbit | I. 3-76 |
| I. 3. E-2 | LOC Power Supply Block Diagram | I. 3-78 |
| I. 3. E-3 | Power Supply Parameters - System | I. 3-87 |
| I. 3. F-1 | Structural Configuration of Lunar Orbiter Capsule | I. 3-90 |

RE-ORDER No. 62-489

# LIST OF ILLUSTRATIONS (Continued)

| Figure | | Page |
|---|---|---|
| I. 3. F-2 | Detail of Lunar Orbiter Capsule Configuration | I. 3-91 |
| I. 3. F-3 | Directional Antenna Inertia Configuration | I. 3-95 |
| I. 3. G-1 | Geometry for Obtaining Thermal Radiative Power from the Lunar Surface | I. 3-97 |
| I. 3. G-2 | Geometry for Obtaining an Expression for d | I. 3-99 |
| I. 3. G-3 | Geometry for Obtaining Cos $\xi_N$ when $\beta$ is Zero | I. 3-100 |
| I. 3. G-4 | Geometry for Obtaining Cos $\xi_N$ when $\alpha$ is Zero | I. 3-102 |
| I. 3. G-5 | Radiative Power of the Lunar Surface as a Function of the Angle from the Terminator Plane | I. 3-104 |
| I. 3. G-6 | $E/\epsilon_N$ as a Function of View Angle $\xi_M$ | I. 3-105 |
| I. 3. G-7 | Thermal Design Aspects of the RTG Model of the LOC | I. 3-107 |
| I. 4. B-1 | TV Subsystem Reliability Diagram (Remote Mapping) | I. 4-2 |
| I. 4. B-2 | TV Subsystem Reliability Diagram (Direct Mapping) | I. 4-3 |
| I. 4. B-3 | Tape Recorder Reliability Diagram | I. 4-3 |
| I. 4. B-4 | TV Transmitter Reliability Diagram | I. 4-3 |
| I. 4. B-5 | Attitude Stabilization Reliability Diagram (Mapping Phase) | I. 4-4 |
| I. 4. B-6 | Attitude Stabilization Reliability Diagram (Post-Mapping Phase, Erection of Spin Axis) | I. 4-4 |

# LIST OF TABLES

Table Page

I. 2. C-1 Three-Sigma Error Limits in Approach Trajectories . . . . . . . I. 2-6
I. 2. D-1 Summary of Orbits Before and After Injection . . . . . . . . . . . . I. 2-13
I. 2. D-2 Alternative TV System Parameters . . . . . . . . . . . . . . . . . . . I. 2-25
I. 2. D-3 f-Number versus Attitude Stabilization Rate . . . . . . . . . . . . . I. 2-26
I. 2. D-4 TV Surveying System Parameter Summary . . . . . . . . . . . . . I. 2-27
I. 2. D-5 Vidicon and Image Orthicon Technical Summary . . . . . . . . . . I. 2-29
I. 2. D-6 Van Diggelen's Lunar Photometric Function . . . . . . . . . . . . . I. 2-30
I. 2. E-1 Operational Sequence of Events . . . . . . . . . . . . . . . . . . . . . I. 2-41

I. 3. A-1 Comparison of Rocket Motors for Capsules having a Gross Weight of 400 and 450 Pounds . . . . . . . . . . . . . . . . . . . . . I. 3-3
I. 3. A-2 Performance and Physical Characteristics of Solid Propellant Retromotor (For 450 Pound Capsule and 1250 MPS Velocity Change) . . . . . . . . . . . . . . . . . . . . . I. 3-5
I. 3. B-1 Values for Investigation by Computer Program . . . . . . . . . . . I. 3-18
I. 3. B-2 Weight and Power Requirements for Stabilization (Pure Jet System) . . . . . . . . . . . . . . . . . . . . . . . . . . . I. 3-33
I. 3. C-1 Analysis Data of a Straight Frequency - Modulation System Operated at $f_b = 62.5$ kc . . . . . . . . . . . . . . . . . . I. 3-37
I. 3. C-2 Analysis Data of a Frequency - Modulation Feedback System Operated at $f_b = 62.5$ kc . . . . . . . . . . . . . . . . . . I. 3-38
I. 3. C-3 Representative Specifications for the Nimbus AVCS Tape Recorder . . . . . . . . . . . . . . . . . . . . . . . . . . . . . . I. 3-39
I. 3. C-4 Encoder Parameters for 3-Watt Telemetry Subcarriers . . . . . I. 3-44
I. 3. C-5 Encoder Parameters for 1/4-Watt Telemetry Subcarriers . . . . I. 3-44
I. 3. C-6 Parameters for the Proposed Telemetry Subassembly . . . . . . I. 3-45
I. 3. C-7 Parameters of Various Selected Antenna Designs . . . . . . . . . I. 3-48
I. 3. C-8 A Tabulation of the Corporate Feed VSWR . . . . . . . . . . . . . I. 3-55
I. 3. C-9 Summary of Telecommunications Subsystem Size Weight and Power Requirements . . . . . . . . . . . . . . . . . . . . . . . I. 3-57
I. 3. D-1 Major Parameters of the Video Subsystem . . . . . . . . . . . . . . I. 3-59
I. 3. D-2 TV Lens Characteristics . . . . . . . . . . . . . . . . . . . . . . . . . . I. 3-66
I. 3. D-3 Estimated Size and Weight of the Video Subsystem . . . . . . . . . I. 3-68
I. 3. E-1 Power and Weight Requirements for the LOC Power Supply . . . I. 3-88

I. 4. D-1 Failure Effects Analysis TV Subsystem . . . . . . . . . . . . . . . . I. 4-6
I. 4. D-2 Failure Effects Analysis Tape Recorder . . . . . . . . . . . . . . . . I. 4-9
I. 4. D-3 Failure Effects Analysis TV Transmitter . . . . . . . . . . . . . . . I. 4-10
I. 4. D-4 Failure Effects Analysis Attitude Stabilization System A - Pure Jet Control . . . . . . . . . . . . . . . . . . . . . . . . . . . . . . I. 4-11
I. 4. D-5 Failure Effects Analysis Attitude Stabilization - Post - Mapping Phase System A - Pure Jet Control . . . . . . . . . . . . I. 4-15

# Section I

# SUMMARY

## A. INTRODUCTION

Part I of this report deals with a system integration study of a Lunar Orbiter Capsule (LOC). The LOC was to be designed as a payload for the Ranger Spacecraft. The primary objective of the capsule was to take lunar-surface television pictures that would detail the lunar-surface characteristics needed for the design support of the Apollo mission. The system integration study constituted a part of the Phase II effort under JPL Contract No. 950340. The objectives of this part of Phase II were to evaluate the effects of trade-offs determined during Phase I and to recommend and prepare functional specifications for a specific system configuration.

The results of the LOC preliminary configuration study were reported to JPL on 28 September 1962.* The present report covers many of the results previously reported and also details the entire effort up to the date of contract cancellation, 10 October 1962. The results presented should be considered preliminary because of cancellation of the studies before completion of many of the tasks originally described in the contractual work statement.

## B. SUMMARY OF RESULTS

### 1. SYSTEM CONCEPT

The structural configuration of the recommended LOC is shown in outline form in Figure I.1.B-1. The bottom portion constitutes an adapter structure which would permit mounting of the LOC on the Ranger Spacecraft. The system comprises five major subsystems. The retro-propulsion subsystem would provide for injection of the capsule into an orbit about the moon from the transit trajectory. In order to ensure that the cameras point at the lunar surface for picture taking and that the communications antennas point toward the earth for data transmission, an attitude control subsystem is incorporated. A communications subsystem would provide channels for TV data transmission, command, and telemetry and would also include a tracking transponder and data storage. The television subsystem uses two cameras; these cameras take pictures alternately, with one camera tube being erased while the other is being exposed. The final subsystem is the power supply, which provides for both the constant and the peak loads required by the other subsystems.

### 2. RETROPROPULSION SUBSYSTEM

A solid-propellant rocket with spin stabilization during retrofiring is recommended for the LOC. The proposed motor is a 3000-pound-thrust unit having a vacuum specific impulse of 280 seconds and a total velocity increment of 1250 meters per second. A unit

---

* RCA Report No. AED-1616, "Lunar Orbiter Preliminary Configuration Report," 25 September 1962

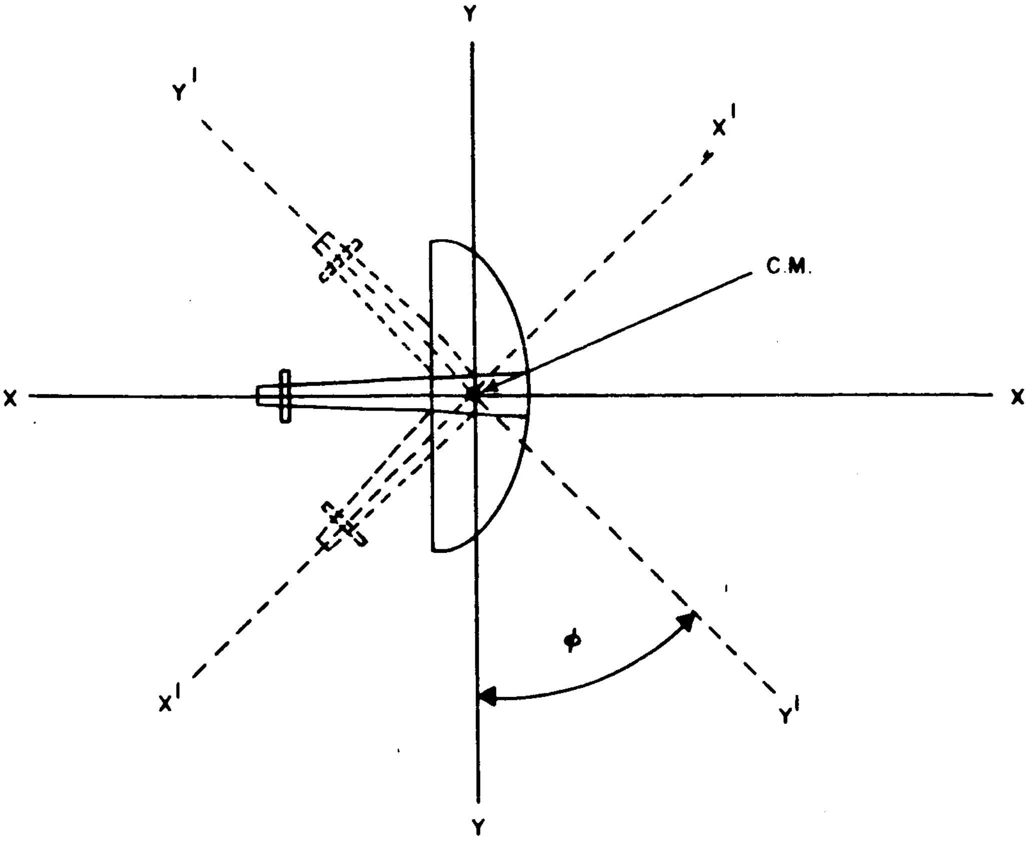

Figure I.1.B-1. Directional Antenna Inertia Configuration

similar to the solid-propellant spin-up system of Ranger 3-5 would provide spin stabilization. The spin rate during retrofiring would be approximately 300 rpm.

### 3. ATTITUDE CONTROL SUBSYSTEM

A conventional three-axis, jet-controlled subsystem operating in a limit-cycle mode is recommended. This subsystem would maintain the LOC principal axes coincident with the moon-centered axes for a period of at least 1 month in a lunar orbit. Roll and pitch errors are detected by a two-axis horizon scanner. Yaw error is detected by either a two-axis gyro-compass or a roll/yaw rate-gyro combination. A back-up lunar sensor incorporating a passive mosaic-type sensor is also recommended. A torquer with six thrust nozzles (two per axis) and a common regulator valve operating at 0.01-pound thrust is proposed. An over-all stabilization accuracy of ±1 degree, with stabilization rates no greater than 0.01 degree per second, is recommended.

The attitude control subsystem proposed should be capable of an operational lifetime of greater than 1 month. This subsystem has been selected, despite the high power requirements and difficult development schedules, because it offers the greatest flexibility and growth potential. Furthermore, the techniques developed for this subsystem would be directly applicable to future lunar orbiters, including manned systems.

## 4. TELECOMMUNICATIONS SUBSYSTEM

The telecommunications subsystem recommended would comprise three major units, all operating at L-band frequencies. These units are as follows:

(a) Tracking Transponder - a two-way, phase-locked doppler unit similar to that presently used on the Ranger Spacecraft.

(b) Video Transmitter - a 20-watt unit similar to that presently used on the Ranger 6-9 capsules.

(c) Command Subsystem - compatible with the Deep Space Instrumentation Facility (DSIF) command capabilities and utilizing as much Ranger command circuitry as practicable.

An omnidirectional antenna providing look angles of approximately 100 degrees in elevation and 360 degrees in azimuth would be used with the transponder and command units. A directional antenna having approximately a 30-degree beamwidth and an on-axis gain of 15 db would be used for the video transmission link. The directional antenna could be trainable in elevation at ground command for approximately 70 degrees (±35 degrees about a nominal orientation) in suitable increments. At least 10 minutes of contact time with earth stations would be assured per lunar orbit. The capability of the transponder and video transmitters would determine the telemetry information available from the capsule. In general, a high-power (3 watts) telemetry subsystem for the transponder is recommended, with priority given to telemetry associated with the operating status of the capsule and required to predict the future capability of the capsule for operational programming.

## 5. TELEVISION SUBSYSTEM

The recommended television subsystem consists of two 1-inch, electromagnetically focused and deflected vidicons and associated camera circuitry. A resolution of approximately 25 meters per TV line, with a total of 700 resolution lines per TV camera, and contingous coverage is recommended. A system using both high-resolution and low-resolution cameras (10 meters and 85 meters per TV line, respectively) could be utilized. Optics having an effective f-number of approximately 1.5 would be used to map the lunar surface at sun angles between 30 and 60 degrees (but notlimited to these angles) with reasonable sensor sensitivity. Iris control by ground command is also proposed to provide for optimum camera subsystem utilization under the wide dynamic range of surface illumination characteristics anticipated. The camera subsystem should be capable of operating in both direct and remote modes on ground-station command. For remote operation, a tape recorder would store the video data obtained while the LOC is not in position for direct video-data transmission to earth. In general, the area for direct video transmission would be between plus and minus 20 degrees of lunar longitude when centered about the nominal earth-moon line. The tape-recorder bandwidth should be at least 62.5 kilocycles, and the recorder should be capable of either continuous or start-stop recording of video data for a total of approximately 8 minutes, or of storing 100 TV frames of approximately 1000 scan lines per frame. The frames would have a horizontal resolution of about 700 TV lines per camera.

## 6. POWER SUPPLY

The power-supply subsystem must be capable of supplying both the constant loads required for the attitude control subsystem and the peak loads required by the TV and telecommunications subsystems. In general, the constraints on the LOC would prohibit the use of only a solar-cell array without foldable panels. A power subsystem utilizing either a combination of a radioisotope thermoelectric generator (RTG) and a solar-cell array, or an RTG only is recommended. During the TV operational phase of the LOC mission, an average continuous unregulated power-supply output of 65 watts is recommended. The power supply should also be capable of handling peak load requirements of approximately 190 watts for short periods.

# Section 2
# SYSTEM ANALYSIS

## A. MISSION OBJECTIVES

The primary objective of the Lunar Orbiter Capsule (LOC) was to secure television pictures of the lunar surface that had sufficient resolution and coverage to delineate lunar surface characteristics of importance to the Apollo mission. Specifically, the LOC mission was to survey various areas of the lunar surface for relative roughness in order to select a landing site, and ascertain the difficulty of performing a landing of a manned vehicle within the selected area. It was anticipated that one or more orbiting payloads might be flown within the flight schedules for Rangers 10 through 14. As a secondary mission objective, a tracking transponder, similar to the units presently planned for use on the Ranger Spacecraft, was to be included in the LOC to determine the selenodetic gravitational potential constants. This experiment also would provide orbital data to establish the operational program of the television equipment. Additional scientific experiments were to be flown whenever sufficient payloads and other design criteria would permit. Each additional experiment, however, would have been included on a non-interference basis and would not have diverted attention from the primary objective, that is, obtaining TV pictures of the lunar surface.

## B. DESIGN CRITERIA

### 1. LOC System Criteria

Simplicity and reliability were the governing criteria for the Lunar Orbiter Capsule in meeting the required mission objectives. The LOC required the necessary retropropulsion for (1) achieving a lunar orbit with characteristics commensurate with the TV experiment, and (2) orienting and stabilizing the vehicle to the lunar local vertical for the lifetime of the television experiment and primary mission objective. The power, communications, and command control capability were to be supplied, as required to accomplish these goals. Inclusion of additional experiments also would be made on a non-interference basis.

### a. Competing Characteristics

Competing characteristics in the LOC system criteria were treated in the following order:

(1) Reliability of Subsystems (in order of importance):

  (a) Retropropulsion capability

  (b) Attitude control and stabilization

    - (c) Video transmission link
    - (d) Television subsystem
    - (e) Transponder subsystem
    - (f) Prognostic and diagnostic telemetry
- (2) Limiting resolution
- (3) Coverage
- (4) Schedule
- (5) Cost
- (6) Biological sterility

## 2. SPACECRAFT BUS CRITERIA

Considerations of the spacecraft bus design criteria are presented here for technical completion only. No further considerations of bus design are given in this report.

One design goal for the LOC was that changes in the Ranger 6, 7, 8, and 9 bus configuration would be made only (1) as required to accommodate the LOC with a simple interface to permit the incorporation of non-interfering experiments, or (2) to incorporate mandatory engineering change orders resulting from experience with Ranger Spacecrafts 3 through 9. In the event that more than a single interface in the bus configuration was required, the changes would be minimized and would require full approval by JPL. Each change would be evaluated in terms of its effect on the bus and the alternatives available in the design of the LOC without inclusion of the change.

The bus requirements were to deliver the LOC to the vicinity of the moon on a nominal 66-hour transit trajectory within the accuracy limits obtainable with a single mid-course maneuver. The necessary ground-commanded terminal maneuver to orient the LOC, prior to separation and injection into lunar orbit, would be a bus requirement within the tolerances of the attitude control and command systems for Ranger Spacecrafts 6 through 9.

### a. Competing Characteristics

Competing characteristics in the spacecraft bus criteria were treated in the following order:

- (1) Reliability of subsystems (in order of importance):
    - (a) Terminal-phase orientation and attitude control
    - (b) Injection-point determination

(c) Bus functions prior to terminal phase (separation, stabilization, mid-course maneuver, etc.) as checked out in previous flights.

(d) Bus failure-detection telemetry

(e) Passenger experiments and associated data-handling systems

(2) Compatibility of LOC and bus

(3) Schedule

(4) Suitability of designs and documentation for continued exploitation of Ranger

(5) Cost

(6) Biological sterility

b. Definition of Weight Characteristics

The gross weight of the spacecraft was not listed as a competing characteristic because its value was fixed by the available vehicle performance and the chosen trajectory. The desired approach to the weight problem was: (1), to minimize the weight of each component, and (2) to reduce the number of components, if necessary, to reduce the total weight. If the spacecraft with all desired components were underweight, the performance excess would normally be manifested in an altered trajectory or increased propellant residuals. This may, in turn, lead to higher reliability and/or greater accuracy of injection. Ballast would not normally be used except when required for balancing the spacecraft. The LOC weight allowance has been assumed to be 450 pounds. This assumes an 825-pound injected weight and a 375-pound bus.

## C. TRAJECTORY CONSIDERATIONS

### 1. PLAN OF OPERATION

The Ranger Spacecraft, flying a near-standard 66-hour trajectory, will deliver the Lunar Orbiter Capsule to the vicinity of the moon and orient the LOC so that the retromotor can be fired to inject the Lunar Orbiter Capsule into an orbit about the moon. The desired orbit should be nearly circular at 250-km altitude, with a final inclination of 35 degrees.

There are uncertainties associated with the spacecraft guidance during powered flight prior to reaching the point of injection into lunar orbit. There may also be small attitude errors in final orientation for retrofire. In addition, there may be errors in the transit orbit as determined by ground tracking. These uncertainties must be considered in selecting the orbits for optimum TV coverage and in sizing the retrorocket to minimize weight. The achievable orbits in the presence of the transit-orbit arrival uncertainties and with the recommended velocity increment are developed and discussed in this section.

The following discussion deals with the selection of the required retrorocket velocity increment and operational procedures for attaining reasonable performance with a minimum impulse retrorocket.

## 2. CAPSULE INJECTION INTO LUNAR ORBIT

The most important single aspect of the 66-hour transit trajectory is the uncertainty in altitude and inclination at the time of arrival. In the JPL "Guidance Considerations for the Establishment of Lunar Orbits" (TM-312-177), C. Sauer states that the three-sigma dispersion in radius of closest approach is 117 km for an equatorial orbit, and slightly less for a polar orbit. C. Sauer cites $B \cdot R$ as 132 km, where B is easily calculated as 3945 km. B is the asymptotic miss radius for the approach trajectory. R is a member of a set of vectors designated as RST. The three-sigma dispersion in inclination is $57.3 \frac{B \cdot R}{B}$, or 1.92 degrees.

The $\Delta V$ required in order to circularize at 250 km is highly variable, depending primarily on the radius of closest approach (RCA) of the transit trajectory to the moon. This can vary from 1.24 km per second to 0.97 km per second over the expected three-sigma variation in radius of closest approach, ignoring the effects of gravity (maximum effect of gravity here is less than 0.03 km per second).

Since a solid propellant retromotor of fixed impulse is desired for reliability, a means of disposing of the excess impulse must be specified. Since thrust termination procedures are not sufficiently developed and would require on-board measurement of velocity increments, a yaw maneuver was proposed in the previous LOC study phase, in which the thrust vector is turned partly out of the orbit plane. In this manner, only the $\Delta V$ required for circularizing is actually used; the remainder rotates the orbit plane about the local radius vector (from the moon to the satellite) to some new position. This has been reported in some detail in the Phase I Study report.

In order to assure that a non-impacting trajectory results from a three-sigma miss on the low side of the nominal approach, even though a three-sigma miss on the high side passes through the orbit radius of interest and can be circularized there, it is necessary to bias the orbit altitude to at least six sigma (or 234 km) above the surface. The aim point for the transit trajectory will be $3\sigma$ (or 117 km) below the circular orbit altitude desired. The nominal altitude of 250 km has been chosen on this basis, but any altitude between 100 km and 400 km would satisfy requirements for coverage and resolution reasonably well. The aim point is, therefore, 1871 km radius or 133 km altitude.

The $\Delta V$ required in order to circularize at 250 km altitude an approach three-sigma low in RCA is 1.24 km/sec. If this is adopted as the retrorocket specification, then lower approaches will not be circularized but can be made into slightly elliptical orbits, with no plane change. Any approach higher than minus three sigma in radius (i.e., 16 km altitude) will be circularized at 250 km, with the orbit plane rotated to the left or right about the point of retrofire.

The Δ V required can be slightly reduced by increasing the design orbit altitude to 300 km and biasing-up the entire dispersion pattern for RCA by 50 km. The minus three-sigma RCA is now 1804 km (or 66 km altitude), and the Δ V required is 1.18 km/sec. All approaches between 66 km and 300 km altitude will be circularized at 300 km altitude, or 2038 km RCA.

An alternative procedure which might be considered would be to fix the aim point at 183 km altitude (1921 km RCA) but to perform the circularizing maneuver at 250 km, as before, instead of 300 km. Trajectories as low as 66 km could be circularized at 250 km, with a Δ V of 1.14 km/sec. Any approach higher than 250 km would be circularized at that altitude, this range of maneuvers requiring a slightly less than 1.0 km/sec Δ V. This work has led to construction of a trade-off curve, Figure I. 2. C-1, where probability and aim point altitude are plotted against retromotor Δ V. For this alternative arrangement, any RCA error above +1.72 sigma would result in circularization at RCA. An RCA error between -3 sigma and +1.72 sigma would result in circularization at 250 km. Both of the above cases produce a plane change or yaw maneuver. For an RCA error below -3 sigma, an elliptical orbit would be obtained.

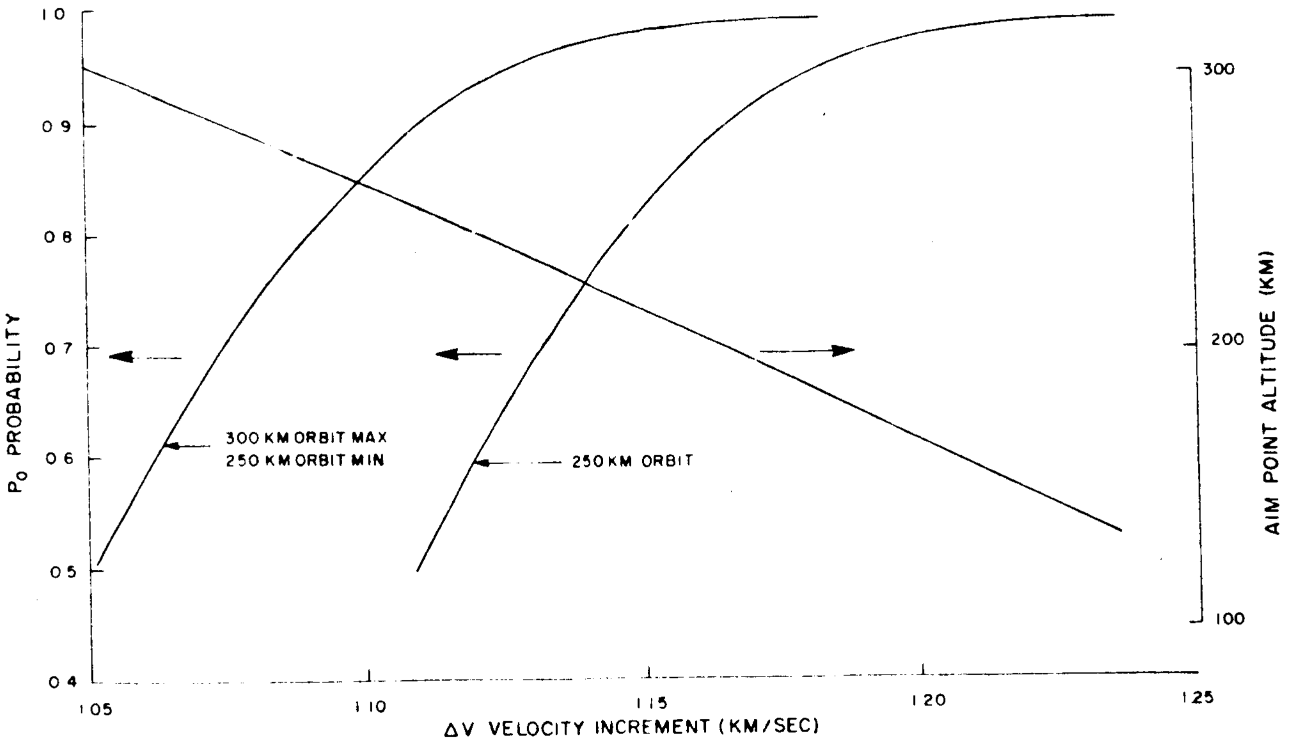

Figure I. 2. C-1. Probability and Aim Point Altitude vs. Velocity Increment

Because of the probability of obtaining an orbit altitude above 250 km, thereby degrading the intended resolution of the TV subsystem, the relatively expensive aim point of 1871 km RCA (or 133 km altitude) is recommended. This requires a Δ V of approximately 1.25 km per second, and an additional weight of 11.3 pounds compared to a retromotor providing 1.15 km/sec. However, this Δ V and added weight provide a certain measure of assurance in attaining a good photographic orbit.

The plane rotation resulting from the dumping of excess Δ V is described in detail in the Lunar Orbiter Capsule Study Final Report (Phase I), dated 3 August 1962. The principal effect of the plane change is to shift both the inclination and longitude of the node to new values. These new values must be coordinated with the requirements of the photographic experiment for coverage of particular areas with specific lighting angles. In conjunction with the Ranger Spacecraft restraints, these restrictions will establish the allowable launch window.

For a retromotor capability of 1.25 km/sec Δ V, all combinations of the approach trajectories in Table I.2.C-1 can be circularized at 250 km altitude.

TABLE I.2.C-1

THREE-SIGMA ERROR LIMITS IN APPROACH TRAJECTORIES

| Radius of Closest Approach | | Approach Inclination | |
|---|---|---|---|
| Error Limit | km | Error Limit | Degrees |
| -3 Sigma | 1754 | -3 Sigma | 25.3 |
| Nominal Aim Point | 1871 | Nominal Aim Point | 27.2 |
| +3 Sigma | 1988 | +3 Sigma | 29.1 |

Table I.2.D-1 (in Part D of this Section) lists final values of node and inclination achieved for a northern hemisphere, trailing limb, lunar approach, with a right yaw maneuver. Discussion of interactions between achieved final orbit and photocoverage is also covered in Part D of this Section.

For most of the trajectory and injection studies in this work, the approach asymptote was taken to be in the lunar equatorial plane, from the direction of 45 degrees west lunar longitude.

The air-point study should be recalculated with an accurate trajectory program to include true positions and velocities for the earth, moon, sun, and spacecraft, and to achieve the desired final orbit, knowing the properties of the yaw maneuver. This must be conducted in conjunction with the construction of at least rudimentary firing tables, since the direction of approach to the moon depends on the time and direction of the earth launch.

The most essential requirements of the injection maneuver are an accurately known trajectory, attitude, and retromotor performance. Unfortunately, each of these elements, at present, leaves some performance to be desired, but improvements are promised in the near future.

Increased accuracy of Doppler measurement by the Deep Space Instrumentation Facility (DSIF) is expected to make possible the refinement of position and velocity of a spacecraft from the presently achievable 30 km and 0.2 meter per second to 1.5 km and 0.01 meter per second by 1965. This should permit even more accurate determination of position in a lunar orbit, assistance being provided to trajectory control and also to photogrammetry.

Attitude control for thrust positioning can be improved by normal development in sensors and gyros, and by increased weight allowances for certain critical parts. Drift rates of 0.1 degree per hour, and position accuracy of 0.2 degree from reference are undesireable for this injection. Better devices could provide a better orbit. (Refer to the Error Sensitivity Table in the Phase I Final Report, page II-13.)

Retromotor performance will be satisfactory as soon as sensors for grain temperature have been incorporated, and when the calibration and Δ V prediction for the retromotor have been demonstrated. There is still an opportunity to use thrust termination devices in place of a yaw maneuver, if such devices become applicable, because of their improved accuracy and reliability. (An extensive discussion of the mechanics of the injection maneuver is covered in The Phase I Study Final Report, Section II.)

### 3. INJECTION ERROR STUDY

The injection maneuver is a non-linear process. Conventional error analysis methods have been largely designed for analysis of linear (or approximately linear) systems. It was intended to preserve the non-linear character of the injection process for this study (since the input deviations were not "small") by applying a method utilizing conditional probability integrals, and evaluating these multiple integrals by computer. This method consists of finding the probability of the (i +1) phase of the maneuver reaching a certain value, having previously established the i-phase. The important variables were judged to be: (1) radius of closest approach, (2) inclination of approach, (3) velocity of approach, (4) altitude and attitude of retrofire, and (5) Δ V of the retromotor. Such a study would lend itself to the effort of redesigning the system specifications and the mission profile in order to secure the highest probability of successful arrival in final orbit within specified limits.

This work had just begun at contract termination. The results of the Phase I Study are the only results available to date for the injection maneuver; these results are documented in the Phase I Final Report, Section II.B-3.

## D. IN-ORBIT CONSIDERATIONS

### 1. TV COVERAGE OPTIMIZATION

There are substantial uncertainties in the arrival conditions for the approach trajectory. The most important of these is the uncertainty in radius of closest approach, or periselene. In general, the solid-propellant, fixed-impulse retromotor chosen for the injection maneuver can only circularize the orbit by using its excess Δ V to make an orbit plane-change maneuver. Because of this injection maneuver, both the inclination and the node of the final orbit become uncertain. These uncertainties are non-linear functions of the various uncertainties in the approach trajectory. (This situation was explored during Phase I of the LOC Study, and is discussed in the Phase I Final Report, dated 3 August 1962, on JPL Contract No. 950340.)

The problem of optimizing the TV coverage is thus made doubly difficult. Not only must an inclination and node longitude be chosen for the orbit at injection (so as to provide the most desirable history of photocoverage for the 30 to 40 days of mission life) but the orbit itself must be chosen to minimize the possibility of having photocoverage severely restricted by extreme variations in the orbit. This optimization problem was to have been studied with the use of a 7090 computer program. This program would have preselected the optimal time and location for photocoverage, as restricted by solar elevation angle limits. Various initial orbits were to have been tried, and desirable injection windows selected, which would provide the best compromises available for maximizing coverage for the first 30 days, and especially for the first 15 days. This work would have generated detailed launch-window constraints from photocoverage considerations.

As a visualization aid and for rough preliminary planning, a Mercator projection of the lunar surface was overlaid with a transparent sheet having solar elevation contours centered on the equator, and with a transparent sheet having an orbit ground track for a specific inclination. This ground track can be adjusted to the node longitude required; then the approximate injection and launch windows can be derived by moving the solar contour pattern to correspond to various times of injection. This process, as described, ignores the libration of the moon, the true subsolar point, and motion of the orbit and solar contours after injection, but, even so, can furnish useful information. This process was to be supplemented with the computer study, discussed in detail in paragraph D. 2 of this section.

Figure I. 2. D-1 illustrates a nominal injection orbit at first quarter. Inclination is 35 degrees; the orbit is direct or eastward; and the descending node is at 105.5 degrees east lunar longitude. Television coverage with illumination, between 20 and 60 degrees solar elevation (or 70 and 30 degrees solar zenith angle respectively), is not obtained in the area of primary interest,* but is obtained above 22 degrees north latitude and between 9 and 29 degrees south latitude. This will be swept across the face of the moon by the rotation of the moon, providing some good coverage, but rather high solar elevation angles near the equator.

Figure I. 2. D-2 shows the same orbit with illumination of half-quarter, half-way between the new moon and first quarter. Here, TV coverage is good between 23 degrees north and 0° latitude, and again below 29° south. This pattern provides better coverage than that of Figure I. 2. D-1, but both will change with time due to regression of the orbit plane and the apparent annual motion of the sun.

---

*(± 90° longitude and ± 20° latitude)

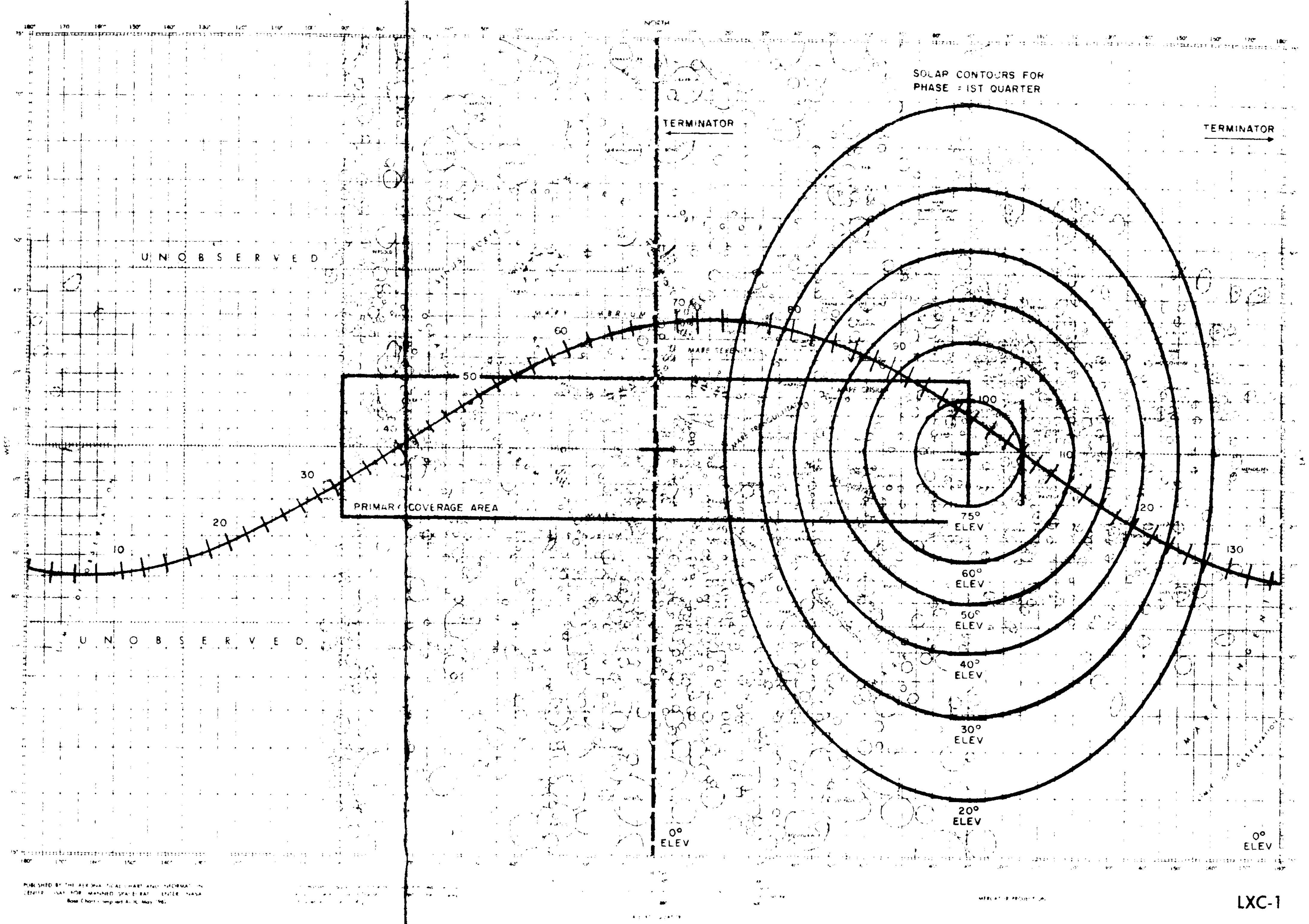
NORTH
SOLAR CONTOURS FOR
PHASE = 1ST QUARTER
TERMINATOR
TERMINATOR
UNOBSERVED
UNOBSERVED
PRIMARY COVERAGE AREA
10
20
30
40
50
60
70
80
90
100
110
120
130
75° ELEV
60° ELEV
50° ELEV
40° ELEV
30° ELEV
20° ELEV
0° ELEV
0° ELEV
WEST
MERCATOR PROJECTION
LXC-1

(35° Inclination; Descending Node, 105.5° Long. E)

Figure I.2.D-1. Nominal Injection Orbit at First Quarter

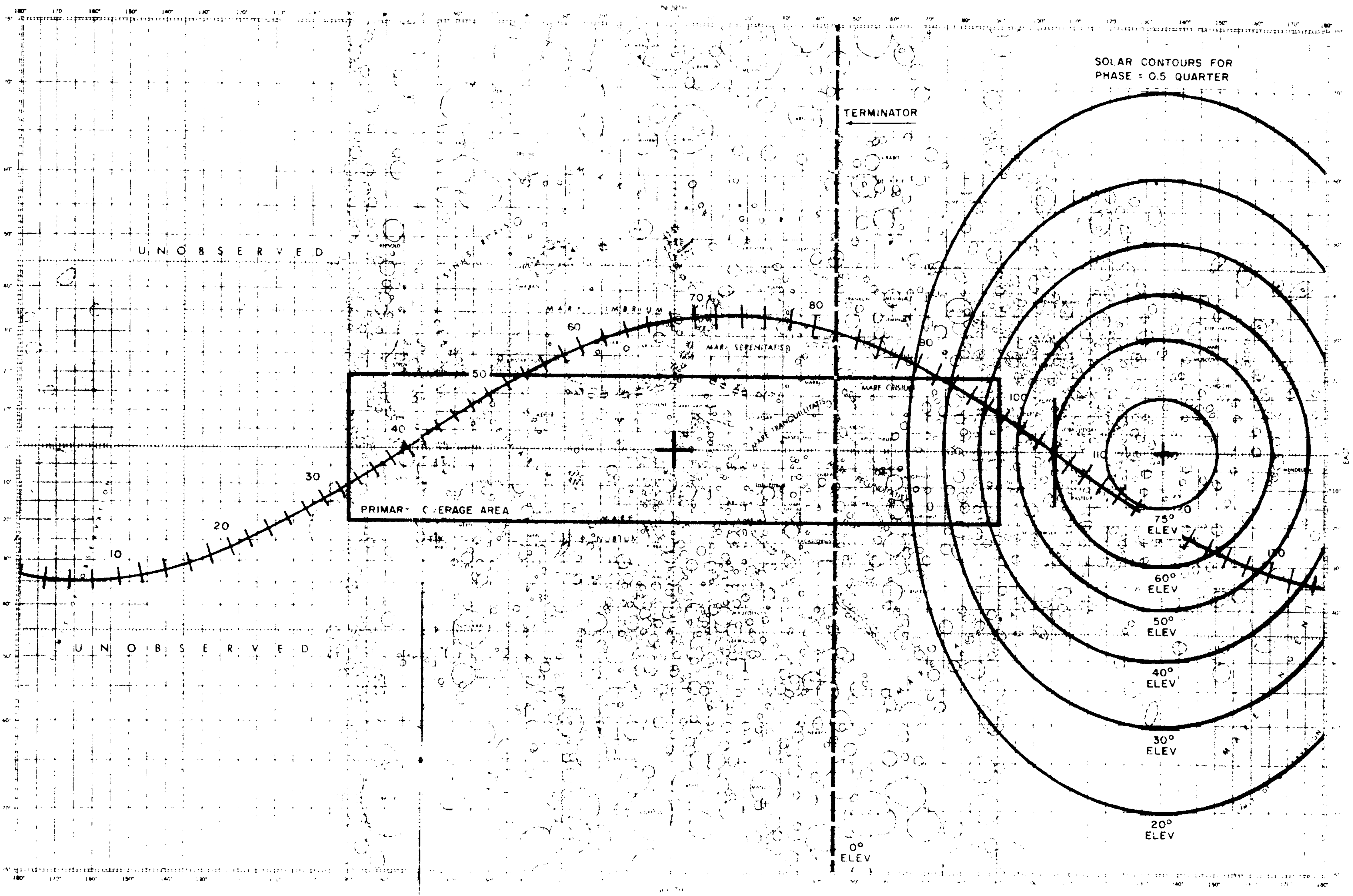
SOLAR CONTOURS FOR
PHASE = 0.5 QUARTER
TERMINATOR
UNOBSERVED
UNOBSERVED
PRIMARY COVERAGE AREA
MARE IMBRIUM
MARE SERENITATIS
MARE CRISIUM
MARE TRANQUILLITATIS
MARE FECUNDITATIS
MARE NUBIUM
WEST
EAST
10
20
30
40
50
60
70
80
90
100
110
120
75° ELEV
60° ELEV
50° ELEV
40° ELEV
30° ELEV
20° ELEV
0° ELEV
180°
170°
160°
150°
140°
130°

PUBLISHED BY THE AERONAUTICAL CHART AND INFORMATION CENTER, USAF FOR MANNED SPACECRAFT CENTER, NASA
Base Chart Compiled ACIC May 1962

LXC-1

(35° Inclination; Descending Node, 105.5° Long. E)

Figure I. 2. D-2. Nominal Injection Orbit With Illumination at Half-Quarter

Figure I. 2. D-3 shows the nominal orbit with illumination for 1. 5 quarter. Television coverage is available from 35° N to 7° S latitude. This is better than either of the previous two at injection, and shows promise of continued good performance for at least one week.

As indicated in Table I. 2. D-1, which summarizes the inclination and node longitude for various orbits of likely occurrence, the effect on inclination and node longitude of variation in radius of closest approach is severe. Figure I. 2. D-4 shows a non-nominal orbit, corresponding to extreme deviations in radius of closest approach and in approach inclination. This is approximated by a 25-degree inclination orbit, with the node at 122° E. longitude. Illumination is shown for injection at 0. 5 quarter. Usable initial TV coverage should extend from approximately 19 degrees north to 5 degrees north latitude.

Figure I. 2. D-5 shows a non-nominal orbit injected at first quarter. Southern photo coverage is possible after one week.

As can be clearly seen from these examples, optimization of photocoverage and selection of launch window are not simple tasks, but procedures have been developed, and will be explained, for describing the performance of each configuration to be examined; this will permit selection of an optimum design orbit and launch window.

TABLE I. 2. D-1

SUMMARY OF ORBITS BEFORE AND AFTER INJECTION

| Radius of Closest Approach (km) | Initial Inclination | Descending Node E. Longitude | Final Inclination |
|---|---|---|---|
| 1754 | 25.3° | 122.2° | 26.3° |
| 1871 | 25.3° | 104,1° | 33.4° |
| 1988 | 25.3° | 108.4° | 43.0° |
| 1754 | 27.2° | 123.0° | 28.1° |
| (Nom) 1871 | 27.2° | 105.5° | 35.0° |
| 1988 | 27.2° | 109.2° | 44.7° |
| 1754 | 29.1° | 123.7° | 30.0° |
| 1871 | 29.1° | 106.8° | 36.7° |
| 1988 | 29.1° | 110.1° | 46.5° |

Approach: Trailing Limb, Northern Hemisphere, Right Yaw Maneuver

## 2. PHOTOCOVERAGE STUDY

The success achieved in mapping the surface of the moon depends, to a great extent, on the amount of adequate illumination available during any orbit. This implies that time history of favorable illumination-intervals be investigated for a specific set of injection conditions. Such a range of illumination is defined by solar elevation angles of 20 to 60 degrees. Thus, by varying the injection conditions and examining the resultant fluctuation in acceptable illumination, a final set of conditions can be selected for optimizing photocoverage. Subsequently, the following problem and question arises: given a set of injection conditions, what are the selenographic coordinates (hence, time interval by direct calculation for a circular orbit) at which the spacecraft enters into and exits out of an area of acceptable illumination? To resolve this problem, the following method was considered.

If the assumption is made that the orbital plane of the spacecraft remains fixed relative to the surface of the moon during a photocoverage interval*, then a closed solution can be performed. The solution consists of determining the points of intersection of two circles on a unit sphere, centered at the center of the moon. Of the two circles, one is a great circle and represents the projection of the spacecraft's motion onto the unit sphere. The center of the circle lies at the pierce-point of the orbit normal with the sphere. Appendix D contains the necessary equations for determining the coordinates of this point. The second circle, with center at the subsolar point (see Appendix D), represents the area concentric to the sun-moon line, sufficiently illuminated for photocoverage purposes. The radius of this solar contour circle is an input parameter, and can be chosen to represent the magnitude of the illumination constraint.

Once the location and dimension of each circle has been determined, the trigonometric expressions outlined in Appendix D may be applied, directly yielding the desired pairs of coordinates. If $(\delta_1, \alpha_1)$ and $(\delta_2, \alpha_2)$ represent the coordinates, namely declination and right ascension, of the two points of intersection, then the time interval ($\Delta t$) of favorable illumination is simply:

$$\Delta t = \frac{T}{2\pi} \text{ arc cos } \left[\sin \delta_1 \sin \delta_2 + \cos \delta_1 \cos \delta_2 (\alpha_2 - \alpha_1)\right] \qquad (1)$$

where: T is the anomalistic period of the spacecraft.

The above scheme was intended to be programmed for use on the digital computer, and would operate in the following manner. A set of initial conditions would be prepared, consisting of orbital elements valid at the exact date of injection, start time, stop time, time increment, and solar contour radius. The program would, at first, perform a solution (see footnote 1) at start-time, and subsequently at each new time-instant, as indicated by the time increment, until the stop-time value is reached. Each solution would exhibit six quantities: two pairs of coordinates, and two time intervals. The collection of output data would be presented as a time history of illumination-interval, permitting rapid comparison with additional runs utilizing

---

* Actual motion during a photocoverage interval will be less than 3/4 of a degree in lunar longitude, which is acceptable for this model.

[1] If the geometry is such that the spacecraft does not pass through a region of acceptable illumination, then the results of the tests described in Appendix D will direct the program to omit any further computation for the date.

RE-ORDER No. 62-484

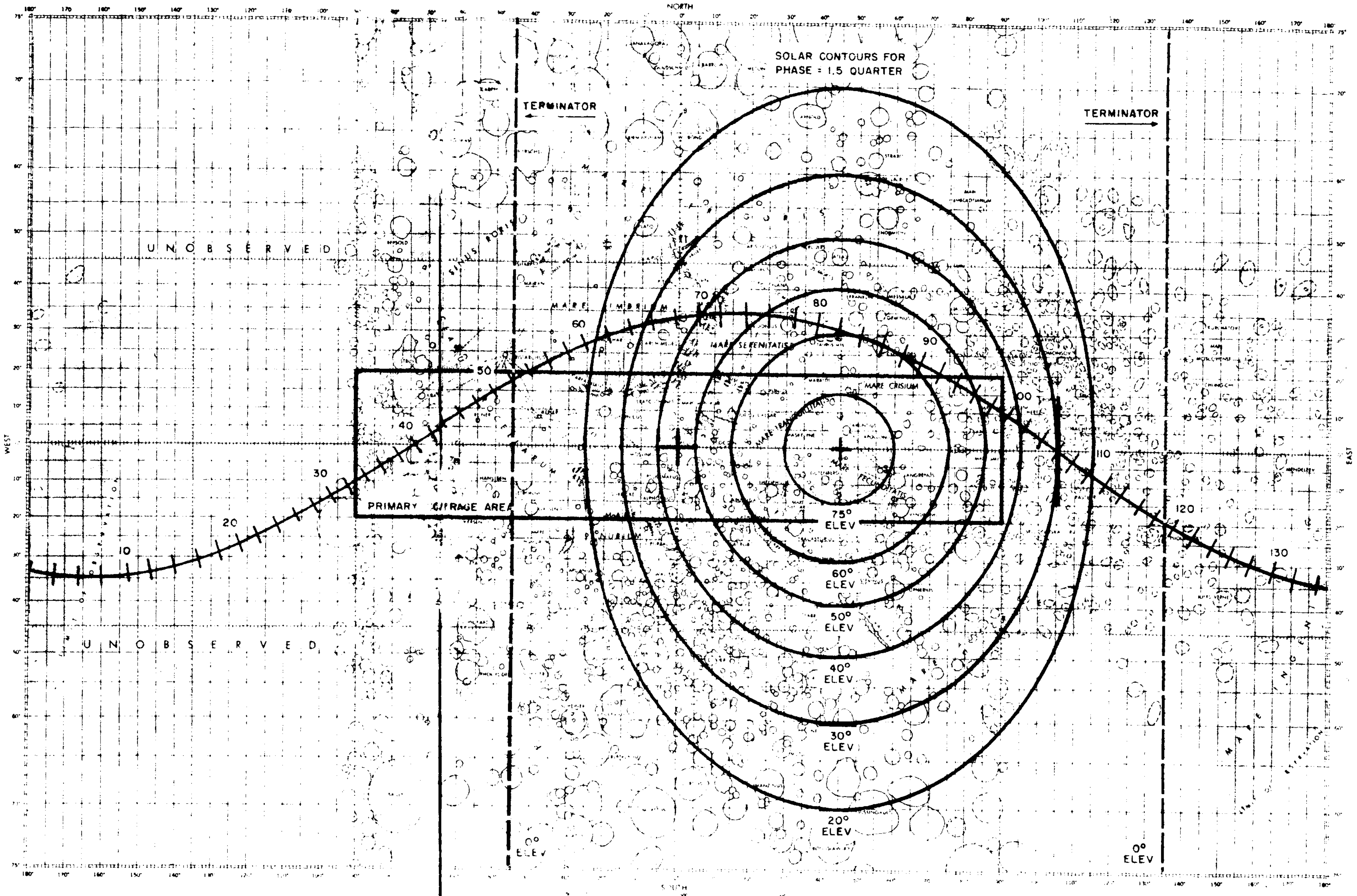
NORTH
SOUTH
WEST
EAST
SOLAR CONTOURS FOR
PHASE = 1.5 QUARTER
TERMINATOR
TERMINATOR
UNOBSERVED
UNOBSERVED
PRIMARY LANDING AREA
MARE CRISIUM
MARE SERENITATIS
MARE IMBRIUM
SINUS RORIS
75° ELEV
60° ELEV
50° ELEV
40° ELEV
30° ELEV
20° ELEV
0° ELEV
0° ELEV
10
20
30
40
50
60
70
80
90
100
110
120
130

PUBLISHED BY THE AERONAUTICAL CHART AND INFORMATION
CENTER USAF FOR MANNED SPACECRAFT CENTER NASA
Base Chart Compiled ACIC May 1962

LXC-1

(35° Inclination; Descending
Node, 105.5° Long. E)

Figure I. 2. D-3. Nominal Injection Orbit
With Illumination at 1.5 Quarter

RE-ORDER No. 62-4F9

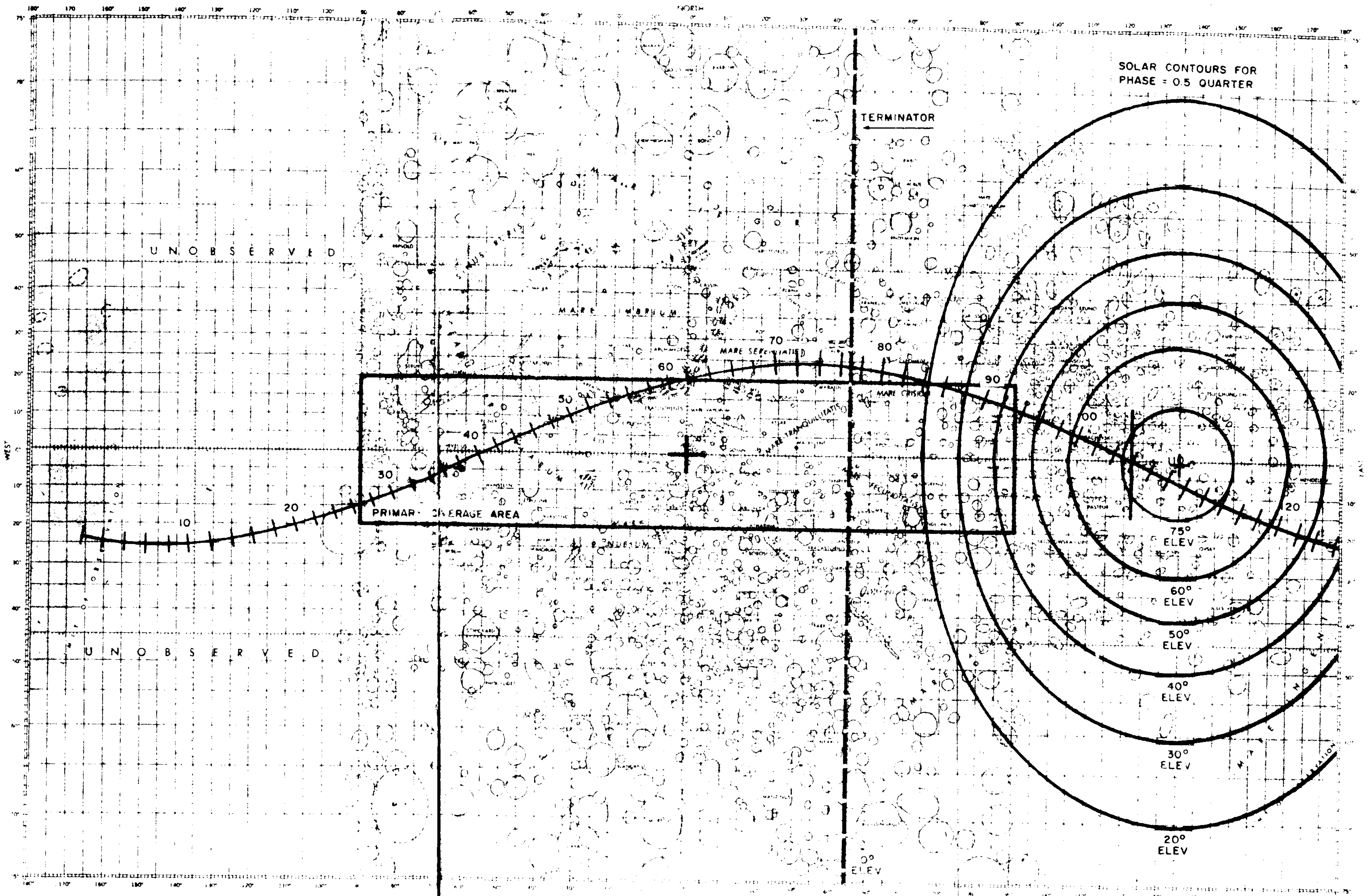
NORTH
WEST
EAST
SOLAR CONTOURS FOR
PHASE = 0.5 QUARTER
TERMINATOR
UNOBSERVED
UNOBSERVED
PRIMARY COVERAGE AREA
MARE NUBIUM
MARE SERENITATIS
MARE CRISIUM
MARE TRANQUILLITATIS
10
20
30
40
50
60
70
80
90
100
20
75° ELEV
60° ELEV
50° ELEV
40° ELEV
30° ELEV
20° ELEV
0° ELEV

PUBLISHED BY THE AERONAUTICAL CHART AND INFORMATION CENTER USAF FOR MANNED SPACECRAFT CENTER NASA
Base Chart Compiled ACIC May 1962

LXC-1

(25° Inclination; Descending Node, 122° Long. E)

Figure I.2.D-4. A Non-Nominal Injection Orbit at Half-Quarter

RE-ORDER No. 62-489

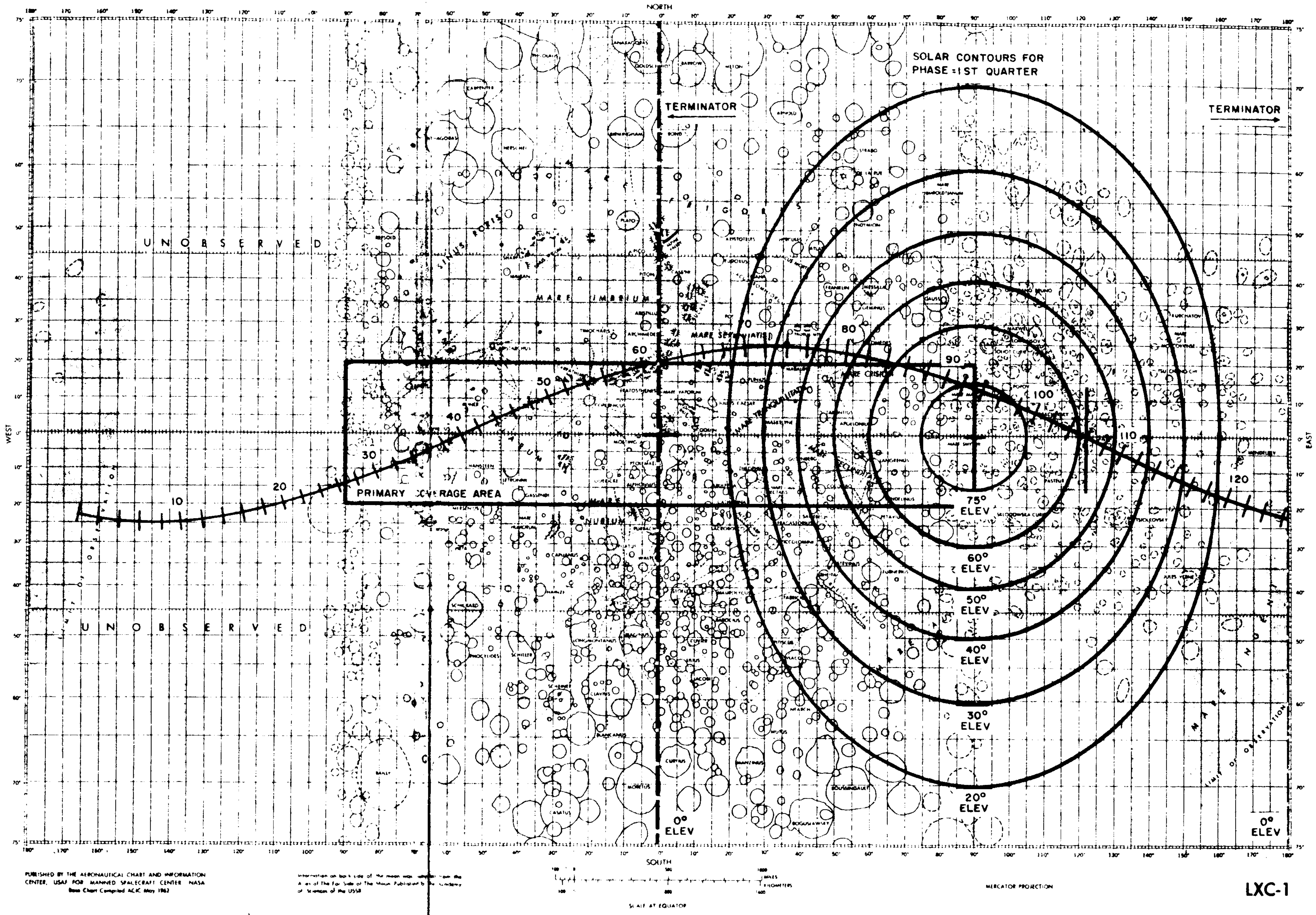
SOLAR CONTOURS FOR
PHASE = 1ST QUARTER
TERMINATOR
TERMINATOR
NORTH
SOUTH
EAST
WEST
UNOBSERVED
UNOBSERVED
PRIMARY COVERAGE AREA
MARE IMBRIUM
SINUS RORIS
MARE SERENITATIS
MARE CRISIUM
MARE TRANQUILLITATIS
MARE NUBIUM
10
20
30
40
50
60
80
90
100
110
120
75° ELEV
60° ELEV
50° ELEV
40° ELEV
30° ELEV
20° ELEV
0° ELEV
0° ELEV
MERCATOR PROJECTION
SCALE AT EQUATOR
LXC-1

PUBLISHED BY THE AERONAUTICAL CHART AND INFORMATION CENTER, USAF FOR MANNED SPACECRAFT CENTER NASA
Base Chart Compiled ACIC May 1962

Information on back side of the moon was adapted from the Atlas of The Far Side of The Moon Published by the Academy of Sciences of the USSR

(25° Inclination; Descending Node, 122° Long. E)

Figure I.2.D-5. A Non-Nominal Injection Orbit at First Quarter

different injection conditions. In a similar fashion, the solar contour radius might be varied, establishing, for each set of initial conditions, a family of time histories. Figures I. 2. D-6, 7, and 8, although developed graphically (see footnote 1), are typical of the results that might be obtained by such a process.

## 3. TV SURVEYING SYSTEM PERFORMANCE

Because of the importance of the TV system to the overall mission, and to provide the necessary background for understanding new studies, the TV system configuration and performance data originally presented in the LOC Preliminary Configuration Report, AED Document 1616, are included here.

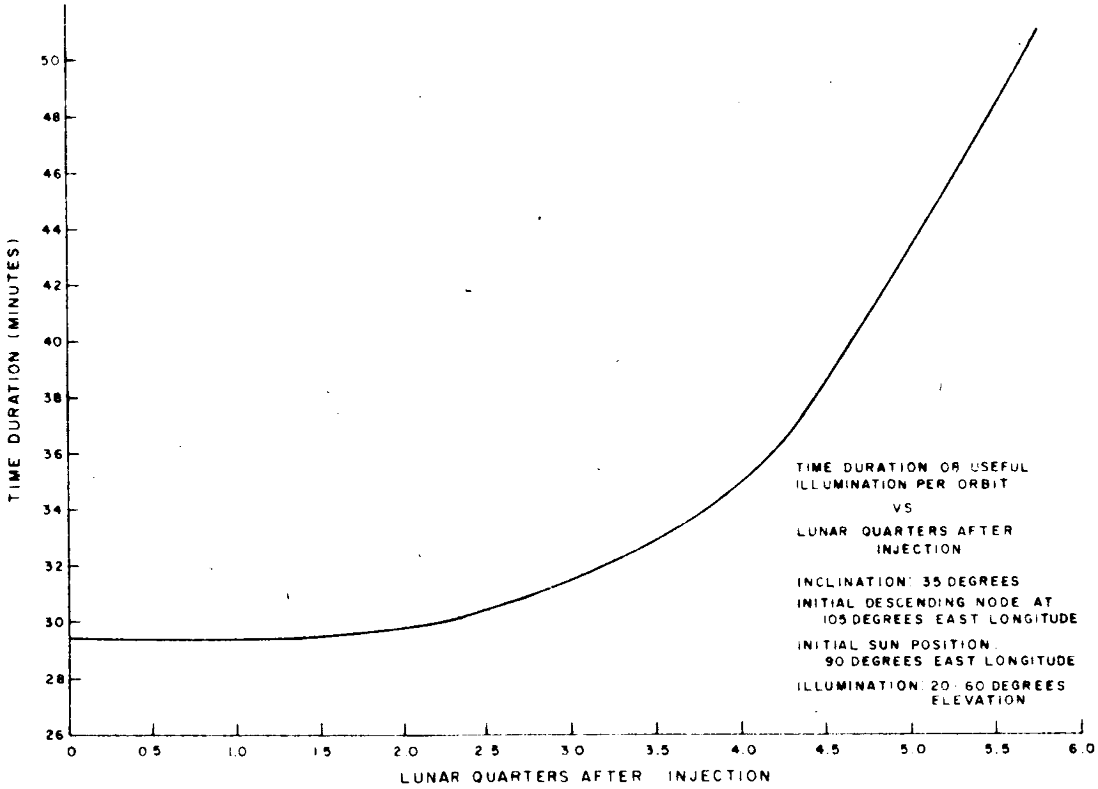

Figure I. 2. D-6. Usefull Illumination Per Orbit For Initial Sun Position of 90° East Longitude

---

[1] The graphical method of determining favorable illumination-intervals consists of an overlay technique, using a sub-satellite ground track and a set of limiting solar contour circles. By proper positioning of these representations, relative to a Mercator projection of the moon, a visual interpolation can be made for time-in and time-out crossings. These intersections indicate the time (measured from ascending node time origin) at which the satellite enters and leaves an area of acceptable illumination. The difference of these times is the illumination-interval, shown as the ordinate in Figures I. 2. D-6, 7, and 8.

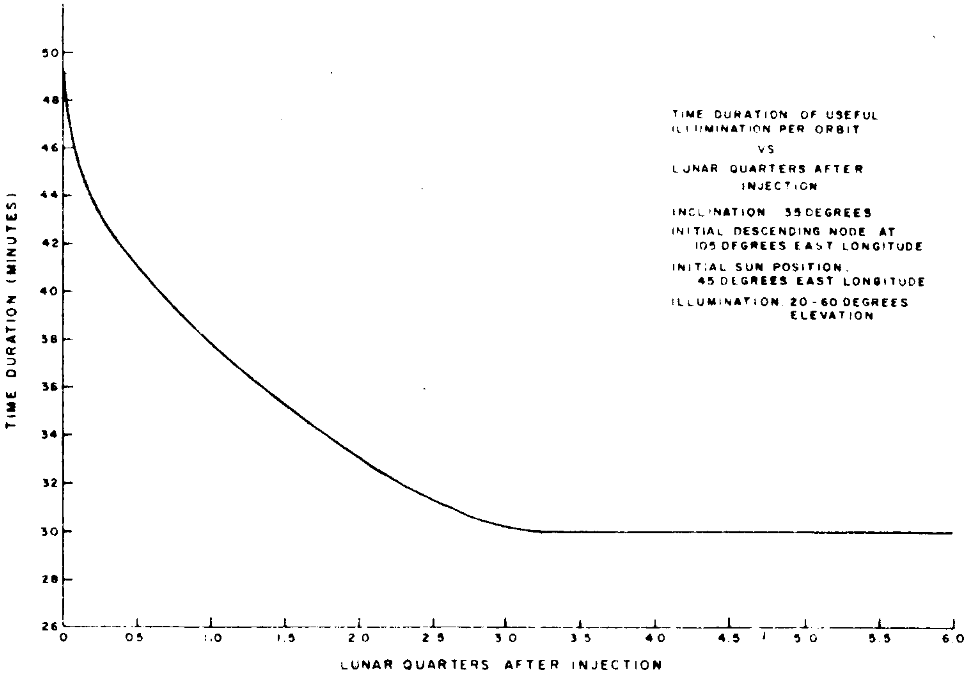

Figure I. 2. D-7. Useful Illumination Per Orbit For Initial Sun Position of 45° East Longitude

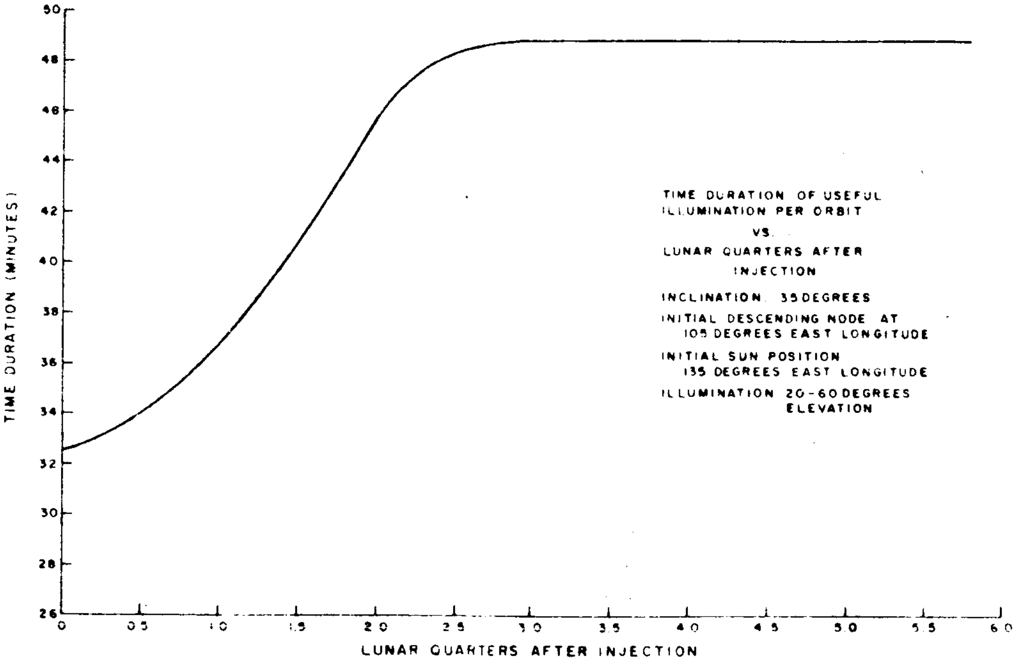

Figure I. 2. D-8. Useful Illumination Per Orbit For Initial Sun Position of 135° East Longitude

The performance of the TV surveying system is determined primarily by the desired resolution and coverage, sensor sensitivity, allowable image motion, communication bandwidth, and achievable orbit, and, to a lesser extent, by the power profile of the cameras, the tape recorder characteristics, and the uncertainties in the orbit and launch date.

The primary area of interest lies between 20 degrees north longitude and 20 degrees south longitude on the visible face of the moon; that is, between 270 degrees east lunar longitude and 90 degrees east longitude. Within this area of interest, there are various areas, such as the vicinity of the craters Kepler and Copernicus, and the Ranger 3 through 9 impact areas in Oceanus Procellarum, which are of special interest. Since the primary objective of the LOC is to compare various sites with respect to their suitability as Apollo landing sites, it is not necessary to map the entire area between plus and minus 20 degrees latitude, but only to be able to obtain data within that area for selected sites with a sufficient resolution and coverage so that comparisons of the surveyed sites can be made. In general, the approach to the television survey of these areas leads to two possible choices. Because of limitations in the television subsystem, communications bandwidth, contact time, and power supply, surveying of large areas at the maximum resolution obtainable by the LOC will not permit continuous coverage of these areas; only sample coverage can be achieved. If the desire for continuous coverage is maintained, then the maximum resolution will be dictated by the requirements of nominal overlap between successive frames along each orbit, or the capability of taking frames on adjacent orbits which also overlap. These two overlap conditions are called endlap and sidelap, respectively.

The longitude span to be surveyed and the requirement for reasonably high resolution have dictated the presence of a surface-stabilized camera system. Resolution and coverage, RF bandwidth, and transmission time combine to dictate that the orbit altitude lie within a few hundred kilometers of the lunar surface, and be nearly circular. The difficulty in controlling the arrival conditions of the transit trajectory with a single mid-course maneuver, and the desire for a minimum-weight retromotor, lead to a choice of a minimum orbit altitude no lower than 250 km. Image motion during the exposure for a non-compensating system becomes more severe at low altitudes and high resolutions, but is not too severe for most of the cases of interest to the LOC. The 250-km altitude orbit has been found to be a satisfactory design point and is recommended.

With the altitude fixed, the orbit inclination is the dominant factor in setting frame width if sidelap is desired, since the perpendicular spacing between orbits varies with the sine of the inclination at the equator. Also, the mappable arc along the orbit within the 20-degrees north and south latitude zone is determined by the inclination, although illumination may be a more restrictive constraint to potential coverage extent.

The allowable power, bandwidth, and transmission time fix the number of bits (and, therefore, the characteristics of the TV scan pattern) and, in combination with the foregoing, the resolution per TV line in the picture. Camera usage, when more than one camera is present, can admit variation, such as two cameras viewing side-by-side across the orbital track, or a high and low resolution camera centered on the orbital track. Readout and erase of the camera must be accomplished within the desired frame repetition time. The readout time of the camera, in general, will be adjusted so that the readout bandwidth is matched to the bandwidth capability of the tape recorder or video transmitter. Since simplicity is a design goal, a single-speed tape recorder and a single frame-rate and readout bandwidth are considered desirable. Existing satellite tape recorder hardware has at least the capability of a 62.5-kc signal bandwidth, with a 120-kc bandwidth achievable with a moderate development program.

A one-inch vidicon was chosen as the sensor because of its relatively high resolution, adequate sensitivity, and experience on related programs. The effective number of resolution lines for this camera is approximately 700.

Table I. 2. D-2 summarizes the investigation of alternative arrangements of cameras, tape recorder, and optical subsystem elements. In general, three possible arrangements have been considered for two possible tape-recorder bandwidths. As is shown, the difference in the tape bandwidth does not affect the operational principles of the three basic camera configurations, but does vary the total information capability on a per-orbit basis which is commensurate with the increased bandwidth. However, of the six configurations listed, only configuration 2 would allow for continuous tape motion; all others would operate in a start-stop manner between frame groups.

The present design goals include two vidicon camera systems, which must remain as preliminary until a final tabulation of weights and power requirements for the entire LOC is determined. Thus, Table I. 2. D-2 considers the possibility of a single camera system (configurations 1 and 4) which includes the capability for continuous coverage. It should also be pointed out that, with a single vidicon and a double set of optics with some rotating elements, configurations 3 and 6 could be obtained. This would lead to some differences in operation, but the coverage and resolution, as shown for configurations 3 and 6, could be obtained with a single vidicon.

In the LOC Preliminary Configuration Report, configuration 2 was recommended as the best overall choice in terms of reliability, resolution, and photocoverage.

A difference of only a factor of 2 to 3 in resolution over configuration 2 is obtained by going to the highest resolution of these configurations (10 meters), and should not lead to a tremendous improvement in the amount of surface characteristic data extractable from the television frames. Furthermore, the fact that continuous coverage at high resolution would not be obtainable with configurations 3 and 6 might hinder the interpretation of the data, since both coverage and resolution are important parameters in the data reduction process. In case two vidicons are not within the capability of the early LOC, reconsideration of this choice may be valid.

A catadioptric lens system of f/1.5 has been selected, and, for a camera sensitivity of 0.2 ft-candle-second at a SNR of 32.5 db, this will permit observations of the lunar surface with a minimum albedo of 0.09 and one TV line of smear per exposure, due to attitude motion rates of $4 \times 10^{-3}$ rad/second at sun-zenith angles of approximately 60 degrees (i.e., 30 degrees from sun terminator). This lens will permit observation of albedos to 0.06 with a 29 db S/N ratio and a sensitivity of 0.1 ft-candle-second at the same sun angles (see Table I. 2. D-3).

# TABLE I. 2. D-2

# ALTERNATIVE TV SYSTEM PARAMETERS

| Parameter | Tape Recorder Bandwidth = 60 kc/s | | | | Tape Recorder Bandwidth = 120 kc/s | | | |
|---|---|---|---|---|---|---|---|---|
| | (1) One Camera | (2) Two Cameras Across Orbit | (3) Two Cameras | | (4) One Camera | (5) Two Cameras Across Orbit | (6) Two Cameras | |
| | | | High Res. | Low Res. | | | High Res. | Low Res. |
| Orbital Altitude (km) | 250 | 250 | 250 | 250 | 250 | 250 | 250 | 250 |
| Orbital Inclination (degrees) | 35° | 35° | 35° | 35° | 35° | 35° | 35° | 35° |
| Field of View (km) | 30 | 16 | 6.5 | 54 | 30 | 16 | 6.5 | 54 |
| Number of TV Lines | 650 | 650 | 650 | 650 | 650 | 650 | 650 | 650 |
| Resolution/TV Line (meters) | 45 | 25 | 10 | 85 | 45 | 25 | 10 | 47 |
| Camera Read Out Time (seconds) | 4.78 | 4.78 | 4.78 | 4.78 | 2.48 | 2.48 | 2.48 | 2.48 |
| Tape Start-Stop Time (seconds) | 1.00 | 0 | 1.00 | 1.00 | 1.00 | 1.00 | 1.00 | 1.00 |
| Total Record Time/ Frame Group (secs) | 5.78 | 9.56 | 10.56 | 10.56 | 3.48 | 5.96 | 5.96 | 5.96 |
| Number of Frames (Total) | 83 | 100 | 90 | 90 | 137 | 160 | 160 | 160 |
| Separation Between Frames centers along orbit (km) | 21.1 | 13.3 | 49 | 49 | 31.1 | 13.3 | 27.8 | 27.8 |
| Linear Coverage (km) | 1750 | 665 | 2220 | 2220 | 2900 | 1060 | 2220 | 2220 |
| % Coverage Between ± 20° Lat. | 79 | 30 | 100 | 100 | 132 | 48. | 100 | 100 |
| Time Between Frames (seconds) | 15.4 | 9.58 | 35.8 | 35.8 | 15.4 | 9.58 | 20 | 20 |
| Erase Time (seconds) | 10.6 | 4.78 | >20 | >20 | 12.9 | 6.8 | >15 | >15 |
| Total Survey Time (mins) | 21.2 | 8.1 | 27 | 27 | 27 | 13 | 27 | 27 |
| Allowable Exposure Time for 1 TV Line Smear and 1.0 millirad/sec Attitude Stabilization (ms) | 27 | 15.2 | 6 | 57 | 27 | 15.2 | 6 | 28.6 |
| Effective Focal Length (mm) | 93 | 175 | 430 | 50 | 93 | 175 | 430 | 93 |

## TABLE I. 2. D-3
## f-NUMBER VERSUS ATTITUDE STABILIZATION RATE

| Attitude Stabilization Rate | Exposure* Time (millisecs) | Sun-Zenith Angle Degrees | Photometric Function | f-Number for: S/N = 32.5 db Exp. = 0.2 ft-cand-secs. | | | f-Number for: S/N = 29 db Exp. = 0.1 ft-cand-sec. |
|---|---|---|---|---|---|---|---|
| | | | | albedo = 0.18 | 0.09 | 0.06 | albedo = 0.06 |
| $1.0 \times 10^{-3}$ rad/sec | 15 | 60 | 0.22 | 2.4 | 1.7 | 1.4 | 2.0 |
| $2.0 \times 10^{-3}$ rad/sec | 13 | 60 | 0.22 | 2.3 | 1.6 | 1.35 | 1.9 |
| $3.0 \times 10^{-3}$ rad/sec | 12 | 60 | 0.22 | 2.2 | 1.5 | 1.25 | 1.75 |
| $4.0 \times 10^{-3}$ rad/sec | 10 | 60 | 0.22 | 2.0 | 1.4 | 1.10 | 1.60 |

* Exposure time based on 1 TV line smear including motion of vehicle over the lunar surface of 1.37 km/sec and a lunar orbit altitude of 250 kilometers.

A summary of the parameters of the TV system, with expected performance characteristics are listed in Table I. 2. D-4.

## TABLE I. 2. D-4

## TV SURVEYING SYSTEM PARAMETER SUMMARY

| Parameters | Performance Characteristics |
|---|---|
| Orbit: | |
| Altitude | 250 km |
| Inclination | 35 deg |
| Surface Speed | 1.37 km/sec |
| Camera: | |
| Video Bandwidth | 62. 5 kc |
| Number of Cameras | 2 |
| Field of View per Camera | 18 km square |
| Combined | 18 x 34 km |
| Scan Lines | 1,024 |
| Resolution Lines | 700 vertical<br>695 horizontal |
| Surface Resolution | 25. 7 meters/TV lines |
| Readout Time | 6. 0 sec |
| Erase Time | 6. 0 sec |
| Frame Repetition Rate | 12. 0 sec |
| Mapping Time | 8 min or 480 sec |
| Mapped Arc | 660 km |
| Lens: | |
| Focal Length | 153 mm |
| f/n (max.) | 1. 5 |
| Aperture | 100 mm |
| Exposure Time | 17 m/sec |
| Smear | 1 TV line/exposure |
| Smear Rate | 4 milli-rad/sec |
| Tape Recorder: | |
| Tape Speed | 30 inches/sec |
| Motion | Continuous |
| Length | 1200 feet |
| Number of Frames | 80 total |
| Total Recording Time | 8 minutes |
| Total Playback Time | 8 minutes |

It became clear, in the light of subsequent discussions at JPL and at NASA Headquarters, that a configuration similar to No. (3) in Table I. 2. D-2 might be more useful, since it could provide both a high and low resolution capability, and at the cost of some general mapping coverage and redundancy of cameras. This arrangement is judged more useful since it can contribute more directly to lunar surface roughness studies for support of the manned-landing program. Such a system would have essentially the same design parameters as the dual medium angle system, except for optics, coverage and resolution. The details are listed in Table I. 2. D-2, under configuration (3).

Frame sizes of 6. 5 km square and 54 km square will be seen at 250 km altitude. Effective resolutions of approximately 10 and 85 meters per TV line can be expected. Optical system focal lengths of 430 mm and 50 mm are suggested, and should be as fast as possible, with variable aperture or shutter speed. Table I. 2. D-3 provides some data on f-numbers, from which it may be seen that either f/1. 5 or f/2. 0 would probably suffice for most of the conditions.

Frames will be taken at intervals of 35. 8 seconds. A suggested frame arrangement is one wide-angle frame, with one narrow-angle frame taken near the center of the wide-angle frame as a "surface detail sampler". The wide-angle frame will assist in locating the narrow-angle frame and will provide general survey capability of a quality which cannot be matched by earth telescopes except near the center of the visible disc. Other operational ratios, such as two or three narrow-angle frames for every wide-angle frame can easily be arranged, as requested. Each such arrangement has operational advantages and disadvantages, and should be carefully considered before freezing the specification.

Start-stop operation of the tape recorder, rather than continuous operation, will be necessary. However, a very long swath will be available at low resolution: 2220 km, as opposed to 660 km with the previously discussed medium-angle system.

## 4. VERTICAL RESOLUTION BY SHADOW MEASUREMENT

In response to a discussion with Dr. E.M. Shoemaker of NASA, the possibility was explored of adapting the LOC optical systems and TV sensors to the problem of measuring vertical relief distances, by shadow measurement near the terminator. The results of this work are included in detail in Appendix E, and are discussed briefly here.

It is possible to match the long shadows cast by surface relief at low lighting angles against the additional exposure time required due to the lower average illumination near the terminator. Image smear, due to orbital velocity, is shown not to be a problem, since the actual linear resolution is coarser for the longer shadows, and percentage smear can be held constant. For constant vertical relief resolution, optical system focal length is shown to grow as solar elevation angle is increased, and shadows are thereby shortened. At some point, a maximum focal length will be reached, and for higher solar elevation angles, a constant horizontal resolution is obtained.

Both the vidicon and image orthicon are examined for this mode of operation. Both show promise of applicability to the mission, with some development of optics or ruggedized tubes. It may be seen that the vidicon allows the use of a shorter focal length optical system, but its lack of sensitivity demands a fast lens or relatively poor vertical resolution, whereas the image orthicon uses a long but slow lens system. For a vertical element of 2 meters to be resolved, some representative results are tabulated in Table I. 2. D-5 for the type 4431 vidicon and type 7198 image orthicon.

TABLE I. 2. D-5

VIDICON AND IMAGE ORTHICON TECHNICAL SUMMARY

| Solar Elevation Angle (deg.) | Focal Length (meters) | Vertical Resolution (meters) | Horizontal Resolution (meters) | Exposure* (msec) |
|---|---|---|---|---|
| # 4431 Vidicon | | | | |
| 1 | 0.0896 | 2 | 19.10 | 20.4 |
| 2 | 0.1793 | 2 | 9.55 | 10.2 |
| 3 | 0.2691 | 2 | 6.36 | 6.8 |
| 4 | 0.3590 | 2 | 4.77 | 5.1 |
| 5 | 0.4492 | 2 | 3.81 | 4.1 |
| 10 | 0.4492 | - | 3.81 | 2.0 |
| # 7198 Image Orthicon | | | | |
| 1 | 0.313 | 2 | 19.10 | 20.4 |
| 2 | 0.629 | 2 | 9.55 | 10.2 |
| 3 | 0.940 | 2 | 6.35 | 6.8 |
| 4 | 0.940 | 2 | 6.35 | 5.1 |
| 5 | 0.940 | 2 | 6.35 | 4.1 |
| 10 | 0.940 | - | 6.35 | 2.0 |

* with no image motion compensation, f# = 0.75; with 90% image motion compensation, f# = 2.38, since exposure can now be increased by a factor of 10 for the same smear. For the image orthicon, with no image motion compensation, f# = 10.43

## 5. DESIGN CHARTS

To assist in the rapid assessment of the performance of satellite TV systems, and to aid in establishing the parameters of new designs, RCA has established nomographs for resolution, bandwidth and readout time.

### a. TV Camera f-Number Relations

Figure I. 2. D-9 nomograph facilitates the use of relations between sensor sensitivity, exposure time, optical system parameters, and object field illumination. For example, the f-number of a satellite optical system may be established in the following manner. Enter the "Highlight Exposure" scale with the highlight sensitivity of the pickup tube, and then enter the exposure time. Draw a line through the two previous points to the next scale, "Target Illuminance". Choose the product of albedo and optical system transmission efficiency, and continue a new line to intersect the construction line. This point, with the product of the solar constant and photometric function, will determine the optical system f-number. A useful variation of this procedure will show the minimum solar elevation angle that can be reached with a particular f-number.

This nomograph should be supplemented by tables which list products of solar constant and photometric function versus solar elevation angle for the various photometric lunar surface models. Table I. 2. D-6 shows this product for the Van Diggelen photometric model. It is assumed for this nomograph that all pictures are taken vertically, essentially.

TABLE I. 2. D-6.

VAN DIGGELEN'S LUNAR PHOTOMETRIC FUNCTION

(for zero angle corresponding to longitude of the point measured on the luminance equator)

| Solar Zenith Angle | Photometric Function | Photometric Function x 13,000 |
|---|---|---|
| 0 | 1.00 | 13,000 |
| 5 | 0.80 | 10,400 |
| 10 | 0.68 | 8,840 |
| 15 | 0.60 | 7,800 |
| 20 | 0.56 | 7,280 |
| 30 | 0.46 | 5,980 |
| 40 | 0.38 | 4,940 |
| 50 | 0.29 | 3,770 |
| 60 | 0.22 | 2,860 |
| 70 | 0.14 | 1,820 |
| 80 | 0.07 | 910 |

### b. Lunar Orbit Altitude, Endlap, Frame Size, and Resolution Relations

Figure I. 2. D-10 nomograph shows the inter-relationship of lunar orbit altitude, surface velocity (for a circular orbit), frame interval, frame spacing, frame size, overlap between consecutive frames, and resolution for a TV sensor covering such a frame size. Altitude, photo interval, and frame travel are to be used together, as shown by the example line on the nomograph, drawn from 700 km altitude to 10 km

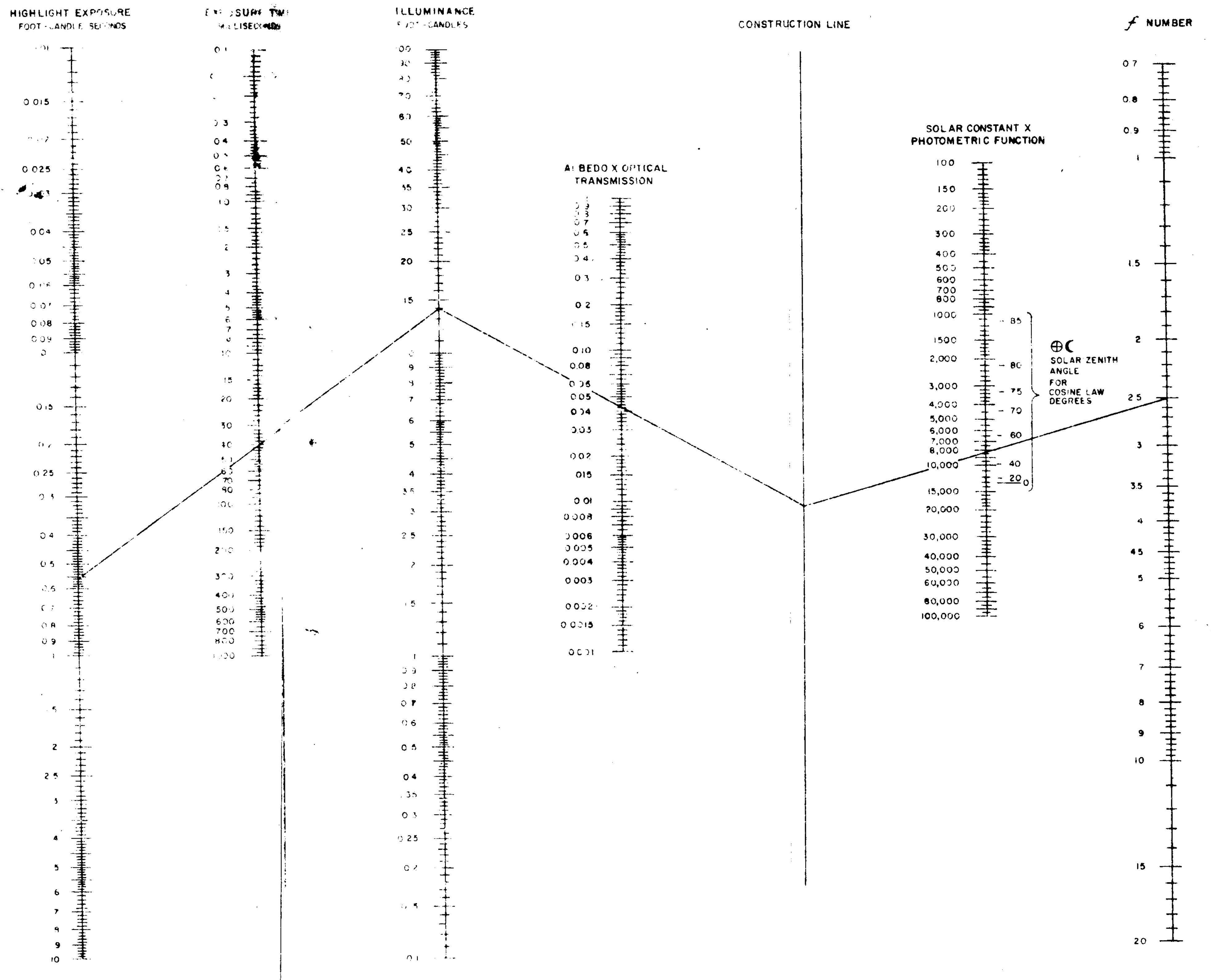

Figure I. 2. D-9. TV Camera f-Number Relations Nomograph

RE-ORDER No. 62-489

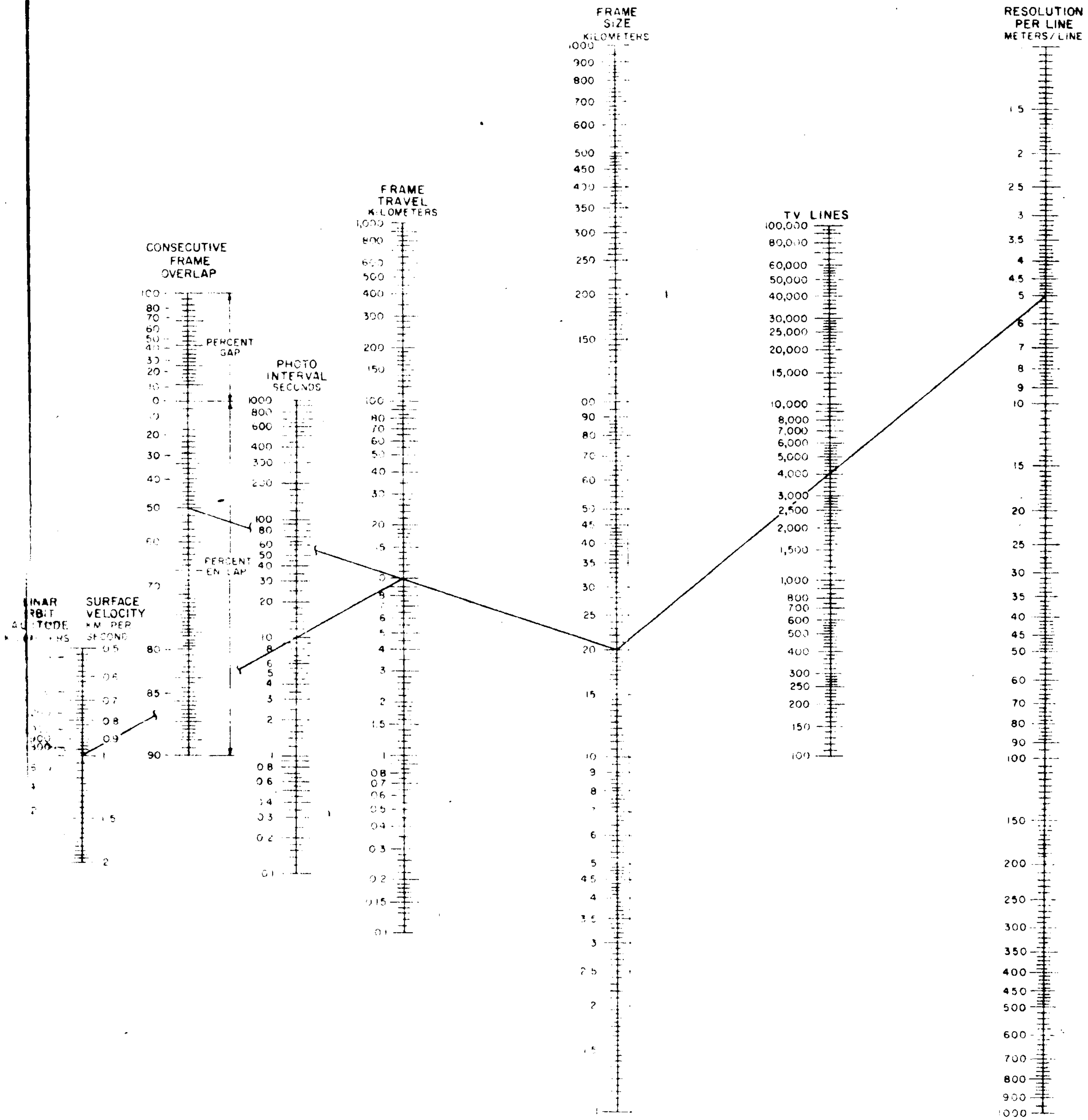

Figure I. 2. D-10. Lunar Orbit Altitude, Endlap, Frame Size, and Resolution Relations Nomograph frame travel. Given frame travel, consecutive frame overlap (as a percent of frame size) can be specified, and a line through these points will yield frame size. Frame size, lines, and resolution per line can then be related by a third construction line.

### c. Lunar Altitude, Resolution, and Smear Relations

The nomograph in Figure I. 2. D-11 relates motion over the lunar surface, exposure time, and allowable smear to the achievable resolution and frame size. A three-segment construction line, as shown in the example, will provide the necessary physical description.

Given 700 km altitude, a desired resolution, and a smear specification, the exposure time and travel per exposure time can be found. The frame size depends on the number of lines and resolution per line.

The Loss in Contrast* scale is based on a transfer function of:

$\frac{\sin \pi x}{\pi x}$, where x is $\frac{\text{Smear in lines}}{\text{2 TV lines}}$

This scale tabulates the fractional loss in contrast, or $1 - \frac{\sin \pi x}{\pi x}$

### d. TV Camera Resolution and Readout Time Relations

Figure I. 2. D-12 nomograph relates the resolution performance of the TV sensor to the total number of bits to be read out, and to the bandwidth required for a particular frame readout duration.

The effective number of scan lines is divided by the vertical sampling loss (or "Kell factor") to find the actual number of scan lines required. A combination of corrective factors, $\frac{KAB}{a_V a_H}$, is used to convert the square of the number of scan lines into total bits (under continuous transmission). For this expression, K is the Kell factor and produces, effectively, the product of vertical bits and horizontal bits;

A is the aspect ratio of the picture, $\frac{\text{H dimension}}{\text{V dimension}}$

B is the resolution ratio, usually 1.0, $\frac{H}{V}$

$a_V$ is the percent of vertical lines (or frame), active

$a_H$ is the percent of horizontal lines (or sweep), active.

---

* from the work of R. M. Scott, "Contrast Rendition as a Design Tool," Photographic Science and Engineering, Vol. 3, No. 5, Sept. - Oct. 1959.

Readout duration is based on two bits per bandwidth cycle, and is set up for slow-scan systems. Frame rate in frames per second is obviously the reciprocal of readout duration in seconds per frame. An example calculation is shown by a three-segment construction line.

## E. OPERATIONAL SEQUENCE OF EVENTS

Table I. 2. E-1 contains a summary of the major events in the mission.

The trajectory is intended to be a near-standard Ranger 66-hour flight sometime near first quarter. At 16 to 20 hours after launch ($T_0$), the trajectory has been determined well enough to permit an economical mid-course, flight-path correction by means of a small, liquid-fueled rocket that is not restartable.

Tracking is continued until approximately two hours before time for the injection maneuver ($T_i$). At this time, the ground control computer calculates the flight path, time and altitude of retrofire, and estimates the final orbit which will be achieved; the computer will also calculate any non-standard injection maneuvers which might be advantageous. These commands are then transmitted; the spacecraft attitude is changed to the retrofire attitude, and a timer is started for the retrofiring initiation. The spacecraft continues to approach until $T_i$, when separation of the payload from Ranger bus proper is initiated, followed by spin-up and retrofire.

The Ranger bus will, in general, continue its trajectory past the moon while the LOC goes into its photographic orbit. Tracking is continued until the LOC orbit is known. Then, the despin sequence is initiated at the most favorable point in orbit for attitude acquisition. A mechanical yo-yo despin device will remove most of the spin; the gas jet attitude system will remove the remainder. Next, the horizon will be searched for and acquired by the active attitude control system, and the LOC will be ready for programming.

TV programming will be carried on as long as the attitude gas supply lasts. This will be a complex operation, similar in many respects to the procedure used for TIROS; locations of new pictures are planned, and the commands and timing requirements for readout and setup are prepared and transmitted to the appropriate ground control station for subsequent relay to the satellite.

At the end of attitude life, or in the event of some critical failure, the back-up experiment will be initiated. On command, the satellite spin axis will be oriented normal to the orbit plane, and satellite spin-up will be initiated by small rockets to a high rotational speed for inertial stability, thus orienting a donut-shaped antenna pattern toward the earth. The earth control stations will then track the satellite to determine its orbit and perturbations to the orbit for a period of months, with the intention of accurately finding the J and L terms of the lunar gravity potential.

RE-ORDER No. 62-489

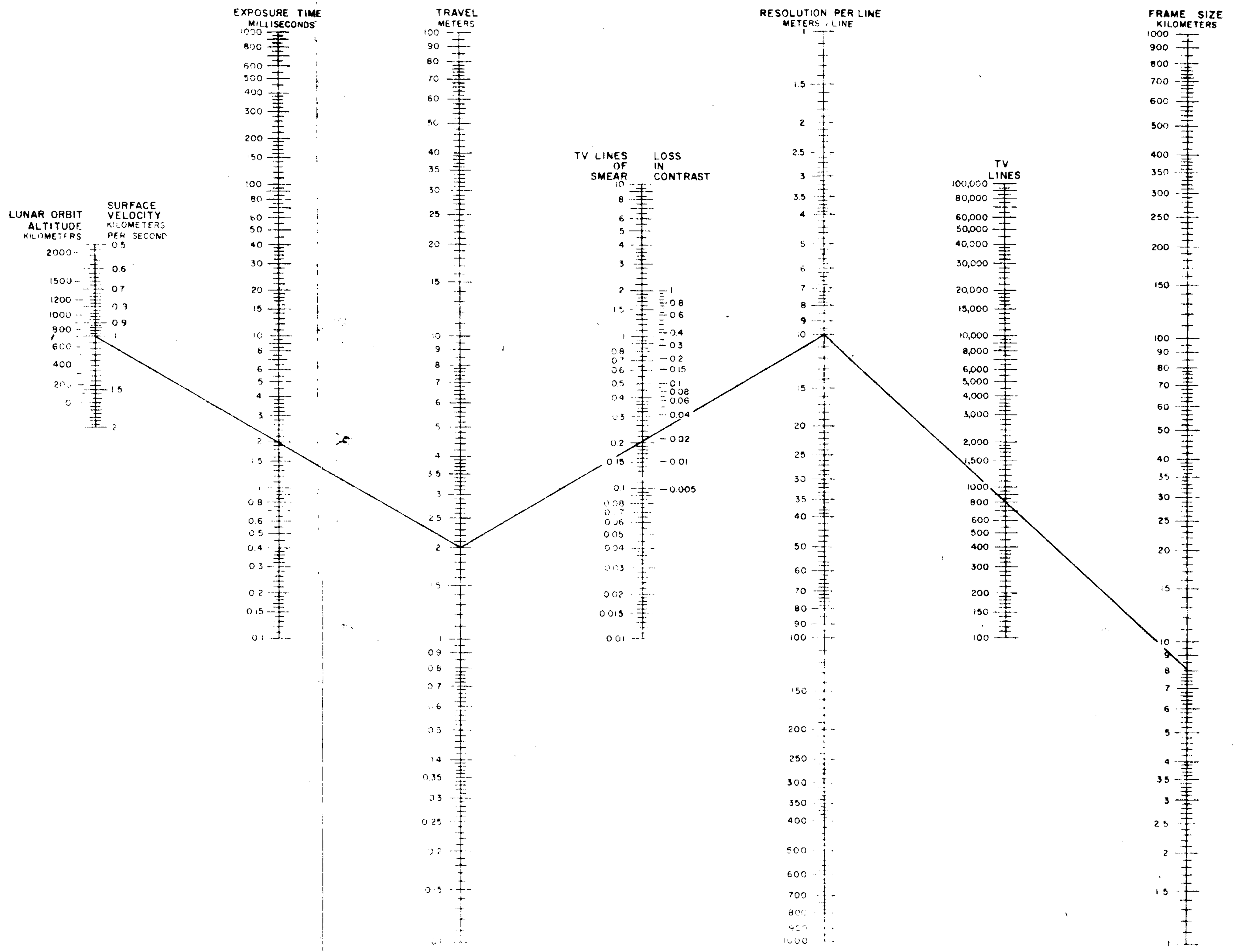

Figure I. 2. D-11. Lunar Orbit Altitude, Resolution and Smear Relations Nomograph

RE-ORDER No. 62-489

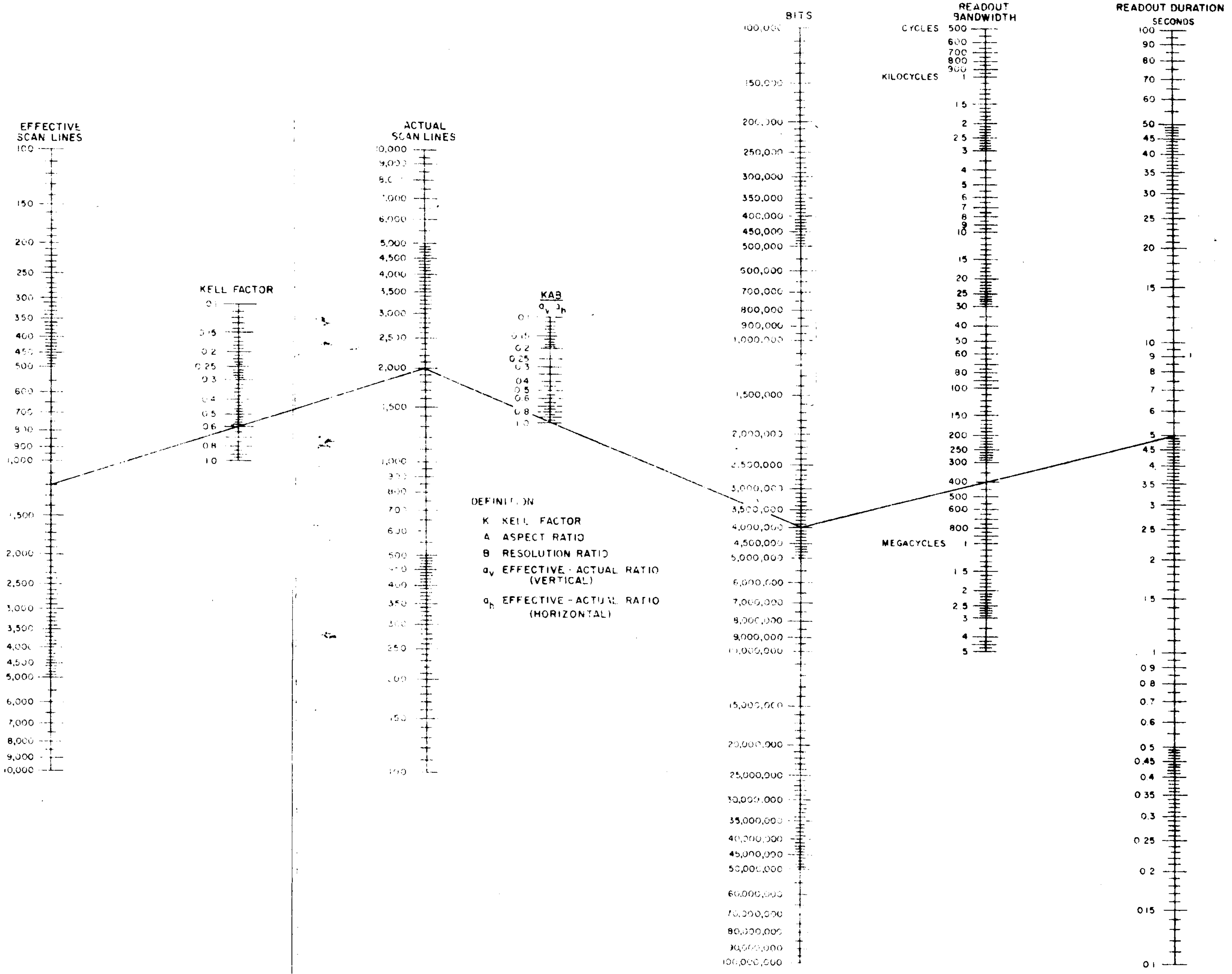

Figure I. 2. D-12. TV Camera Resolution and Readout Time Relations Nomograph

ORDER No. 62-489

## TABLE I. 2. E-1

## OPERATIONAL SEQUENCE OF EVENTS

| Time | Event |
|---|---|
| $T_o$ | Launch |
| until: $T_o$ +16 to 20 hours | Tracking and Orbit Determination |
| $T_o$ +16 to 20 hours | Attitude Change, Mid-course Correction and Re-orientation |
| until: $T_i$ - 2 hours | Tracking and Orbit Determination |
| $T_i$ - 2 hours | Attitude Change for Injection |
| $T_i$ | Injection: Separate; Spin-Up; Retrofire |
| until: $T_i$ +1 to 3 hours | Tracking and Orbit Determination |
| $T_i$ +1 to 3 hours | Lunar Vertical Acquisition: |
| (until acquired) | De-spin; acquire horizon; switch to active attitude control |
| $T_i$ +30 to 40 days (until attitude gas exhausted) | Program for TV: command for TV operation, antenna orientation telemetry; select direct or storage mode of operation. |
| At gas exhaustion | Command orientation of satellite spin axis normal to orbit plane; fire spin-up rockets. |
| To equipment failure (est. 1 year) | Tracking and Orbit Determination (Geodetic Experiment) |

# Section 3
# PRELIMINARY SYSTEM DESIGN ANALYSIS

## A. RETROPROPULSION

The subsystem for injecting the capsule into an orbit about the moon from the transit trajectory consists of a solid-propellant rocket with spin stabilization during firing. Spin-up is accomplished with the Ranger 3, 4 and 5 solid propellant spin gas generation subsystem.

### 1. SOLID PROPELLANT RETROMOTOR

The design configuration recommended for the retropropulsion subsystem (see LOC Preliminary Configuration Report) was a 3000-pound thrust solid-propellant rocket motor with the following design characteristics:

(1) Spherical casing

(2) PBAA/Aluminum/$NH_4CLO_4$ propellant composition with vacuum specific impulse of 280 seconds and density of 0.063 $lbs/in^3$

(3) Conical semi-recessed nozzle

These recommended design characteristics were based upon the following pertinent points:

a. A thrust level of 3000 pounds was selected because:

(1) The motor size is compatible with the capsule dimensional constraints;

(2) Steady state accelerations are approximately the same as experienced during earth launch; and

(3) The resultant burning time is compatible with design technology and operational condition.

b. The propellant specific impulse and density necessitate no development program.

c. A spherical shape was selected over a cylindrical shape because:

(1) The motor is three inches shorter, which is in the right direction when considering boost vehicle moments and capsule structural weight;

(2) Lower motor inert weight results because of an improved structural factor (0.108 vs 0.13), which is in the right direction with payload weight as a critical item; and

(3) The spherical design is a developed item.

d. In consideration of solid rocket design constraints, modification of the Ranger 3, 4 and 5 retromotor would result in cost and schedule very close to that of a new design for the following reasons:

(1) The greater than 20 pounds decrease in propellant weight would require a grain configuration development effort;

(2) Different attachment would require a case development effort; and

(3) Modifications (1) and (2) above are of sufficient scope to necessitate a full flight-proof-test program.

Table I.3.A-1 provides a comparison of two rocket motors for capsules having gross weights of 400 and 500 pounds. The heavier capsule is recommended for the LOC mission.

The rocket motor performance and physical characteristics used for defining the preliminary configuration (Figure I.3.A-1) are listed in Table I.3.A-2. A work statement on the solid-propellant retrorocket (Appendix A) was sent out to obtain data from industry for use in defining the final recommended rocket motor configuration. The companies receiving this request were Thiokol Chemical Corporation (Elkton Division), Hercules Powder Company (Bacchus Division), and Rocketdyne, Wacco Solid Plant. The information requested was cancelled, prior to receipt of data, because of contract cancellation.

## 2. MAJOR INTERFACES

### a. Loads

The rocket motor case will be used to transmit the dynamic and static loads from the capsule to the Ranger Bus.

### b. Arming

The ignition system must be armed prior to capsule separation. Ranger safety rules will necessitate that this event occur after "Agena" first-burn to eliminate the requirement for a destruct subsystem.

### c. Firing Time

The point in time at which the motor is fired must be varied to compensate for the change in motor performance as a function of propellant temperature. This will be accomplished prior to separation of the capsule from the Ranger Bus.

## TABLE I.3.A-1

## COMPARISON OF ROCKET MOTORS FOR CAPSULES HAVING A GROSS WEIGHT OF 400 AND 450 POUNDS

| Pertinent Factor | | 400 Pounds | 450 Pounds |
|---|---|---|---|
| Payload Weight | (pounds) | 232.9 | 261.9 |
| Motor Weight | (pounds) | | |
| Total | | 167.1 | 188.1 |
| Propellant | | 149 | 167.8 |
| Inert | | 18.1 | 20.3 |
| Motor Shape | | sphere | sphere |
| Diameter Motor | (inches) | 17.36 | 18.26 |
| Total Length Motor | (inches) | 27.86 | 28.76 |
| Burning Time | (seconds) | 13.63 | 15.37 |
| Total Impulse | (pound-seconds) | 40,900 | 46,100 |
| Acceleration | (g's) | | |
| Initial | | 7.5 | 6.67 |
| Burnout | | 11.8 | 10.5 |
| Ignition | | less than 40 | less than 40 |
| Rate of On-Set | (g's/second) | 150,000 | 150,000 |

d. Capsule Separation

The capsule must be separated from the Ranger Bus prior to retro firing.

e. Orientation

The capsule must be properly oriented prior to firing of the retromotor.

f. Spin-Up

The capsule must be spinning during retro-firing to maintain thrust misalignment requirements within acceptable limits.

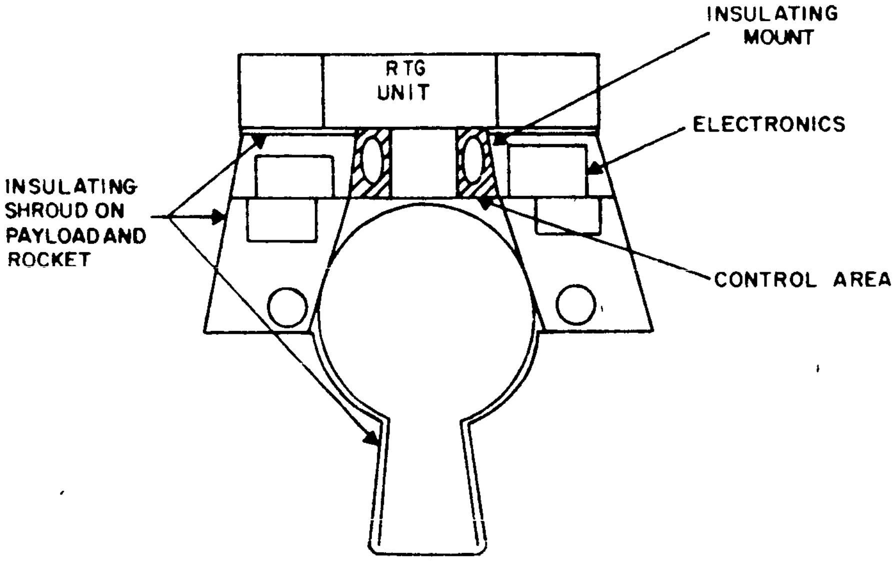

Figure I.3.A-1 LOC Solid Propellant Retromotor, Preliminary Design Configuration

g. Fire

Initiation of firing will necessitate a 28-volt signal.

h. Motor Separation

The motor will be separated from the capsule by the application of a 28-volt signal to the separation device. The separation velocity must be sufficient to prevent collision between the capsule and burnt motor case and will vary according to the installation configuration. Also, separation must be delayed sufficiently to prevent collision as a result of motor outgassing after burnout. Delay time will be from three to six minutes. The maximum motor external temperature will be 400° F at the nozzle and will be developed approximately one minute after burnout.

i. Exhaust Plume

The plume probably will not cause excessive increase in capsule temperature, but may cause solar cell performance degradation because of metallic deposits. This item will necessitate altitude test at AEDC.

j. Temperature Limits

The motor temperature must be maintained between 40° F and 90° F.

## TABLE I.3.A-2

## PERFORMANCE AND PHYSICAL CHARACTERISTICS OF SOLID PROPELLANT RETROMOTOR (FOR 450 POUND CAPSULE AND 1250 MPS VELOCITY CHANGE)

| Pertinent Data | Characteristic |
|---|---|
| Performance: | |
| Thrust | 3000 lbs (average) |
| Burning Time | 15.37 sec |
| Specific Impulse | 280 $\frac{\text{pounds-seconds}}{\text{pounds}}$ |
| Thrust Coefficient | 1.867 |
| Specific Heat Ratio | 1.17 |
| Chamber Pressure | 600 psia (average) |
| Nozzle Expansion Ratio | 24 |
| Nozzle Half-Angle | 16 deg. |
| Acceleration (g's) | |
| Initial | 6.67 |
| Burnout | 10.5 |
| Ignition | less than 40 |
| Rate of on-set (per second) | 150,000 |
| Physical: | |
| Propellant Composition | PBAA (13%)/Aluminum (15%) $NH_4CLO_4$ (71%)/ Additives (1%) |
| Propellant Weight | 167.8 lbs (includes sliver loss) |
| Structural Factor (includes mounting ignitor and sliver) | 0.108 |
| Inert Weight | 20.3 lbs |
| Thrust Trace Characteristics | neutral and stable |
| Sliver (usable) | 2% |
| Thrust Misalignment* | 0.101 inch |
| Volumetric Efficiency | 92% |

*Displacement is measured at the nozzle throat; this is assumed to be sufficient to account for the up-setting moment on the capsule caused by thrust vector displacement and angular misalignment.

## 3. SPIN ROCKETS

Preliminary analysis indicates that Ranger 3, 4 and 5 spin-rocket installations would be sufficient. Thus, this system, which consists of a simple gas generator (0.6-pound propellant) supplying three symmetrically disposed torque nozzles, is recommended. In view of this recommendation, little effort was expended in this area.

## B. ATTITUDE CONTROL SUBSYSTEM

The final report on Phase I of the Lunar Orbiter Capsule Study included descriptions of two alternative stabilization systems — a pure jet, 3-axis control system (identified as System A), and a system comprising a counter-rotating platform mounted on a spinning main body (identified as System B). Only the 3-axis system was considered in any detail during Phase I. However, after discussion with potential vendors, it became apparent that the development time of a horizon scanner for this application would be in excess of 12 months and that the cost would be of the order of 1.2 million dollars. Therefore, an alternative approach, requiring a much simpler sensor, was briefly examined. In the first month of Phase II, this alternative approach (System B) was analyzed further, and the preliminary designs for both systems were evolved in sufficient detail to enable a fair comparison to be made between them. (A discussion of System B is presented in Appendix C). In the second and third months of Phase II, preliminary specifications for the subsystems and components were to have been derived on the basis of the selected design. This final phase of the work was not, of course, completed.

Table III of the LOC Preliminary Configuration Report lists the advantages and disadvantages of both systems (A and B); hence, they will not be repeated here. However, in summary, the advantages of System A are:

1) Very low residual error rates permitting long exposure times for TV.

The advantages of System B are:

1) Fewer development problems (particularly with regard to sensors).

2) Greater weight and power margin.

On the basis of these characteristics, System A was selected and further analysis of the attitude control subsystem for this design commenced. The problem of horizon-scanner development remained. The estimates of time-to-delivery from either of the two most probable manufacturers (Barnes Engineering and A. T. L.)* did not exceed 15 months. However, these estimates were based on the assumption that few, if any, development problems would be encountered. In the opinion of RCA, the proposals contained insufficient evidence of the feasibility of development in the estimated time for the company to embark with confidence on a design incorporating a lunar IR horizon scanner without some "back-up" approach.

For this reason, much of the effort subsequent to publication of the configuration report was devoted to devising a back-up system which would require the least modification of the primary system incorporating a mechanical IR horizon scanner. The alternative method would employ a lit-side horizon sensor only, the drift during darkness being limited by a "strap-down", 3-gyro mechanism. Two single-degree-of-freedom gyros would be required to obtain yaw control in any event (in each case, the vehicle was to have been stabilized with respect to lunar axes) and a third would possibly be required to provide pitch information; thus, it is conceivable that modifications to the logic only would be required to transform from one system to the other. A block diagram of one possible form of an alternate system is shown in Figure I.3.B-1. Both time and funds were insufficient to investigate the characteristics of this system on an analog computer and thereby derive specifications for the components. The gyros required would undoubtedly be of higher grade. However, ordinary spring-restrained rate gyros were unsatisfactory for the primary system (continuous horizon-sensing approach) in any event; thus, inertial-grade* components would be employed in either system. Perkin-Elmer, Inc. completed a preliminary study of a fully passive "lit-side" lunar horizon sensor at RCA's request. The conclusions of this study are summarized later in this section.

---

*Advanced Technology Laboratories

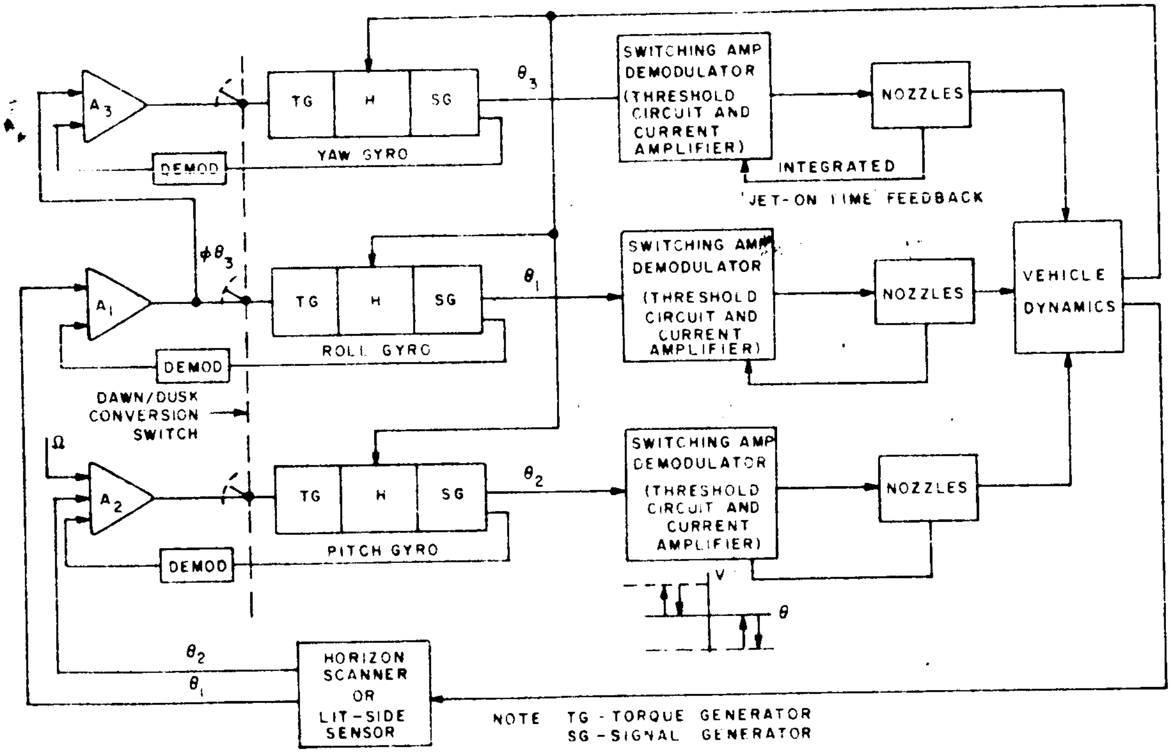
A3
TG
H
SG
YAW GYRO
θ3
DEMOD
SWITCHING AMP DEMODULATOR (THRESHOLD CIRCUIT AND CURRENT AMPLIFIER)
NOZZLES
INTEGRATED
JET-ON TIME FEEDBACK
φθ3
A1
TG
H
SG
ROLL GYRO
θ1
DEMOD
SWITCHING AMP DEMODULATOR (THRESHOLD CIRCUIT AND CURRENT AMPLIFIER)
NOZZLES
VEHICLE DYNAMICS
DAWN/DUSK CONVERSION SWITCH
Ω
A2
TG
H
SG
PITCH GYRO
θ2
DEMOD
SWITCHING AMP DEMODULATOR (THRESHOLD CIRCUIT AND CURRENT AMPLIFIER)
NOZZLES
V
θ
θ2
θ1
HORIZON SCANNER OR LIT-SIDE SENSOR

NOTE TG - TORQUE GENERATOR
SG - SIGNAL GENERATOR

Figure I.3.B-1 Block Diagram of an Alternate Attitude Control Subsystem

## 1. SUBSYSTEM ENGINEERING

The major systems effort during Phase II was devoted to the layout and configuration of System B, the pinned system. However, System A was recommended; hence, the analysis of System B is presented in Appendix C to this report. The mechanical problems involved in the approach of System B were greater than those arising on the jet-stabilized design. These problems have a direct bearing on the performance of the stabilization. It will be sufficient here to recall that factors such as bearing clearances, bearing friction fluctuations, dynamic balance, shift of the principal axis, and inertia distribution directly influence stabilization accuracies. The last two of these factors were considered in some detail, and an analysis of each is included in Appendix C.

---

*High-precision components required for inertial-guidance systems.

a. Pure Jet System

The effort on System A (the jet system) subsequent to issuance of the Phase I final report can be divided in 3 main parts:

(1) Analog simulation of horizon-scanner/gyro-compass system;

(2) Discussions with potential subcontractors and evaluation of their proposals; and

(3) Preliminary investigation of a possible back-up system.

Further analysis of the final phases of the mission (spin-up and erection) was not considered of primary importance at this stage because the techniques are similar to those employed on existing AED satellites and are well understood. The only problem area of significance appeared to be converting the horizon scanner to a horizon pulse generator to act in conjunction with the solar aspect indicator to uniquely determine attitude after spin-up. AED was assured by the manufacturers that conversion could be made automatic and accomplished simply by de-energizing the rotating-mirror drive motor. In any event, if this were not possible, a separate detector could be provided.

The de-spin and acquisition technique recommended originally in the Phase I Final Report was somewhat modified, principally because the attitude control system itself was redesigned around a yaw sensing technique using two single-axis gyros rather than around a gyro compass. (Subsequent discussion with manufacturers showed that the time schedule for development of a gyro compass would be inconsistent with the time schedule of the LOC project.) It was further decided that acquisition should be automatic. Therefore, a knowledge of the final orientation of the vehicle (after de-spin) was not considered to be mandatory (see Section III. 2. g of the Phase I Final Report) and, in particular, it would not be necessary to minimize the spin axis drift during the time between retrofire and acquisition. Two gyros, both of which could be used in a rate mode, would be included in the modified attitude control system; hence, only one more (which might be required in any event) would be needed to close the loop of an active despin system using the attitude control jets. However, as with the gyro-compass system, the benefit of retaining the small residual spin of approximately two degrees per second remains. In this event, as before, the plane normal to the spin axis (which contains what are to become the vehicle yaw and roll axes) can be taken as invariant over one, or possibly two, orbits. Therefore, the line of intersection of this plane and the orbit plane will also be invariant and must at some time coincide with the local vertical. Consequently, a single rotation about the original spin axis would bring the vehicle "yaw" axis into coincidence with the local vertical, assuring acquisition of two references simultaneously. In fact, it was found that no augmentation of components of the jet system would be required for this maneuver (although the loop gains needed adjustment).

The discussion in the Phase I Final Report (Section III 3e) of this and the following phase still applies in other respects.

1) Analysis of Equations of Motion - The equations of motion as defined on Page III-39 of the Phase I Final Report on the Lunar Orbiter Capsule Study were utilized in further analysis of the vehicle motion. The small-angle equations were used in order to simplify the analysis to linearized form. The reference axis, from which the body axis angular displacement is measured, rotates at the instantaneous angular body rate (a constant rate). This is assumed in the calculations for a circular orbit.

The small-angle displacements in roll, pitch, and yaw are given by the complex equation:

$$\ddot{\theta} + (\lambda - 2)\,\omega j\,\dot{\theta} + (\lambda - 1)\,\omega^2\,\theta = L/A$$

$$\ddot{\theta}_2 - L/B$$

where:

$\theta = \theta_1 + j\,\theta_3$

$\theta_1$ = roll angle

$\theta_2$ = pitch angle

$\theta_3$ = yaw angle

$L = L_1 + j\,L_2$

$L_1$ = roll torque

$L_2$ = pitch torque

$L_3$ = yaw torque

$A = C$ = cross axis moment of inertia

$B$ = spin axis moment of inertia

$\Omega = \omega$ = spin axis rotation rate

$\lambda = \dfrac{B}{A}$

The eigenvalues for the roll-yaw coupled set become:

$s = j\,(1 - \lambda)\,\omega,\ j\,\omega$

where $(1-\lambda)\,\omega$ is the vehicle precession rate relative to the rotating coordinate system, and $\omega$ is the vehicle spin rate. In terms of a vehicle stabilized relative to a moon-oriented framework rotating with velocity $\Omega$ about the roll axis:

$$\omega = \Omega .$$

In the Lunar Orbiter Capsule study, the inertia ratio of the vehicle will be very close to unity; hence the factor $(\lambda-1)$ is approximately equal to zero. A further simplification of the coupled equation is possible:

$$\ddot{\theta} + \dot{\theta}\,(\lambda-2)\,j\,\Omega = L$$

or

$$\ddot{\theta}_1 - (\lambda-2)\,\Omega\,\dot{\theta}_3 = {}^{L_1}/_{A} \qquad \text{(Roll channel)}$$

$$\ddot{\theta}_3 + (\lambda-2)\,\Omega\,\dot{\theta}_1 = {}^{L_3}/_{C} \qquad \text{(Yaw channel)}$$

$$\ddot{\theta}_2 = {}^{L_2}/_{B} \qquad \text{(Pitch channel)}$$

The control requirements of the Lunar Orbiting Capsule are essentially divided into two phases; initial acquisition, and stabilization with reference to the lunar local framework. During the stabilization phase of the mission, attitude control is accomplished by torquing jets on each of the principal axes of the vehicle. In turn, these jets are activated by position signals arising in horizon scanner sweeps on the roll and pitch axes and rate information developed from the gyro compass on the yaw axis.

The jets are utilized in On and Off modes, with cut-in and cut-out determined by position and rate data from the scanners. Phase advance in the jet timing system, for purposes of stability, is obtained by adding a rate term to the position signal. Hence, the conditions for cut-in and cut-out become:

$$\text{Jet cut-in} \qquad \theta = \theta_o - \frac{\Delta\theta}{2} - \beta\,\dot{\theta}_{ci} - \epsilon_{ci}$$

$$\text{Jet cut-out} \qquad \theta = \theta_o + \frac{\Delta\theta}{2} - \beta\,\dot{\theta}_{co} - \epsilon_{co}$$

where:

$\theta$ = Position for jet cut-in and cut-out (degrees)

$\Delta\theta$ = Time (position) delay zone, (degrees)

$\theta_o$ = One-half the total dead zone (degrees)

$\beta$ = phase advance constant $\left(\frac{\text{degrees}}{\text{degrees/sec}}\right)$

$\epsilon_{ci}, \epsilon_{co}$ = Additional phase advance terms to be described

Figure I.3.B-2 shows the limit cycle phase plane diagram.

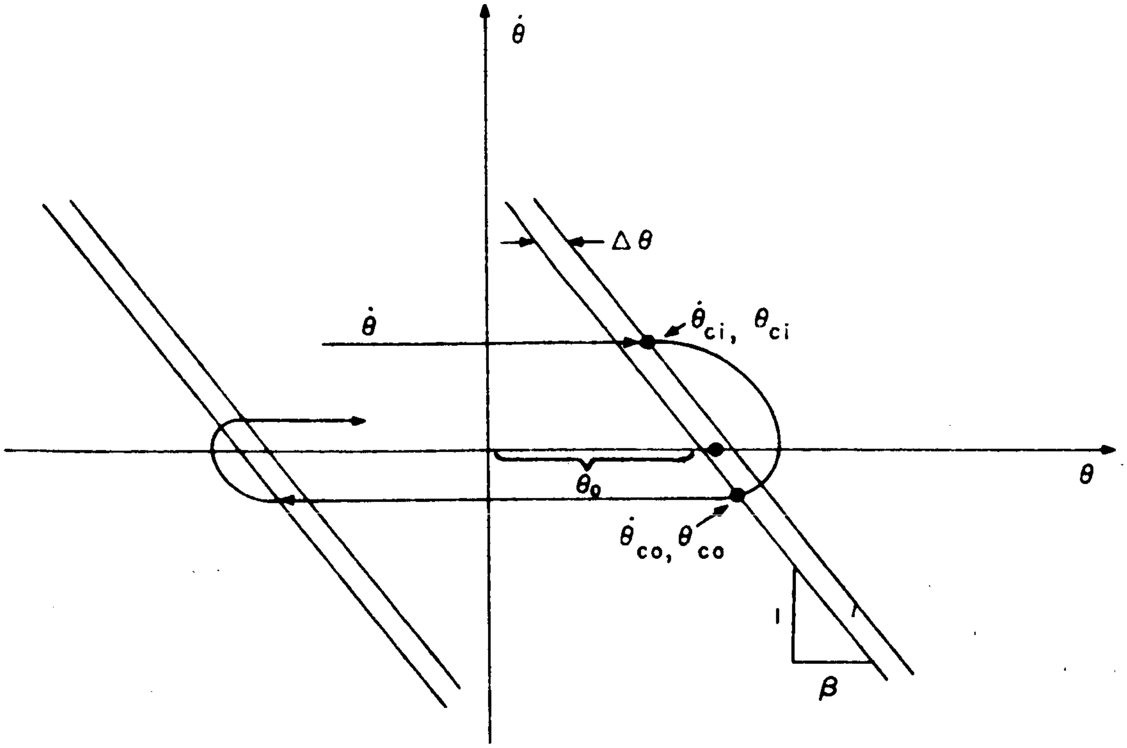
$\dot{\theta}$
$\Delta\theta$
$\dot{\theta}$
$\dot{\theta}_{ci}, \theta_{ci}$
$\theta_0$
$\theta$
$\dot{\theta}_{co}, \theta_{co}$
1
$\beta$

Figure I.3.B-2 Limit Cycle Phase-Plane Diagram

Figure I. 3. B-3 illustrates the programming utilized in the analog computation of vehicle response and gas consumption. The right-hand side of the figure represents the vehicle dynamics in the rate and yaw channels expressed in the linearized equations. The transfer function from input torque to position out is:

$$\text{(Roll)} \qquad \theta_1 = \frac{L_1 + \dot{\theta}_3 \, A \, (\Omega) \, (2-\lambda)}{A \left(s^2 + \lambda - 1\right)}$$

$$\text{(Yaw)} \qquad \theta_3 = \frac{L_3 + \dot{\theta}_1 \, C \, (\Omega) \, (\lambda - 2)}{A \left(s^2 + \lambda - 1\right)}$$

For jet switching and compensation, the left-hand side of the figure illustrates the system proposed initially. In the roll channel, the horizon scanner detects the position error, $\theta_1$. This information, in combination with $\dot{\theta}_1$, is used to form the sum $\theta_1 + \beta \, \dot{\theta}_1$ which is thresholded at $\theta_0$ for triggering the jets. Compensation for the cross-velocity-coupling inherent in the vehicle dynamics is accomplished by the addition of a term proportional to the cross axis velocity, $\dot{\theta}_3$.

2) Analog Computer Programming - The programming of the Analog computer follows essentially the flow diagram of Figure I. 3. B. 4. However, the dynamics of the vehicle were simplified by setting $(\lambda - 1)$ equal to zero.

The analog programming shown in Figure I. 3. B-3 is accomplished in the conventional manner. The phase advance and the switching and torque circuits are delineated. The time delay zone is obtained by the use of amplifiers 2 and 3. Amplifier 2 is voltage-limited until the input voltage exceeds the values imposed by potentiometers 13 and 14.

The dead zone circuitry is similarly constructed. In this latter case, the input voltage must exceed the voltage imposed on potentiometers 49 and 50.

The input driving voltage to the vehicle dynamics is obtained by pulse generation and subsequent clipping to assure a constant amplitude. The series diodes prevent leakage of reverse voltage to the torque input. The torquing circuit is shown in Figure I. 3. B-5. Integrator 16 is the pulse-width counter, and accumulates the total impulse for the runs.

Note that noise input points are specified on the analog program sheet. These are indicated by the symbol $\epsilon$ into Amplifier 1 (in the roll gyro channel), Amplifier 2 (in the horizon sun channel), and Amplifier 33 in the yaw gyro channel. Random noise was injected at these points; the noise having a magnitude approximately 10 percent of the dead zone angle spread and 10 percent of the design limit cycle velocity.

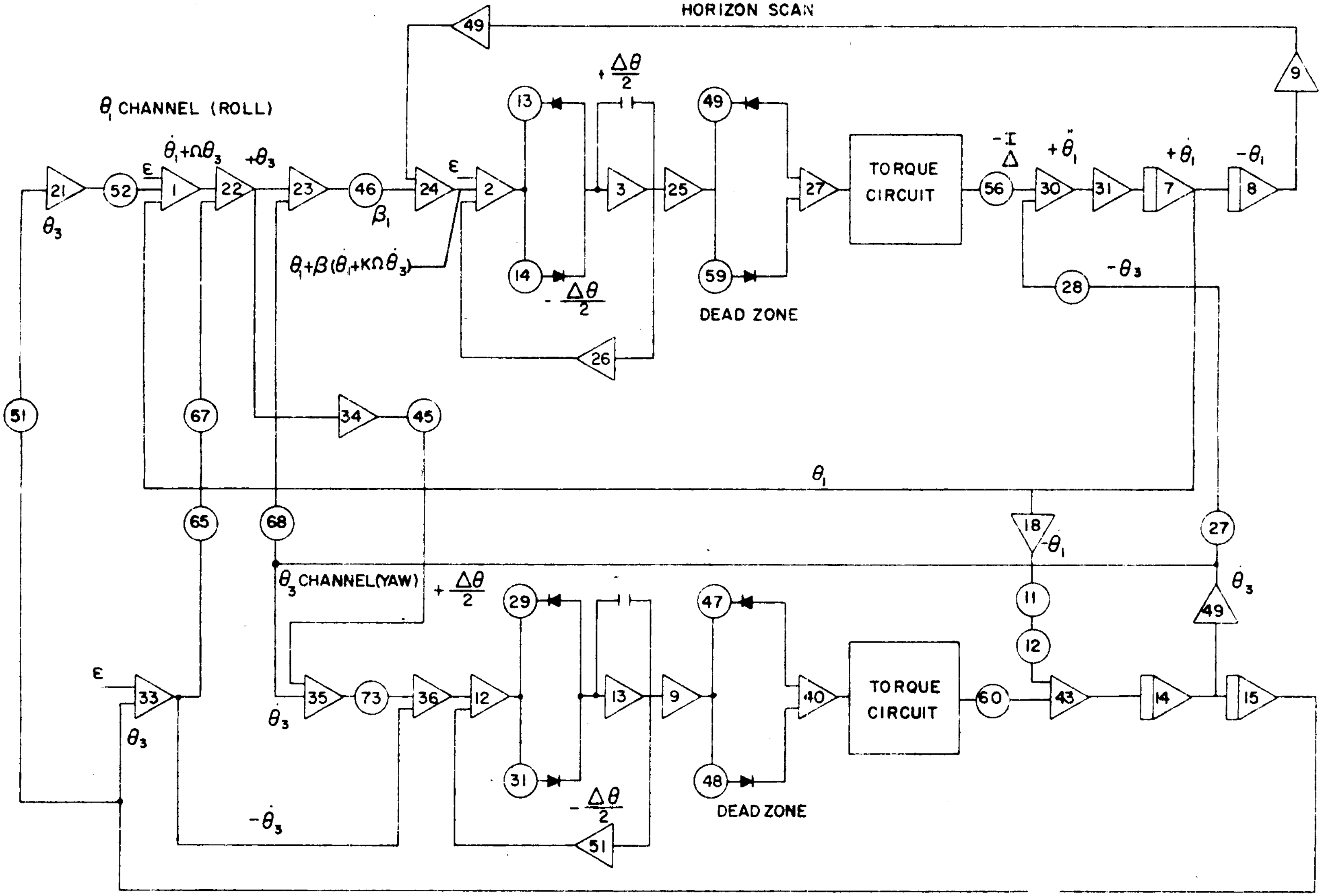
HORIZON SCAN
$\theta_1$ CHANNEL (ROLL)
$\theta_3$ CHANNEL(YAW)
$\dot{\theta}_1+\Omega\theta_3$
$+\dot{\theta}_3$
$\beta_1$
$\epsilon$
$\theta_1+\beta(\dot{\theta}_1+K\Omega\dot{\theta}_3)$
$+\frac{\Delta\theta}{2}$
$-\frac{\Delta\theta}{2}$
DEAD ZONE
TORQUE CIRCUIT
$-\frac{I}{\Delta}$
$+\ddot{\theta}_1$
$+\dot{\theta}_1$
$-\theta_1$
$-\theta_3$
$\theta_1$
$-\theta_1$
$\dot{\theta}_3$
$\theta_3$
$-\dot{\theta}_3$
21
52
1
22
23
46
24
2
13
14
3
25
49
59
27
26
56
30
31
7
8
9
28
51
67
34
45
65
68
18
11
12
33
35
73
36
12
29
31
13
9
47
48
40
51
60
43
14
15
49
27

Figure I. 3. B-3 Analog Program for Roll - Yaw Analysis

RE-ORDER No. 62-489

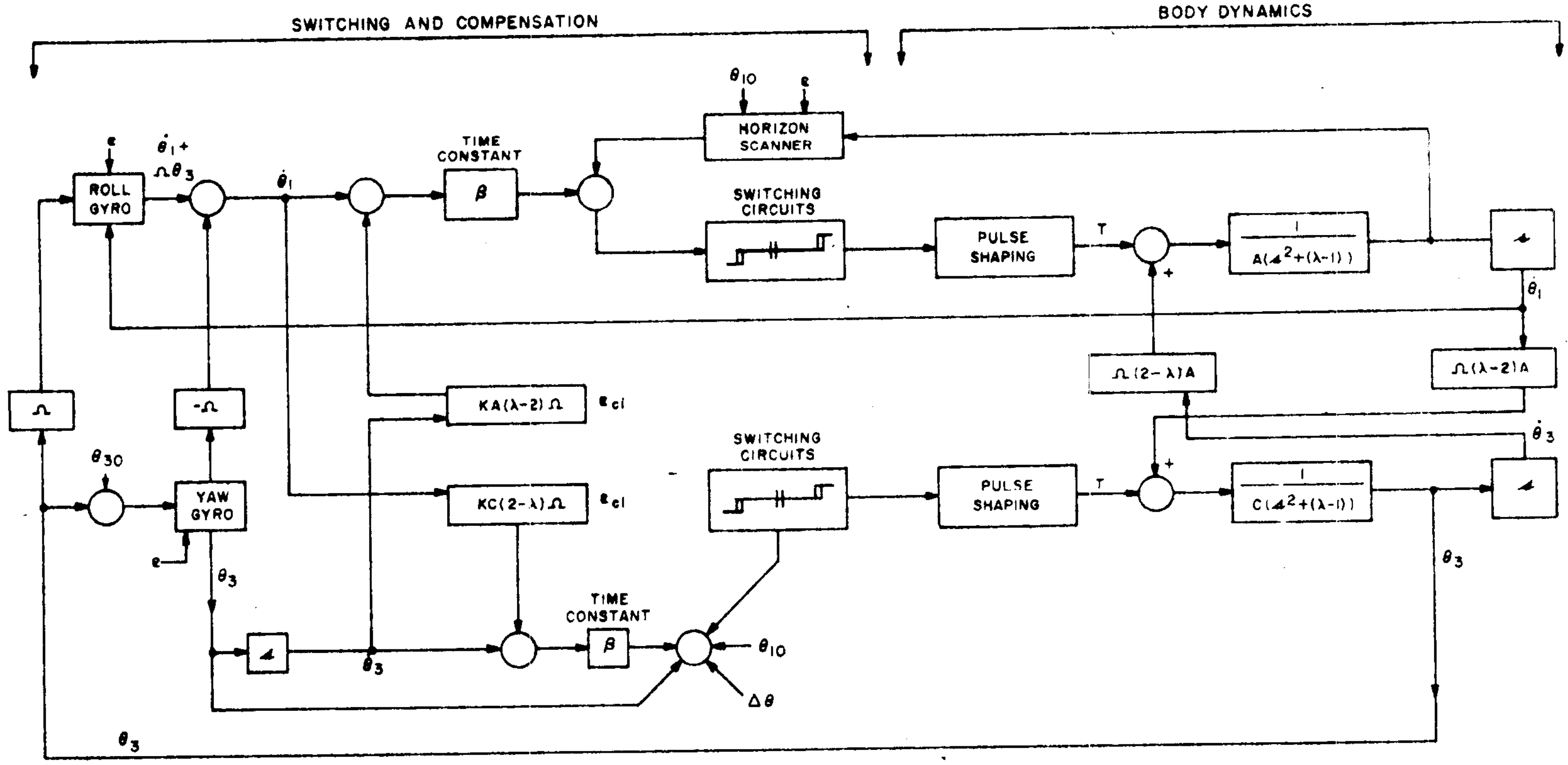
SWITCHING AND COMPENSATION
BODY DYNAMICS
ROLL GYRO
YAW GYRO
$\epsilon$
$\dot{\theta}_1 + \Omega\theta_3$
$\dot{\theta}_1$
$\theta_{10}$
$\theta_{30}$
$\theta_3$
$\dot{\theta}_3$
HORIZON SCANNER
TIME CONSTANT
$\beta$
SWITCHING CIRCUITS
PULSE SHAPING
T
+
$\frac{1}{A(s^2+(\lambda-1))}$
$\frac{1}{C(s^2+(\lambda-1))}$
$\Omega(2-\lambda)A$
$\Omega(\lambda-2)A$
$KA(\lambda-2)\Omega$
$KC(2-\lambda)\Omega$
$\epsilon_{cl}$
$\Omega$
$-\Omega$
$\Delta\theta$

Figure I.3.B-4 Programming for Vehicle Response and Gas Consumption

RE-ORDER No. 62-459

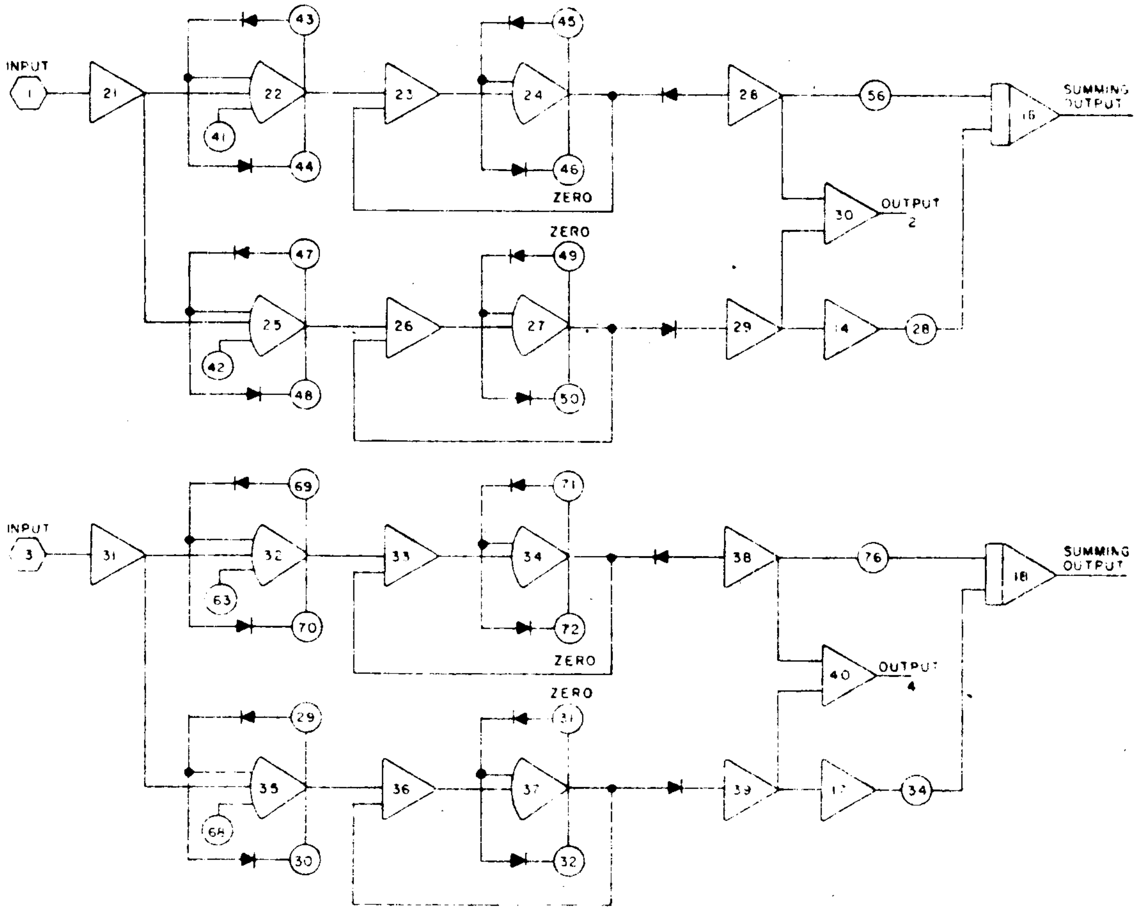
INPUT
1
21
22
41
43
44
23
24
45
46
ZERO
28
56
30
OUTPUT
2
16
SUMMING
OUTPUT
25
42
47
48
26
27
49
50
ZERO
29
14
28
INPUT
3
31
32
63
69
70
33
34
71
72
ZERO
38
76
40
OUTPUT
4
18
SUMMING
OUTPUT
35
64
29
30
36
37
31
32
ZERO
39
17
34

Figure I.3.B-5 Torquing Circuitry Block Diagram

Figure I.3.B-6 shows the schematic of the low-pass filter used to pass noise signals from the random-noise generator into the switching channels. This is essentially a maximally flat Butterworth filter, with a low-pass corner at three cycles per second. The transfer function is:

$$\frac{\theta_{in}}{\theta_{out}} = \frac{\omega^3}{s^3 + 2s^2\omega + 2s\omega^2 + \omega^3} \qquad \text{(Filter Transform)}$$

with one real and two complex poles.

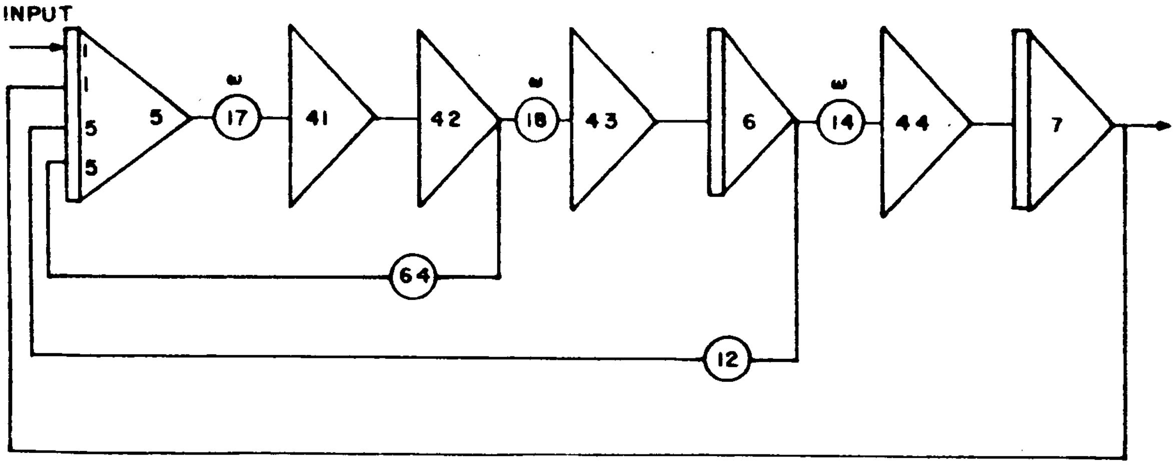

Figure I.3.B-6 Block Diagram of the Low-Pass Filter

Table I.3.B-1 shows the values investigated by this computer program for this study.

3) Conclusions - The analog programming was checked against computed values of velocity decrement in the transient mode. For the case of each individual channel, the analog results paralleled those obtained by the use of the curve shown on Page III-45 of the Phase I final report (Figure III-B-14, Velocity Relations for Limit Cycle Control). Gas consumption, computed by iteration from the analytic data, was confirmed. The addition of the cross-coupling terms changed the patterns only slightly. The straight-line dead zone plots of the single-channel results changed to flat arcs.

### TABLE I. 3. B-1
### VALUES FOR INVESTIGATION BY COMPUTER PROGRAM

| Parameter | Value |
|---|---|
| Moments of Inertia | |
| $B = I_{spin}$ | 6 sl. ft.$^2$ |
| $A=C = I_{cross}$ | 0.95 (6) sl. ft.$^2$ |
| $\Omega$ | one orbit in two hours |
| $\theta_o$ | ± 1°, 1-1/2° |
| $\Delta\theta$ | 0.1° |
| $\beta$ | 10, 5 |
| k | 1, 0.5 |
| Jet thrust | 0.01 lb. |
| Jet moment arm | 1 ft. |
| Limit cycle velocity | 0.01°/sec. |

The addition of 10 percent noise to the input channels increased propellant consumption. However, it is significant that added noise is sometimes effective in returning the dead-zone velocity to practically zero. This is due to the random occasions in which the noise triggers the jet cut-off at the proper time. The vehicle drifts very slowly across the dead zone under these conditions. Such a passage takes typically from 30 to 60 minutes.

Figures for gas consumption with noise added are:

1. Dead zone ± 0.5°

   $\frac{\Delta\theta}{2}$ ± 0.05°

   Noise 10% of $\theta_o$ and of 0.01°/sec. (Both channels)

   $\beta = 5$

Total impulse, 5.45 lb sec./day

$$\frac{\text{Roll channel gas consumption}}{\text{Yaw channel gas consumption}} = \frac{130}{87}$$

II. Dead zone = ± 1°

$$\frac{\Delta\theta}{2} = \pm 0.05°$$

Noise added 10% of $\theta_o$ and 0.01°/sec.

$\beta = 5$

Impulse required, 3.29 lb sec./day (Both channels)

$$\frac{\text{Roll channel gas consumption}}{\text{Yaw channel gas consumption}} = \frac{4}{3}$$

III. Dead zone = ± 0.5°

$$\frac{\Delta\theta}{2} = \pm 0.05°$$

Noise added = Zero

$\beta = 5$

Impulse required, 3.12 lb-sec./day (Both channels)

$$\frac{\text{Roll channel gas consumption}}{\text{Yaw channel gas consumption}} = \frac{51}{50}$$

b. Horizon Scanner Back-up System

Before embarking on a discussion of the approach proposed in the event of serious problems being encountered in horizon scanner development, a description will be given here of the first two-single-axis gyro system conceived as an alternative to the gyrocompass. This system was not presented in either of the earlier reports because at that time, the availability of a two-axis gyrocompass within the time period of this project was anticipated. Both time and funds were insufficient to complete a computer study of this technique; however, earlier work at AED had established feasibility. The disadvantage of the method lies in the fact that coupling is introduced through the sensors, adding to the effect of that already existing because of the shape of the vehicle itself (unequal inertias). Therefore, it is to be expected that propellant consumption using this system would be higher than that for the gyro-compass system.

A clear idea of the method can be obtained from the block diagram for the roll and yaw channels (see Figure I.3.B-7). The gyros are used solely in the rate mode.

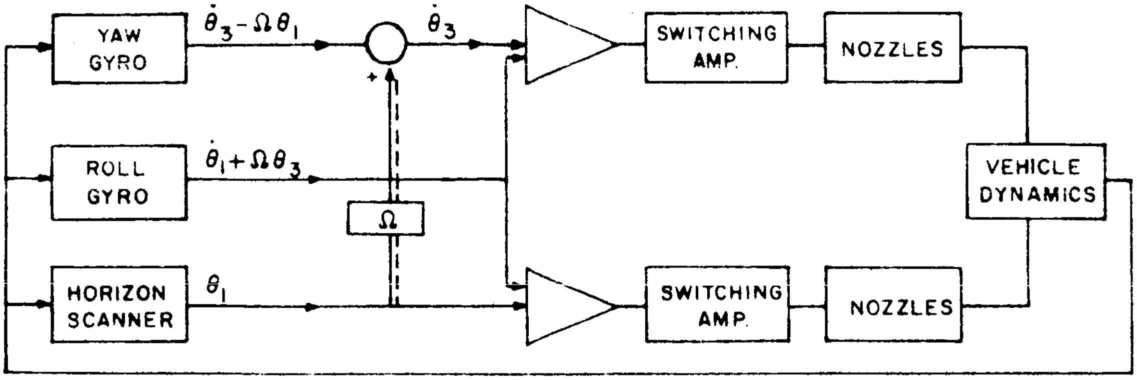
YAW GYRO
ROLL GYRO
HORIZON SCANNER
$\dot{\theta}_3 - \Omega\theta_1$
$\dot{\theta}_1 + \Omega\theta_3$
$\theta_1$
$\dot{\theta}_3$
+
$\Omega$
SWITCHING AMP.
SWITCHING AMP.
NOZZLES
NOZZLES
VEHICLE DYNAMICS

Figure I. 3. B-7 Block Diagram of the Roll and Yaw Channel of the Horizon Scanner Back-up System

The notation is the same as that used in the Phase I Final Report: $\theta_1$, $\theta_3$ are small angular displacements from moon-centered roll and yaw axes and $\Omega$ is the orbital angular frequency. Also for the vehicle's principal moments of inertia (A, B, C) in roll, pitch and yaw, the roll and yaw equations of motion (as given previously) are, for small values of $\theta_1$ and $\theta_3$:

$$A\ddot{\theta}_1 + (A + C - B)\Omega\dot{\theta}_3 + 4(B - C)\Omega^2\theta_1 = L_1$$

$$C\ddot{\theta}_3 - (A + C - B)\Omega\dot{\theta}_1 + (B - A)\Omega^2\theta_3 = L_3$$

Neglecting the small restoring torque arising from the last terms on the right-hand sides of these equations, the control torques $L_i$ must contain terms proportional to $\theta_i$ and $\dot{\theta}_i$. The outputs from the three sensors are:

| | | |
|---|---|---|
| Horizon Scanner | — | $\theta_1$ |
| Roll gyro | — | $\dot{\theta}_1 + \Omega\theta_3 = \omega_1$ (day) |
| Yaw gyro | — | $\dot{\theta}_3 - \Omega\theta_1 = \omega_3$ (day) |

Thus, $L_1$ will contain the required terms if it is of the form

$$L_1 = a_1\theta_1 + b_1\omega_1$$

where $a_1$ and $b_1$ are constants, and, similarly, if:

$$L_3 = a_3 \omega_1 + b_3 \omega_3$$

the required yaw angle and its derivative will be included. Algebraically:

$$L_1 = \left(a_1 \theta_1 + b_1 \dot{\theta}_1\right) + \left(b_1 \Omega \theta_3\right)$$

$$L_3 = \left(a_3 \Omega \theta_3 + b_3 \dot{\theta}_3\right) + \left(a_3 \dot{\theta}_1 - b_3 \Omega \theta_1\right)$$

The second term in each of these expressions contains the additional coupling terms referenced above and, in fact, the motion is unstable because of their presence. However, it has been shown that stability is achieved if the term containing $\dot{\theta}_1$ in $L_3$ is removed. This is readily accomplished by introducing the cross-feedback loop shown dotted in Figure I. 3. B-7.

When System A was finally selected for detailed study and the pinned system discarded, it became necessary (in the opinion of AED) to develop a further alternative for use if scanner development should fall behind schedule. The system selected was one incorporating the "lit" side mentioned earlier. In this case it would be necessary for the alternative to be identical, in nearly all respects, to the primary system (with the exception of the horizon sensor itself) so that minimum modification would be required in the event of a reappraisal. The rate gyro approach is certainly adaptable if a gyro is included in the pitch loop in addition to those in roll and yaw. It has one disadvantage however, in that the horizon scanner output tends to be noisy. This problem can, to an extent, be overcome by "integrated jet-on time" feedback (see the Phase I Final Report); however, the gyros are required in any case as an inertial reference during darkness (in the back-up system), and may as well be utilized during horizon-scanner operation as signal filters. The gyros were used in this way in the system ultimately selected for detailed study. The system devised is shown in Figure I. 3. B-1. A torque generator feedback loop is shown around each unit; however, in this system, the gyros are used in an integrating rate and not a rate mode as before. Thus, the output of the signal generator is compared with the horizon error signal from the scanner to continuously update the gyro. Noise on the scanner input can be removed if the gain in the forward loop is not too high. Conversion to night-time operation can be accomplished by simple switching as shown.

During daylight, when the scanner is operating, all three gyros are continuously updated; hence, the tolerable drift rate is simply a function of the duration of inertial stabilization (zero for the primary system and not more than one hour for the back-up system). Consequently, a drift rate of one degree per hour would be satisfactory; this rate is well within the tolerance of any existing inertial-grade gyro. A more stringent requirement is placed on the pitch gyro (in the back-up system) because of the need to compensate for the orbital angular velocity (approximately 180 degrees per hour). A specified drift of one degree per hour would require torque generator linearity of 0.5 percent, a value which is marginal. A larger drift (e.g., two to three degrees per hour) may have to be tolerated; however, this will not seriously affect propellant consumption.

The switching time reference can be taken from the master clock, the sun, or from the 'lit-side' sensor itself. Perkin-Elmer took the latter condition as a requirement in their study of the sensor and indicated that it was quite feasible.

Unlike the first system described, the arrangement permits minimizing the cross-talk in the sensors although such cross-talk cannot be completely eliminated. Consequently, it was anticipated that the propellant requirements computed for the original gyro-compass system would apply approximately in this case. However, no firm conclusions could be drawn without recourse to a simulation similar to that carried out in the former case, and it is regretted that this work was not completed before termination of the contract.

Inter-axis coupling and noise can be minimized by proper selection of the summing amplifier and torque generator gains. For the case of the roll gyro, assume the summing amplifier gain to be A volts/volt, the torque generator gain to be G rads/sec./volt (e.g., assume that the reaction to the torque is purely viscous), $\zeta$ to be the noise on the H. R. signal, $\delta$ to be the drift of the gyro, and $\dot{\theta}_T$ to be the rate of float rotation due to the torque generator. Then.

$$A\left(\theta_1 + \zeta - \theta_o\right) = \theta_\epsilon$$

$$\dot{\theta}_T = G\,\theta_\epsilon$$

$$\theta_T + \theta_1 + \int \Omega\,\theta_3 + \delta = \theta_o$$

(note that $\dot{\theta}_1 + \Omega\,\theta_3$ is the roll component of angular velocity.)

Eliminating $\theta_T$ from these relations yields:

$$\theta_o = \theta_1 + \frac{\Omega\,\theta_3 + S\,\delta + G\,A\,\zeta}{S + GA}$$

$$\theta_\epsilon = A\,\zeta - A\,\frac{\left(\Omega\,\theta_3 + S\,\delta + GA\,\zeta\right)}{S + GA}$$

where S denotes $\frac{d}{dt}$. Note that drift rate and not drift appears in these expressions. Consequently, the error resulting from drift will be negligible. Also, the frequency $\zeta$ will be large compared with the frequency $\dot{\theta}_1$; thus, the noise in the roll channel will be suppressed by the gyro. Further, in the first equation, the coupling term can be minimized by increasing the product GA. However, if this product is very large ($\theta_o \rightarrow \theta + \zeta$), the advantage of using the gyro as a filter is lost. Therefore, some optimum value of the gain product exists.

It can be seen from the second equation that the output of the summing amplifier gives a measure of the yaw error, $\theta_3$. In the steady state:

$$\theta_o = \theta_1 + \frac{\Omega \theta_3}{GA}$$

$$\theta_\epsilon = A \left[ \zeta - \frac{\Omega \theta_3}{GA} \right] \qquad \text{(A large)}$$

The problem with a simple system, consisting of only one gyro, should be clear from these relations. Describing the coupling in the first of the equations as "noise" it can be seen that varying the quotient $\frac{\Omega}{GA}$ merely improves the signal-to-noise ratio in one channel at the expense of the other. Therefore, it is necessary to introduce a second (yaw) filter to smooth the signal $\theta_\epsilon$; a second gyro is proposed for this purpose. This course is feasible because $\zeta$ is much greater than $\theta_1$. As an example, if $\theta_1$ and $\theta_3$ are in degrees, the quotient $\frac{\Omega}{GA}$ is dimensionless (where $\Omega$ is in radians per second, G is in seconds, and A is dimensionless).

If 10 percent coupling can be tolerated in the roll channel, then

$$\frac{\Omega}{GA} \leq \frac{1}{10}$$

$\left[\theta_1 \text{ and } \theta_3 \text{ are, to all intents and purposes D-C.}\right]$

$$\Omega = 0.82 \times 10^{-3}$$

$$\therefore \quad GA >> 3.3 \times 10^{-3}$$

Also:

$$\theta_\epsilon = A \left( \zeta - \frac{\theta_3}{10} \right)$$

Thus, yaw resolution is critically affected by roll noise in the horizon scanner and a larger dead-zone would undoubtedly have to be tolerated in this channel. Although such a characteristic leaves much to be desired, yaw accuracy is not as critical as roll or pitch. Without analog simulation, it would be premature to report that this system is better than the rate gyro system. However, at the termination of study, it was considered that one of these two approaches would be adopted for the LOC.

62-489

## 2. HORIZON SENSORS

The major developers and manufacturers of optical sensors were invited to submit proposals for a sensor capable of providing two-axis error information using selenographic coordinates for vehicle attitude control (in the pitch and roll axes). Three major companies submitted proposals that described reliable methods of detecting the local vertical from a lunar oriented, 3-axis-stabilized vehicle, in a lunar orbit at an altitude of 200 ± 50 km. Two of the proposed methods use horizon-splitting techniques to derive two-axis information, while the third method utilizes a horizon tracking method that will be employed in the Gemini satellite. Barnes Engineering suggested an electro-mechanical infrared scanner, sensitive in the long-wavelength spectrum, which employs two space-tested motors, bolometers, and specially designed mirrors to scan and detect the lunar horizon at two points per axis. This proposed device was studied and was found to be sound in principle. It would be satisfactory for the LOC mission if the weight and power consumption could be reduced to an acceptable level. The developers indicated that it was possible to reduce the weight to 8 pounds and the power requirement to 10 watts with little sacrifice in reliability and operational life. This IR scanner is described in greater detail later in this section.

A second horizon-splitting technique was proposed by the Perkin-Elmer Corporation utilizing a simplified mosaic sensor arrangement which requires no moving parts and very simple logic. This method was based on a sensor arrangement designed at RCA for the purpose of eliminating mechanical parts and reducing power and weight. This proposed sensor would operate with a high degree of reliability in the visible spectrum, and would be used for continuous control on the sunlit portion of the moon with an accuracy of ± 0.5 degree of arc.

The horizon-tracking scheme developed for the Gemini mission by Advanced Technology Laboratory was also proposed for the lunar orbiting satellite. Using a long-wavelength infrared detector, the sensor is oscillated through ± 2 degrees while tracking the horizon of the object disk, when the vehicle yaw axis coincides with the local vertical. The oscillations provide spacial filtration and tend to minimize the effect of bodies protruding from the object disk. When properly oriented, this sensor would provide linearly proportional error signals with an accuracy greater than 1 degree over a large variation of subtended angles.

All three of the proposed methods have merits that would be beneficial in the successful operation of a lunar photographic mission. In the investigations of sensors applicable for this mission, the following evaluation chart was used to derive a figure of merit for each of the three sensors (the numbers represent the order of preference).

| | Barnes | Perkin-Elmer | ATL |
|---|---|---|---|
| Reliability | 2 | 1 | 2 |
| Development Problems | 3 | 1 | 2 |
| Power and Weight | 3 | 1 | 2 |

RE-ORDER No. 62-489

| | Barnes | Perkin-Elmer | ATL |
|---|---|---|---|
| Flexibility | 1 | 2 | 1 |
| Lifetime | 1 | 1 | 1 |
| Cost | 3 | 1 | 2 |
| Accuracy | 1 | 1 | 1 |

In nearly all categories, the Perkin-Elmer sensor design has advantages for application in this mission. Although the initial intent was to consider a contractual agreement with either Barnes Engineering or ATL, the late entry submitted by Perkin-Elmer would have been considered as a primary sensor having a high probability of success in this lunar photographic mission. However, there was a suggestion that this project should carry a program for the development of a general-purpose lunar-horizon sensor. For this reason, the system incorporating this visible detector was proposed, at termination of contract, as a back-up approach.

a. Perkin-Elmer Corporation Mosaic Sensor

A simplified lunar horizon sensor is proposed involving no moving parts and an unusually simple logic. The sensor is designed to provide attitude information with an accuracy of ± 0.5 degree for lunar reconnaissance at a distance of 250 ± 50 km. Even greater accuracy is obtainable with some increase in system complexity.

The vehicle's inertial platform is used in conjunction with a "gyro updating" concept to take advantage of the high signal-to-noise ratio provided by the sunlit lunar horizon. Thus, sensor-derived attitude control is used when orbiting the sunlit side and gyro information when orbiting the dark side of the moon.

A simple three-valued digital logic is used in conjunction with 40 mosaic photoconductor elements to provide the required output error signal. A Dawn-Terminator Sensor and a solid-state counter provide a delayed command signal to start and stop operation so that accuracy will not be degraded in either terminator region.

The use of a unique type of parallel logic and a pair comparison technique provides insurance against catastrophic failures. Failure of any one mosaic sensor element or any logic circuit component will produce a maximum error of 1 bit or 0.375 degree in one axis. Additional random failures will tend to cancel out rather than increase the error. This, combined with the completely passive sensor operation, leads to maximum reliability of the device.

The proposed optical inertial attitude system employs highly reliable devices within the existing state of the art to provide local vertical without the need for far-infrared sensing or a complex computer logic. The Mosaic Lunar Attitude Sensor consumes only 2 to 3 watts of d-c power and weighs less than 2.5 pounds.

Attitude information with respect to local vertical is required of an artificial moon satellite operating at an altitude 250 ± 50 km from the lunar surface. The satellite orbit is inclined 30 degrees with respect to the moon's ecliptic. The space-vehicle subsystem must provide an analog signal to correct pitch and roll error with respect to local vertical. A sensor tolerance of ± 0.5 degree in pitch and roll is specified. The lunar horizon subtends a half-angle of 58°30' to 63°40' for this geometry (see Figures I.3.B-8 and I.3.B-9). The suggested mission requirements would be to photograph or televise the lunar surface; hence, attitude orientation of the camera with respect to the moon is required primarily during the daylight portion of the orbit. The mission characteristics provide for a minimum operational period of 30 days. All areas of the moon will be sunlit at some time during this interval.

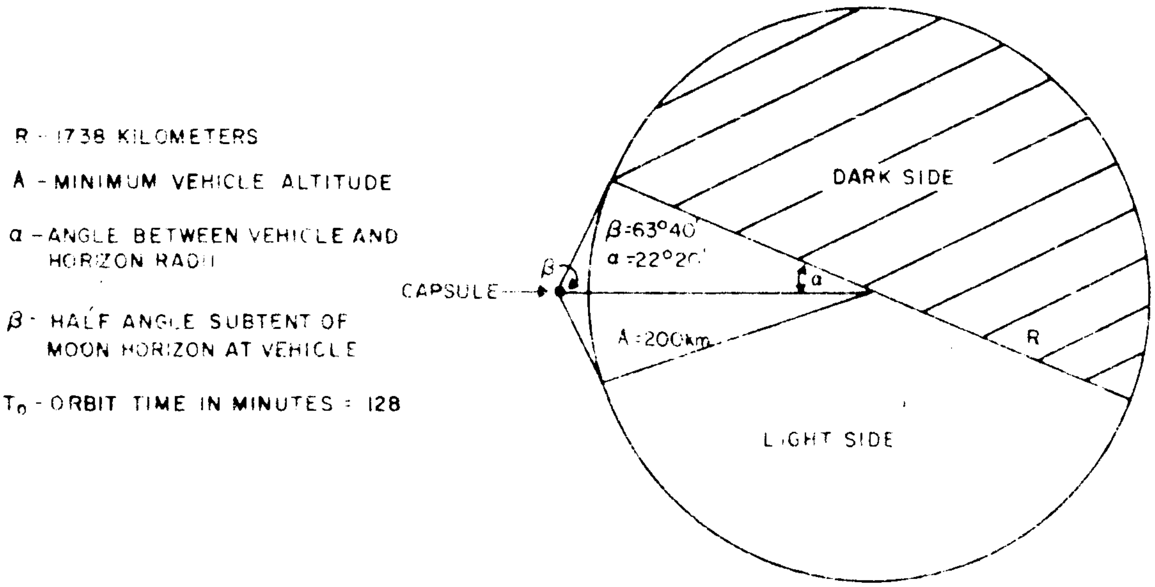
R - 1738 KILOMETERS
A - MINIMUM VEHICLE ALTITUDE
α - ANGLE BETWEEN VEHICLE AND HORIZON RADII
β - HALF ANGLE SUBTENT OF MOON HORIZON AT VEHICLE
$T_0$ - ORBIT TIME IN MINUTES = 128
DARK SIDE
β = 63°40'
α = 22°20'
β
α
CAPSULE
A = 200 km
R
LIGHT SIDE

Figure I.3.B-8 Vehicle-Moon Relationship at Minimum Altitude

Attitude orientation while orbiting over the dark side of the moon is only incidentally required, in order to facilitate the attitude re-acquisition phase on returning to the sunlit side of the moon and to stabilize the transmitting antenna.

The dawn and dusk terminator regions will be covered in a period of time equal to $\left(\frac{2 \times 10.1}{\cos 30°}\right)$ minutes when the orbit is inclined to the equator by 30 degrees. Thus, a total time of 23.1 minutes must be deleted from the maximum daylight operating region.

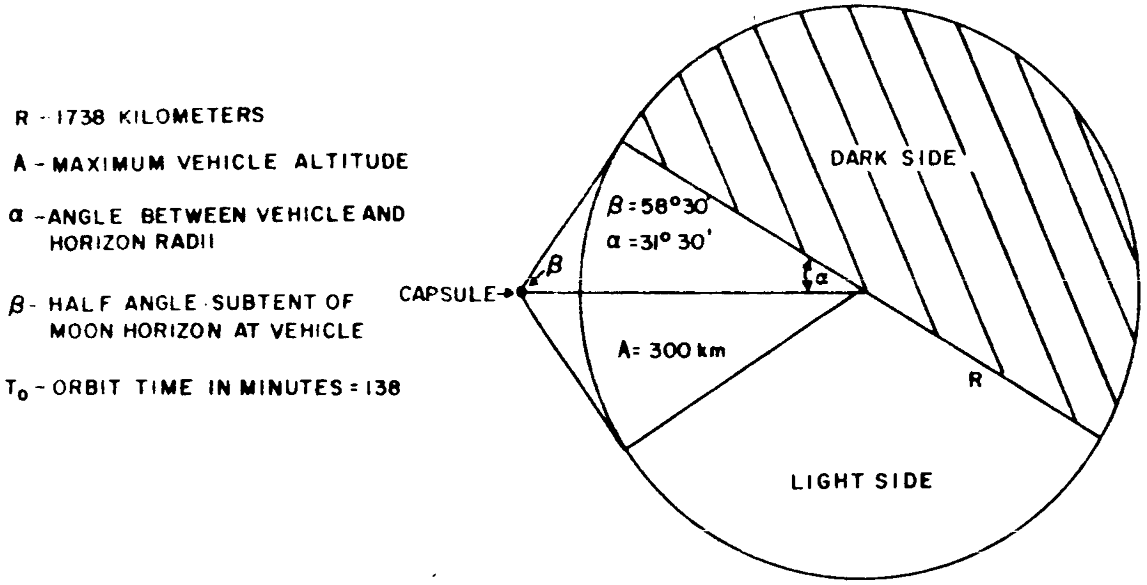
R - 1738 KILOMETERS
A - MAXIMUM VEHICLE ALTITUDE
α - ANGLE BETWEEN VEHICLE AND HORIZON RADII
β - HALF ANGLE SUBTENT OF MOON HORIZON AT VEHICLE
$T_0$ - ORBIT TIME IN MINUTES = 138
DARK SIDE
β = 58° 30'
α = 31° 30'
β
α
CAPSULE
A = 300 km
R
LIGHT SIDE

Figure I. 3. B-9 Vehicle-Moon Relationship at Maximum Altitude

The dark side of the moon reaches a low temperature of 120° K. Its thermal radiation is supplemented by earthlight during a portion of the month. Earthlight provides an illumination of up to $1.8 \times 10^{-3}$ lumens per square cm. As for the moon's own radiation, 120° K corresponds to a spectral response in the far infrared region (24 to 30 microns).

The bright side of the moon has a brightness of 13,700 to 14,700 foot-candles at normal incidence and has a mean albedo of 0.073. Its minimum albedo is 0.02; its maximum 0.3.

A visible-light sensor presents a simple method of obtaining the local vertical on the sunlit side of the moon, where it is needed. The inertial platform is utilized to maintain coarse attitude after dusk, thus minimizing re-acquisition correction after each "dawn".

It is proposed to use a photoconductor mosaic composed of four mosaic strips, each subtending a narrow field in one of four quadrants (see Figure I. 3. B-10). Each mosaic strip is composed of ten photoconductive elements, and each element is connected with the corresponding element in the matrix in the opposite quadrant. The output voltage from any element pair is zero if the elements are both illuminated or both dark. If only one element is "on", an output voltage will be developed, the polarity being dependent on which of the two quadrants is illuminated. In this manner, all of the useful information is derived from the lunar horizon.

The logic circuitry is used to determine the output voltage of every element pair in each axis. By summing the output voltage in each axis, an analog voltage proportional to attitude error is developed for both pitch and roll.

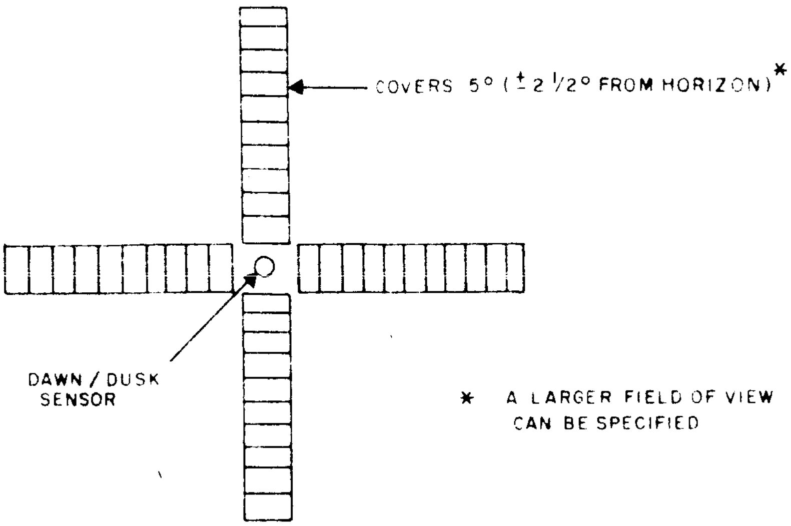
COVERS 5° (± 2 1/2° FROM HORIZON)*
DAWN / DUSK SENSOR
* A LARGER FIELD OF VIEW CAN BE SPECIFIED

Figure 1.3.B-10 Mosaic Arrangement of Visible-Light Sensor

A null condition will result when there are an equal number of "on" elements on two opposing sides of the mosaic detector in the pitch and roll axes respectively. This null condition is equivalent to local vertical orientation in each axis.

An 0.75-degree field per mosaic element, with a 40-mm focal length, provides a cell element size of approximately 0.5 mm (0.020 inch) which is considered entirely feasible by the photoconductor manufacturer. A dichroic filter can be added to each lens to provide heat rejection when accidentally looking at the sun.

A mosaic detector array to view the sunlit side of the moon can be built using photoconductor elements. Photoconductors include both photoresistors and phototransistors. At the present time, the reliability of phototransistors is less well established and the minimum state-of-the-art cell size is greater. Therefore, RCA would plan to use photoresistors, hereafter referred to as photoconductors. Cadmium selenides and cadmium sulfides, with peak sensitivities of 6900 and 5500 angstroms respectively, are elements of proven reliability. Cadmium sulfide has a slightly longer time constant (53 msec) than cadmium selenide but is less temperature-sensitive and has a higher on-off ratio. The reliability of cadmium sulfides has been thoroughly investigated by the Jet Propulsion Laboratory and others. CdS photoconductors have been successfully used on the Ranger and Mariner spacecraft as part of a sun sensor.

As indicated earlier, light levels on the sunlit side of the moon vary from fifteen to several thousand foot-candles. For an f/2 lens, this light level range will provide a cell illumination of from one to several hundred foot-candles, giving an "on" state of from 1000 to 20,000 ohms. An "off" state will be greater than 500,000 ohms.

This on-off ratio of 25 to 1 greatly exceeds the minimum signal-to-noise requirements and obviates the need for sophisticated data processing.

A separate element looking straight down will serve as the "dawn" sensor. Light on this sensor will turn on a solid-state counter which, in turn, will transfer attitude command from the gyro to the sensor control 15 minutes after dawn and switch back to gyro control 38 minutes later. This program will eliminate sensor attitude errors caused by partially illuminated fields of view even under the worst conditions of altitude, orbit inclination, and albedo.

A more elaborate control system could be used to give partial capability in twilight and dawn areas; however, the complexity involved does not appear justified.

Sensing element reliability is increased by the unique parallel logic used. Failure of any individual element pair will not affect the operation of the other element pairs. Redundancy has been used within each mosaic to further increase reliability.

b. Barnes Engineering Horizon Scanner

The optical arrangement of each of two heads comprises a collector mirror, a "paddle-wheel" scanning mirror, filters, and thermistor IR detectors. Each of two heads provides signals indicative of vehicle attitude relative to the lunar local vertical about one axis. The scanning mirror is arranged such that it scans the IR detector's instantaneous field of view from an angle of 105° above the vehicle yaw axis to an angle of 45° above the yaw axis in two scan sectors situated 180° opposite in space, generating two live-scan "fans" ($0 - A_1 - A_2$ and $0 - B_1 - B_2$) in space (see Figure 1.3.B-11). The "A" and "B" fans are generated in time sequence.

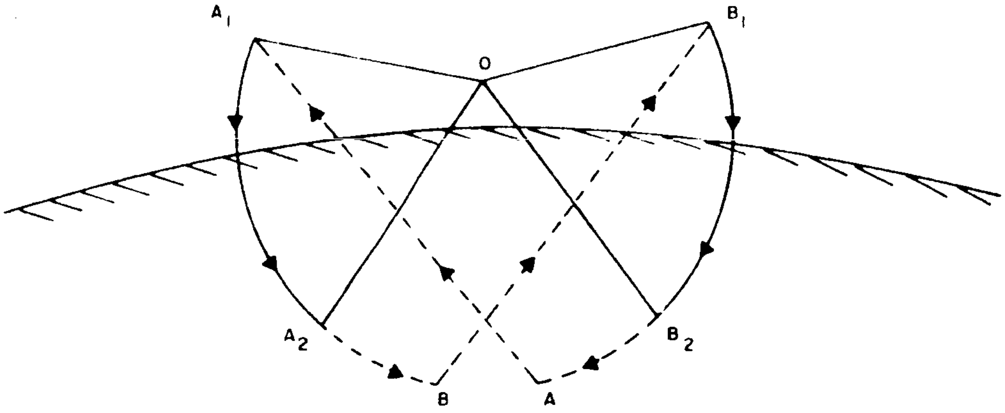

$O-A_1 - A_2$ AND $O\ B_1-B_2$ ARE ACTIVE SCAN PATHS

$A_2-B-B_1$ AND $B_2-A-A_1$ ARE ELECTRONICALLY BLANKED

Figure 1.3.B-11 Geometry of Barnes Engineering Horizon Scanner

A double-thermistor infrared detector eliminates sun and earth signals to prevent erroneous signals. The infrared detector comprises two 1-mm x 5-mm thermistor flakes separated by 3 mm. This results in an instantaneous optical field of view comprising two 1° x 5° fields separated by 3° in a direction normal to the scanning plane. This field of view is scanned in space by the "paddle-wheel" scanning mirror, which rotates about an axis normal to the optical axis. The paddle-wheel scanning mirror construction results in scanning half the aperture during each active scan period. Thus, the semicylindrical scanning beam is deflected off one of the "Vee" mirrors, thus rotating the scan plane 90 degrees such that it is parallel to the mirror spin axis. When the other semi-circular section of the paddle-wheel scanning mirror begins its scan period, it deflects the scanning beam off the other Vee mirror, causing the detector's instantaneous field of view to scan in a direction 180 degrees opposite to the previous scan.

The scanning mirror is double-sided; hence, two scans of opposite horizon edges are made for each revolution of the scanning mirror. Therefore, it can be seen that the center of the instantaneous field of view scans a sector of a 168-degree apex angle cone in space per axis. In a discussion with the designers, the following points were brought out:

1. The scanner is a new development;
2. Two scanning heads are necessary for two-axis control;
3. The scanner is linear over a wide range;
4. The total weight is 12 lbs;
5. The signal-to-noise ratio is 29 to 1;
6. The operational life is 21,000 hours;
7. Irregularities will not result in errors greater than 0.8 degree at an altitude of 200 km;
8. By proper processing, the effect of earth-glow, Lunar Terminator, or direct sun are minimized;
9. The initial cost estimate for design and development is $945,000, while flight models are estimated at $50,000 each; and
10. The development time, including testing, would be between 12 and 15 months.

### c. ATL Horizon Tracker

The horizon tracker uses a dual motion of the field-of-view of a single infrared telescope. As shown in Figure 1.3.B-12, the unit scans back and forth along a 160-degree sector of the horizon at a frequency of 1 cps. Concurrently, the line of sight

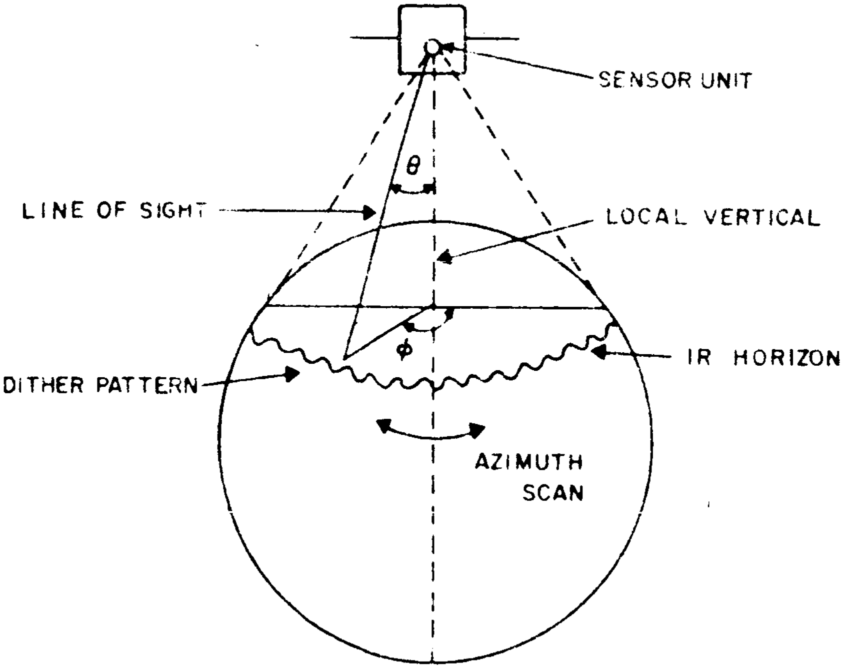

Figure I.3.B-12 Geometry of ATL Horizon Tracker

is oscillated or "dithered" by a mirror through 4 degrees at 30 cps at right angles to the horizon. The horizon edge is tracked at this high speed, and the variation in average position of the line of sight, as measured at the mirror during different portions of the slow-speed azimuth scan, is used to drive the angle of tilt from the yaw axis.

It is now well established that some disturbances (e.g., lunar mountains, earth glow, solar radiation) exist on the moon's infrared horizon. The ATL scanning system averages the horizon angles over a complete 160-degree sector rather than relying on data from three or four fixed points; hence, it is far less susceptible to such disturbances than a fixed-point system would be. In addition, the field of view of the infrared telescope never moves more than 2 degrees away from the horizon; therefore, infrared gradients within the moon beyond 2 degrees from the horizon can have no effect on the system. A third advantage of such a scanning method is that null accuracy is not affected by electronic or mechanical drifts, because, at null, the angle of the line-of-sight to the horizon (measured at the mirror) is constant throughout the azimuth scan. The pitch and roll outputs are derived from the time variations in this angle through a-c amplifiers. At null, there are no time variations in the angle, thus, the signal-processing amplifiers have zero output. The null accuracy therefore, is limited only by mechanical tolerances (which can be held to seconds of arc) and the properties of the moon's horizon itself. The averaging effect of the 160-degree scan minimizes even the effect of horizon anomalies.

RE-ORDER No. 62-459

In normal operation, the mirror dithers the line of sight across the horizon with a peak displacement of 2.0 degrees. The servo action positions the mirror such that the duty cycle of the dither, (e.g., the ratio of the time the detector sees to the total dither period) is very nearly 50%. Thus, the average mirror position is close to the horizon.

A search phase of the servo, used for initial acquisition, causes the line-of-sight to sweep repetitively over a 70-degree range until an infrared gradient is recognized. Logic circuitry prevents recognition of any gradient except the first positive one encountered during the downward sweep (i.e., the horizon).

Error-signaling-processing circuits compare the Positor-position signals at different phases of the azimuth drive and derive pitch and roll outputs.

In preliminary discussions with the representatives of ATL, the following information was brought out:

1. A modified version of the Gemini sensor would be applicable. (Development of the Gemini sensor is in line with the present 8-month schedule).
2. Accuracies of 1° or better in two axes are obtainable.
3. The sensor is linear over a range of ±7°.
4. The weight of a single-head unit plus electronic packaging will be approximately 7 pounds.
5. The signal-to-noise ratio is 5 to 1 at a temperature of 120°K.
6. The field of view in the acquisition mode has an elevation of 70°, and an azimuth of 160°.
7. The sensor's operational life in a vacuum is 26,000 hours.
8. Preliminary analysis indicates that effects resulting from horizon or surface irregularities are nominal. (The effects of crossing the lunar terminator must be studied.)
9. The possibility of lunar terminator lock-on must be studied.
10. A preliminary cost schedule includes:

| | |
|---|---|
| Development | $351,000. |
| Prototype | 176,000. |
| Ground equipment dev. | 38,000. |
| Ground equipment prod. | 68,000. |
| Flight models | 50,000. each |

## 3. SUMMARY OF WEIGHT AND POWER REQUIREMENTS FOR ATTITUDE CONTROL

Table I.3.B-2 presents the weight and power requirements for the pure jet attitude control subsystem. Because of the possibility of using either of two horizon sensors, the table includes both possibilities. It is obvious that the back-up system shows an immense improvement from both standpoints. It should also be pointed out that sufficient A/C gas is included for a minimum of 40 days operation, based upon the results of the computer program described earlier in this section.

TABLE I.3.B-2

WEIGHT AND POWER REQUIREMENTS FOR STABILIZATION
(PURE JET SYSTEM)

| Component | Weight (lbs) | Power (watts) |
|---|---|---|
| Horizon Scanner | 12* | 12 |
| ('Lit-Side, Sensor)** | (2 1/2) | ( 3) |
| Team Damper | 2 | |
| De-Spin Mechanism | 3 | |
| Spin-up Rockets | 2 | |
| Solar Aspect Sensor | 0.5 | |
| Tank, gas, nozzles, regulator, etc. | 17.5 | |
| Control Electronics | 5 | 1 |
| 3 MIG Gyros | 3 | 9 |
| Total | 45 (35.5) | 22 (13) |

* Barnes Engineering conservative estimate

** Alternative to horizon scanner

## C. TELECOMMUNICATIONS

The data acquired during the preliminary study (Phase I) of the Lunar Orbiter Capsule were re-evaluated during Phase II of the Study Contract to determine the requirements for the telecommunications subsystem. As a result of this work, the subsystem envisioned should provide: (1) command and timing signals to the lunar orbiting capsule after its separation from the Ranger bus; (2) tracking signals which would permit the determination of the lunar-capsule orbital elements; and (3) telemetry data which would be analyzed to evaluate all subsystem performance. This subsystem should also be capable of transmitting television pictures of the lunar surface from the capsule to the earth.

The telecommunications subsystem (to perform the required functions) would include circuits for communications, a tape recorder with capability for storing data until it is later transmitted, a tracking transponder, circuits for command control and timing, circuits for telemetry data acquisition and transmittal, and antennas for transmitting the data from the capsule to the earth. Tentatively, the TV transmitter will be a low-power version of the one designed for RA 6-9; the tape recorder will be a modified Nimbus AVCS; the transponder will be identical to the one used in RA 6-9; the command and telemetry circuits will be the same as the RA 6-9, but will require some new hardware; and two antennas (a dish and an "omni") will be used. The circuits and hardware scheduled for use in the telecommunications subsystem would require minimum development effort, and would provide maximum compatibility with the Ranger facilities and program.

A brief description of each of the major subassemblies included in the telecommunications subsystem is given here. More detailed descriptions of their components and operation are presented later in this section.

(1) Video Transmitter - The recommended TV transmission subassembly uses many of the components used in the RA 6-9 payload. A single 20-watt transmission channel is used. Based on the assumption that the DSIF will contain a frequency-modulation feedback democulator which is recommended, a worst-case RF link analysis was performed. The data indicate that a 20-watt, 960-Mc transmitter operating with a 30-inch dish antenna will result in a 29-db peak-to-peak RMS signal-to-noise ratio (in a 62.5-kc baseband) with a margin of 7 db. This means that the RA 6-9 transmitter can be operated at 20-watts, which will eliminate one intermediate power amplifier and reduce the input power requirements. Furthermore, the RA 6-9 power amplifier will be used in its present configuration (pressurized) until data indicate that the pressurized vessel is unnecessary.

(2) Tape Recorder - The tape recorder scheduled for use in the LOC is a modified Nimbus AVCS recorder which has a 62.5 kc bandwidth at a tape speed of 30 inches per second. The video data are recorded by frequency-modulating a subcarrier oscillator. Since the TV mapping of the lunar surface will require both direct and remote operation, the tape recorder will also store video data until it can later be transmitted back to earth. The recorder has capacity for 8 minutes of recording in one direction, and this time can be increased by using multiple tracks. The recorder is also capable of start-stop operation.

(3) Tracking Transponder - A two-way doppler transponder will be installed on the capsule. This will permit the DSIF to track the LOC by both doppler and angle techniques. The transponder will also serve as the command receiver and telemetry transmitter. The Ranger L-band, Mod. III transponder used in the Ranger bus is the one recommended for the LOC. The high-power (3-watt) power amplifier is necessary because of the wide-band attitude control telemetry requirements. The transponder will operate in conjunction with the omni-directional antenna.

(4) Command Control - The command subassembly recommended for the LOC is the one used in the RA 6-9 bus. Use of this command subassembly thus makes the LOC compatible with the Ranger DSIF command procedures. The command detector and decoder will be identical to those in Ranger, but the central computer and sequencer function will require a new design. The detailed requirements of each of the subsystems requiring command are not presently known; therefore, details can be determined later.

The central timing source for the LOC will be a clock, and will be used by all subassemblies and subsystems. This clock would be used in such functions as remote picture taking.

(5) Telemetry - The telemetry subassembly recommended for the LOC is similar to that used in the RA 6-9 bus, thus permitting the use of the present DSIF data reduction methods and equipment. The number of telemetry channels can be reduced to conserve weight and power, and would be advantageous because of the long mission time when compared to that of Ranger. Although the detailed requirements for telemetry data are not presently known, the assumption has been made that all data rates, with the exception of the attitude control sensors, will be very slow and slow commutating rates may, therefore, be used. Engineering telemetry for the TV system will be multiplexed with the video information and this will be done in a manner similar to that used on RA 6-9.

(6) Antenna Design - For LOC TV transmission, a 30-inch dish antenna with a circularly polarized feed is recommended. The dish will be hinged in elevation to permit steering of the boresight axis by command as the orbital plane precesses. The antenna beamwidth will be 30 degrees at the half-power points and will yield a maximum gain of 15 db.

The LOC will also have an omni-directional antenna consisting of an array of eight half-wave slot radiators, each of which is excited by a cavity. The eight cavities are fed equal in-phase signals using 7 power dividers. The azimuth beamwidth of the omni antenna is 360 degrees and the elevation beamwidth is 120 degrees. The antenna is linearly polarized and will produce a gain of -3 db.

## 1. VIDEO TRANSMITTER

The basic LOC Video Transmitter will be similar to the present Ranger 6 through 9 transmitter (refer to RCA Specification RSP-1150). The differences occur primarily as a result of the reduced power output requirement and the use of a single transmitter channel.

The following component blocks are deleted or modified from the present Ranger 6 through 9 video transmitter:

| Deleted | Modified |
|---|---|
| 1. Intermediate power amplifier (IPA) number 2. | 1. Change the transmitter modulator to limit baseband input to 62.5 KC. |
| 2. 4-port hybrid ring. | 2. Reduce power amplifier output to 20 watts minimum (reduce plate voltage from 1000 volts to 600 volts). |
| 3. Dummy load. | |
| 4. Directional coupler. | 3. Redesign power supply to reduce power consumption reflected by the above deletions and changes. |

The LOC video transmitter design will contain less parts, operate at reduced voltage and power stresses and will, therefore, have a greater chance of mission success.

The results of a comparative analysis of a straight frequency-modulation system (FM) and a frequency-modulation feedback system (FMFB), are shown in Tables I.3.C-1 and I.3.C-2. The development of a FMFB demodulator is recommended.

## 2. TAPE RECORDER

One mode of operation of the LOC television system requires storage of the video information prior to transmission to earth. A tape recorder design exists (the Nimbus AVCS Tape Recorder) that will meet the requirements of LOC. The representative specifications for this recorder are shown in Table I.3 C-3. The design of the recorder includes provisions for three (3) 62.5 KC video channels plus a 50 kc timing channel. This design is for use in a frequency division multiplex system (FDM).

The LOC system requires a single video channel with direct frequency modulation of the video transmitter by the video baseband. Therefore, the addition of a tape demodulator is required between the tape playback amplifiers and the transmitter modulator and the block diagram is shown in Figure I.3.C-1. The demodulator can be added to the tape recorder by deleting the unused playback amplifiers. The basic Nimbus tape recorder design is capable of start-stop operation, which adds to the flexibility of system design. The recorder can be modified to record and playback an increased video baseband of 120 KC, if this should be required. A tape speed change from 30 inches per second to 60 inches per second and doubling the tape FM modulator

## TABLE I.3.C-1

## ANALYSIS DATA OF A STRAIGHT FREQUENCY-MODULATION SYSTEM OPERATED AT $f_b = 62.5$ kc

| No. | Parameter | Value | Tolerance | Notes |
|---|---|---|---|---|
| 1 | Total Transmitter Power | 13dbw | +1dbw<br>-0dbw | 25 watt Resdel P.A. run at 20 watts min. |
| 2 | S/C Circuit Loss | 0.7db | ±.3db | Estimate-no diplexing to antenna-short cable |
| 3 | S/C Antenna Gain | 15db | +.5db<br>-0db | 30" Antenna for 30° BW |
| 4 | S/C Antenna Pointing Loss | 3db | +.3db<br>-3db | 30° BW Fixed Antenna |
| 5 | Space Loss | 204.2db | +1.2, -0.0db | Calc: 252,000 stat. Mi. 960Mc |
| 6 | Polarization Loss | 0.14db | ±.1db | Same as RA-6-9 |
| 7 | Ground Antenna Gain | 45.7db | ±.8db | JPL Memo 4/16/62<br>Horn Feed<br>Diplexed Operation<br>per C.A. Helritz<br>Paramp 130-150°K<br>Moon 30°K<br>Diplexer .25 ±.03db<br>Antenna 33 ± 25°K<br>RX Line .2±.1 |
| 8 | Ground Circuit Loss | 0.45db | ±.13db | |
| 9 | Total Receiver Power | -134.79dbw | +5.83dbw<br>-1.63dbw | |
| 10 | System Noise Temperature | 258.5°K | +0<br>-48.7°K | |
| 11 | Receiver Noise Density (KT) | -204.5dbw | +0dbw<br>-.9dbw | |
| 12 | Noise BW | 265KC | ±.5KC | FM m=1.12<br>$f_b$ = 62.5KC |
| 13 | Noise Power | -150.3dbw | +0.5dbw<br>-1.4dbw | |
| 14 | C/N Ratio | 15.51db | +7.23db<br>-2.13db | |
| 15 | Threshold | 12db | | |
| 16 | Performance Margin (worst case) | 1.38db | | |
| 17 | Modulation Gain | 9db | | m = 1.12<br>NIF = $3 m^2(m+1)$ |
| 18 | S/NRatio (at threshold) | 21db | | |
| 19 | $S_{pp}/N_{rms}$ (at threshold) | 30db | | |

## TABLE I.3.C-2

## ANALYSIS DATA OF A FREQUENCY-MODULATION FEEDBACK SYSTEM OPERATED AT $f_b = 62.5$ kc

| No. | Parameter | Value | Tolerance | Notes |
|---|---|---|---|---|
| 1 | Total Transmitter Power | 13dbw | +1, -0 | 25 watt Resdel P.A. run at 20 watts min. |
| 2 | S/C Circuit Loss | 0.7db | ±0.3db | Estimate-no diplexing to antenna-short cable |
| 3 | S/C Antenna Gain | 15db | +0.5, -0db | 30" Antenna for 30°BW |
| 4 | S/C Antenna Pointing Loss | 3db | | 30° BW Fixed Antenna |
| 5 | Space Loss | 204.2db | | Calc: 252,000 stat. Mi. $960M_c$ |
| 6 | Polarization Loss | 0.14db | | Same as RA-6-9 |
| 7 | Ground Antenna Gain | 45.7db | | JPL Memo 4/16/62<br>Horn Feed |
| 8 | Ground Circuit Loss | 0.45db | | Diplexed Operation<br>per C.A. Helritz |
| 9 | Total Receiver Power | -134.79dbw | +5.83dbw<br>-1.63dbw | Paramp 130-150°K<br>Moon 30°K |
| 10 | System Noise Temperature | 258.5°K | +0<br>-48.7°K | Diplexer .25 ± .03 db<br>Antenna 33 ± 25°K<br>RX Line .2±.1 |
| 11 | Receiver Noise Density | -204.5 dbw | +0<br>-0.9dbw | |
| 12 | Noise BW | 365 Kc | ±.5db | FM $m = 1.12$<br>$f_b = 62.5$ KC |
| 13 | Noise Power | -148.9dbw | +.5dbw<br>-1.4dbw | |
| 14 | C/N Ratio | 14.11db | +7.23db<br>-2.13db | |
| 15 | Threshold | 4.9db | | |
| 16 | Performance Margin (worst case) | 7.08db | | |
| 17 | Modulation Gain | 15.1db | | $m = 1.92$ NIF $= 3m^2(m+1)$ |
| 18 | SNR (at threshold) | 20 db | | |
| 19 | $S_{pp}/N_{rms}$ (at threshold) | 29db | | |

[illegible] No. 62-419

## TABLE I.3.C-3

## REPRESENTATIVE SPECIFICATIONS FOR THE NIMBUS AVCS TAPE RECORDER

| | | |
|---|---|---|
| Tape, one mil mylar base | | 1/2 inch wide |
| Length of tape | | 1200 feet |
| Tape speed | | 30 inches/sec. |
| Records in one direction for 8 minutes | | |
| Plays back in opposite direction for 8 minutes | | |
| Starting time | | Less than 1 second |
| Stopping time | | Less than 2 seconds (dynamic brake used) |
| Voltage input | | -24.5 volts DC |
| Power input (initial surge for one second) | | 15 watts |
| Power input (steady state) | | 10 watts |
| Channels | | 4 total |
| Video | 3 (72 kc to 120 kc -6.5 VDC into -11.5 VDC) | |
| Timing | 1 (50 kc 50% AM) | |
| Erase | | DC Permanent Magnet |
| Enclosure Size | 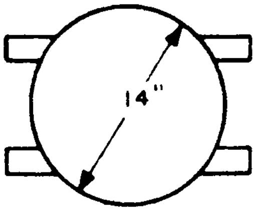 | 8 inches high |
| Weight | | 17 pounds |
| Angular momentum compensated to ±0.02 lb.-in.-sec. | | |
| Impedances: | Power Converter Input | 2,000 ohms |
| | Modulator Input | 40,000 ohms |
| | Timing Input | 620 ohms |
| | All Channel Outputs | 1,500 ohms |

Output Levels - All channels unloaded 6 Volts (p-p)

Wow and flutter - Measured values N12 Recorder 3-19-62

| Frequency (cps) | Wow & Flutter % rms |
|---|---|
| 0.5 to 30 | 0.015 |
| 30 to 300 | 0.04 |
| 300 to 5000 | 0.085 |
| DC to 5000 | 0.11 |

The above do not represent spec limits, but are typical values.

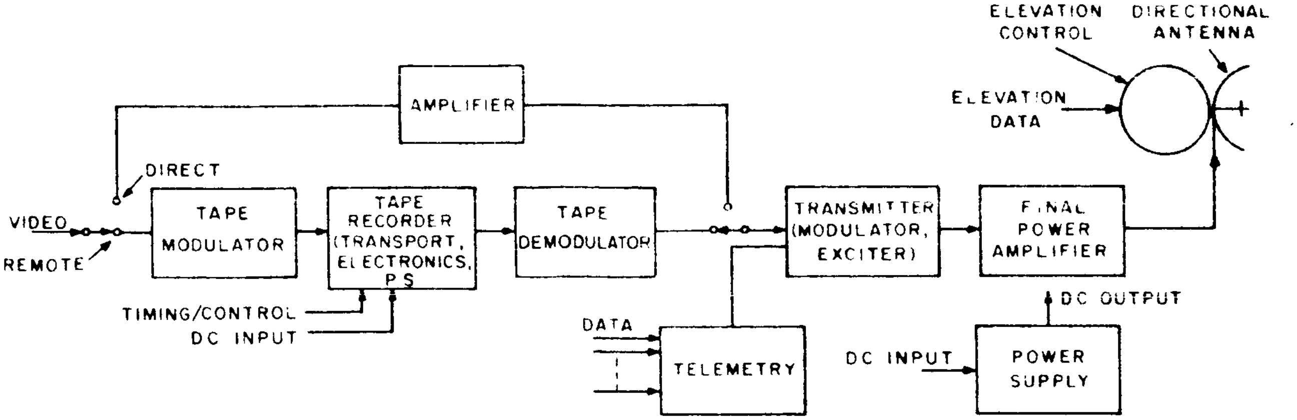
AMPLIFIER
DIRECT
VIDEO
REMOTE
TAPE MODULATOR
TAPE RECORDER (TRANSPORT, ELECTRONICS, P S
TAPE DEMODULATOR
TIMING/CONTROL
DC INPUT
TRANSMITTER (MODULATOR, EXCITER)
FINAL POWER AMPLIFIER
ELEVATION CONTROL
DIRECTIONAL ANTENNA
ELEVATION DATA
DATA
TELEMETRY
DC OUTPUT
DC INPUT
POWER SUPPLY

Figure I.3.C-1 Block Diagram of the Video Transmission Subassembly

output would be required to accommodate the increased video bandwidth. Suitable changes would have to be made to the playback amplifiers.

## 3. TRACKING TRANSPONDER

The tracking transponder serves several purposes for the LOC; it provides a coherent tracking signal for use by the deep space instrumentation facility (DSIF) in doppler determination and angle tracking of the capsule, and the transponder also serves as the command receiver and telemetry transmitter. A block diagram of the transponder is shown in Figure I.3.C-2. The transponder configuration will use a single "omni" antenna, diplexed, for use by the receiver and transmitter. A single transmitter power amplifier will be used rather than the Ranger bus configuration.

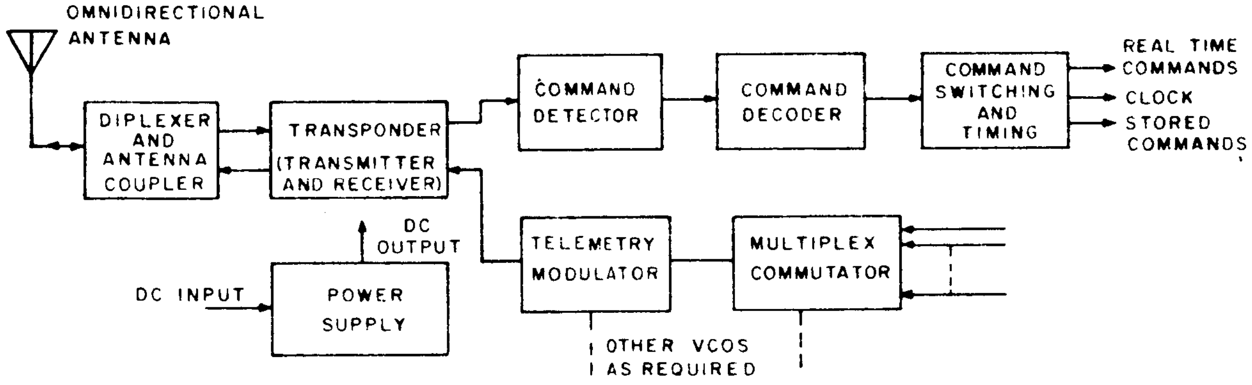
OMNIDIRECTIONAL ANTENNA
DIPLEXER AND ANTENNA COUPLER
TRANSPONDER (TRANSMITTER AND RECEIVER)
COMMAND DETECTOR
COMMAND DECODER
COMMAND SWITCHING AND TIMING
REAL TIME COMMANDS
CLOCK
STORED COMMANDS
DC OUTPUT
DC INPUT
POWER SUPPLY
TELEMETRY MODULATOR
MULTIPLEX COMMUTATOR
OTHER VCOS AS REQUIRED

Figure I.3.C-2. Block Diagram of the Tracking Transponder Subassembly

## 4. COMMAND CONTROL

The command subsystem for the LOC will be similar to that used in the Ranger 6 through 9 bus, thus making the LOC compatible with the present DSIF command procedures. There are two basic time limitations on the command system:

1. The acquisition time required for the command detector may be 8-1/2 minutes after the command subcarriers are applied (plus about 3 minutes for RF acquisition).

2. The maximum command rate is one command every 57 seconds.

These limitations would require turning the transponder on for about 12-1/2 minutes if commands are required during the orbit. The command word structure for the LOC will be the same as that for the Ranger RA-6 through RA-9 spacecraft (i.e., 1 framing bit, 5 address bits, and 12 data bits) to make use of the existing Ranger circuitry as much as possible.

Figure I.3.C-3 is a block diagram of the RA-6 Command Detector, Command Decoder, and Central Computer and Sequencer (CC&S). A comprehensive block diagram and functional description of the Command Detector and Command Decoder may be found in Spec. No. RL-4-322, dated 15 March 1962. Information on the CC&S may be found in Spec. No. RL-4-410A dated 5 April 1962.

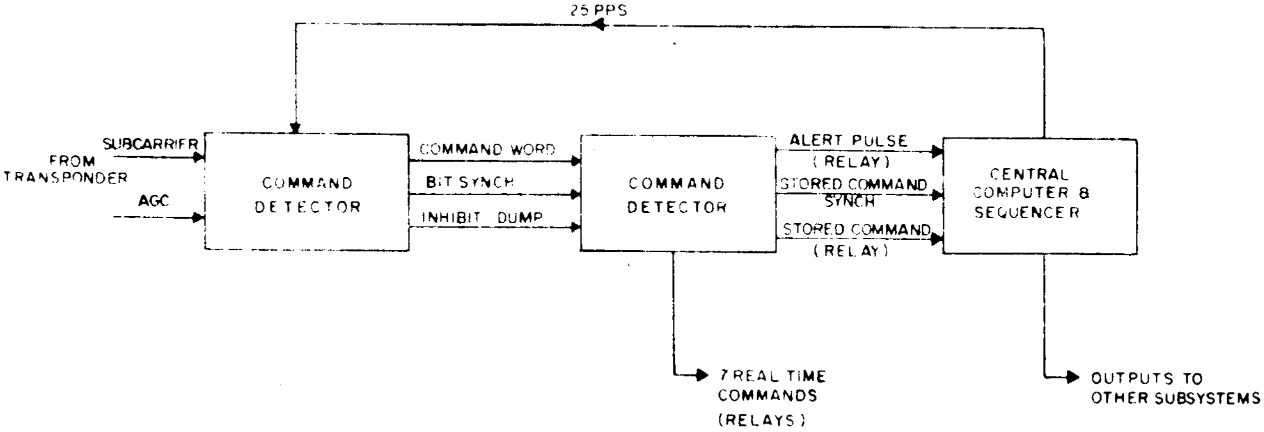
25 PPS
SUBCARRIER
FROM
TRANSPONDER
AGC
COMMAND
DETECTOR
COMMAND WORD
BIT SYNCH
INHIBIT DUMP
COMMAND
DETECTOR
ALERT PULSE
(RELAY)
STORED COMMAND
SYNCH
STORED COMMAND
(RELAY)
CENTRAL
COMPUTER &
SEQUENCER
7 REAL TIME
COMMANDS
(RELAYS)
OUTPUTS TO
OTHER SUBSYSTEMS

Figure I.3.C-3 Block Diagram of the Ranger 6 through 9 Command Subassembly

The Command Detector accepts the command sub-carrier from the receiver, and extracts the digital "1" - "0" information from it. The AGC level is also monitored (a drop in AGC below a preset threshold indicates unacceptable signal to noise ratio of the subcarrier, and an inhibit-dump signal is generated). After the framing bit opens the proper gates, the digital information is fed from the Detector to the Command Decoder, along with an internally generated 1 pps bit sync signal derived from the CC&S 25 pps clock. One command word may be received every 56 seconds: this apparently allows the same 18 bit word to be sent twice in the event of an error or poor signal to noise ratio. Because the Command Detector operates on data in a serial fashion, it poses no inherent restraints on either the length of a command word or its structure. The 56-second reset timing operation may easily be extended or shortened by the addition or subtraction of a flip-flop. The command word is entered, in serial fashion, into the Command Decoder's 17 bit shift register. The framing bit is discarded. The address portion of the command word is decoded, and if a "real time" command is indicated a relay is actuated. If a "stored" command is indicated, the contents of the shift register are serially shifted to the CC&S.

Using the present command word configuration of 5 bits for addressing, there are 32 possible addresses. At present, 7 addresses are used for real-time commands and 6 addresses are used for stored commands. If more than 7 real-time commands are required, additional relays would have to be added and possibly some addition to the address decode matrix would be needed. For more than 6 stored commands a change to the address decode matrix is all that would be required. However, either one of these two increases would probably necessitate changes in the CC&S.

The Ranger CC&S appears to be a highly specialized subsystem, performing rather specific computations and timing functions during prelaunch, launch, flight and pre-impact operations. It is doubtful that this unit can be used in the LOC, although some of its design techniques may prove useful.

A determination of the configuration of the LOC CC&S subsystem would require information from all other LOC subsystems regarding clock pulses, input sequence signals, computations, sweep signals etc. Furthermore, an evaluation must be made to determine whether these signals could best be generated in the CC and S or in the particular subsystem.

## 5. TELEMETRY

A comparison of a 3 watt and a one-fourth watt telemetry transponder system showed that the one-fourth watt transponder is inadequate to transmit the required amount and types of data involved. The major restriction is caused by the necessity for sending unprocessed horizon sensor data as well as commutated data. Any design for a quarter-watt telemetry system, it is felt, would have insufficient margin for reliable operation, and could jeopardize the success of the mission.

### a. High Power Telemetry (3 watts)

The encoder subsystem for a 3 watt telemetry link would have 5 subcarrier channels. A block diagram is shown in Figure I.3.C-4. Channel #1 at 400 cps would be used as a synchronizing channel for the commutators which would be slaved to it. This channel would provide information for decommutation of telemetry information. The synchronizing signal is filtered by a bandpass filter before being mixed with the other subcarriers. Channel #2 at 560 cps will carry unseparated PAM data that is rate limited. There will be 30 channels sampled at a rate of 1 channel per second. This commutator would carry stabilization data and power supply and transponder data. Channel #3 at 730 cps will be time shared between the horizon sensors and a 30 channel, PAM (unseparated), rate-limited commutator used to carry TV telemetry

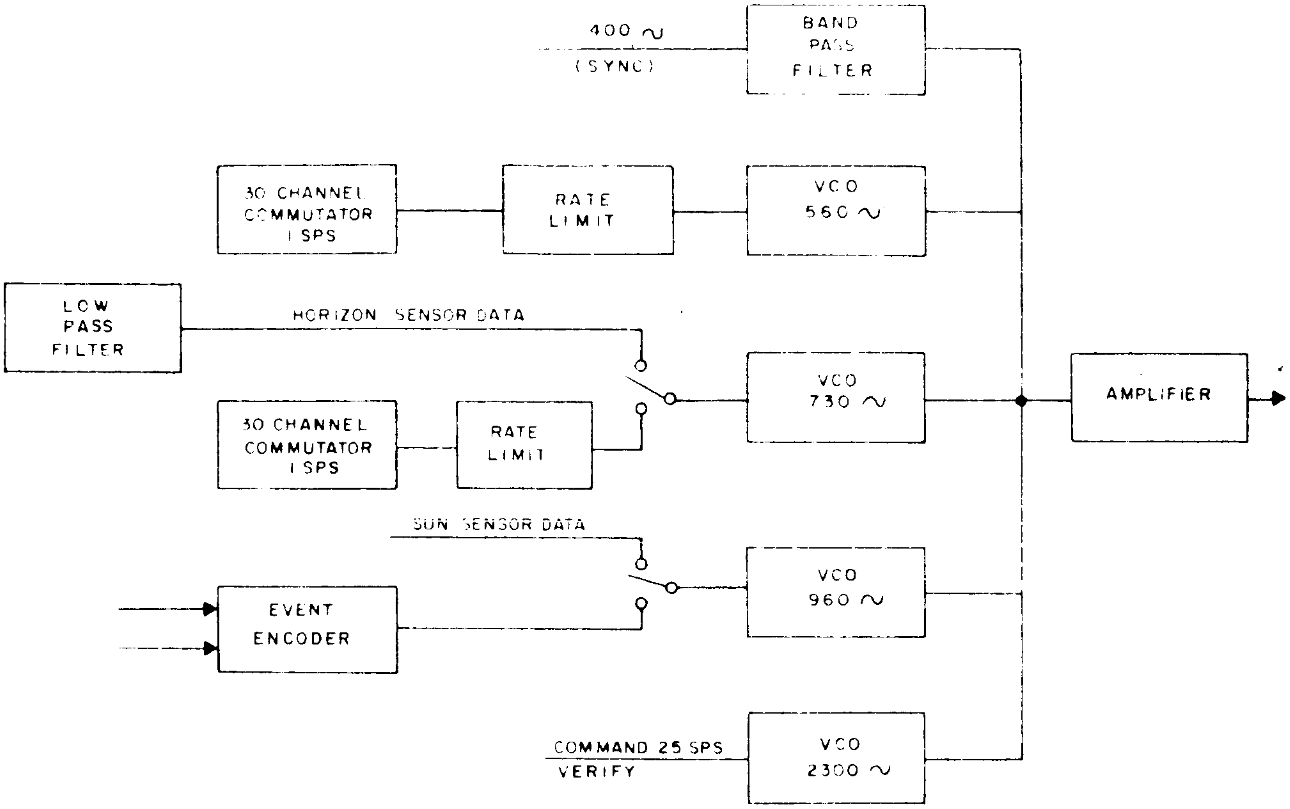
400 ∿
(SYNC)
BAND PASS FILTER
30 CHANNEL COMMUTATOR 1 SPS
RATE LIMIT
VCO 560 ∿
LOW PASS FILTER
HORIZON SENSOR DATA
VCO 730 ∿
AMPLIFIER
30 CHANNEL COMMUTATOR 1 SPS
RATE LIMIT
SUN SENSOR DATA
VCO 960 ∿
EVENT ENCODER
COMMAND 25 SPS
VERIFY
VCO 2300 ∿

Figure I.3.C-4 Block Diagram of Encoder Subassembly for a 3-Watt Telemetry Link with Five Subcarrier Channels

data. The horizon sensor data will be limited by a 10 cycle low-pass filter. The input chosen will be done by command. Channel #4 at 960 cps will be time shared between the sun sensor digital data and an event encoder which will operate only during initial orbit injection and stabilization. Thereafter, the sun sensor data will be permanently fed to the VCO. Channel #7 at 2.3 kc will be used for command verification at a maximum bit rate of 2.5 bps. All 5 channels will be mixed together through an amplifier before application to the transponder.

The parameters for the various subcarriers are given in Tables I.3.C-4 and -5. The values for noise, bandwidth, RF modulation index, and modulation loss were determined using the criteria of JPL Technical Report No. 32-215, "The Pioneer IV Lunar Probe: A Minimum-Power FM/PM System Design", by Ben D. Martin: and from JPL Spec. No. RA345-4-311, "Functional Specification Ranger RA-3, 4, and 5 Spacecraft Telecommunication System", 16 January 1962. Such a system would weigh about 6 pounds and require about 5 watts of power for its operation. This system is the preferred system because it allows ample margin for operation of all subcarriers and could be expanded by another subcarrier or two without appreciably affecting the other subcarriers or the tracking capability of the transponder.

## TABLE I. 3. C-4

## ENCODER PARAMETERS FOR 3-WATT TELEMETRY SUBCARRIERS

| Subcarrier No. | Freq. (cps) | Inform. Rate | Δ f (Cycles) | R. F. Mod. Index (radians) | Noise Bandwidth ($2B_{1o}$ cycles) | R. F. Mod. Loss (db) | Threshold SNR In $2 B_1$ (db) | Margin (db) |
|---|---|---|---|---|---|---|---|---|
| 1 | 400 | 0.3 cps | — | .24 | 2 | 20.6 | 9 | 8.0 |
| 2 | 560 | 1 SPS | 50 | .68 | 50 | 11.0 | 5.6 | 7.0 |
| 3 | 730 | 1 SPS or 10 cps | 50 | 1.02 | *100 | 6.9 | 5.6 | 8.1 |
| 4 | 960 | 1 SPS or 1 bps | 20 | .68 | 42 | 11.0 | 5.6 | 7.8 |
| 7 | 2300 | 2.5 bps | 4 | .53 | 16.7 | 13.5 | 5.6 | 9.3 |

$P_{carrier}$ = 5.3 db modulation loss

* Denotes pre-detection noise bandwidth

## TABLE I. 3. C-5

## ENCODER PARAMETERS FOR 1/4 WATT TELEMETRY SUBCARRIERS

| Subcarrier No. | Freq. (Cycles) | Inform. Rate | Δ f (Cycles) | R. F. Mod. Index (radians) | Noise Bandwidth (cycles) | R. F. Mod. Loss (db) | Threshold (db) | Margin (db) |
|---|---|---|---|---|---|---|---|---|
| 2 | 560 | 1 SPS or 10 N | 50 | 1.65 | 84 | -4.2 | +5.6 | 6 |
| 3 | 730 | 1 SPS or 1 bps | 10 | 1.42 | 25 | -7.2 | +5.6 | 6 |
| 7 | 2.3 kc | 2.5 bps | 4 | 1.27 | 16.7 | -9 | +5.6 | 6 |

$P_{carrier}$ = -10 db modulation loss

## TABLE I. 3. C-6

## PARAMETERS FOR THE PROPOSED TELEMETRY SUBASSEMBLY

| No. | Parameter | Value | Tolerance |
|---|---|---|---|
| 1 | Total Transmitter Power 3 watts | 34.8 dbm | +0.8, -0.0 db |
| 2 | Transmitting Circuit Loss | -2.0 db | +0.5, -0.0 db |
| 3 | Transmitting Antenna Gain (a) | -3.0 db | +3.0, -1.0 db |
| 4 | Transmitting Antenna Pointing Loss | (included in 3) | |
| 5 | Space Loss (b) | -204.2 db | +1.2, -0.0 db |
| | f = 960 MC, R = 405000 KM | | |
| 6 | Polarization Loss (c) | -3.0 db | |
| 7 | Receiving Antenna Gain | 45.7 db | +0.8, -0.8 db |
| 8 | Receiving Antenna Pointing Loss (d) | -2.0 db | +2.0, -1.0 db |
| 9 | Receiving Circuit Loss | -0.5 db | +0.1, -0.1 db |
| 10 | Net Circuit Loss | -179.0 db | +7.6, -3.7 db |
| 11 | Total Received Power | -134.2 dbm | +8.4, -3.7 db |
| 12 | Receiver Noise Spectral Density (N/B) | -174.8 dbm/cps | +0.4, -0.0 db |
| | T System (°K) = 240, +0, -20 | | |
| 13 | Carrier Modulation Loss | -5.3 db | +1.0, -1.0 db |
| 14 | Received Carrier Power | -139.5 dbm | +9.4, -4.7 db |
| 15 | Carrier APC Noise BW ($2B_{LO}$ = 20 ± 4 cps) | 13.0 db/cps | +0.8, -1.0 db |
| | CARRIER PERFORMANCE - TRACKING (one-way) | | |
| 16 | Threshold SNR in $2B_{LO}$ | 0.0 db | |
| 17 | Threshold Carrier Power | -161.8 dbm | +1.2, -1.0 db |
| 18 | Performance Margin | 21.3 db | +10.6, -5.7 db |
| | CARRIER PERFORMANCE - TRACKING (two-way) | | |
| 19 | Threshold SNR is $2B_{LO}$ (e) | 1.0 db | |
| 20 | Threshold Carrier Power | -160.8 dbm | +1.2, -1.0 db |
| 21 | Performance Margin | 20.3 db | +10.6, -5.7 db |

## TABLE I. 3 C-6 (Continued)
## PARAMETERS FOR THE PROPOSED TELEMETRY SUBASSEMBLY

| No. | Parameter | Value | Tolerance |
|---|---|---|---|
| | Data Channel #1, 400 cps | | |
| 1 | Modulation Loss | -20.6 db | +2.0, -2.0 db |
| 2 | Received Data Subcarrier Power | -154.8 dbm | +10.4, -5.7 db |
| 3 | Data APC Noise BW ($2B_{1o} = 2$) | 3.0 db | +1.0, -0.8 db |
| 4 | Threshold SNR in $2B_{1o}$ | 9.0 db | |
| 5 | Threshold Subcarrier Power | -162.8 dbm | +1.4, -0.8 db |
| 6 | Performance Margin | 8.0 db | +11.4, -6.5 db |
| | Data Channel #2, 560 cps | | |
| 7 | Modulation Loss | -11.0 db | +1.0, -1.0 db |
| 8 | Received Data Subcarrier Power | -145.2 dbm | +9.4, -4.7 db |
| 9 | Data APC Noise BW ($2B_{1o} = 50$) | 17.0 db | +0.5, -0.5 db |
| 10 | Threshold SNR in $2B_{1o}$ | 5.6 db | |
| 11 | Threshold Subcarrier Power | -152.2 dbm | +0.9, -0.5 db |
| 12 | Performance Margin | 7.0 db | +10.3, -5.2 db |
| | Data Channel #3, 730 cps | | |
| 13 | Modulation Loss | -6.9 db | +1.0, -1.0 db |
| 14 | Received Data Subcarrier Power | -141.1 dbm | +9.4, -4.7 db |
| 15 | Data APC Noise BW ($2B_{1o} = 100$) | 20.0 db | +0.5, -0.5 db |
| 16 | Threshold SNR in $2B_{1o}$ | 5.6 db | |
| 17 | Threshold Subcarrier Power | -149.2 dbm | +0.9, -0.0 db |
| 18 | Performance Margin | 8.1 db | +10.3, -5.2 db |
| | Data Channel #4, 960 cps | | |
| 19 | Modulation Loss | -11.0 db | +1.0, -1.0 db |
| 20 | Received Data Subcarrier Power | -145.2 dbm | +9.4, -4.7 db |
| 21 | Data APC Noise BW ($2B_{1o} = 42$) | 16.2 db | +0.5, -0.5 db |
| 22 | Threshold SNR in $2B_{1o}$ | 5.6 db | |
| 23 | Threshold Subcarrier Power | -153.0 dbm | +0.9, -0.5 db |
| 24 | Performance Margin | 7.8 db | +10.3, -5.2 db |

TABLE I.3 C-6 (Continued)

PARAMETERS FOR THE PROPOSED TELEMETRY SUBASSEMBLY

| No. | Parameter | Value | Tolerance |
|---|---|---|---|
|  | Data Channel #7, 2.3 kcps |  |  |
| 1 | Modulation Loss | -13.5 db | +1.5, -1.5 db |
| 2 | Received Data Subcarrier Power | -147.7 dbm | +9.9, -5.1 db |
| 3 | Data APC Noise BW ($2B_{1o}$ = 16.7) | 12.2 db | +0.5, -0.5 db |
| 4 | Threshold SNR in $2B_{1o}$ | 5.6 db |  |
| 5 | Threshold Subcarrier Power | -157.0 dbm | +0.9, -0.5 db |
| 6 | Performance Margin | 9.3 db | +10.8, -5.6 db |
|  | Data Channel |  |  |

Comments:

(a) The transmitting antenna is expected to have a gain no worse than this from ± 60 degrees of beam center and all around in azimuth.

(b) Value given is for maximum lunar distance.

(c) Tentatively the polarization for the transmitting antenna is linear. There is some possibility of providing circular polarization.

(d) This assumes no active tracking of the satellite and that the ground antenna is pointed at the moon's center. The margin allows for a pointing error of ± 0.2 degrees.

(e) Transponder SNR +7 db.

62-459

## 6. ANTENNA DESIGN

Two antennas are required for the LOC; a high-gain directional antenna used for video transmission and a low-gain omni-directional antenna used for receiving and transmitting from the transponder. The use of the L-band frequencies is considered for early orbiters, but later orbiters would require the use of the S-band because of DSIF frequency assignments.

The requirements and constraints for antenna design are as follows:

(a) Directional antennas must have a half-power beamwidth of 30°.

(b) Omni-directional antennas must have a half-power beamwidth sufficiently wide in any longitudinal plane of the LOC to insure a minimum gain of -3 db over a look-angle range of ±60° relative to the LOC transverse plane.

(c) Circularly polarized antennas are desirable to obviate a 3-db polarization loss which would be inherent with lineraly polarized feeds. DSIF ground antenna feeds will be circularly polarized.

(d) Antennas may be located on the fore-end of the LOC with due consideration given to stability and shroud clearance. The sides of the LOC may also incorporate antennas if there are no excessive reductions in solar-cell area, violations of the shroud envelope, or obstructions to the radiation pattern.

### a. Directional Antennas

The directional antennas will be employed for RF transmission only. The merits of antenna designs other than parabolical reflectors were investigated and the dish appears to be most attractive, especially when the physical dimensions of other types are considered. The parameters of various selected antenna designs are listed in Table I.3. C-7.

TABLE I.3. C-7

PARAMETERS OF VARIOUS SELECTED ANTENNA DESIGNS

| Antenna | Aperture (wavelengths) | Length (wavelengths) | Comments |
|---|---|---|---|
| Horn | ~ 2 | 2.2 | too bulky |
| Dish | 2.44 | .41 | most attractive |
| Helix | $\pi$ -1 | 3.2 | too long |
| Polyrod | 0.5 | 4.0 | too long |

The L-band wavelength is 12.2 inches and the S-band is about 5.0 inches. A dish at L-band frequencies would be 20 inches in diameter and 5 inches deep. For L-band frequencies, a directional dish antenna is the best chóice. For S-band, however, the choice will not be as clear-cut. Such items as feed design and materials would influence the decision.

A maximum declination of -30° will be incurred by the directional antenna. One antenna problem of major concern is the reflection of energy from LOC surfaces. These reflections will severely perturb the radiation pattern unless reflections are minimized by displacing the antenna from the LOC. Antenna height, therefore, is vital to the achievement of a "clean" 30° beam. Minimum height can only be verified through a model test program which is beyond the scope of the Phase II study. A valid criterion, however, appears to be one utilizing optical-ray techniques which are applicable in the Fresnel or near-field zone of the antenna. For the L-band dish at -30°, the parallel ray reflected from the lowest tip of the reflector must not be obstructed by any surface or structure of the LOC.

Five factors influence the f/d (focal length/diameter) ratio of the L-band dish: (1) primary illumination controls characteristics of the secondary pattern by affecting the aperture amplitude and phase distributions. This control is more difficult for small f/d ratios. (2) Too large a ratio increases the swept-volume and inertia of the antenna. (3) Since the antenna feed will not be a true point source at the focus, it produces focal defects, known as aberrations, which cause the rays to diverge from the ideal parallel beam. This difficulty is minimized when the f/d ratio is about 0.25. The design range for the f/d ratio is usually taken from 0.25 to 0.50. (4) Beamwidth of the primary illumination must be consistent with the angular aperture of the reflector. The f/d ratio must be chosen to provide optimum illumination of the reflector which is usually a 10 db taper in power. (5) The reflection of a center-fed dish is dependent on the f/d ratio and on the diameter as follows:

$$\mathrm{SWR} \approx \frac{d/\lambda + 3\ F/d}{d/\lambda - 3\ F/d}$$

Since the diameter is fixed by the desired 30° beamwidth, the best match will occur at smaller f/d ratios. For $d/\lambda = 2.44$ (Beam = 30°), and $f/d = .375$,

$$\mathrm{SWR} \approx 2.7$$

Vertex-plate matching techniques may be used to correct the impedance mismatch due to the reflector. The VSWR of the antenna is then essentially that of the feed. The plate will increase side-lobe intensity but this is not serious since the specifications on the side lobes are not critical.

The L-band directional antenna design is shown in Figure I.3. C-5. A similar S-band dish is not shown because further investigation on other antenna types is needed. The center 6 inch diameter of the L-band dish is solid because it is illuminated with the highest intensity and enhances surface strength. The remaining reflector area may have a porosity as high as 50% for weight reduction. Aluminum of .08 inch thickness may be employed. The dish should have a rolled edge for rigidity. Surface shape and dish support depend on radial or concentric ribs.

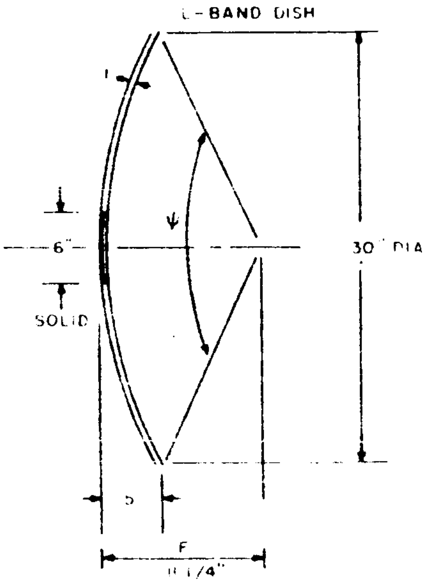

FREQUENCY (f) - 960 mc

WAVELENGTH (λ) - 12.2"

$\frac{F}{D} = \frac{3}{8}$, F = 0.91 λ

DISK DIAMETER (D) - 30" = 2.44 λ

GAIN = 15 db

BEAM WIDTH = 30°

FOCAL POINT (F) - 11 1/4"

ANGULAR APERTURE (ψ) - 135°

DISK THICKNESS (t) - .080"

MATERIAL - ALUMINUM

WEIGHT ≈ 4 LBS.

NOTE: FOR S-BAND CONFIGURATION MULTIPLY DIMENSIONS SHOWN BY 0.42

Figure I.3. C-5. Design of the L-Band Directional Antenna

1) Linearly polarized Feeds - In Phase I of the study a dipole-reflector design was mentioned as the rear feed for the directional antenna. Possible designs include dipole-disk or double-dipole types. Figure I.3. C-6 indicates typical dimensions for a slot-fed dipole-disk feed and Figure I.3. C-7 for a double-dipole. The double-dipole feed is preferable in terms of less weight and minimum aperture blockage.

The primary illumination of the parabolic reflectors may be controlled by adjustment of the several parameters. (1) The transmission line can be 7/8 inch rigid coax which acts as the feed support as well. Aluminum may be employed throughout.

The cable connection to this feed may be RF 8/U which has an attenuation of .08 db/ft at L-band and .14 db/ft at S-band; the weight per foot is .105 lbs. This cable will not be subject to excessive flexture or wear because the antenna excursions will be slow.

---

(1) S. Silver, "Microwave Antenna Theory and Design," Vol. 12, Rad. Lab. Series, McGraw Hill, P. 254

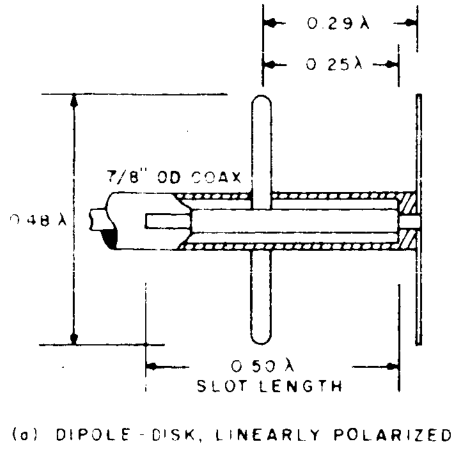
0.29 λ
0.25 λ
7/8" OD COAX
0.48 λ
0.50 λ
SLOT LENGTH
(a) DIPOLE-DISK, LINEARLY POLARIZED

Figure I.3.C-6. Directional Antenna Feed, Dipole Disk, Linearly Polarized

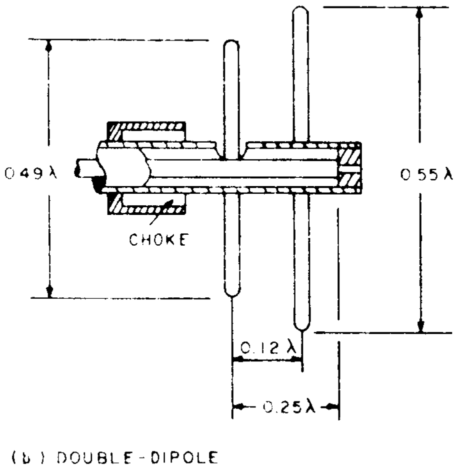
0.49 λ
0.55 λ
CHOKE
0.12 λ
0.25 λ
(b) DOUBLE-DIPOLE

Figure I.3.C-7 Directional Antenna Feed, Double-Dipole, Linearly Polarized

2) Circularly-Polarized Feeds - To obviate a 3 db polarization loss in the rf link, a circularly polarized feed must be used. Two possibilities are a helical feed, and a crossed-dipole feed. The helical feed would have about four turns to provide the primary illumination necessary for a dish. It is the simplest way to achieve circularity; however, use of a helix is not justified because the length of the helix required would be about 0.88λ. The focal length of the dish is 0.91λ. The helix is poor feed design because it is too long and would degrade the secondary pattern both in directivity and side-lobe structure. Essentially the helix cannot be used because the required antenna beamwidth is too large for that feed design.

Feed design employing crossed-dipoles should be investigated. This unit would consist of a turnstile radiator over a ground plane at the parabola focus.

b. Omni-Directional Antenna

1) Linearly Polarized Feeds - The technique for achieving a linearly polarized L-band omnidirectional pattern is essentially unchanged from that proposed in the Phase I study. An array of eight circumferential slot radiators is used to derive the required 120° X 360° pattern. Figure I. 3. C-8 shows in detail the dimensions of the cavity which will excite the flush-mounted slots.

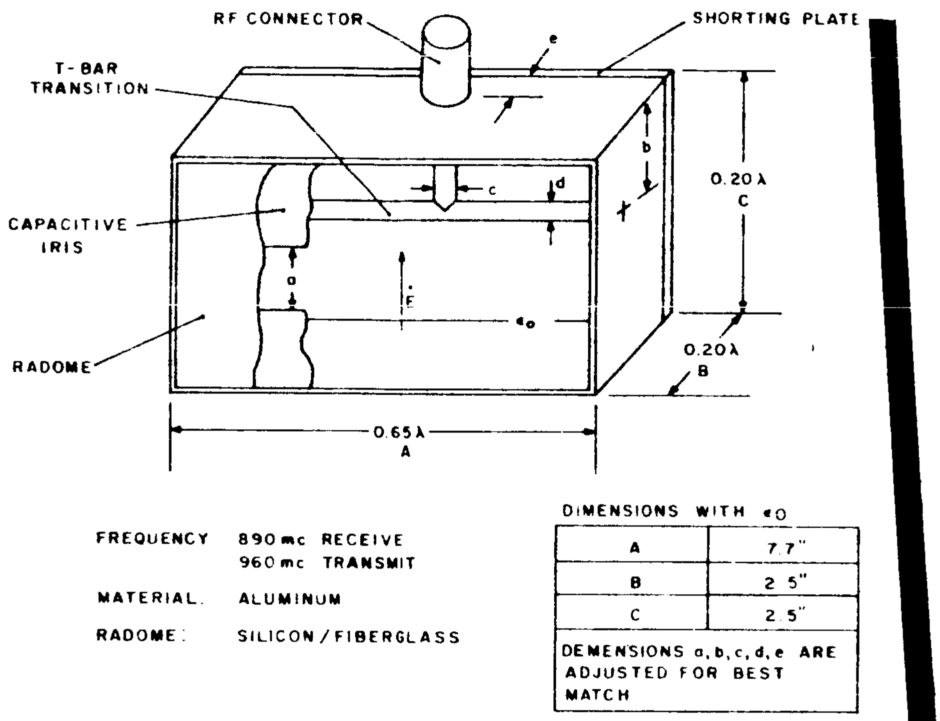
RF CONNECTOR
SHORTING PLATE
e
T-BAR TRANSITION
b
c
d
0.20λ
C
CAPACITIVE IRIS
a
f
$\epsilon_0$
RADOME
0.20λ
B
0.65λ
A
FREQUENCY 890 mc RECEIVE
960 mc TRANSMIT
MATERIAL ALUMINUM
RADOME SILICON/FIBERGLASS
DIMENSIONS WITH $\epsilon_0$
A 7.7"
B 2.5"
C 2.5"
DEMENSIONS a, b, c, d, e ARE ADJUSTED FOR BEST MATCH

Figure I. 3 C-8. L-Band Cavity Backed Slot, Linearly Polarized

The electric field along the cavity-backed slot is not necessarily sinuso[illegible]al or related to a complementary wire antenna. (1) One way to treat the unit is as [illegible] cavity resonator which is energized by some transducer and free to radiate out of t[illegible] slot. The field across the slot is dependent on the excitation of TE and TM cavity [illegible]odes. To insure that the energy stored in the cavity is primarily in the $TE_{01}$ mod[illegible] cavity dimensions are sufficiently large so that this principal mode is above cutoff. An important design parameter is the antenna Q (2) the ratio of the $TE_{01}$ mode s[illegible]red energy per cycle of the radiated power. The Q will be minimum when the st[illegible]d energy is in the $TE_{01}$ mode. The Q will limit the inverse VSWR bandwidth p[illegible]duct which, for a small cavity is $Q = \frac{3}{4\pi^2} \frac{\lambda^3}{V}$ where V is volume in cubic wavelengths. Figure I.3.C-9 shows the equivalent circuit of the cavity. The shunt conductance is the radiation conductance of the slot. The parallel susceptance is a sum of the shunt susceptance of the slot and the TE mode susceptance of the cavity. The series-resonant circuit is the result of the energy stored in the TM modes in the cavity and feed structure. Proper feed and cavity design can eliminate the series reactance and under this condition the above expression for Q is valid. For the cavity of Figure I.3.C-7

---

(1) S. Silver, "Microwave Antenna Theory and Design," Vol. 12, Rad. Lab. Series, McGraw Hill, P. 254

(2) H. Jasik, "Antenna Engineering Handbook", Pages 8 - 12.

$$Q = \frac{3}{4\pi^2} \quad \frac{\lambda^3}{\lambda^3 \; (0.65)\;(.2)\;(.2)} = \frac{3}{4\pi^2}\left(.26\right) = 2.9$$

Time did not permit the calculation of the radiation pattern for the eight slot array.

2) Circularly Polarized Feeds - There were several techniques considered for achieving a circularly polarized radiation from a cavity and these are shown in Figure I.3.C-10. Most techniques essentially introduce a 90° phase shift between two equal and orthogonal field components to effect circular rotation of their resultant field. Figure I.3.C-10a shows a square cavity which is fed by two orthogonal exciters where the necessary phasing is performed by coax line length. In Figure I.3.C-10b, the cavity is rectangular and excited by a probe inclined at 45°. Each orthogonal component of the excited field has a different velocity of propagation due to the different spacing of parallel walls. If the cavity length is chosen judiciously, a 90° phase shift between orthogonal fields will be obtained at the radiating aperture. An alternate approach employing a square cavity would be to obtain the necessary phase shift with a dielectric quarter-wave plate. The rectangular cavity approach appears to be the technique used in TELSTAR antennas. Application of these techniques to LOC design is precluded by the longitudinal bandwidth requirement. Half-power beamwidth is about 120°, however.

When circular polarization is desired, the aperture must be modified to a small or unity aspect-ratio in order to support the necessary orthogonal modes. Consequently, the broad pattern in the plane normal to a slot is sacrificed. There is, however, one approach (2) which should be investigated more thoroughly. Circular polarization is realized with a slot radiator by placing a tilted parasitic dipole in the plane of the aperture and the dimensions for this configuration are shown in Figure I.3.C-10c. One disadvantage of this approach when compared to the linearly polarized radiator is the increased cavity size and weight. An advantage of the linear unit is that its dimensions may be reduced by dielectric loading of the cavity. Appropriate dielectrics for this space application should be studied.

---

(1) G. Ragan "Microwave Transmission Circuits", Volume 9, Rad. Lab. P. 378

(2) E. Wilkinson, "Circularly-Polarized Slot Antenna," Microwave Journal, March, 1961, P. 97.

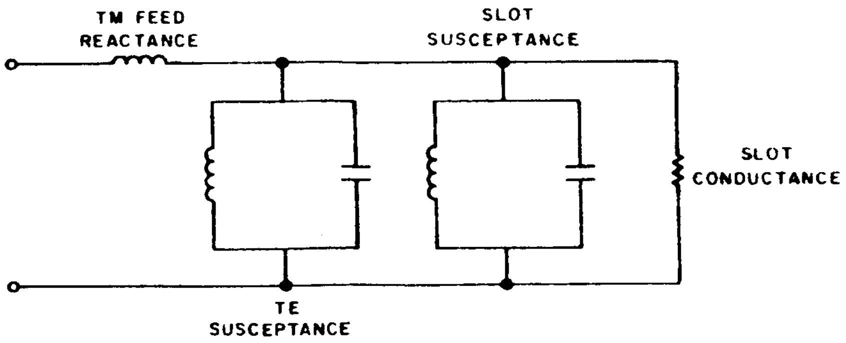
TM FEED
REACTANCE
SLOT
SUSCEPTANCE
SLOT
CONDUCTANCE
TE
SUSCEPTANCE

Figure I.3.C-9. Equivalent Circuit of the Transponder Antenna Slot-Cavity

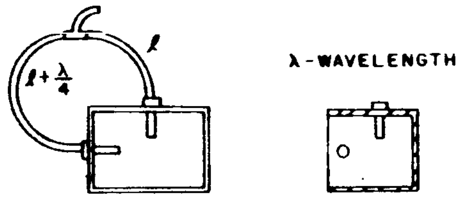
$\ell + \frac{\lambda}{4}$
$\ell$
λ-WAVELENGTH

A. ORTHOGONAL EXITATION WITH CABLE-LENGTH PHASING

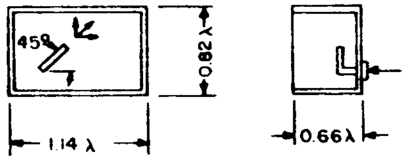
45°
$\ell$
0.82λ
1.14 λ
0.66λ

B. QUADRATURE PHASING OF ORTHOGONAL COMPONENTS
WITH RECTANGULAR CAVITY

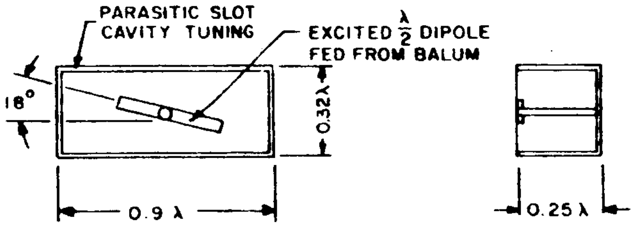
PARASITIC SLOT
CAVITY TUNING
EXCITED $\frac{\lambda}{2}$ DIPOLE
FED FROM BALUM
18°
0.32λ
0.9 λ
0.25 λ

C. DIPOLE EXCITED SLOT (A SLOT EXCITED DIPOLE ALSO MAY BE USED)

Figure I.3.C-10. Techniques Considered For Achieving Circularly Polarized Radiation From a Cavity

The use of a two-turn helix within a flush-mounted circular cavity was investigated. The beamwidth of such units varies from 80° to 100° at half power points and axial ratios are usually no better than 3 or 4 db even on-axis. The principal disadvantage is cavity size, however, which is about one foot in diameter.

3). Corporate Feed Structure - A corporate feed couples the eight cavities of the L-band omni-antenna to the transponder. Equal-amplitude in-phase signals are fed to each cavity by seven power splitters. The variation of the corporate structure mismatch with power splitter and antenna VSWR's is of vital concern. If the VSWR at the corporate feed input is too high, the reflection loss will reduce system margin by decreasing radiated power. A tabulation of the corporate feed VSWR is listed in Table I.3.C-8 and is based on the assumption that all eight cavities exhibit the same mismatch and that the seven power splitters are identical.

TABLE I.3.C-8

A TABULATION OF THE CORPORATE FEED VSWR

$\sigma_\alpha$ = antenna cavity VSWR

$\sigma_t$ = power splitter VSWR

$\sigma_c$ = corporate feed VSWR

| $\sigma_t$ | $\sigma_c$ | | |
|---|---|---|---|
| | for $\sigma_\alpha = 1.0$ | for $\sigma_\alpha = 1.2$ | for $\sigma_\alpha = 1.5$ |
| 1.1 | 1.18 | 1.28 | 1.55 |
| 1.2 | 1.37 | 1.44 | 1.68 |

For simplifying the mathematics in computation, the following effects were ignored: (1) power splitter insertion loss, (2) VSWR masking by line losses which may be .08 db/ft, (3) re-reflection by one splitter of the reflected power from the succeeding splitter.

The VSWR of each antenna should be no greater than 1.5. The power splitter VSWR is about 1.1. The corporate feed VSWR should then be no greater than 1.55 which corresponds to a reduction in radiated power of 0.2 db. Six feet of coax cable are required in the corporate feed so that about 0.5 db of line loss is present. The power splitter insertion loss will be about 0.1 db per split or 0.3 db from corporate feed input to each cavity. Total losses due to line-attenuation, splitter insertion, and reflection will be 1.0 db.

b. Low Power Telemetry (1/4 watt)

The primary limiting factor in the low power system is the necessity of transmitting horizon sensor pulses with rise times of about 40 milliseconds. Since the pulses follow an approximate exponential rise, the maximum rate of frequency change of the subcarrier is approximately given by:

$$\delta = \frac{2.2\,\Delta f}{t_r}$$

where $\Delta f$ is the peak subcarrier frequency change and $t_r$ is the pulse rise time. Solving for the change in terms of peak subcarrier frequency change yields:

$$\delta = 55\,\Delta f \quad \text{cps/sec.}$$

The equivalent noise bandwidth ($2\,B_{10}$) is given by:

$$2\,B_{10} = 6.66\sqrt{\frac{\delta}{3.28}}$$

or

$$2\,B_{10} = 27.2\sqrt{\Delta f}$$

The output signal to noise is proportional to $\Delta f^2$ while the input carrier to noise is proportional to $2\,B_{10}$. Thus a compromise must be reached to give proper operation. Because the subcarrier would be used to send commutated data requiring a high degree of accuracy (better than 5%), this must also be considered. To obtain this degree of accuracy, a deviation of at least 50 cycles is needed. Therefore, $2\,B_{10}$ is equal to 193 cycles. For this case we can use predection filtering to determine the noise bandwidth. For IRIG Channel #2, the bandwidth is 84 cycles. Such a bandwidth requires a modulation index of 1.65 radians if three subcarriers are used. The parameters for the proposed system are listed in Table I.3. C-6.

This system, because of the type and amount of data to be transmitted, must operate in a marginal carrier-to-noise area. Because the modulation index is relatively high for all the subcarriers, a small change in the subcarrier output levels will cause a fairly large change in the received power, both for the carrier and individual subcarriers. Considering the low margin in the entire system, the use of the 1/4 watt system is questionable.

## 7. SUMMARY OF SIZE, WEIGHT AND POWER REQUIREMENTS

A summary of size, weight, and power requirements for the telecommunications subsystem is presented in Table I.3.C-9.

### TABLE I.3.C-9

### SUMMARY OF TELECOMMUNICATIONS SUBSYSTEM SIZE, WEIGHT AND POWER REQUIREMENTS

| Subsystem | Size | Weight (lbs) | Power |
|---|---|---|---|
| TV Transmission | | | |
| Power Amplifier Transmitter | 5" x 5" x 10" | 8 | |
| Power Supply | 5" x 5" x 10" | 4 | 140 watts @ -27V ± 5% |
| Tape Recorder | 14" diam. x 7" | 17 | 10 watts @ -24-1/2V ± 1/2V<br>400 cps ± 1% square wave<br>20V P-P into 2K ohms |
| High gain antenna | 30" dish | 6 | 10 watts @ -27V ± 10%<br>(intermittent) |
| Tracking Telemetry and Control | | | |
| Transponder | 7" x 7" x 5" | 11 | +250V ± 3% @ 23 ma<br>+150V ± 3% @ 12 ma |
| | 7" x 7" x 5" | 6.25 | +15V ± 5% @ 376 ma<br>-15V ± 5% @ 88 ma<br>+5.75V ± 2.5% @ 1.1 amp |
| Telemetry (commutator) | 5" x 5" x 5" | 4 | 5 watts @ +27V ± 10% |
| (VCO) | 4" x 4" x 5-1/2" | 2 | |
| Command & Timing | 8" x 5" x 4"<br>8" x 7" x 4" | 3.25<br>3.00 | -15V ± 5% @ 200 ma<br>-24-1/2V ± 5% @ 100 ma |
| Omni Antenna 8 Cavities | 2" x 3" x 7"<br>10 lbs. total | (1.25 ea.) | None |

RE-ORDER No. 62-459

## D. VIDEO SUBSYSTEM

### 1. Subsystem Description

A block diagram of the video subsystem is shown in Figure I.3.D-1. Two cameras are provided, and each is associated with a Camera Electronics unit. The cameras are exposed alternately at intervals of 6 seconds, so that the total elapsed time between successive exposures of a given camera is 12 seconds. The video-signal outputs of the cameras are added together in a combiner unit. The stored image is read out from each camera alternately over a period of 6 seconds. One camera is erased and prepared for its next exposure while the other is being read.

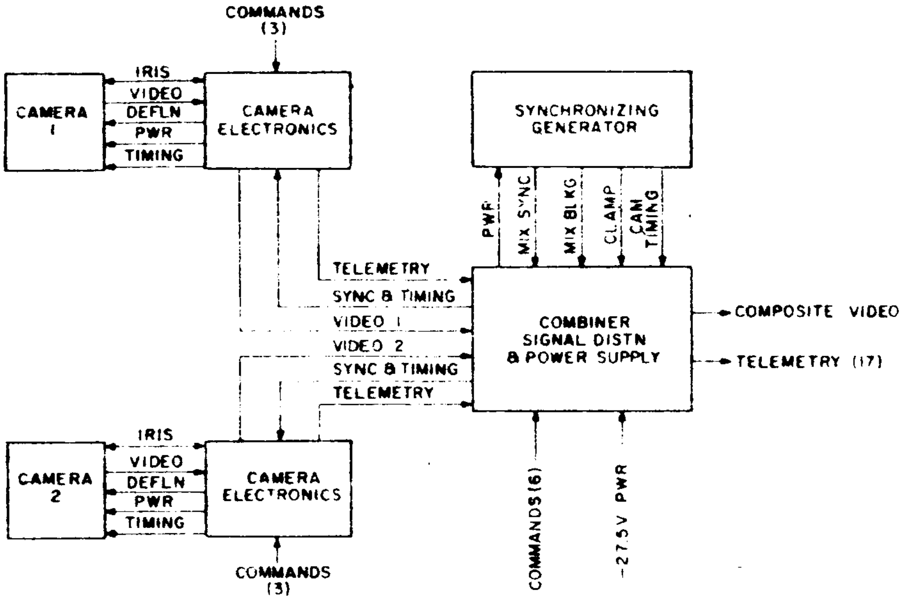
COMMANDS (3)
CAMERA 1
IRIS
VIDEO
DEFLN
PWR
TIMING
CAMERA ELECTRONICS
SYNCHRONIZING GENERATOR
PWR
MIX SYNC
MIX BLKG
CLAMP
CAM TIMING
TELEMETRY
SYNC & TIMING
VIDEO 1
VIDEO 2
SYNC & TIMING
TELEMETRY
COMBINER SIGNAL DISTN & POWER SUPPLY
COMPOSITE VIDEO
TELEMETRY (17)
CAMERA 2
IRIS
VIDEO
DEFLN
PWR
TIMING
CAMERA ELECTRONICS
COMMANDS (3)
COMMANDS (6)
-27.5V PWR

Figure I.3.D-1. Block Diagram of the Television Subsystem

The timing and synchronizing signals associated with camera operation are provided by a synchronizing generator. These signals are routed to the Combiner Signal Distribution and Power Supply, where they are utilized as required by the combiner section and distributed to the two cameras via the corresponding Camera Electronics units.

The Camera Electronics unit supplies the necessary power, timing, and deflection signals to its associated camera, accepting the basic timing pulses from the Synchronizing Generator and providing the appropriate amplifying or wave-shaping. It also has servo circuits to control the camera iris in response to commands from the command receiver, and to deliver telemetry signals to the signal distribution circuits.

Each camera contains a vidicon camera tube with its associated focus-deflection coil assembly and optical system, including the iris and iris drive mechanism and the shutter.

The following tabulation shows the major parameters of the video subsystem:

TABLE I. 3. D-1.

MAJOR PARAMETERS OF THE VIDEO SUBSYSTEM

| | |
|---|---|
| Number of scanning lines | 1024 |
| Frame time (V) | 6 seconds |
| Vertical deflection frequency (read) | 1/6 cps. |
| Vertical deflection frequency (erase) | 7281-7/9 cps. |
| Horizontal deflection frequency | 170 2/3 cps. |
| Horizontal period (H) | 5. 859 milliseconds |
| Horizontal blanking, 0. 05 H | 0. 293 milliseconds |
| Vertical blanking, 0. 015 V | 90 milliseconds |
| Baseband | 62. 5 kc |
| Vertical resolution (nominal) | 700 lines |
| Horizontal resolution | 696 lines |

Straight binary counters are used to obtain the deflection frequencies in order to simplify the required counter chain. With the blanking percentages chosen and the baseband available (62. 5 kc), the frame time is calculated to be 6 seconds. A total of 1024 scanning lines requires a count of $2^{10}$ between vertical and horizontal deflection frequencies, leading to the value shown (170-2/3 cps) for the horizontal deflection frequency.

The vertical deflection frequency is increased during the erase cycle until it is higher by a factor of 42-2/3 than the horizontal deflection frequency, which remains unaltered. This approach has proved to improve the erasure. The reason for adopting the numerical ratio of 42-2/3 is that it provides a triple interlace of the erasure scanning and should effectively prevent the formation of erasure bars that result from phase lock occurring between the horizontal and vertical frequencies, which can happen if the erase vertical frequency is free-running. The ratio is easily realized in a frequency-dividing circuit having a division ratio of 3, as will be discussed later.

A block diagram of the generator counter circuit is shown in Figure I. 3. D-2. The four basic output frequencies are as follows:

$f_o$ - the basic frequency of 1/12 cps, used to time the expose and erase cycles of each camera

$f_V$ - the vertical deflection frequency (1/6 cps), used during the read cycle

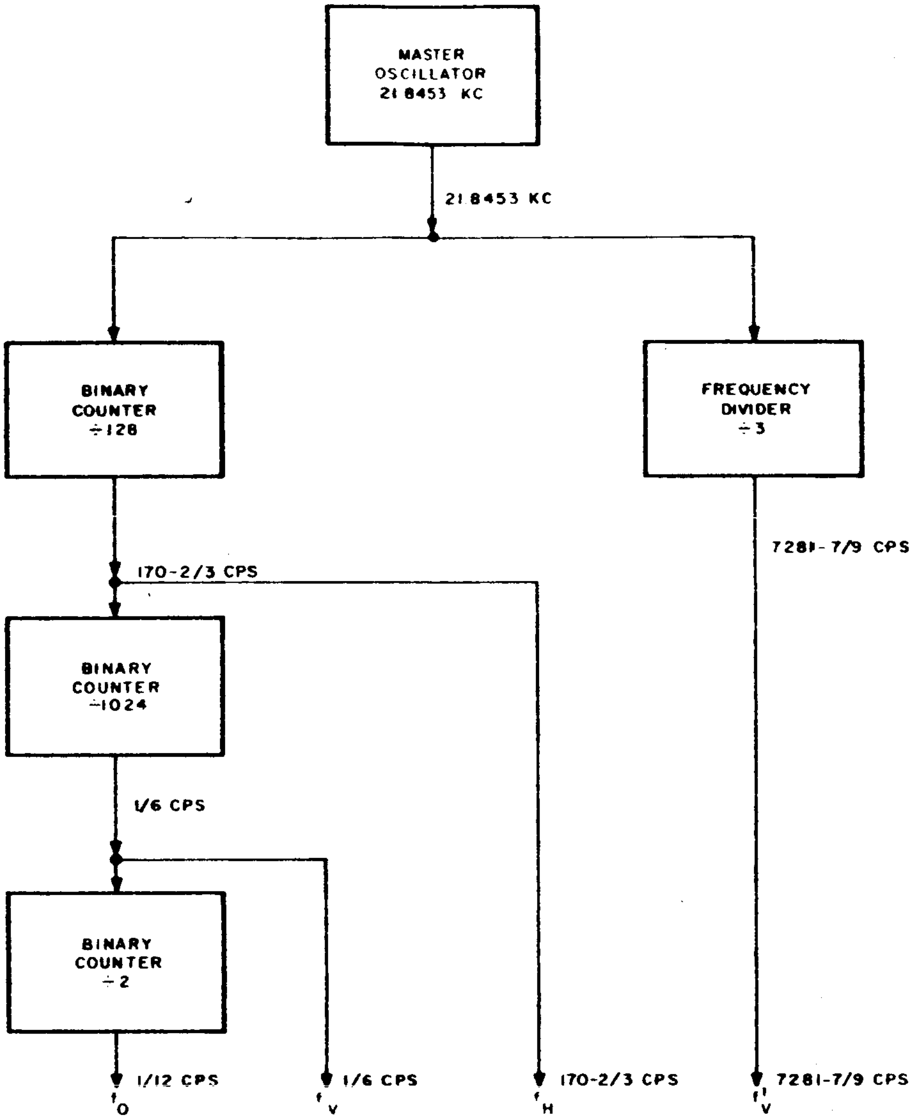
MASTER OSCILLATOR 21.8453 KC
21.8453 KC
BINARY COUNTER ÷128
FREQUENCY DIVIDER ÷3
170-2/3 CPS
7281-7/9 CPS
BINARY COUNTER ÷1024
1/6 CPS
BINARY COUNTER ÷2
1/12 CPS
f O
1/6 CPS
f V
170-2/3 CPS
f H
7281-7/9 CPS
f' V

Figure I. 3. D-2. Block Diagram of the Generator Counter Circuits

$f_H$ - the horizontal deflection frequency, used during both read and erase cycles

$f_V'$ - the vertical frequency, used during the erase cycle.

These basic signals are processed in wave-shaping circuits to provide the required pulses of these respective frequencies for use in the system. The following pulse signals are derived from the above basic frequencies:

Horizontal Sync for Camera Electronics Unit No. 1

Vertical Drive (read) for Camera Electronics Unit No. 1

Vertical Drive (erase) for Camera Electronics Unit No. 1

Horizontal Sync for Camera Electronics Unit No. 2

Vertical Drive (read) for Camera Electronics Unit No. 2

Vertical Drive (erase) for Camera Electronics Unit No. 2

Shutter Pulse for Camera No. 1

Erase Pulse for Camera No. 1

Camera Gate Pulse for Camera No. 1

Shutter Pulse for Camera No. 2

Erase Pulse for Camera No. 2

Camera Gate Pulse for Camera No. 2

Clamp Pulse for Combiner Unit

Mixed Sync for Combiner Unit

Mixed blanking for Combiner Unit

The camera gate pulse is used to alternate between the vertical read and erase drive signals for a given camera, thus placing it alternately in the read and erase modes. The camera gate pulse for one camera is 180° out of phase with that for the other in order to permit the desired staggered timing relationship between read and erase. This is shown in the basic camera timing diagram, Figure I. 3. D-3.

Various other signals are required, but these are formed in the appropriate unit and timed by the above listed pulse signals. For example, the shutter is driven by a shutter drive circuit which is contained in the Camera Electronics unit and driven by the shutter pulse. The required signals for the cathode and G-1 grid of the vidicon are also formed in the Camera Electronics unit.

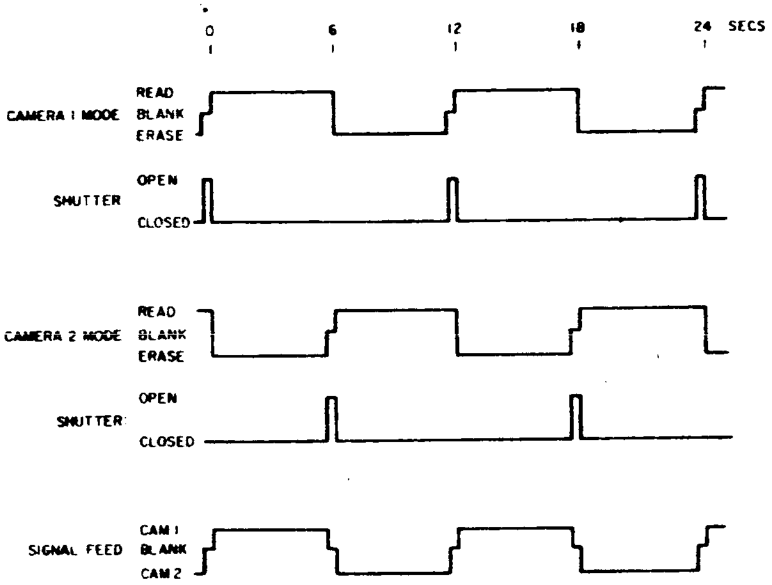

Figure I. 3. D-3. Basic Camera Timing Diagrams

## 2. VIDEO SUBSYSTEM DESIGN

### a. Camera

The camera block diagram is shown in Figure I. 3. D-4. The camera contains a vidicon camera tube mounted in a focus-deflection yoke assembly. Associated with the vidicon is an electromagnetic focal-plane shutter which is timed by means of the shutter pulse to open just before the readout interval (see Figure I. 3. D-3). During readout, an appropriate value of beam current is established by means of suitable signal waveforms applied to the grid and cathode of the vidicon. The return beam is cut off by blanking signals. During erase, a uniform illumination is applied to the vidicon target for a period of about 200 milliseconds. This illumination dissipates the charge left on the photoconductor by the preceding exposure. The beam current is then increased, and the vertical deflection frequency is changed to the value of approximately 7000 cps used for erase, giving about 1000 frames of erase scan during the 6-second erase interval.

Light input to the vidicon is regulated by an electronically controlled iris diaphragm. The iris is actuated by a motor, and its degree of opening is indicated by the voltage at the arm of a potentiometer geared to the iris drive. This voltage is compared to the voltage divider, and the motion operates to balance the resulting Wheatstone bridge. Several pre-set voltage dividers are provided, each corresponding to one of a set of desired apertures. The desired aperture is chosen by selecting the appropriate voltage divider by ground command through the command receiver. Redundant iris drive motors are provided to improve reliability. A video preamplifier raises the level of the vidicon output, and provides a suitable drive for the video amplifier contained in the Camera Electronics unit.

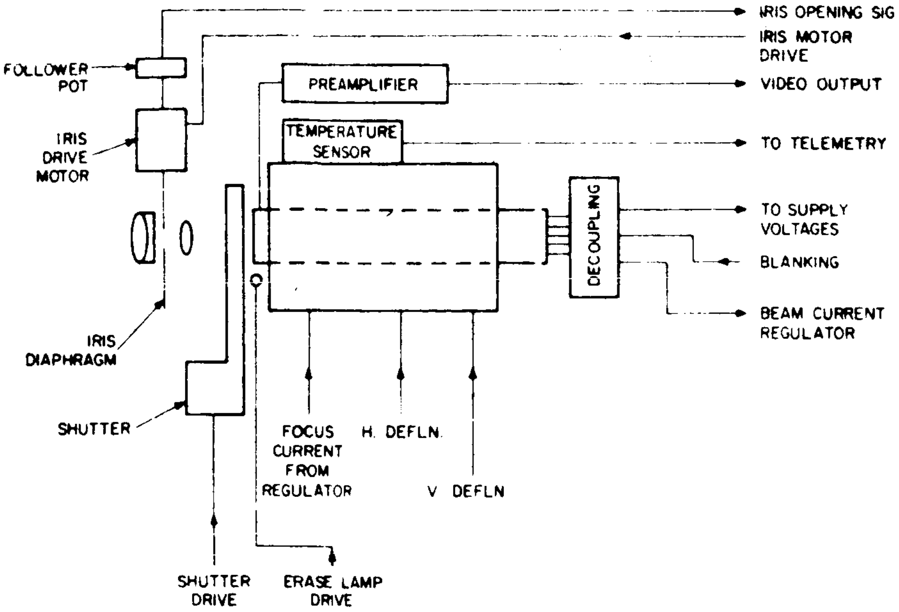
IRIS OPENING SIG
IRIS MOTOR DRIVE
FOLLOWER POT
PREAMPLIFIER
VIDEO OUTPUT
IRIS DRIVE MOTOR
TEMPERATURE SENSOR
TO TELEMETRY
DECOUPLING
TO SUPPLY VOLTAGES
BLANKING
BEAM CURRENT REGULATOR
IRIS DIAPHRAGM
SHUTTER
FOCUS CURRENT FROM REGULATOR
H. DEFLN.
V DEFLN
SHUTTER DRIVE
ERASE LAMP DRIVE

Figure I.3.D-4. Block Diagram of the TV Camera

The temperature of the camera case is sensed and fed out as a telemetry signal.

b. Camera Electronics Unit

The Camera Electronics unit accepts H Sync, V Sync, V' Sync, shutter pulse, erase pulse, and camera gate pulse signals from the synchronizing generator. Using these signals, it develops deflection-current waveforms for both horizontal and vertical deflection, and it commutates the vertical deflection signals between that used for read (1/6 cps) and that used for erase (7281-7/9 cps) by using the camera gating signal. The output circuits are timed from the shutter pulse driving the shutter, and it furnishes output pulses to the erase lamp which are timed from the erase pulse.

The circuit for controlling the iris drive motor to balance the Wheatstone Bridge is part of the Camera Electronics unit. It commands selection of the pre-set voltage dividers to be used in effecting the balance. Power supplies for the camera tube and focus-current and beam-current regulators are included. A video amplifier is provided to raise the signal level provided by the preamplifier in the camera in order to drive the combiner amplifier.

There are seven command inputs, three for selection of the iris opening and four to select alternatives between iris drive motors and clutches. The six telemetry outputs are video, focus current, camera temperature, Camera Electronics unit temperature, vidicon high voltage, and iris opening.

c. Combiner, Distribution, and Power Supply Unit

The basic function of this unit is to accept inputs from the two cameras and to gate them so that their frames occur in sequence. In addition, it inserts horizontal and vertical blanking while clamping each line at black level. A d-c-coupled clipper provides a clean base line accurately related to black. This clipping operation removes any spurious signal occurring in the video by eliminating any part which extends below black. Were this operation not performed, there could be interference with picture sync at the receiver. Following this clipping operation, the signal passes through an AGC amplifier which is intended to keep the signal level reasonably constant to ensure a constant transmitter modulation, thus avoiding unnecessary addition of noise in the transmission link. Finally, mixed synchronizing is added to the signal. Simple rectangular pulses provide the horizontal sync; the vertical sync consists of a serrated signal similar to that used in EIA sync, except that equalizing pulses and double-frequency serrations are not needed since the system is not interlaced. The leading edges of the vertical pulse blocks are coherent with those of the horizontal pulses to retain horizontal sync at the receiver during transmission of the vertical sync.

This unit also distributes power to the Camera Electronics units and the Synchronizing Generator and provides the main ON-OFF switch for the video subsystem. In addition, it distributes sync and timing signals to the Camera Electronics units and provides all telemetry outputs, some of which are generated within the unit. It has a pair of ± 6.3-volt power supplies, which are mutually redundant. It accepts the following commands to select between these supplies.

Power Supply A ON
Power Supply A OFF

Power Supply B ON
Power Supply B OFF

Video Subsystem ON
Video Subsystem OFF

It provides the following telemetry outputs, which represent the complete telemetry information for the video subsystem:

Vidicon Heater 1
Vidicon Heater 2

Horizontal Sync
Vertical Sync

Video
Vidicon Magnetic Focus
Camera Temperature
Camera Electronics Temperature
Vidicon High Voltage
Iris Opening

} Camera No. 1

Video
Vidicon Magnetic Focus
Camera Temperature
Camera Electronics Temperature
Vidicon High Voltage
Iris Opening

Camera No. 2

Composite Video Output

A block diagram of the combiner unit is shown in Figure I.3.D-5. The outputs of the cameras feed into gates which are controlled by camera gate signals. These serve to gate in the video signal while their respectively associated cameras are reading and to gate out the spurious signals generated during erase. The outputs of the gates are added in a resistive adder circuit and are amplified and clamped. Mixed blanking is then added, and the signal is clipped before the d-c component restored by the clamping is lost. The signal now contains an accurate black reference; it is passed through an AGC amplifier to cause its peak-to-peak amplitude to assume a chosen value. Mixed sync is then added in a sync adding stage.

d. Problem Areas

(1) Erase - Adequate erasure within a 6-second period is necessary for satisfactory subsystem performance. RCA experience indicates that an important feature in obtaining erasure involves making a large number of passes of the scanning beam over the target during the erase cycle. Therefore, the system described, which has proved satisfactory in another camera system, is provided.

(2) Smear - Smear results from the motion of the intersection of the optic axis at the surface being imaged. The motion is caused by the velocity of the satellite in combination with its attitude perturbations. Conservative design would indicate that the motion should be small compared to the projection of a scanning line on the lunar surface. However, this places a constraint on the exposure time, and the higher the resolution the greater is the constraint. The shorter the exposure time, the greater must be the image brightness for a given signal-to-noise ratio. Thus, a compromise must be made in which the relative importance of these factors is considered.

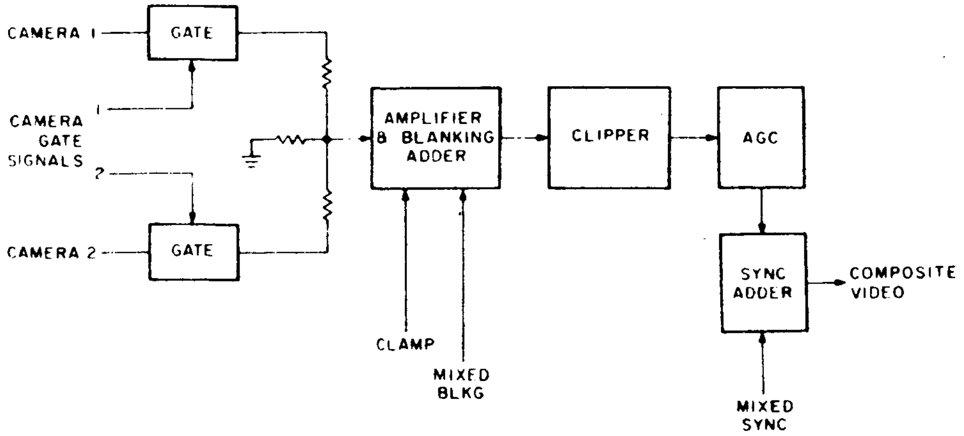

Figure I.3.D-5. Block Diagram of the Combiner Unit

3) Shutter Shock - The actuation of the electromagnetic shutter causes a mechanical shock to be applied to the camera housing as the shutter armature hits the mechanical stop which limits its travel. This shock can cause microphonics to appear in the video output; at least one source of these microphonics is the camera tube itself. The technique of allowing the microphonic oscillations to damp out before starting readout is effective, but it results in reducing the time available for erasure. It is anticipated that some improvement of the present situation will be required.

4) Camera Optics - In support of the video subsystem study for the LOC program, applicable optical lens systems have been investigated. Some of the lens systems considered which are currently available are listed in Table I.3.D-2. The choice of lenses was predicated on weight, size, availability, and optical requirements of scene illuminance and image immobilization (exposure time). The equivalent focal lengths establish the scale factor (ratio of focal length to altitude) required to satisfy the total linear object field coverage, as well as the angular resolution requirements.

TABLE I.3.D-2.

TV LENS CHARACTERISTICS

| EFL (mm) | f/No. | Type | Weight (pounds) | Size (mm) | |
|---|---|---|---|---|---|
| | | | | Dia. | Length |
| 50 | 1.4 | Dioptric | 0.6 | 46.6 | 65.5 |
| 75 | 1.4 | Dioptric | 1.2 | 60 | 112 |
| 100 | 2.0 | Dioptric | 1.5 | 70 | 140 |
| 150 | 1.5 | Catadioptric | 3.0 | 110 | 120 |
| 180 | 1.5 | Catadioptric | 4.0 | 120 | 145 |
| 400 | 1.5 | Catoptric | 12 | 268 | 320 |
| 430 | 1.5 | Catoptric | 13 | 282 | 345 |
| | | | | | |
| 50 | 0.75 | Dioptric | 3 | 85 | 78 |
| 100 | 0.75 | Dioptric | 5 | 180 | 170 |
| 150 | 0.75 | Dioptric | 5 | 254 | 250 |
| 350 | 1.4 | Catadioptric | 12 | 280 | 533 |

The dioptric lenses need no lens modifications, with the exception of the 100-millimeter lens, but will require lens housing modifications to satisfy the environmental qualifications. For the 100-millimeter lens, a lens design modification would be required to obtain a relative aperture of 1.5.

[illegible] No. 62-489

For the intermediate range of focal lengths, a catadioptric lens system is recommended, because a dioptric system having a relative aperture of 1.5 would weigh more. The supporting lens housing is of the same material as the metal reflecting mirror. Beryllium mirrors weigh 1/15 and aluminum 1/6 of a comparable-size quartz mirror. Surfaces of metal mirrors are coated with an amorphous metal coating consisting of a nickel, nickel-phosphor combination.

For the 400-mm to 430-mm focal length, a possible system is the Baker three-reflecting-element catoptric anastigmat. The optical schematic of this lens system is shown in Figure I.3.D-6. This system was suggested by the Perkin-Elmer Corporation. Itek, Incorporated suggested a Cassegrainian system having a quartz aspheric corrector plate located at the center of curvature of the primary reflective lens. The location of the secondary reflecting lens is such as to locate the vidicon behind the primary lens. A field flattener would be located in front of the focal-plane shutter. The Itek system is slightly longer than 430 mm, and the Perkin-Elmer system has an over-all length approximately 0.75 of the focal length. The weights of both systems are approximately the same; 10 to 12 pounds.

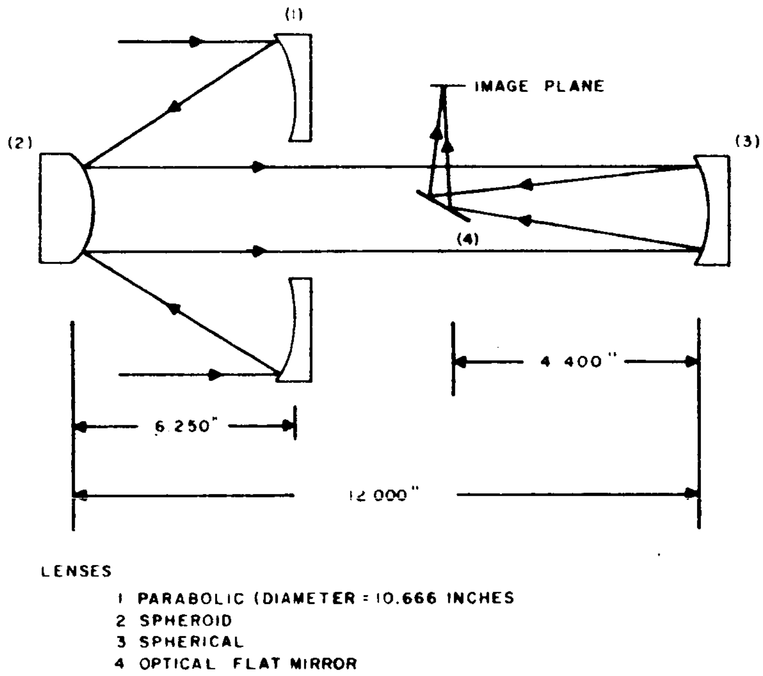

Figure I.3.D-6. Optical Schematic of a Catadioptric Anastigmat

## 3. SUMMARY OF WEIGHT AND POWER REQUIREMENTS

The estimates of weight and power requirements are based on recorded data from the Nimbus TV systems, to which this system bears some similarity. Points of difference include the following:

(a) The Nimbus system includes no synchronizing generator, so some additional weight must be allowed for this.

62-459

(b) The Nimbus system employs three cameras; the proposed system has only two.

(c) The erasure required in the proposed system must take place within a single frame time, whereas several frames are used in Nimbus.

The following tabulation shows the approximate sizes and weights of the units:

TABLE I. 3. D-3.

ESTIMATED SIZE AND WEIGHT OF THE VIDEO SUBSYSTEM

| Units | Over-all Dimensions (Inches) | Weight (lb) | Number Required | Weight per System (lb) |
|---|---|---|---|---|
| Camera | 8 x 6-1/2 x 7* | 7 | 2 | 14 |
| Camera Electronics | 6 x 13 x 2 | 5.7 | 2 | 11.4 |
| Sync Generator | 6 x 13 x 2 | 4.3 | 1 | 4.3 |
| Combiner - Power Supply | 6 x 13 x 2 | 5 | 1 | 5 |
| Total Weight (not including lenses) | | | | 34.7 |

*Not including lenses. Main body roughly conical in shape, 6.5 inches diameter x 7 inches high. The 8-inch dimension represents the 1.5-inch protrusion of the shutter on one side.

The total power drain is estimated to be in the order of 50 watts total.

## 4. GROUND STATION EQUIPMENT

### a. Description of Ground Equipment

A block diagram of the ground-station system is shown in Figure I. 3. D-7. Facilities are provided for both magnetic-tape storage of the pre-detected video information furnished by the ground communications equipment and direct display of the detected video on a high-quality kinescope, where the images are filmed by a 35-mm camera. In addition, the magnetic tape can be played back through the system at any time, in which case the detected video is also displayed on the kinescope and the images in turn are filmed by the 35-mm camera.

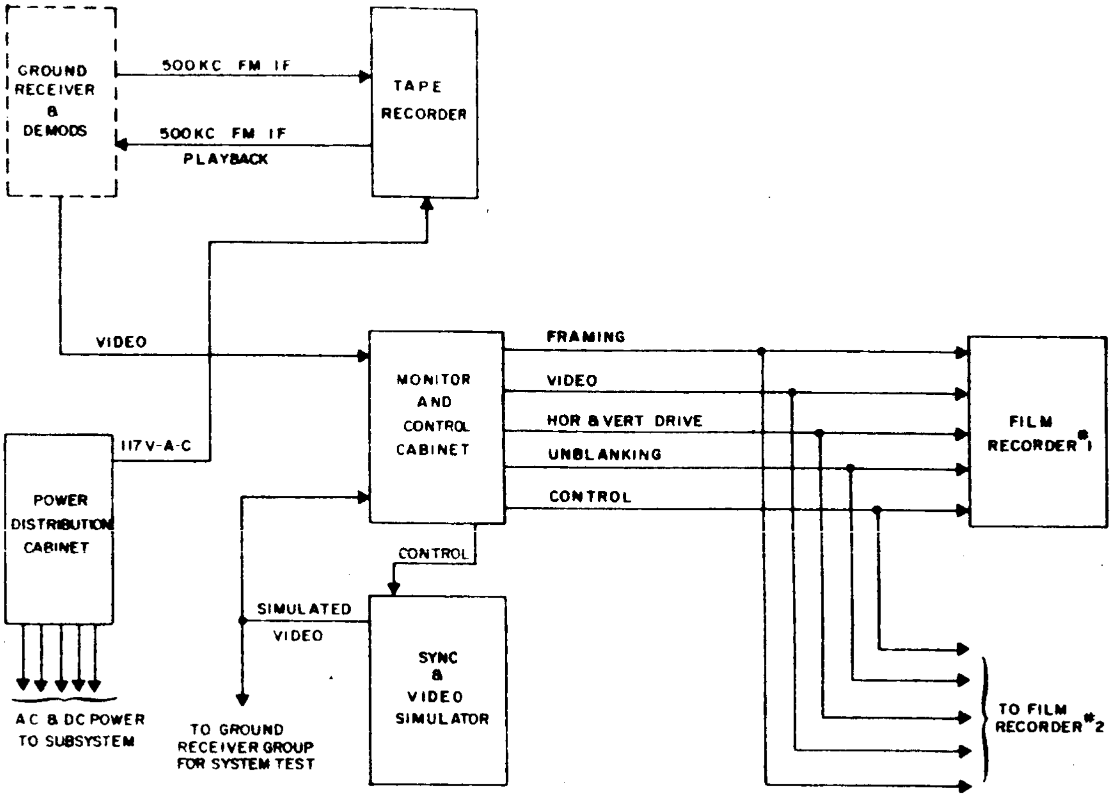
GROUND RECEIVER & DEMODS
500KC FM IF
TAPE RECORDER
500KC FM IF PLAYBACK
VIDEO
MONITOR AND CONTROL CABINET
FRAMING
VIDEO
HOR & VERT DRIVE
UNBLANKING
CONTROL
FILM RECORDER #1
117V-A-C
POWER DISTRIBUTION CABINET
CONTROL
SIMULATED VIDEO
SYNC & VIDEO SIMULATOR
AC & DC POWER TO SUBSYSTEM
TO GROUND RECEIVER GROUP FOR SYSTEM TEST
TO FILM RECORDER #2

Figure I.3.D-7. Block Diagram of the TV Recording and Display Equipment

The system contains the following major subsystems:

Ground Receiver and Demodulators (Figure I.3.D-8)

Power Distribution Cabinet (Figure I.3.D-9)

Monitor and Control Cabinet (Figure I.3.D-10)

Sync and Video Simulator (Figure I.3.D-11)

Film Recorder (Figure I.3.D-12)

Further details of each unit are given in the referenced figures.

RE-ORDER No. 62-459

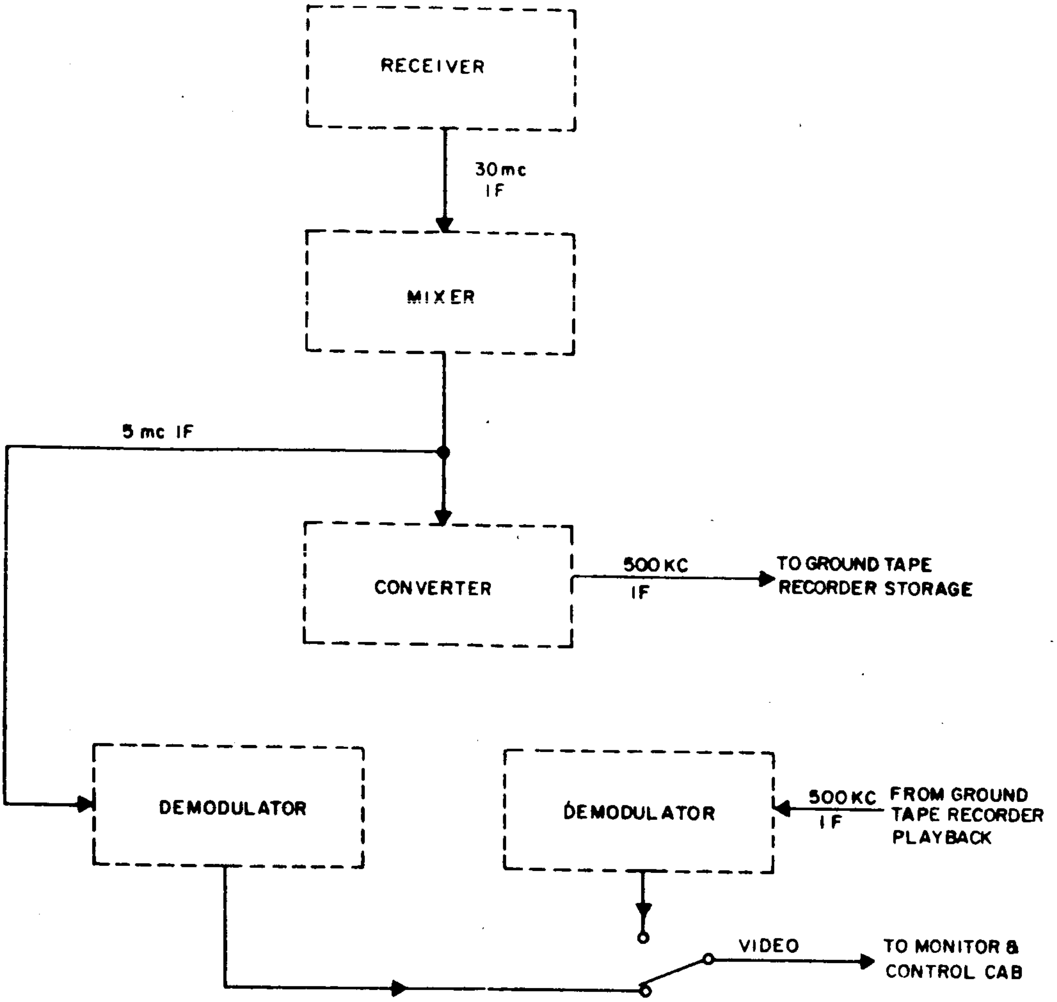
RECEIVER
30 mc IF
MIXER
5 mc IF
CONVERTER
500 KC IF
TO GROUND TAPE RECORDER STORAGE
DEMODULATOR
DEMODULATOR
500 KC IF
FROM GROUND TAPE RECORDER PLAYBACK
VIDEO
TO MONITOR & CONTROL CAB

Figure I.3.D-8. Block Diagram of Ground Receivers and Demodulators

Most of the a-c and d-c power for the system is supplied from the power distribution cabinet. One notable exception is the kinescope high-voltage supply, which is part of the film recorder equipment.

The processed video signal, horizontal and vertical sync, and control signals for the film recorder and kinescope are provided by the monitor and control equipment. This same equipment is utilized for processing the simulated video signal, the direct video signal, or the magnetic-tape playback information.

The sync and video simulator unit is utilized to generate a composite simulated video signal. This signal is utilized in testing and checking the television display equipment. As a more complete test, the simulated video can be transferred to the ground communications equipment, there to be passed through a simulated transmission link before being fed to the display equipment.

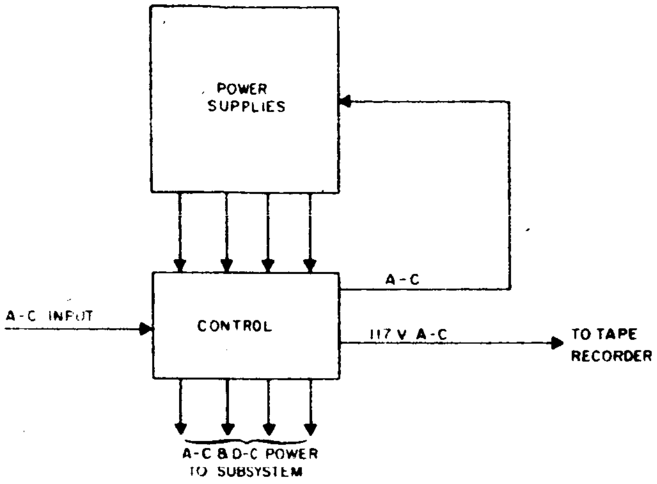
POWER SUPPLIES
A-C
A-C INPUT
CONTROL
117 V A-C
TO TAPE RECORDER
A-C & D-C POWER TO SUBSYSTEM

Figure I.3.D-9. Block Diagram of Power Distribution Cabinet

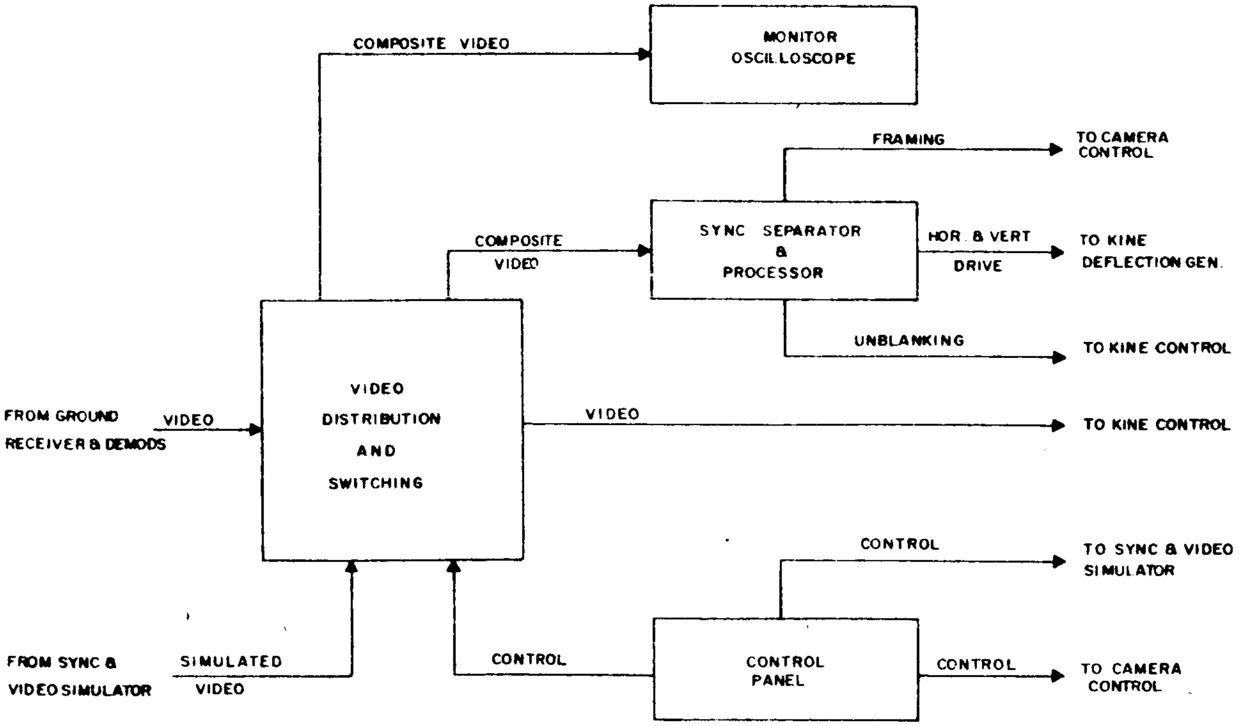
COMPOSITE VIDEO
MONITOR OSCILLOSCOPE
FRAMING
TO CAMERA CONTROL
COMPOSITE VIDEO
SYNC SEPARATOR & PROCESSOR
HOR & VERT DRIVE
TO KINE DEFLECTION GEN.
UNBLANKING
TO KINE CONTROL
FROM GROUND RECEIVER & DEMODS
VIDEO
VIDEO DISTRIBUTION AND SWITCHING
VIDEO
TO KINE CONTROL
CONTROL
TO SYNC & VIDEO SIMULATOR
FROM SYNC & VIDEO SIMULATOR
SIMULATED VIDEO
CONTROL
CONTROL PANEL
CONTROL
TO CAMERA CONTROL

Figure I.3.D-10. Block Diagram of the Monitor and Control Cabinet

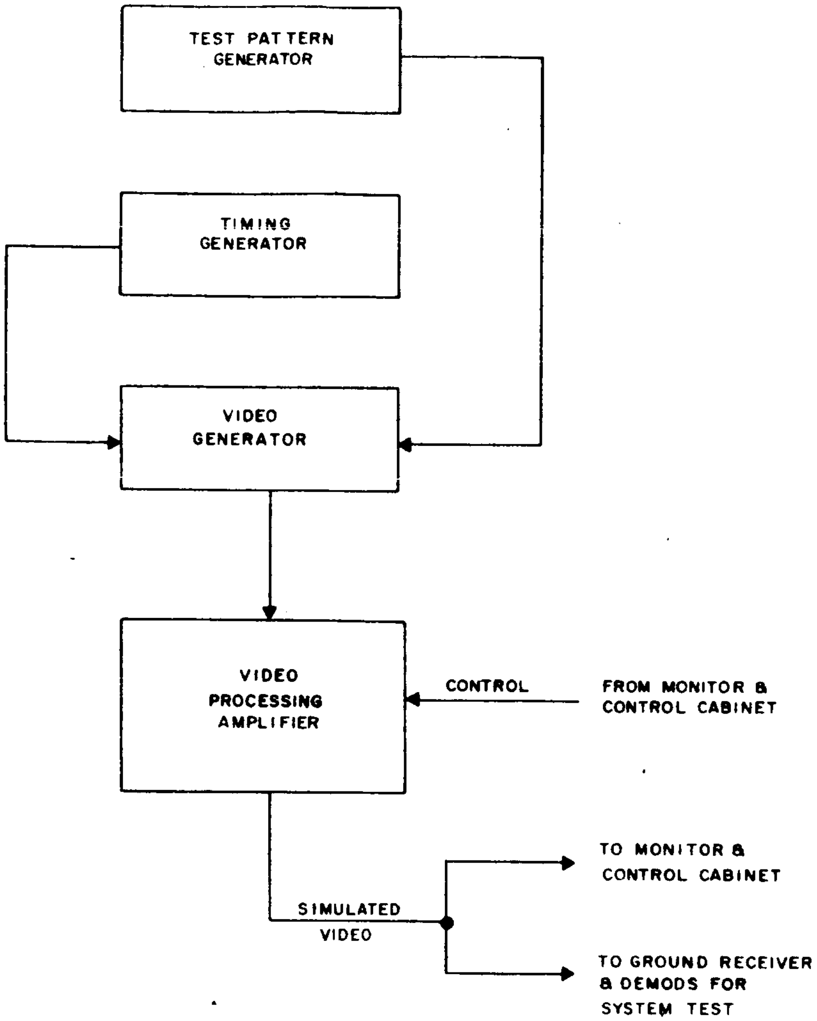
TEST PATTERN GENERATOR
TIMING GENERATOR
VIDEO GENERATOR
VIDEO PROCESSING AMPLIFIER
CONTROL
FROM MONITOR & CONTROL CABINET
SIMULATED VIDEO
TO MONITOR & CONTROL CABINET
TO GROUND RECEIVER & DEMODS FOR SYSTEM TEST

Figure I. 3. D-11. Block Diagram of the Sync and Video Simulator

The film recorder cabinet contains the high-quality kinescope on which the slow-scan TV imaging is performed. A 35-mm pulse-advanced camera is provided to obtain a filmed record of the images displayed on the kinescope. In addition, a Polaroid camera is provided for quick-look pictures to determine the moment-to-moment status of the kinescope display as desired by the operator.

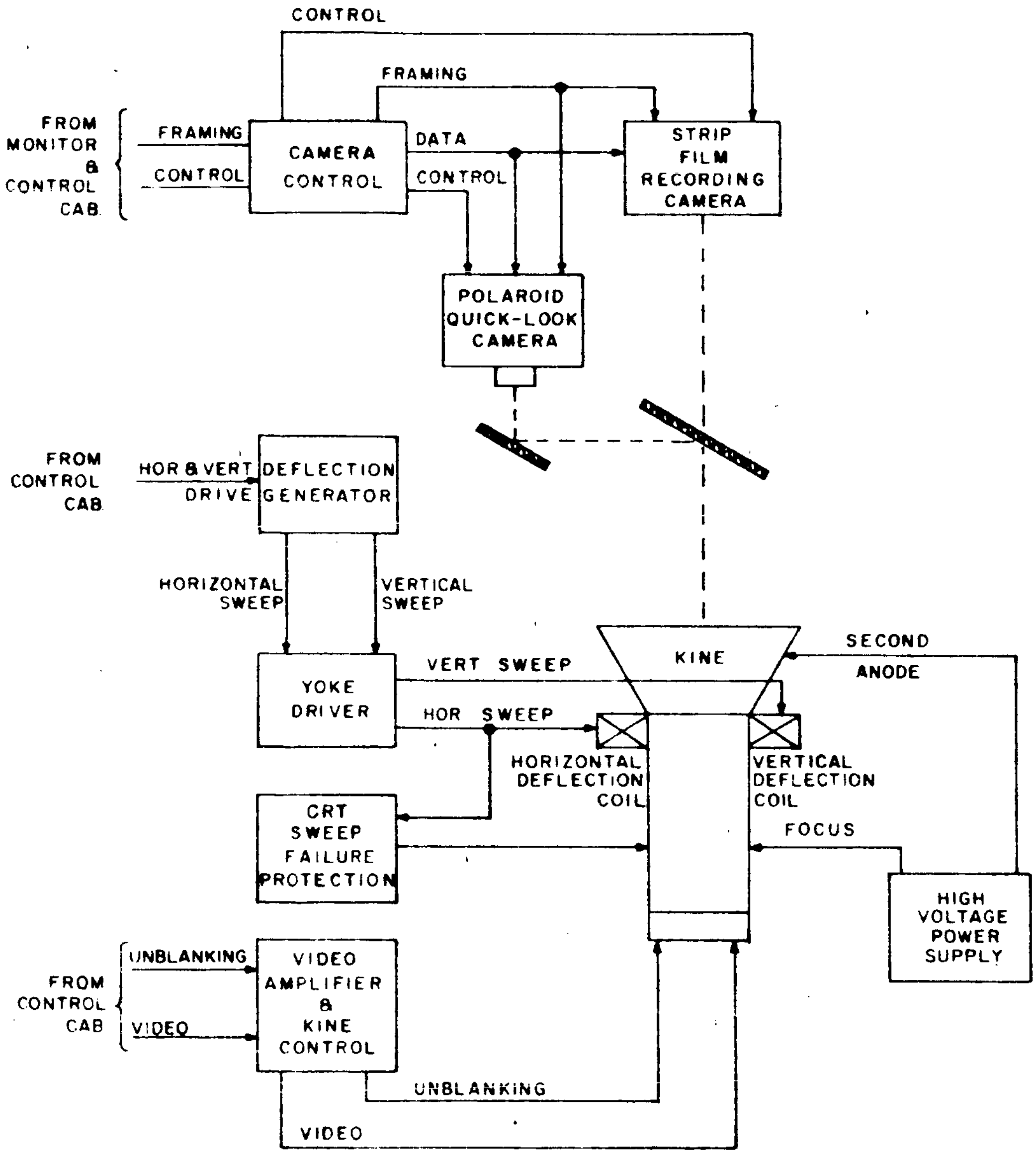
CONTROL
FRAMING
FROM MONITOR & CONTROL CAB
FRAMING
CONTROL
CAMERA CONTROL
DATA
CONTROL
STRIP FILM RECORDING CAMERA
POLAROID QUICK-LOOK CAMERA
FROM CONTROL CAB
HOR & VERT DRIVE
DEFLECTION GENERATOR
HORIZONTAL SWEEP
VERTICAL SWEEP
YOKE DRIVER
VERT SWEEP
HOR SWEEP
KINE
SECOND ANODE
HORIZONTAL DEFLECTION COIL
VERTICAL DEFLECTION COIL
CRT SWEEP FAILURE PROTECTION
FOCUS
HIGH VOLTAGE POWER SUPPLY
FROM CONTROL CAB
UNBLANKING
VIDEO
VIDEO AMPLIFIER & KINE CONTROL
UNBLANKING
VIDEO

Figure I.3.D-12. Block Diagram of the Film Recorder

1) Tape Recorder Cabinet - The tape recorder cabinet contains a wide-band, continuous, linear, magnetic tape system to record and play back the pre-detected video and telemetry signals received from the ground communications equipment. This recorder should have a bandwidth of approximately 1 megacycle. Presently available recorders having this bandwidth provide a minimum of 15 minutes recording time on a standard 14-inch reel at a tape speed of 120 inches per second. Thus, one reel would provide sufficient storage for the anticipated video output of the TV camera subsystem for one complete orbit.

Normally, the composite video signal from the ground communications equipment would be processed directly and supplied to the video display equipment for concurrent recording on the 35-mm film. Thus, the ground tape recorder would provide essential storage facilities for the video information in case of a malfunction during the direct display and film recording process. In addition, this magnetic tape record provides archival storage of the TV subsystem data in a desirable form.

2) Monitor and Control Cabinet (Figure I.3.D-10) - The equipment contained in the monitor and control cabinet consists of an oscilloscope monitor, sync separators, and a control and function indicator panel. The oscilloscope monitor is provided so that either real or simulated composite video may be monitored as desired. The sync separator unit contains the equipment necessary to generate horizontal and vertical sync pulses from the composite video provided by the communications ground equipment. It is anticipated that each sync separator unit will consist of a local oscillator which can be locked to the sync timing information contained in the composite video signal. The horizontal and vertical free-running local-oscillator frequencies will be nominally an integer multiple of the frequencies generated internally in the TV camera system (170-2/3 cps and 1/6 cps for the horizontal and vertical rates, respectively.

The control panel contains switches which control the system power, tape recorder, equipment functional mode, and the film recorder. The various functions will be indicated by lighted switches and indicators, making full use of color coding wherever feasible.

In addition, the monitor and control cabinet will provide equipment to generate a film camera pull-down pulse from the vertical sync, and distribute video, sync, blanking, and drive signals within the TV Recording and Display equipment. Gating of video and pulse waveforms to the appropriate kinescope, monitor, and film camera units will also be provided, as well as the drive circuits for the control-panel indicators and film-camera data boards.

3) Sync and Video Simulator (Figure I.3.D-11) - This unit is provided to supply various video signals for system checkout and calibration. The unit will contain the equipment and control panel necessary to generate and select the following simulated video signals:

(a) Horizontal Bars

(b) Vertical Bars

(c) Grating Pattern (combination of 1 and 2)

(d) Gray Scale (halftones)

(e) Resolution Pattern (sine-wave bursts in vertical pattern)

(f) Composite Pattern (combination of 3, 4, and 5)

[illegible] 62-489

Horizontal and vertical sync will be superimposed on all of these signals so that each is a composite video signal. Much of the circuitry for this unit will consist of standard digital circuits and building blocks in plug-in module form.

4) Film Recorder (Figure I.3.D-12) - The Film Recorder displays a full frame of video on a high-resolution cathode-ray tube for photographically recording the TV information. The equipment consists of a kinescope unit, a film camera with data board, and a Polaroid Land camera.

The kinescope unit utilizes a 5-inch CRT to display a full frame of video over the usable diameter of the CRT face. This image is passed through suitable optics to a pulse-advanced 35-mm film camera, where it is recorded on a nominal 18-by-24-mm format. The film is advanced a frame at a time during the vertical blanking time (90 milliseconds). The actual video pictures are recorded in an area 18-by-18-mm, the remaining frame area being used to record a data board containing a real-time clock, a frame counter, and a data slate board for hardwritten information.

In addition, a half-silvered mirror is utilized to reflect the kinescope image to a Polaroid camera for random-access photos of the CRT display, which in turn are processed for viewing in 10 seconds.

5) Video Sync Alternative - The sync separation scheme described above presupposes that the sync information is contained in the composite video signal and that amplitude stripping techniques can be used to remove the sync information. In other words, the peak-to-peak composite signal is greater in amplitude than the peak-to-peak video signal by the amount of sync amplitude. Thus it is apparent that, for a given FM transmission bandwidth, the greater the sync amplitude in the composite signal, the smaller the peak-to-peak video signal that can be transmitted. Thus, a greater peak-to-peak video signal could be sent through a given FM transmission link if the sync information were removed entirely or incorporated in the composite signal in other than an additive amplitude way.

One scheme which would allow the elimination of sync information from the actual video signal would be to transmit horizontal sync alone on a separate narrow-band channel. Since this would result in no transmitted vertical sync information, the ground-station recording film camera would require a continuous slow-motion drive, rather than a pulse-advance film drive. The horizontal sync would be generated by wave-shaping the ground-received signal and controlling the phase of the output sync.

This system would depend on the availability of an additional narrow-band channel. Also, the total bandwidth for the video-plus-sync channels would have to be determined before deciding if this approach would be feasible.

## E. POWER SUPPLY

### 1. INTRODUCTION

Detailed analyses of the power requirements, power source and electric storage design, and regulatory electronic circuitry were within the scope of the intended study. Specifications for the power system required and a plan for power supply development were not intended to be within the scope of the present report. A continuing evaluation of new developments in industry, advancements in the state of the art, and in specific system requirements, was intended to parallel all phases of the study.

Following is a brief description of tasks attempted and completed during the course of the study, as well as some of the difficulties encountered.

At the beginning of the program, primary emphasis was placed on load analysis, that is, voltage and power requirements of various vehicle loads, and the time sequence of load occurrence. Results are shown partly in Figure I.3.E-1 and partly in various other sections of this report.

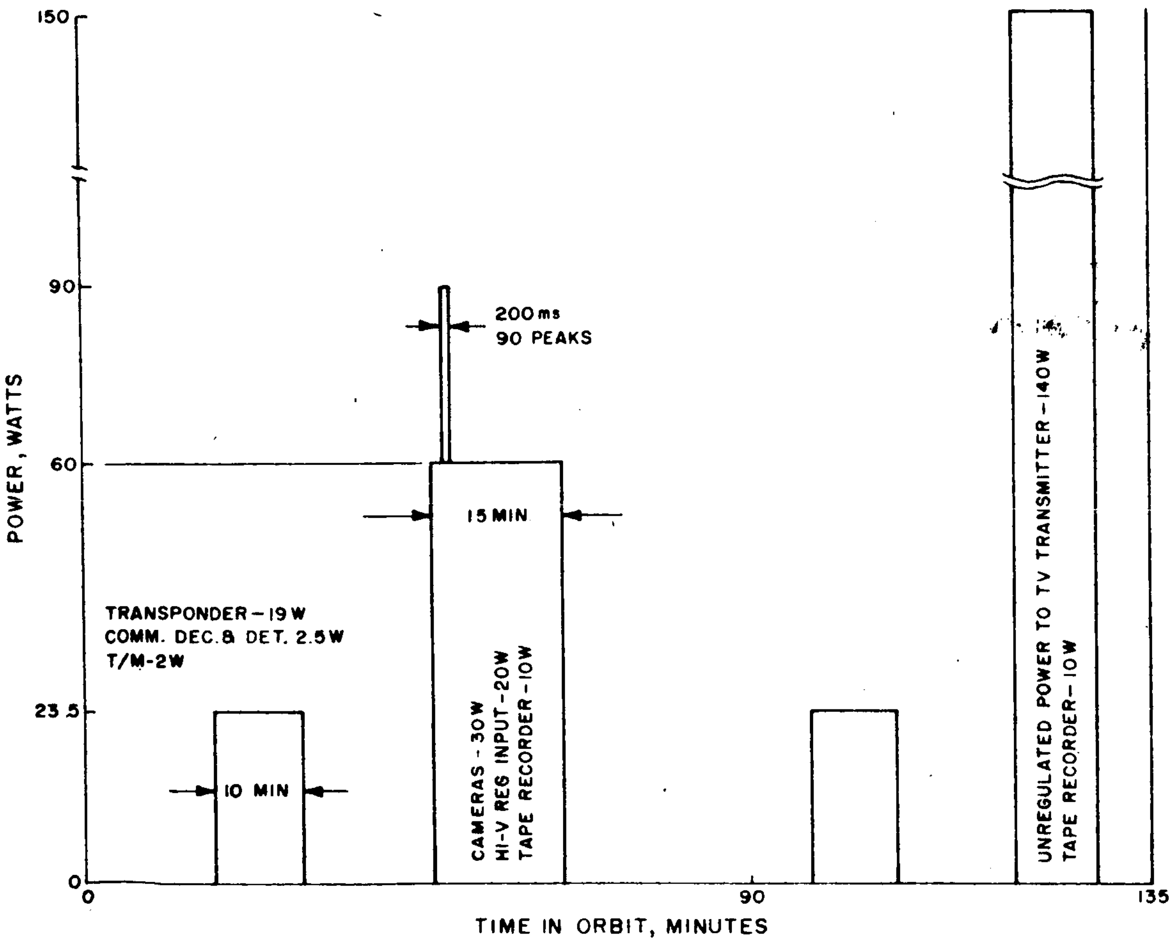

Figure I.3.E-1. LOC Power Profile Less Continuous Load $P_c$ for the First 40 Days in Orbit

Once the load analysis was considered completed, design of the power source was initiated with the investigation of an appropriate solar-cell array. Working together with the thermal and structures skill centers it became immediately apparent that the greatest difficulty lay in obtaining sufficient vehicle area for solar-cell mounting; all preliminary calculations revealed that, depending on mission profile assumed, the projected vehicle area needed to support the required power profile would be approximately 12 to 15 square feet—a requirement which would interfere severely with the intended size and weight limitations. It has been suggested that the projected area in question should be limited to 8 or 10 square feet, if possible.

These circumstances pointed towards a combined RTG–solar-cell source. With this idea in mind, a study of the weight tradeoffs was begun. This study, in its entirety, is included as a part of this report. It is shown that, using some of the already available vehicle skin area for solar-cell mounting, and combining the power thus obtained with that from an RTG of appropriate size (exact size depending on the exact array configuration allowed), an adequate source of power could be realized using state-of-the-art techniques and available component parts.

To complete the study, some attention needs to be given to the electronics requirements, although circuitry and packaging techniques of an adaptable nature have already been developed by RCA for other space systems. The battery type required remains to be pinned down, although a thorough study of battery requirements has already been made and is included below. From the systems viewpoint, the exact conditions of RTG and solar-cell array load-sharing must be analyzed; no great difficulties, however, need be anticipated in this area since the current-voltage characteristics of both types of sources are ideally suited for load matching, perhaps even without an assist from any specialized electronics.

To the problem areas encountered it must be added that since the system had to be designed for two different missions of different power requirements (TV and Tracking), not only had two different designs to be created, but also the design requirements of one had to be compatible with those of the other. Considerable time was required to complete the necessary analytical work. Weight and power trade-off curves included in this section show the intricate relationships among the power source characteristics, system weight, required electrical storage, and duration of mission in the Tracking mode.

## 2. SUMMARY

The analysis of a power supply system comprising both a solar array and a radioisotope - thermoelectric power source has been performed for the system configuration shown in Figure I.3.E-2. Other configurations are possible, for example, one with the RTG output connected directly to its own group of loads, rather than to a common unregulated bus as shown.

In what follows, the solar array is described in terms of the required vehicle surface area $A_s$. The RTG is described in terms of a number ($P_r$) of watts, where $P_r$ is the number of watts required at the end of the 40th day (the end of the TV mission). In this analysis all $P_r$ values are based on the half-life of Polonium 210.

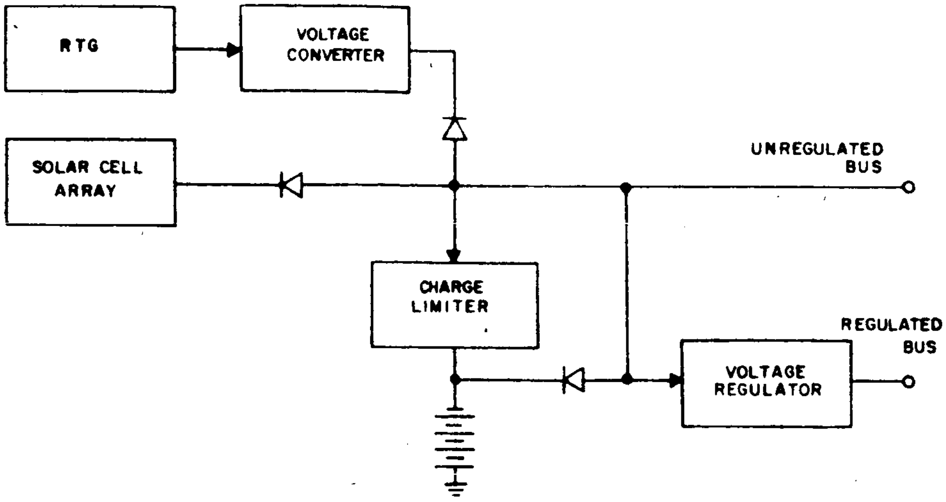

Figure I. 3. E-2. LOC Power Supply Block Diagram

It has been found that for the LOC mission (specifically, "System A"), a radioisotope-thermoelectric generator rated at 40 to 60 watts at the end of the TV mission, in conjunction with a suitable amount of solar-cell array battery power, will meet the power requirements of that mission and cause the system to survive at least 60 days in the Tracking mode (see Figure I. 3. E-1 for TV-mode power profile). The weight of such a power system would be just under 80 pounds total, although further weight optimization is considered possible.

The analysis has been carried out step by step, and several expressions of a general nature have been derived. Given a new set of assumed numbers, the numerical analysis can be repeated without further difficulties.

## 3. ENERGY BALANCE, DERIVATIONS AND ANALYSIS

Figure I. 3. E-2 shows a simplified block diagram of the system. As indicated, the unregulated bus is supplied jointly by a solar-cell array and a radioisotope - thermoelectric generator (RTG).

The average power at the unregulated bus ($P_u$) is:

$$P_u = \sigma P_s + P_r \tag{1}$$

where $\sigma$ is the fractional time in the sun, $P_s$ is the average daytime power output from the solar-cell array, and $P_r$ is the output of the RTG device at the output terminals of the voltage converter.

The array output $P_S$ is determined from a well-known expression often used in solar-array design:

$$P_s = 130 \; P_f \; AED \tag{2}$$

where

$P_f$ is the cell packing factor, of the order of 0.8 to 0.9; 0.85 will be used in what follows,

A is the projected effective vehicle area required for solar cells, in square feet,

E is the effective air mass zero efficiency of the solar cells at approximately +25° to +30°C,

D is the combined array degradation factor due to wiring losses and off-optimum operation, assumed 0.92,

and 130 is the solar constant in watts/ft.$^2$

Equation (2) is assumed to be time-independent; that is, over a period of approximately one year or so, the array output is assumed to remain constant for the LOC mission. RTG output, however, will decrease in time, the amount of decrease being a function of the rate of decay of the radioactive material used to generate heat. Let the output of the RTG be defined as follows:

$$P_r = P_o \exp \left(- \frac{t}{k}\right) \tag{3}$$

The constant k may be determined from the following boundary conditions:

when $t = t_{\text{half-life}}$, then $P_r = 0.5 \; P_o$.

If the radioactive material is Polonium 210, with a half-life of 138 days, then

$$0.5 \; P_o = P_o \exp \left(- \frac{138}{k}\right) \tag{4}$$

where $P_o$ is watts of output at $t + \tau = o$; $\tau$ is the number of days standby prior to insertion into moon orbit, and t is the number of days in moon orbit.

Based on the isotope half-life alone, and assuming constant efficiency of the thermoelectric elements over a wide temperature range, the constant k is found to be 197 days. The assumed effective efficiency, however, serves to modify this number, causing the effective rate of decay to appear to be faster than that implied by the number just found. A study has been made to show that, for the required 40-day lifetime in the TV mode, the constant k is such as to cause the equation to assume the following form:

$$P_r = P_o \exp\left[-0.011\ (t + \tau)\right] . \tag{5}$$

Equations (1), (2), and (5) define the amount of power available at the unregulated bus at any time t, as well as the energy available over any reasonable increment of time $\Delta t$ taken about any time t. As for the amount of energy required, it is a function of the agreed-upon load profile and the internal power-supply losses. Therefore, regardless of the type of source(s) or the relative amount of energy originating at either of the two (or more) sources used, the amount of orbit energy required for a single orbit at, say, the VR input (Figure I.3.E-2) is a fixed number which can be determined. The VR input is a realistic point at which to determine the per-orbit energy requirements since the voltage level there is the same as the unregulated bus, and because it is the only point in the system from which current is drawn by all the loads. At that point the total energy requirement per orbit (in watt-hours) is the sum of the daytime $(WH)_d$ and nighttime $(WH)_n$ requirements, where the latter consists of two parts: first, the direct nighttime energy from the RTG which, in a manner of speaking, knows no "nighttime," and second, assuming that the RTG energy alone is not always sufficient to supply nighttime loads, the net difference which must be supplied by the batteries. This net difference is equal to the difference between the total nighttime requirement $(WH)_n$ at the VR input and the energy supplied by the RTG. To be consistent with the idea of the amount of energy required from the sources, that is, to refer nighttime energy requirements to the unregulated bus, the above net difference must be divided by the battery watt-hour charge-discharge efficiency, $e_b$, expressed as a fraction, i.e.,

$$\sum (WH) = (WH)_d + \left[\frac{(WH)_n - (1 - \sigma)\ TP_r}{e_b}\right] + (1 - \sigma)\ TP_r \tag{6}$$

where T = orbital period (135 min. for LOC); and other symbols as defined earlier.

Let $(WH)_d$ and $(WH)_n$ be known. The Power profile in Figure I.3.E-1 will be used; as seen, this profile shows peak requirements only. The constant power $P_c$ (not shown) will be assumed to be variable for the time being. Assuming that the power supply regulation efficiency is 78% during nighttime and during the one large daytime peak shown, and 68% during the remainder of daytime. Referring to Figure I.3.E-1,

$$(WH)_d = \frac{1}{0.68}\left[\left(\frac{75}{60}\right) P_c + 23.5 \left(\frac{10}{60}\right)\right] + \frac{1}{0.78}\left[\left(\frac{15}{60}\right) P_c + 60 \left(\frac{15}{60}\right)\right] ,$$

or

$$(WH)_d = 2.16P_c + 25 \text{ watt-hours} \tag{7}$$

Note that the 0.2-second peaks shown in Figure I.3.E-1 have been neglected; they are significant only in the regulator and perhaps battery designs. For the nighttime requirements:

$$(WH)_n = \frac{1}{0.78}\left[\frac{45}{60}P_c + 23.5\,\frac{10}{60} + 10\,\frac{10}{60}\right] + 140\,\frac{10}{60}$$

$$(WH)_n = 0.96\,P_c + 30.5 \text{ watt-hours} \qquad (8)$$

Note that the 140-watt peak is at the unregulated voltage level, and therefore not subject to the 78% efficiency factor.

Equations (7) and (8) can be substituted into equation (6). But prior to that let it be noted that $(1 - \sigma)T$ of equation (6) is $\frac{45}{60}$ hours; likewise, $P_r$ is given by equation (5).

Making all of the substitutions and simplifying, the result is an expression for the total energy requirements per orbit required from any and all sources of available power:

$$\sum(WH) = 3.69\,P_c - 0.44\,P_o \exp\left[-0.011\,(t + \tau)\right] + 73.5. \qquad (9)$$

It is seen that the smaller the RTG, from the point of view of electrical output, the more total energy is required (negative term small). This is a consequence of the fact that relatively more nighttime power will have to be supplied by the battery, in turn raising the total energy by the amount needed to overcome increased battery losses resulting from the implied larger discharge.

If the time element is included in Equations (1), (2), and (3), the total energy per orbit available from both sources can be found.

$$\sum(WH) = TP_u$$

$$\sum(WH) = \frac{90}{60}\,(130)\,(0.85)\,(0.92)\,AE + \frac{135}{60}\,P_o \exp\left[-0.011\,(t + \tau)\right] \qquad (10)$$

or

$$\sum(WH) = 153\,AE + 2.25\,P_o \exp\left[-0.011\,(t + \tau)\right] \qquad (11)$$

To be within energy balance, the required energy must equal the available energy. Equating the right-hand members of equations (9) and (11) and simplifying, the result is the overall system energy-balance equation based on the first-40-day profile and a constant power $P_c$:

$$AE + 0.0176\,P_o \exp\left[-0.011\,(t + \tau)\right] - 0.0241\,P_c - 0.480 = 0 \quad (t \leq 40 \text{ days}) \qquad (12)$$

To determine the energy-balance equation for operation after the first 40 days, it is customary to let the constant term of equation (12) (0.48) equal zero. However, there is in this case one minor difference. Since there are assumed to be no peaks of any sort when $t > 40$ days, the daytime regulation efficiency is constant of 68%, instead of 68% for 75 minutes and 78% for the remaining 15 daytime minutes used in the determination of Equation (7). A technically correct expression, therefore, should have a slightly different coefficient for $P_c$. By applying the analytical technique developed above, the energy balance expression for operation after the first 40 days becomes:

$$AE + 0.0176\ P_o \exp\left[-0.011\ (t + \tau)\right] - 0.0244\ P_c = 0 \qquad (t > 40) \qquad (13)$$

Let the two equations covering both energy balance conditions be altered further by adapting them to a specific mode of LOC operation, i.e.,

let $P_c = 27$ watts when $t \leq 40$ days

and $P_c = 25$ watts when $t > 40$ days

Let it be further assumed that the standby time is two weeks ($\tau = 14$ days).

Since the RTG source power is a decreasing function of time, the energy balance equation (12) must specifically apply for the condition of $t = 40$ days. Equation (13) will be left with $t$ as a variable, for it will later be useful in determining the amount of time the system can survive in the Tracking mode which follows the first 40 days.

If the amount of power required from the RTG source at $t = 40$ days is defined as $P_r$, then

$$P_r = P_o \exp\left[-0.011\ (t + 14)\right] \qquad (t = 40 \text{ days})$$

and if $t_t$ is defined as the time of operation in tracking mode, then substitutions can be made into Equations (12) and (13). Simplified, they are:

$$AE + 0.0176\ P_r - 1.13 = 0 \qquad (t \leq 40 \text{ days}) \qquad (14)$$

$$AE + 0.0176\ P_r \exp\left[-0.011 t_t\right] - 0.61 = 0 \qquad (t > 40 \text{ days}) \qquad (15)$$

Let E be the solar-cell efficiency at approximately +28°C. Let it also be assumed that the actual temperature of the solar array is + 60°C in the TV mode and +40°C in the Tracking mode. These operating temperatures will cause any assumed E to drop, necessitating an increase in the available area A to keep the AE product constant. E is assumed to decrease at a rate of 0.6% per centigrade degree of temperature rise. That assumption and the fact that the maximum angle between the sun vector and normal to the array (vehicle side) is of the order of 30° will cause the maximum projected surface area $A_s$ (side-area seen looking normal to the side surface) to be greater than the A of Equations 14 and 15 by an amount given by

$$A_s = A \left[\frac{1 + 0.006\ (60-28)^\circ\mathrm{C}}{\mathrm{Cos}\ 30^\circ}\right] \doteq 1.38A \qquad (t \leq 40 \text{ days}) \qquad (16)$$

Similarly,

$$A_s = 1.24\ A \qquad (t > 40 \text{ days}) \qquad (17)$$

It is probably true that when the angle is 30° the temperature is somewhat below the maximum.

Equations (16) and (17) imply the worst case combination which may therefore constitute the only assumed safety factor in the array design in this analysis.

If $E = 0.1$ (10% @ +28°C)

and $A = A_s/1.38$ (Equation 16),

then

$AE = 0.0725\ A_s$.

Making substitutions into Equation (14) and simplifying,

$$A_s + 0.243\ P_r - 15.6 = 0 \qquad (t \leq 40 \text{ days}) \qquad (18)$$

Similary, by substituting Equation (17) into Equation (15), we obtain

$$A_s + 0.218\ P_r \exp\left[-0.011\ t_t\right] - 7.56 = 0, \text{ thereafter.} \qquad (19)$$

## 4. WEIGHT ANALYSIS

The weight of a solar array is taken to be 1.1 pounds per square foot, including solar cells and a nominal structure. On that basis, the weight of an array consisting of cells mounted on a side of a cylinder is $1.1\pi A_s$, where $A_s$ has been defined in the previous section as the maximum projected surface area. The weight of all power supply electronics, when packaged, may be taken as 6 pounds for the LOC. The weight of an RTG will be assumed to be based on a specific power of 1.12 watts ($P_r$ Equations (14) and (15)) per pound.* For the battery weight, consider the numerator of the fractional member of Equation (6) which represents total battery discharge per orbit (strictly speaking this is actually not the total battery discharge per orbit; the daytime peak shown in Figure E-1 may draw some stored battery power assuming near-optimum system design. The amount of energy drawn, however, will be relatively small, and, assuming the presence of an RTG, will take place only around the 40th day.):

---

*This number is based on a manufacturer's unofficial quote using Pb-Te thermoelectric elements, and assuming that $P_r$ is the power at the end of the 40th day.

$$\text{Battery discharge} = (WH)_n - (1 - \sigma)\ TP_r \text{ (watt-hours)}$$

Making substitutions from Equation (8), and noting that

$$(1 - \sigma)\ T = \frac{45}{60} \text{ hrs, then}$$

$$\text{Battery discharge} = 0.96P_c + 30.5 - 0.75\ P_r = 54.5 - 0.75\ P_r, \tag{20}$$

since $P_c = 27$ watts.

Equation (20) represents the amount of battery discharge per orbit in the TV mode. The weight of the battery is determined by its ability both to absorb a given rate of charge and to furnish a required maximum rate of discharge to a load. For nickel-cadmium batteries, the maximum safe rate of charge is 3 watts per pound of batteries. Furthermore, during the TV mode, recharge time per orbit is 75 minutes (90 minutes daytime less a 15-minute peak load duration). Also, the watt-hour charge-discharge efficiency may be safely assumed to be 63%.

$$\text{Ave. watts charge} = \frac{54.5 - 0.75\ P_r}{0.63\ \frac{(75)}{60}} \tag{21}$$

$$= 69.2 - 0.95\ P_r \text{ (watts)}$$

which is the required charge rate. Based on 3 watts per pound, the required battery weight is

$$\frac{\text{watts charge}}{\frac{3 \text{ watts}}{\text{pound}}} = 23 - 0.317\ P_r = \gamma' \tag{22}$$

It can be shown that, in this case, as long as the battery weight is $\gamma'$ or more, the percent depth of discharge is 23.6% or less:

$$d = \frac{\text{watt-hours discharge/orbit}}{\text{watt-hours capacity}} \cdot 100 \tag{23}$$

The numerator of Equation (23), is given by Equation (20). For Ni-Cd batteries, the specific capacity is 10 watt-hours per pound, hence, watt-hours capacity = 10 $\gamma'$ where $\gamma'$ is given by Equation (22).

$$\therefore \quad d = \frac{(54.5 - 0.75\ P_r)\ \text{watt-hours}}{10\ \dfrac{\text{watt-hours}}{\text{pound}}\ (23-0.317\ P_r)\ \text{pounds}} \cdot 100 = 23.6\% \qquad (24)$$

A depth of discharge of this magnitude or less is considered acceptable.

In a similar manner, a weight $\gamma''$ can be determined, based on a maximum permissible rate of discharge of 10 watts discharge-to-load per pound. In the case of interest, discharge is no less a limiting factor than the average rate of charge analyzed in some detail above. In what follows, $\gamma'$ will be defined as the weight of an unpackaged battery in the equations involving total power-supply weight.

The total power-supply-system weight $\gamma$ is, therefore,

$$\gamma = 1.1\ \pi A_s + 6 + \frac{P_r}{1.12} + 1.15\ \gamma' \qquad (25)$$

where $\gamma'$ is the battery weight determined from Equation (22). The factor of 1.15 accounts for packaging.

In Equation (25), the first term of the right-hand member is the weight of the solar cell array, the second term the weight of the regulatory electronics, the third term the weight of the RTG, and the fourth term is the battery weight. From Equation (18),

$$A_s = \left[15.6 - 0.243\ P_r\right] \text{ft}^2 .$$

Substituting $A_s$ into Equation (25) and simplifying,

$$\gamma = \left[86.6 - 0.31\ P_r\right] \text{pounds} \qquad (26)$$

## 5. RESULTS AND CONCLUSIONS

Table I.3.E.1 shows the results of the equations derived in the preceding sections.

The first column in Table I.3.E.1 is the solar-array area, $A_s$. It will be recalled that $A_s$ is the required projected vehicle area which must be made available for solar-cell mounting; the actual projected area of the solar cells is, therefore, somewhat lower than $A_s$. The second column is a set of solutions of Equation (18) for $P_r$, given $A_s$ in the first column. $\gamma$ in the third column is found from Equation (26); it is the total "unadjusted" system weight, and is a function of the various possible combinations of $A_s$ and $P_r$ in the first two columns. The "adjustment" referred to is that of the battery weight, to make sure that the battery is credited with sufficient weight to enable it to meet various system requirements, e.g. maximum watts discharge. The value of this adjustment is found and given in Table V-1 as $\Delta\gamma$ which, when added to $\gamma$ in the third column, results in the total power supply system weight of a working system given in the next-to-last column under Total Weight. Appropriate footnotes (part of Table E-1) show some further detail regarding battery weight adjustment.

Finally, the last column is a set of solutions of Equation (19) for $t_t$, given $A_s$ and $P_r$ of the first two columns.

Figure I. 3. E-3 shows graphically the results presented in Table I. 3. E-1. The top curve shows the total system weight as a function of solar-array area $A_s$. Total system weight does not appear to be affected a great deal by the particular solar cell - RTG proportion selected, particularly within a solar-array range of approximately 0 to 10 sq. ft, although the system weight is minimal in the all-RTG system ($A_s = 0$). The "RTG power, 40th day" curve is a plot of $P_r$ as a function of $A_s$. As indicated, as $P_r$ goes down, battery weight must increase to support a larger share of night-time loads. Two curves of array power are drawn: one, for the TV mode, and the other, for the Tracking mode; the difference between the two curves is due to different array temperatures, which are +60°C and +40°C, respectively.

As the array contribution to the overall power requirements is allowed to increase, the number of days of operation in the tracking mode is also increased until the array area is 7.58 sq. ft. or larger, under which condition the Tracking mode will be sustained indefinitely. This is shown by the curve labled "days Tracking mode".

In conclusion, analysis indicates that the mission requirements of 40 days TV mode and $t_t$ days Tracking mode can be accomplished by 15.63 sq. ft. of projected solar-cell array area, by an RTG weighing roughly 58 pounds and supported by suitable batteries to sustain peak loads, or by a judiciously chosen proportion of each type of source. The optimum system is probably somewhere within the region of requirements resulting in 2 to 7 square feet of projected array area, depending on the desired life in the Tracking mode, ease of procurement of the RTG of the required characteristics, and solar-cell area availability. Weight would be a secondary consideration due to the demonstrated relative constancy of total system weight within the range of greatest interest.

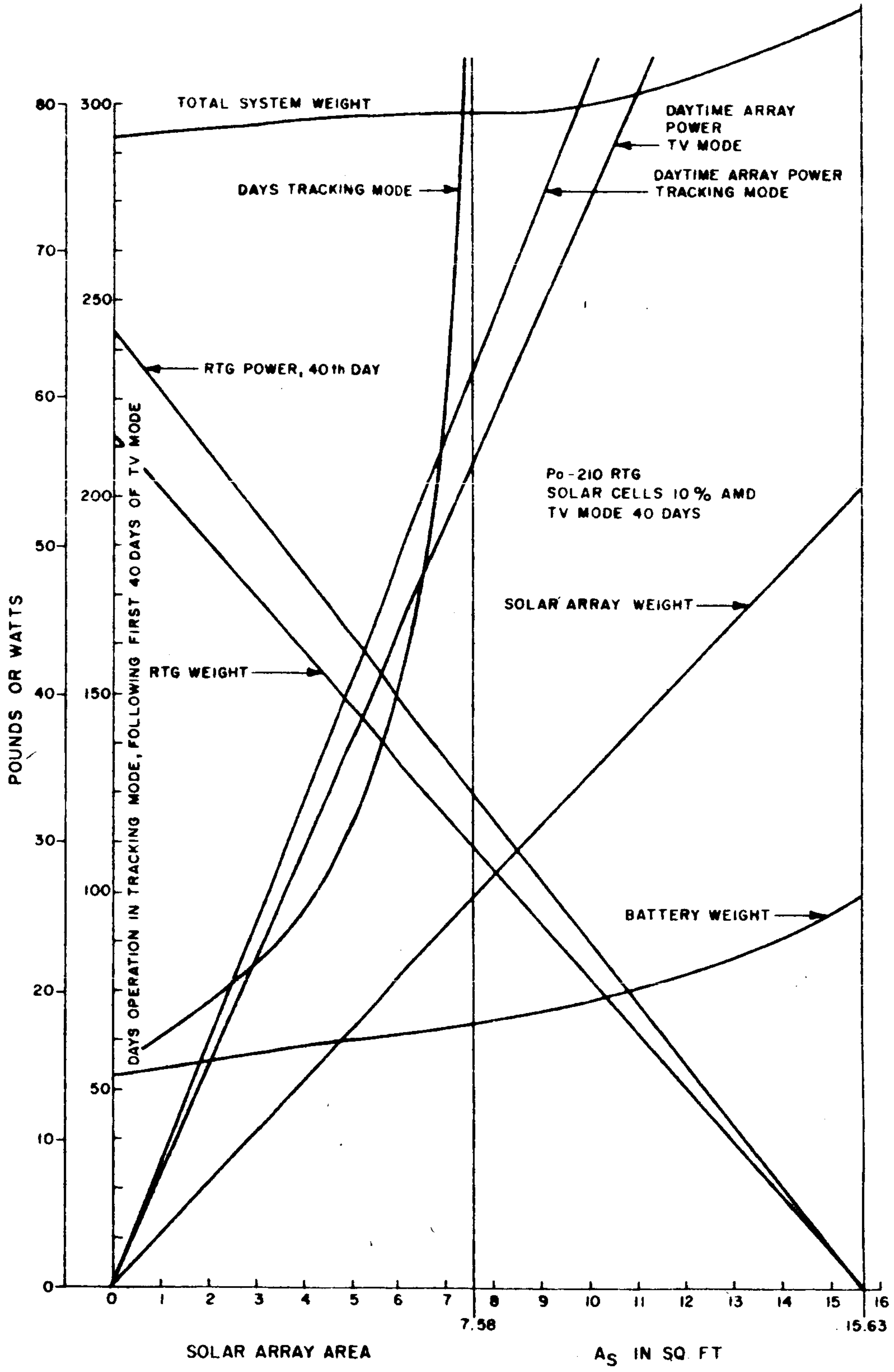

Figure I. 3. E-3. Power Supply Parameters - System

## TABLE I.3.E-1

## POWER AND WEIGHT REQUIREMENTS FOR THE LOC POWER SUPPLY

| $A_s$ (sq. ft.) | RTG Power @ 40 Days (Watts) ($P_r$) | $\gamma$ (Pounds) | Battery Weight (Pounds) | | $+\Delta\gamma$ Battery** Adjustment to $\gamma$ (Pounds) | Total Weight (Pounds) | Days Operation in Tracking Mode |
|---|---|---|---|---|---|---|---|
| | | | $\gamma$ | adj.* | | | |
| 0 | 64.4 | 66.6 | 2.6 | 12.3 | 11.2 | 77.8 | 56.0 |
| 1 | 60.3 | 67.9 | 3.8 | 12.7 | 10.2 | 78.1 | 63.1 |
| 2 | 56.2 | 69.2 | 5.2 | 13.1 | 9.1 | 78.3 | 71.7 |
| 3 | 52.0 | 70.5 | 6.5 | 13.6 | 8.2 | 78.7 | 82.6 |
| 4 | 47.9 | 71.8 | 7.8 | 14.0 | 7.1 | 78.9 | 95.0 |
| 5 | 43.8 | 73.0 | 9.1 | 14.4 | 6.1 | 79.1 | 119.0 |
| 6 | 39.6 | 74.3 | 10.4 | 14.8 | 5.1 | 79.4 | 159.0 |
| 7 | 35.5 | 75.6 | 11.7 | 15.2 | 4.0 | 79.6 | 226.0 |
| 7.58 | 33.1 | 76.3 | 12.5 | 15.4 | 3.3 | 79.6 | indefinite |
| 10 | 23.2 | 79.4 | 15.7 | 16.4 | 0.8 | 80.2 | indefinite |
| 12.5 | 12.9 | 82.6 | 18.9 | 18.9*** | 0 | 82.6 | indefinite |
| 15.63 | 0 | 86.6 | 23.0 | 23.0*** | 0 | 86.6 | indefinite |

* $\gamma'$ adjusted for 10 watts discharge per pound; otherwise $\gamma'$ is based on 3 watts charge/pound @ 23.6% depth of discharge.

** difference between adjusted battery weight and $\gamma'$ multiplied by 1.15: to be added to $\gamma$.

*** no adjustment for watts-discharge/pound required.

## F. MECHANICAL DESIGN OF LUNAR ORBITER CAPSULE

### 1. DESIGN CONSTRAINTS

The structural configuration of the lunar-orbiter capsule and the system design parameters evolved from the external design constraints imposed by the mission requirements, the spacecraft bus, the launch-vehicle envelope, and the payload capability. Internal constraints based primarily upon meeting successful mission performance requirements, are maintenance of satisfactory inertia ratios and provision of satisfactory thermal control and structural integrity.

Prime consideration was given in the mechanical design of the lunar-orbiter capsule to negate any need for change in either the spacecraft bus or launch vehicle. This goal was essentially satisfied by staying within the design envelope of the Agena-B nose cone and clearing the solar paddles of the spacecraft bus. This was accomplished by the use of an aircraft-type, riveted, sheet-metal, conical adapter skirt that mates the lunar-orbiter capsule to the spacecraft bus. The upper portion of the adapter skirt fastens to the retro-rocket case through a Marman-type, "quick-disconnect" flange. The lower portion of the skirt extends down and mounts to the spacecraft bus. Ejection of the capsule from the spacecraft bus is accomplished by activation of either of two redundant explosive bolts in the Marman-type separation clamp. Separation velocity is imparted to the capsule by the spin-up motors prior to firing the retro-rocket.

Restrictions on the launch vehicle and on the spacecraft bus payload and envelope influenced the selection of the capsule power supply and the attitude and stabilization system. The structural configuration (see Figures I.3.F-1 and I.3.F-2) includes a 65-watt radioisotope thermoelectric generator (RTG) and a three-axis, gas-jet stabilization system. Other systems under consideration were a solar-cell-array power supply and a spin-stabilized attitude-control system.

Internal design constraints were primarily concerned with maintaining satisfactory mass moment-of-inertia ratios

$$\left[\frac{I \text{ spin axis rotating mass}}{I \text{ transverse for static rotating mass}}\right]$$

greater than 1.0 during the spin-up portions of the mission, as well as to provide satisfactory transient environmental temperature control for the various system components and RTG heat dissipation temperature regulation. A basic "disc-like" structure was designed to support the system components. This requires ejection of the retro-rocket motor after burnout and ejection of the directional antenna and part of the directional antenna support prior to the final tracking-transponder experiment.

High density packaging of capsule equipment is accomplished by mounting equipment to both sides of a baseplate. The upper side of the baseplate is flat to provide for ease of mounting equipment. The lower side has six radial ribs which provide the necessary stiffness and strength to endure launch vibration, in-flight acceleration, and rotational loads. Structural weight is held to a minimum partially by using the retro-rocket case as a main structural member to transfer the capsule load to the

E-ORDER No. 62-489

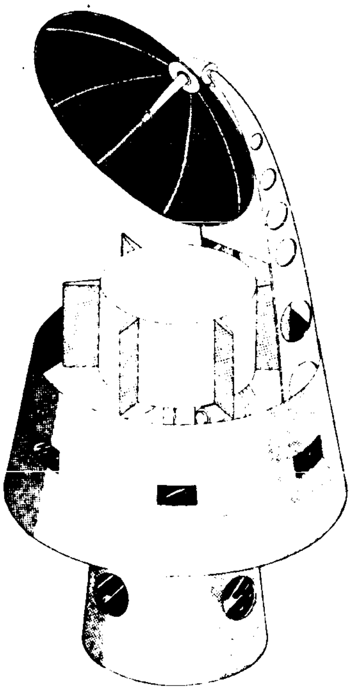

Figure I.3.F-1. Structural Configuration of Lunar Orbiter Capsule

spacecraft bus via the adapter. In addition, the torus-shaped gas-storage container and the thermal-control radiation panels perform a dual role when integrated into the system by further increasing the structural stiffness. The basic baseplate structure provides great latitude for the addition of possible further experiments on future missions, assuming some of the present payload will not be required.

With the center of mass located at approximately station 445.0, the mass moments of inertia are approximately estimated as follows:

$I_{xx}$ = 8.23 slug-ft$^2$

$I_{yy}$ = 10.28 slug-ft$^2$

$I_{zz}$ = 8.97 slug-ft$^2$

Approximate estimates are given at this time since the RTG unit had to be relocated, and no new figures are available.

## 2. SYSTEM COMPONENTS (Refer to Figures I.3.F-1 and I.3.F-2)

### a. Retro-rocket and Spin-Up Rockets

The retro-rocket and spin-up rockets are of the solid-propellant variety, selected because of their simplicity and reliability. A spherical retro-rocket case with protruding thrust nozzle is especially suitable for the lunar-orbiter capsule because its compact

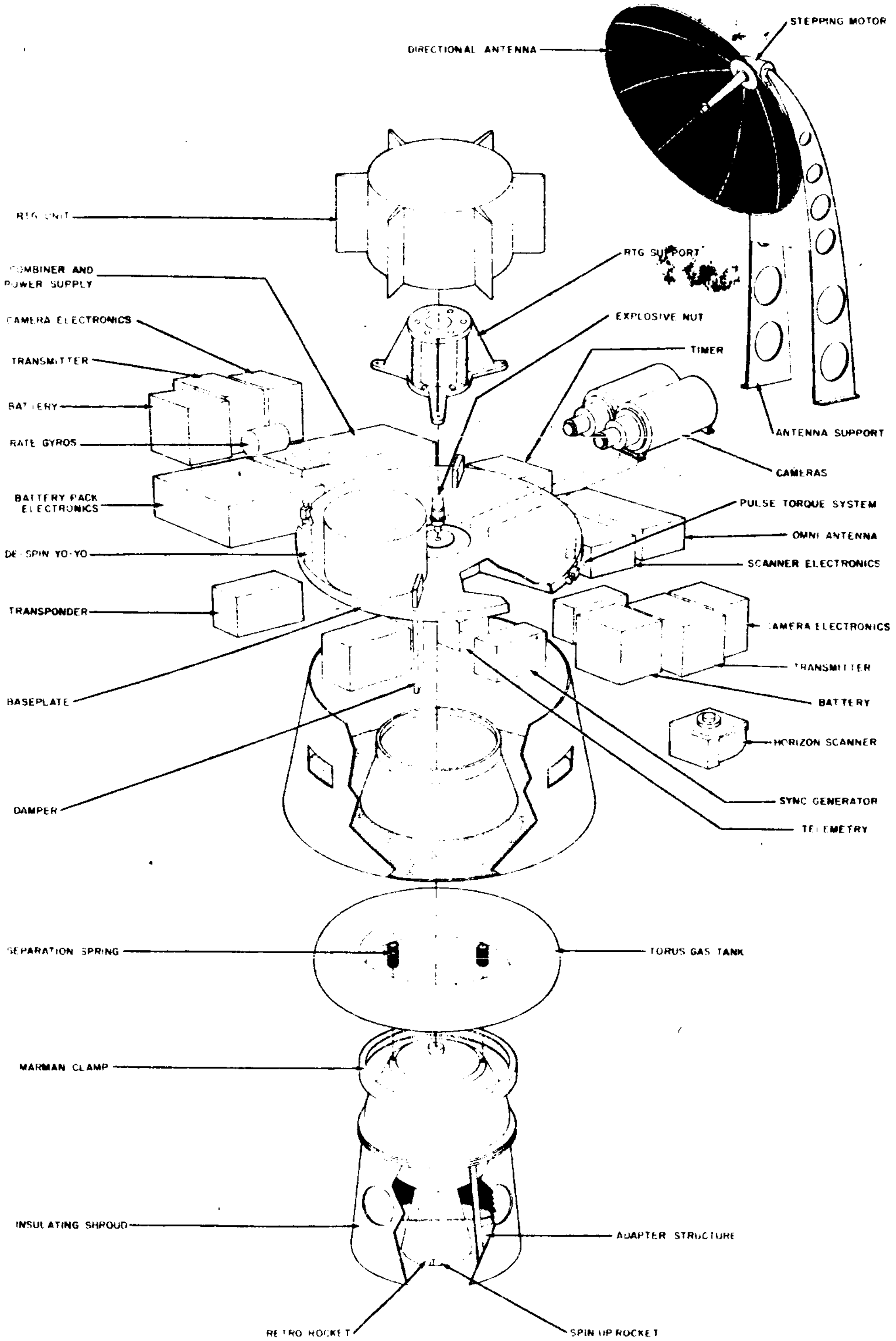
DIRECTIONAL ANTENNA
STEPPING MOTOR
RTG UNIT
COMBINER AND POWER SUPPLY
RTG SUPPORT
CAMERA ELECTRONICS
EXPLOSIVE NUT
TIMER
TRANSMITTER
BATTERY
RATE GYROS
ANTENNA SUPPORT
CAMERAS
BATTERY PACK ELECTRONICS
PULSE TORQUE SYSTEM
OMNI ANTENNA
DE-SPIN YO-YO
SCANNER ELECTRONICS
TRANSPONDER
CAMERA ELECTRONICS
TRANSMITTER
BASEPLATE
BATTERY
HORIZON SCANNER
DAMPER
SYNC GENERATOR
TELEMETRY
SEPARATION SPRING
TORUS GAS TANK
MARMAN CLAMP
INSULATING SHROUD
ADAPTER STRUCTURE
RETRO ROCKET
SPIN UP ROCKET

Figure I.3.F-2. Detail of Lunar Orbiter Capsule Configuration

envelope and shortened nozzle length appreciably affect the payload center-of-mass and mass moment-of-inertia restrictions of the spacecraft bus. The solid spin-up rockets are similar to those employed with great success on the TIROS weather satellite.

Three solid-propellant spin-up rockets are to be mounted to the exhaust nozzle of the retro-rocket at a small angle to provide a thrust increment to the capsule after separation from the spacecraft bus. They also provide a rotational stability to the capsule to minimize any error in misalignment of the retro-rocket thrust. Thermal and inertial considerations require ejection of the retro-rocket casing. This takes place after burnout by the activation of an explosive bolt which separates the retro-rocket motor from the main structural baseplate. Eight nested springs at the mating face provide the necessary separation velocity for a clean, uniform separation.

### b. Directional L-Band Antenna

The directional antenna is rigidly secured to the baseplate by a sheet-metal gooseneck structural mount. This allows the center of mass of the directional antenna to be located at the principal axis of the capsule, which in effect ensures little disturbance to the capsule stability during orientation of the antenna dish necessary for the procurement of television pictures of the lunar surface. The dish is secured to the mount at launch by a pin-puller type catch which disengages prior to activation of the stepper motor to rotate the directional-antenna dish. Ejection of the antenna and a portion of the mount is effected by activation of an explosive bolt immediately after final spin-up for the final transponder tracking experiment. This is discussed more fully in Section I. 3. C.

### c. Three-Axis Attitude-Control System

A conventional three-axis, gas-jet torquing system is to be used. It consists of a torus storage tank, six 0. 01 - 0. 05-lb. solenoid-operated thrust nozzles, two per axis, with a common regulator valve. The nozzles will be mounted around the mid-section of the capsule and in mutually perpendicular planes, to eliminate coupling problems. Either a nitrogen or a liquid ammonia gas system shall be used; liquid ammonia requires a lower storage tank pressure and is therefore preferable. This subsystem is selected primarily because if offers a greater degree of flexibility and growth potential to the lunar-orbiting capsule than a spin-stabilized system. In addition, techniques developed for this system would be directly applicable to later lunar orbiters, including manned systems.

### d. Thermal Shield

The thermal shield consists essentially of two concentric cylinders joined together at the bottom with a thin flat sheet-metal dish. It maintains the capsule in a satisfactory temperature range during the mission for transit and operating modes. In addition, it stiffens the underside area of the baseplate and equipment compartments. It can also serve as a guide for jettison of the retro-rocket so as not to induce any undesirable loads to the capsule. The shield will be permanently fastened to the baseplate for the entire mission.

e. Omnidirectional Antenna

The omnidirectional antenna will consist of eight slot radiators, mounted circumferentially and equidistant beneath the baseplate. They will be energized through eight coaxial cables. The thermal shield will include 8 electrically-transparent covers over cut-outs in the region of the slot radiator.

f. TEAM Dampers*

Two TEAM dampers will be located 180° apart symmetrically with respect to the center of mass of the payload capsule and parallel to the spin axis. Cut-outs will be provided in the baseplate to facilitate mounting the dampers.

g. The De-spin Assembly

The de-spin assembly will be wound about the structural frame at the center of mass of the capsule. It will provide the necessary change in angular momentum to de-spin the capsule after the initial spin-up after orbit injection. This system has proven to be highly reliable in the TIROS satellite series.

h. Final Spin-Up Rockets

As in the initial spin-up rockets, the final spin-up rockets will be of the solid-propellant variety. Two sets of rockets will be mounted essentially at the center of the capsule mass as it exists for the final transponder-tracking phase of the mission. One set will be fired to achieve a low-velocity rate prior to achievement of the spin axis normal to the ecliptic plane. The second set will be used for final high-speed spin-up after proper orientation has been obtained.

i. Vidicons

Two vidicon units will be mounted to the top of the baseplate, in line with the horizon scanners. Optical line-up with the horizon scanners is essential at installation to the capsule.

j. Horizon Scanners

Either one or two horizon-scanner units will be mounted to the capsule in such a way as not to disrupt the beam field of view.

k. Digital Solar-Aspect Sensor

The digital solar-aspect sensor is used to establish the spin-axis normal to the ecliptic plane during the final spin-up mode.

---

* See page III-20 of the Final Report on Lunar Orbiter Capsule, AED-1542, dated 31 July 1962 for a discussion of the "TEAM" precession damping mechanism.

### 1. Gyros and Other Electronic Components

If active scanners are used, a gyro compass or two, single-degree of freedom, system is necessary for yaw-axis control. If a static unit is used, a three-axis system will be used as a stable platform. Other electronic system components will be mounted for accessibility and convenience to other related components.

## 3. PROBLEM AREAS

### a. The Radioisotope Thermoelectric Generator (RTG) Power Supply

This unit requires special handling. If a low half-life material is used, replacement RTG's would have to be readily available from the RTG manufacturing facility.

Provision would have to be made to dissipate the heat generated during the launch mode, or until the spacecraft shroud is ejected. One suggested method is to use an umbilical draft system to suitably cool the RTG prior to launch. Thermal dissipation, during the near-earth phase, would have to be checked.

### b. Directional L-Band Antenna

As indicated in the "Lunar Orbiter Capsule Preliminary Configuration Report", AED-1616, dated 25 September 1962, page III-15, item 16, the antenna is located so that its center of gravity is on the payload spin axis. The offset of the gooseneck frame from this axis would be compensated for by other equipment. As a result, the only remaining product-of-inertia term is the product-of-inertia of the antenna about its own center-of-mass. Although rotation of the antenna would add some additional product-of-inertia, this should not be large enough to be of any real consequence.

In the formula* for the product of inertia as a function of angular rotation:

$$I_{x'y'} = \frac{1}{2}(I_x - I_y)\sin 2\phi + I_{xy}\cos 2\phi \qquad \text{(See Figure I.3.F-3.)}$$

$I_{xy}$, the product-of-inertia term, is zero about the principal axes $I_x$ and $I_y$ because the x axis is an axis of symmetry. $I_{x'y'}$, the new product of inertia, after rotation through an angle $\phi$, is then equal to the first term only. The product-of-inertia term can be eliminated altogether by merely making $I_x = I_y$ by the addition of some electronic components behind the reflector. Effectively then, all axes through the center-of-mass become principal axes of the antenna.

The principal axes of the payload would be established collinear with the spin axis for the transfer and retro-rocket spin-up mode.

---

* See Appendix I of Engineering Mechanics by Timoshenko and Young and the Section on Principal Axes and Principal Moments of Inertia.

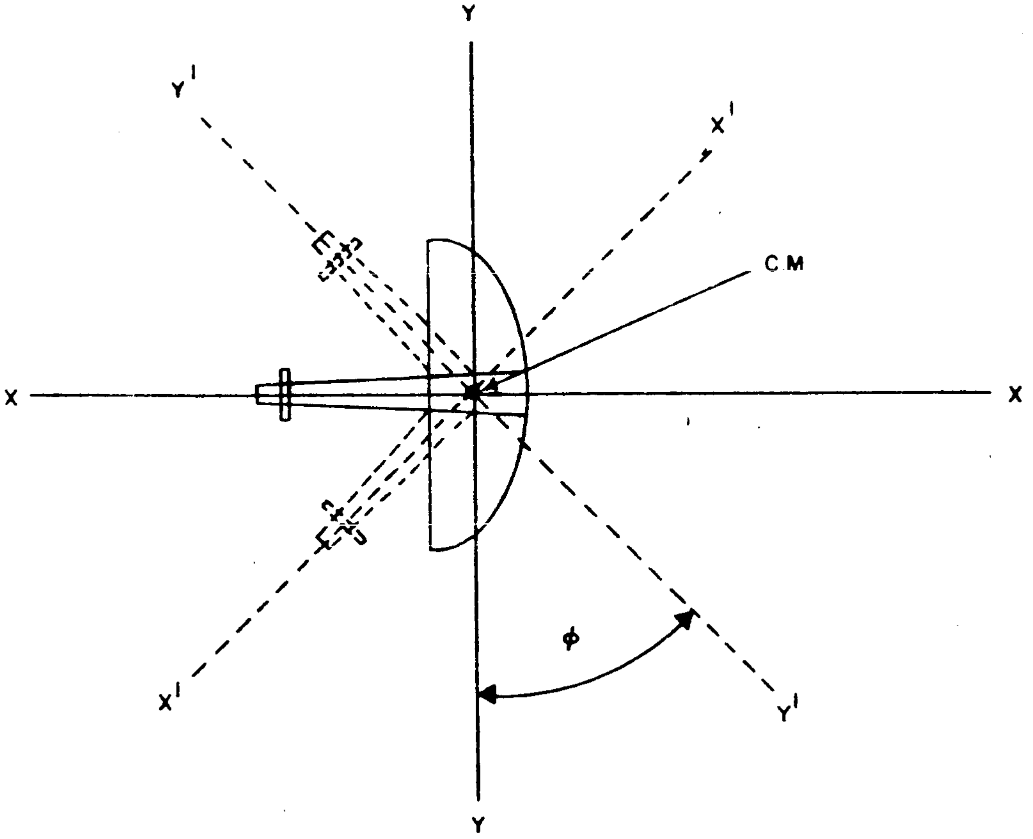

Figure I. 3. F-3 Directional Antenna Inertia Configuration

In order to obtain a suitable inertia ratio for the spin-up phase, one or more components no longer useful for this phase would be ejected. This may be accomplished in two ways:

1) eject the antenna and part of the gooseneck support frame in order that the principal axis of the payload does not shift, or

2) eject the antenna and the complete gooseneck support frame.

Technique No. 1) is the simpler, if the required inertia ratio can be achieved by this technique alone. As indicated before, the principal axes would not be changed; and the pulse jets and TEAM dampers would operate in the same manner. It would appear that this method is feasible, since the inertia contributed by the antenna and the upper part of the gooseneck is relatively large, and represents the masses farthest from the transverse axis. The contribution of the lower part of the gooseneck support to transverse inertia is somewhat less, because it is designed to support only a four-pound antenna. Furthermore, the gooseneck is designed with a light mass distribution in the free portion and a heavy distribution at the base.

A principal-axis shift would occur if the entire gooseneck support also were ejected. This could be eliminated by attaching electronic components integrally to the frame or by ejecting additional components. A small, principal-axis shift could be tolerated if it were small, and, if necessary, the pulse jets could be lined up with respect to the new principal axes. It is doubtful that this would be required.

### c. Retro-Rocket Ejection

A more detailed investigation must be made as to how the spin-up rocket may be ejected without bumping the payload proper. Evaluation also must be made of the centrifugal force contribution resulting from rotation during the retro-rocket spin-up phase of the mission.

RE-ORDER No. 62-459

## G. THERMAL CONTROL

### 1. INTRODUCTION

The thermal design effort for Phase II of the LOC Study program comprised two main areas:

(1) Development of a computer program for accurately determining the lunar orbit thermal radiation environment, and

(2) Final thermal design of the LOC.

A detailed thermal analysis of the LOC itself could not be initiated until the vehicle configuration was established. The program was cancelled just as this configuration was established; hence, the work actually performed in the thermal control area was primarily devoted to determining the lunar orbit thermal radiation environment.

### 2. THERMAL RADIATION ENVIRONMENT OF A LUNAR ORBIT

Preliminary data on the thermal radiation environment were accumulated during Phase I of the LOC study program. To provide more accurate data, a computer program was developed during Phase II to obtain the IR and solar-reflected radiation inputs to a plane area at various orbit altitudes and at various angles to the position vector. The geometry for obtaining these inputs is shown in Figure I. 3. G-1.

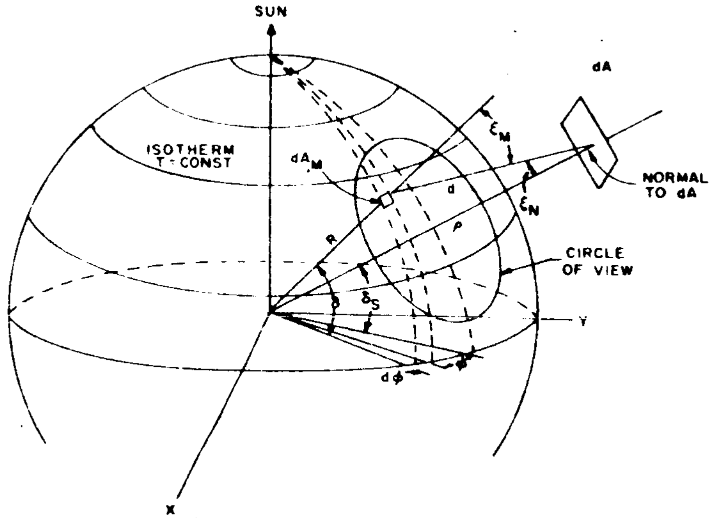

ρ = DISTANCE FROM CENTER OF EARTH TO AREA dA
d = DISTANCE FROM $dA_M$ ON MOON'S SURFACE TO dA
R = EARTH'S RADIUS VECTOR TO $dA_M$
$\epsilon_M$ = ANGLE BETWEEN R AND d
$\epsilon_N$ = ANGLE BETWEEN d AND NORMAL TO AREA
δ = ANGLE BETWEEN R AND XY PLANE
$\delta_S$ = ANGLE BETWEEN ρ AND XY PLANE
φ = ANGLE BETWEEN PROJECTION OF R ON XY PLANE AND PROJECTION OF ρ ON XY PLANE

Figure I. 3. G-1 Geometry for Obtaining Thermal Radiative Power from the Lunar Surface

The basic equation for the IR radiation input is:

$$dP = \epsilon_M \sigma T_M^4 F_{MdA} \, dA_M \quad \text{(watts)} \tag{1}$$

where:

$dP$ = power transferred to a surface element, $dA$, of the satellite from a surface element, $dA_M$, of the moon

$F_{MdA}$ = geometric view factor from the moon's surface element ($dA_M$) to the satellite's surface element ($dA$)

$\epsilon_M \sigma T_M^4$ = radiative power from the moon's surface element ($dA_M$)

Using the geometry of Figure I.3.G-1 $F_{MdA}$ is given by:

$$F_{MdA} = \frac{\cos \xi_M \cos \xi_N}{\pi d^2} R^2 \cos \delta \, (d\delta) \, (d\phi) \, (dA) \tag{2}$$

Substituting this expression in Equation (1) and dividing by $dA$ yields:

$$\frac{dP}{dA} = dI_{Th} = \epsilon_M \sigma T_M^4 \frac{\cos \xi_M \cos \xi_N}{\pi d^2} R^2 \cos \delta \, d\delta \, d\phi \left(\text{watts/in}^2\right) \tag{3}$$

Performing the integration indicated in Equation (3) yields:

$$I_{Th} = \int\int \epsilon_M \sigma T_M^4 \frac{\cos \xi_M \cos \xi_N}{\pi d^2} R^2 \cos \delta \, d\delta \, d\phi \tag{4}$$

To solve this equation, the factors $\cos \xi_M$, $\cos \xi_N$, and $d$ must be expressed in terms of $\delta$, $\phi$, and $B$, where $B$ is equal to $R/\rho$. To simplify both the derivation and computation, all cases were excluded for which $\alpha$ and $\beta$, the angles to the position vector (see Figure B-1 in Appendix B), are different from zero simultaneously (e.g., either $\alpha$ or $\beta$ or both may be zero, but cannot be non-zero simultaneously). Thus, an equation was derived for all values of $\alpha$ with $\beta$ equal to zero and a second equation was derived for all values of $\beta$ with $\alpha$ equal to zero. The input for any arbitrary angle can then be determined by an appropriate combination of the two equations.

To derive an expression for $d$ which is valid in both of the cases described above, the triangle defined by line segments $R$, $\rho$, and $d$ is used. (This triangle is shown in Figure I.3.G-2.) The Law of Cosines yields:

$$d^2 = \rho^2 + R^2 + 2 R\rho \cos \eta \tag{5}$$

RE-ORDER No. 62-459

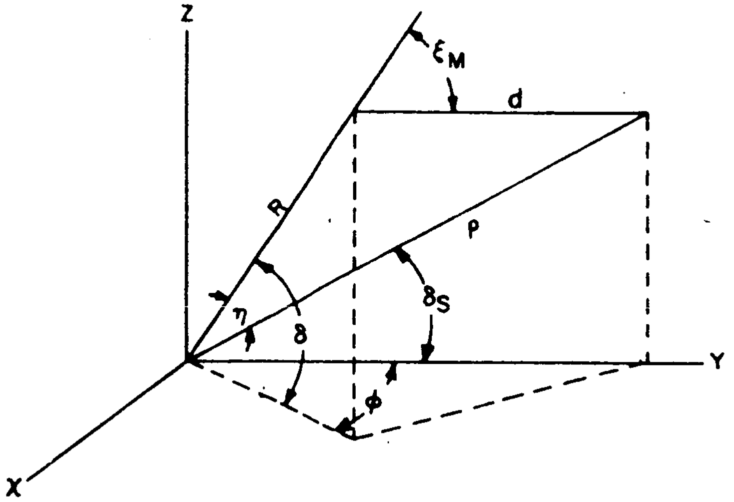

Figure I. 3. G-2 Geometry for Obtaining an Expression for d

The principles of vector analysis are used to derive an expression for cos $\eta$.

$$\cos \eta = \frac{\vec{R} \cdot \vec{\rho}}{R\rho}$$

$$= \cos \delta \cos \delta_s \cos \phi + \sin \delta \sin \delta_s \qquad (6)$$

Thus:

$$\frac{d^2}{\rho^2} = 1 + B^2 - 2B\left(\cos \delta \cos \delta_s \cos \phi + \sin \delta \sin \delta_s\right) \qquad (7)$$

where:

$$B = \frac{R}{\rho}$$

The factor cos $\xi_M$ is also independent of both $\alpha$ and $\beta$, and is given by (from triangle $Rd\rho$):

$$\cos \xi_M = \frac{1}{2\rho d}\left(\rho^2 + d^2 - R^2\right)$$

$$= \frac{\rho}{2d}\left(1 - B^2 + \frac{d^2}{\rho^2}\right) \qquad (8)$$

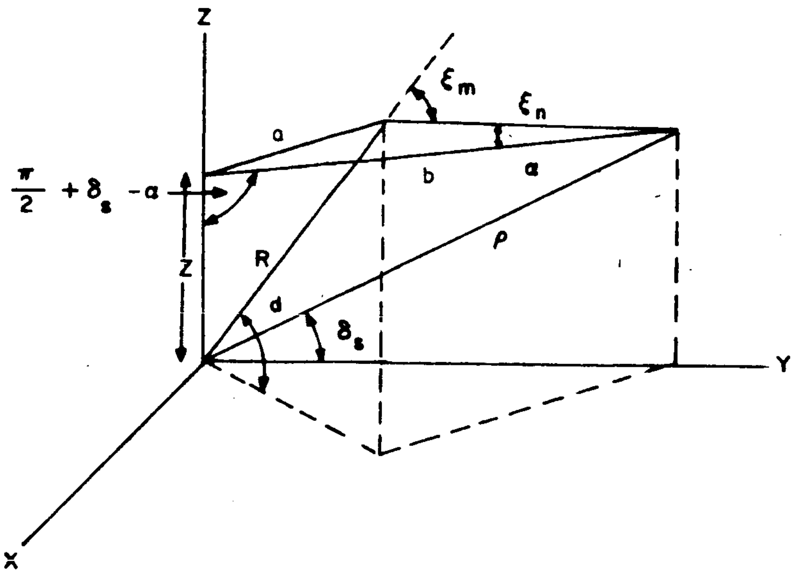

Figure I. 3. G-3 Geometry for Obtaining Cos $\xi_N$ when $\beta$ is Zero

Figure I. 3. G-3 shows the geometry for deriving an expression for cos $\xi_N$ when $\beta$ is zero. In this figure, b is the extension from the normal of the plate to the Z axis and a is the distance from $dA_M$ to the intersection of b and the Z axis. Applying the Law of Cosines to triangle abd gives:

$$\cos \xi_N = \frac{1}{2db}\left(d^2 + b^2 - a^2\right) \tag{9}$$

From the Law of Sines:

$$\frac{b}{\sin\left(\frac{\pi}{2} - \delta_s\right)} = \frac{\rho}{\sin\left(\frac{\pi}{2} + \delta_s - \alpha\right)} \tag{10}$$

Solving Equation (10) for b yields:

$$b = \frac{\rho \cos \delta_s}{\cos\left(\delta_s - \alpha\right)}$$

From triangle ZRa:

$$a^2 = Z^2 + R^2 - 2RZ \cos\left(\frac{\pi}{2} - \delta\right)$$

$$Z = \frac{\rho \sin \alpha}{\cos\left(\delta_s - \alpha\right)}$$

Therefore:

$$a^2 = \rho^2 \left[\frac{\sin\alpha}{\cos\left(\delta_s - \alpha\right)}\right]^2 + R^2 - 2R\rho\,\frac{\sin\alpha\,\sin\delta}{\cos\left(\delta_s - \alpha\right)} \tag{11}$$

Thus, for $\beta$ equal to zero:

$$\cos\xi_N = \frac{\rho}{2d}\,\frac{\cos\left(\delta_s - \alpha\right)}{\cos\delta_s}\left[\frac{d^2}{\rho^2} + \frac{\cos^2\delta_s - \sin^2\alpha}{\cos^2\left(\delta_s - \alpha\right)} - B^2 - 2B\,\frac{\sin\alpha\,\sin\delta}{\cos\left(\delta_s - \alpha\right)}\right] \tag{12}$$

Substituting Equations (7), (8), and (12) in Equation 4 yields, for all values of $\alpha$:

$$\begin{aligned} I_{Th} = \int_{\delta\min}^{\delta\max}\int_{\phi\min}^{\phi\max} & \left[f(\delta,\phi)\cos\delta\right]\left[\frac{\cos\delta\cos\delta_s\cos\phi + \sin\delta\sin\delta_s - B}{\left[1 + B^2 - 2B\left(\cos\delta\cos\delta_s\cos\phi + \sin\delta\sin\delta_s\right)\right]^2}\right] \\ & \left[\frac{\cos\left(\delta_s - \alpha\right)}{\cos\delta_s}\right]\left[\frac{\cos^2\delta_s - \sin^2\alpha}{\cos^2\left(\delta_s - \alpha\right)} + 1 - 2B\left(\cos\delta\cos\delta_s\cos\phi + \sin\delta\sin\delta_s\right.\right. \\ & \left.\left. - \frac{\sin\delta\sin\alpha}{\cos\left(\delta_s - \alpha\right)}\right)\right] d\delta\, d\phi \end{aligned} \tag{13}$$

where $f(\delta, \phi)$ is equal to $\epsilon_M \sigma T_M^4$. The limits on $\delta$ and $\phi$ are derived in Appendix B. Also given in this appendix are several other expressions for $I_{Th}$ which must be used in portions of the region of integration where Equation (13) cannot be used because of the term $1/\cos\delta_s$.

Figure I.3.G-4 shows the geometry for obtaining $\cos\xi_N$ when $\alpha$ is equal to zero. In this case, the extension of the normal (a) will intersect the x axis at a distance b from the origin. From Figure I.3.G-4.

$$\cos\xi_N = \frac{1}{2ad}\left(a^2 + d^2 - h^2\right) \tag{14}$$

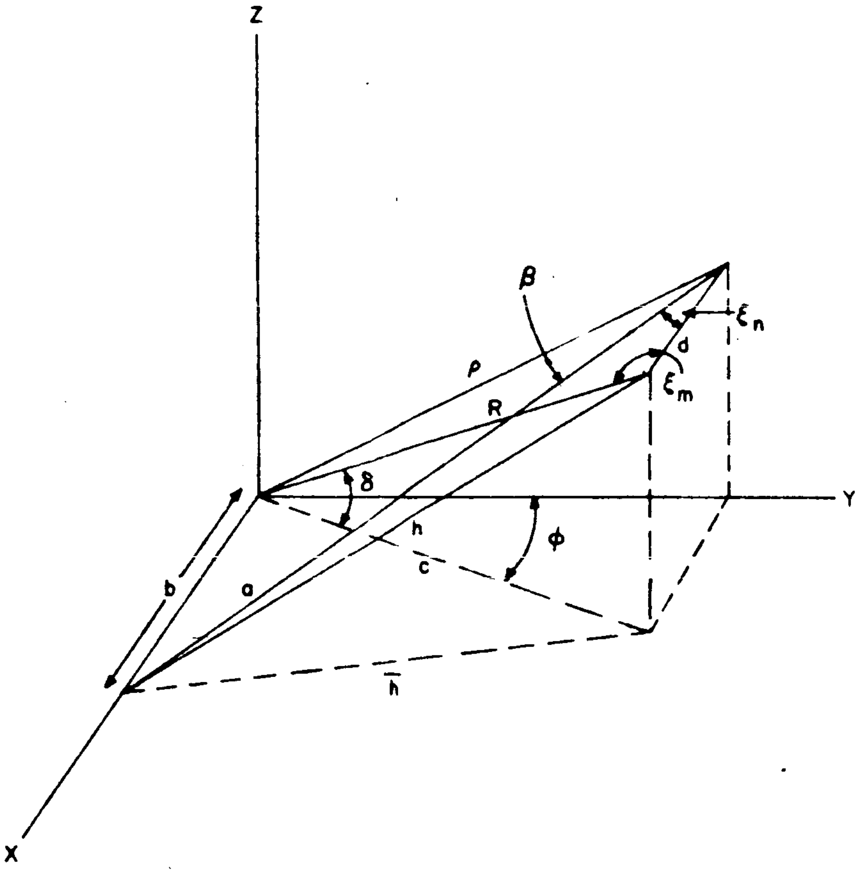

Figure I. 3. G-4 Geometry for Obtaining Cos $\xi_N$ when $\alpha$ is Zero*

where:

$$a = \frac{\rho}{\cos \beta}$$

$$h^2 = \bar{h}^2 + R^2 \sin^2 \delta$$

$$\bar{h}^2 = c^2 + b^2 - 2bc \cos\left(\frac{\pi}{2} - \varphi\right)$$

$$= c^2 + b^2 - 2bc \sin \phi$$

$$c = R \cos \delta$$

$$b = \rho \tan \beta$$

*Projections "a" and "b" are differently defined in Figures I. 3. G-3 and I. 3. G-4.

Solving for $\bar{h}$ yields:

$$\bar{h}^2 = R^2 \cos^2 \delta + \rho^2 \tan^2 \beta - 2 R \rho \cos \delta \tan \beta \sin \phi$$

Thus, when $\alpha$ is equal to zero:

$$\cos \xi_N = \frac{\rho}{2d} \cos \beta \left( \frac{1}{\cos^2 \beta} + \frac{d^2}{\rho^2} - B^2 - \tan^2 \beta - 2 B \cos \delta \tan \beta \sin \phi \right) \qquad (15)$$

Substituting Equations (7), (8), and (15) into Equation (4) yields:

$$I_{Th} = \frac{B^2}{\pi} \int_{\delta \min}^{\delta \max} \int_{\phi \min}^{\phi \max} f(\delta, \phi) \cos \delta \left[ \frac{\cos \delta \cos \delta_s \cos \phi - \sin \delta \sin \delta_s - B}{\left\{ 1 + B^2 - 2B \left( \cos \delta \cos \delta_s \cos \phi \right) \right\}^2} \right]$$

$$\left[ \cos \beta - B \left( \cos \delta \cos \delta_s \cos \phi \cos \beta + \cos \beta \sin \delta \sin \delta_s - \sin \beta \cos \delta \sin \phi \right) \right] d\delta d\phi \qquad (16)$$

The limits of integration for Equation (16) are derived in Appendix B (case B). To find the distribution of radiative power ($\epsilon_M \sigma T_M^4$), Bulletin 106 of the Lowell Observatory* was used to plot the radiative power as a function of $\delta$. A curve fit was then made with the function:

$$\epsilon_M \sigma T_M^4 = k \sin^{\frac{2}{3}} \delta \qquad (17)$$

as recommended by A. Markow.** Figure I. 3. G-5 shows the point of measurements and curves for values of k of 0. 8 watts per square inch and 0. 85 watts per square inch. Mr. W. M. Sinton* suggested that the measured values appear to be about 5 percent high. (The atmospheric transmission characteristic at the time of measurement was very good and the atmospheric correction used was slightly conservative.) Therefore, the value of 0. 8 watts per square inch was used for k. This agrees quite well with the theoretical prediction derived during the preliminary study.*** When multiplied by 0.95 to account for the 5-percent noted previously, the value of 0.8 watt per square inch is also the mean radiative power at the subsolar point as calculated by W. M. Sinton. The radiative power at the subsolar point as a function of the lunar phase angle of the moon's surface element) has also been published.* Plotting this measured value

---

* W. M. Sinton, et. al., "Isothermal Contours of the Moon", Lowell Observatory Bulletin 106.

** A. Markow, "The Moon, A Russian View", University of Chicago Press, 1962.

*** Final Report on Lunar Orbital Capsule Study, Contract No. 950340, dated 31 July 1962.

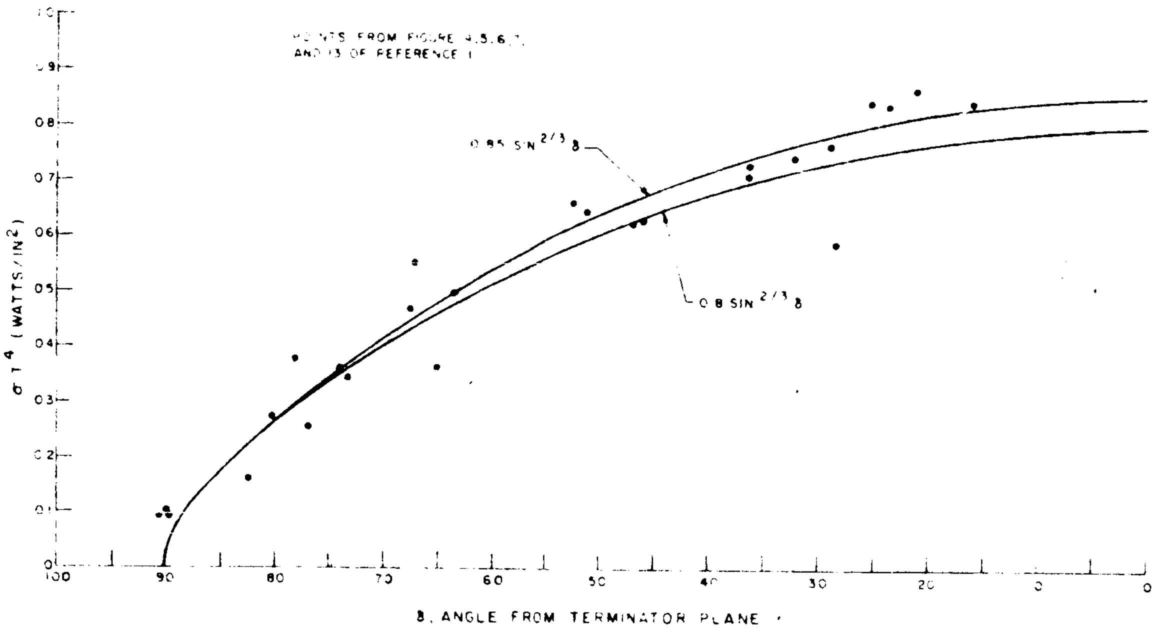

Figure I. 3. G-5 Radiative Power of the Lunary Surface as a Function of the Angle from the Terminator Plane

as a function of the view angle, $\xi_M$, and normalizing the values with respect to the values of $\epsilon / \epsilon_N$ (emission normal to the surface element) yields the emission characteristic, of the lunar surface as a function of the emission angle. The result of these calculations, shown in Figure I. 3. G-6, shows that the lunar surface cannot be treated as a diffuse emitter. (For a diffuse emitter, Lambert's Law would be represented in the figure by a straight line for which $\epsilon / \epsilon_N$ is equal to one.)

There is no well-accepted explanation for the peculiar emission characteristic. The peculiarity may result from lunar surface roughness (i. e., when viewed from an angle, only the relatively cold slopes of the mountains and valleys can be seen) or from the emission characteristic of a non-conducting surface.* To compare the measurements with the values obtained in this latter case, Figure I. 3. G-6 includes a curve representing the theoretical emission characteristic of a non-conducting surface having an index of refraction, N, of 2. (In this case, $\epsilon_N$ is the emissivity for emission normal to the surface element.) The obvious agreement with the measured values appears to justify the use of this curve to represent lunar surface emission. Thus, emission from the lunar surface can be given by:

$$
\begin{aligned}
\epsilon_M \sigma T_M^4 &= f(\delta, \phi) \\
&= k\, F\left(\xi_M\right) \sin^{\frac{2}{3}} \delta \qquad (18)
\end{aligned}
$$

---

* M. Jakob, "Heat Transfer", Vol. 1, John Wiley & Sons, New York 1949

RE-ORDER No. 62-459

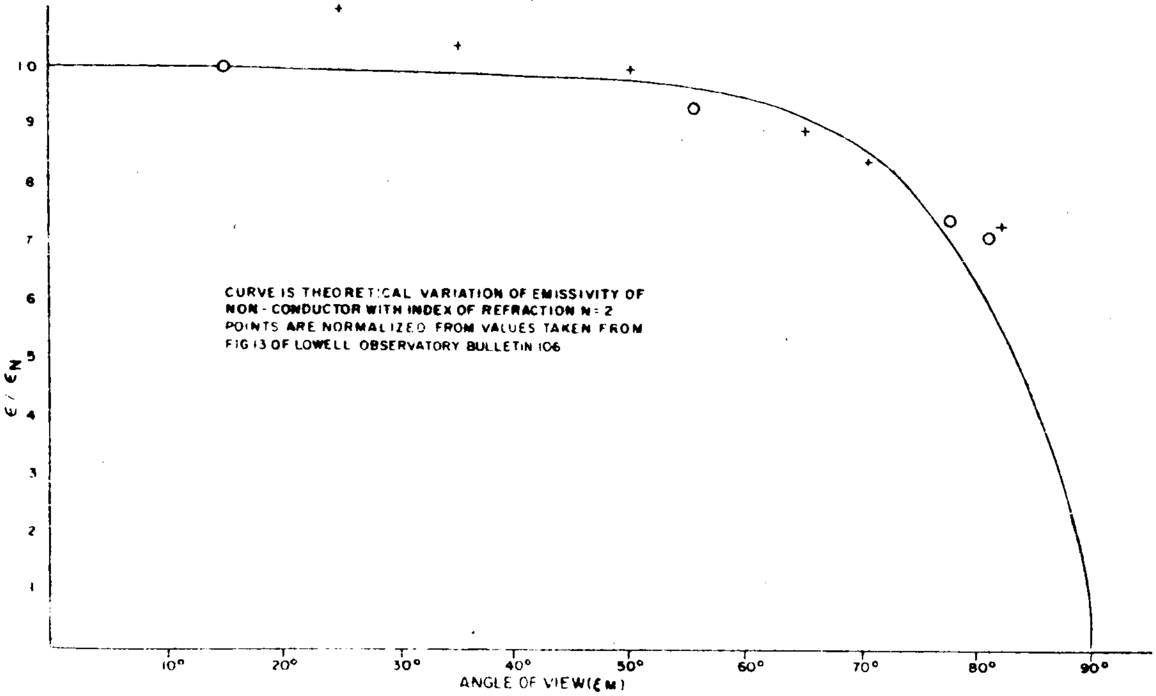

Figure I. 3. G-6 $\epsilon/\epsilon_N$ as a Function of View Angle $\xi_M$

The values of F ($\xi_M$) are tabulated in Appendix B. Using Equation (18), the value of k should be higher than that calculated from Sinton's measurements as the mean value for the subsolar point because the variation in the brightness of emission as a function of direction is already accounted for. Thus, the value of k should be selected according to the values measured at full moon. According to Lowell Observatory Bulleton No. 106, this value is 0.88 watt per square inch. With a 5-percent correction, it becomes 0.84 watt per square inch.

Substituting for k in Equations (17) and (18) yields:

$$\epsilon_M \sigma T_M^4 = 0.8 \sin^{\frac{2}{3}} \delta \tag{19}$$

$$\epsilon_M \sigma T_M^4 = 0.84 F \left(\xi_M\right) \sin^{\frac{2}{3}} \delta \tag{20}$$

The computations were made for each of these two functions at a given orbital altitude for various values of $\delta_S$. To show the influence of the emission characteristic, F ($\xi_M$), the constant in Equation (20), 0.84, was replaced by 0.8 to give the change in $I_{Th}$ resulting from the emission characteristic alone.

The computations were carried for 15-degree steps in the value of $\delta_S$, starting at the subsolar point and ending when only the non-illuminated surface could be seen ($\delta_S = \arccos \beta$). To account for the difference in the night temperature of the lunar surface at sunrise or sunset, two constant values of night temperature were assumed, according to an emissive power 0.014 watt per square inch or 0.008 watt per square inch. For values of $\delta_S$ for which the circle of view included part of the non-illuminated surface, the computations were made for both of these values. In cases where there was no significant difference in the computational results, one of the values was discarded.

The results of the computer program are the IR radiation density for a lunar orbit at orbital altitudes from 50 to 5000 kilometers and for various angles between the plane satellite surface and the position vector.

This same computer program can be used to determine the radiation input to the satellite due to reflected solar radiation. The only change that must be made is in the factor $\epsilon_M \sigma T_M^4$, which must be replaced by a brightness function, $B(\delta, \phi)$. The lunar surface is not a perfectly diffuse reflector; hence the function $B(\delta, \phi)$ is not, as it would be according to Lambert's Law, simply $Sa \sin \delta$ (where S is the solar constant and a is the mean albedo).

At the time of cancellation, information was being accumulated to determine the distribution of the brightness of sunlight reflected from the lunar surface.

## 3. VEHICLE THERMAL DESIGN

The thermal design of the vehicle itself (RTG-powered model) was concerned with maintaining the temperature within allowable limits during the mission. For convenience, the mission was divided into three phases:

(1) The transit phase;

(2) The TV and tracking phase, with 3-axis-stabilized attitude control; and

(3) The spin-up phase, occurring after 30 to 40 days in phase 2, during which only the tracking transponder would be operated.

The main objective of the thermal design effort was to avoid the need for active thermal control while still AC holding the temperature within allowable limits during all phases. This control is achieved, as shown in Figure I.3.G-7, by surrounding the electronic equipment with an insulating shroud which would probably consist of a few separated layers of light aluminized Mylar. The shroud would cover the entire vehicle except for an area directly behind the retro-rocket and an area surrounding the camera optics. These two areas would be used for additional thermal control during the last two phases. With this configuration, the temperature control during the three phases of the mission is achieved as detailed in the following paragraphs.

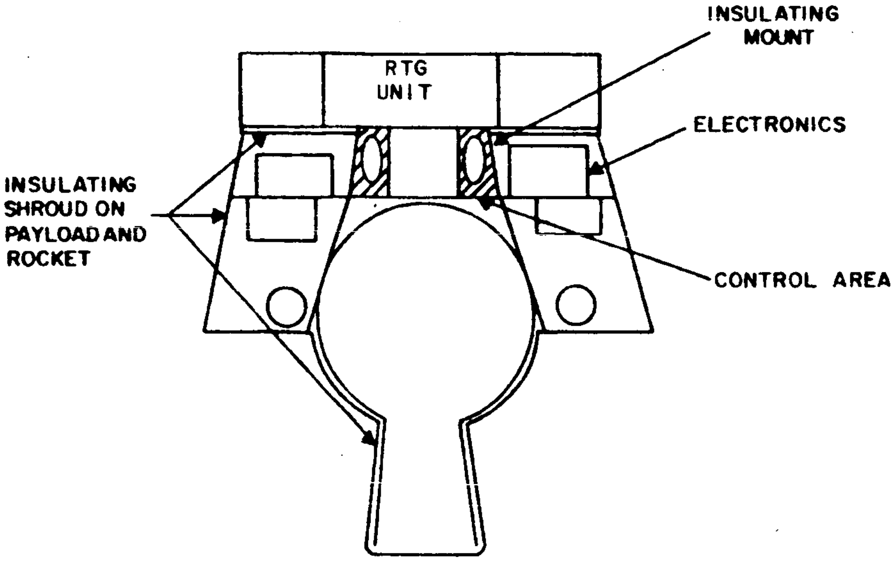

Figure I. 3. G-7 Thermal Design Aspects of the RTG Model of the LOC

During Phase 1, the transit phase, the temperature of the electronic equipment must be no lower than 0°C. During the transit trajectory, the vehicle is oriented such that the spin axis always points toward the sun; hence, there is almost no direct solar input into the vehicle. Even without the insulating cover, the solar radiation would strike the sides at such a low angle that the surface would act as a mirror. The solar input to the top would be blocked by the RTG power supply unit and the antenna. This RTG power supply offers a possibility of avoiding the thermal shield originally proposed for keeping a solar-cell-powered vehicle at proper temperatures during the transit phase. Two practical methods are available for keeping the equipment at the proper temperature during this phase:

(1) Using the heat generated by the RTG power supply; or

(2) Using the electrical power of the RTG to operate a small resistor which would supply enough heat to compensate for the small amount lost through the insulating cover.

The first method has the advantage of simplicity; however, heat transfer to the equipment from the RTG unit cannot be interrupted by simple means once the vehicle is injected into the lunar orbit. At that time, the equipment will be turned on, and it will no longer be desirable to have heat flowing into the equipment from the RTG. There is also the additional problem that the cold-junction temperature of the RTG decreases exponentially with time, corresponding to the decreasing output of the radioisotope fuel. It would then be extremely difficult to hold the heat transfer from the unit to the equipment at a constant level.

To avoid this drawback, the electrical power from the RTG unit can be used to heat the equipment through a resistive strip heater. Using this technique requires the RTG be thermally isolated from the electronic by an insulating mount. The amount of power required can be determined by considering how much heat will be lost through the insulating cover. By using only a single layer of aluminized Mylar, the emissivity of the outer surface can be reduced to at least .05. The heat loss would then be:

$$Q_{LOST} = A_s \epsilon \sigma T^4 \tag{21}$$

where:

$A_S$ = total radiating surface $\left(1500 \text{ in}^2\right)$

t = .05

T = 0°C (273°K)

$\delta$ = Stephan-Boltzmann constant

With these values:

$$Q_{LOST} = 37 \text{ watts} \tag{22}$$

Therefore, a resistor capable of dissipating 40 to 45 watts will keep the equipment sufficiently warm. After the transit phase, the heater can be turned off easily. During transit phase, it is also necessary to surround the rocket with an insulating shroud in order to keep its temperature from falling too low.

Upon entering a lunar orbit, Phase II, the TV and tracking phase, the retrorocket is to be jettisoned. When the rocket and its protective covering are jettisoned the area behind the rocket (denoted as "control area" in Figure I.3.G-7) is left exposed. This area can be used to radiate away part of the additional heat created when the electrical equipment is turned on. The amount of area needed can be approximately found from:

$$A_s \epsilon \sigma T^4 + A_{CA} \epsilon_{CA} \sigma T^4 = Q_{eL} \tag{23}$$

where:

$A_{CA}$ = additional control area needed

$\epsilon_{CA}$ = emissivity of area

$Q_{eL}$ = average heat dissipation of the electrical equipment. = 60 watts

For a temperature, T, of 30°C (303°K):

$$A_{CA}\,\epsilon_{CA} = \frac{Q}{\sigma T^4} - A_s\epsilon \tag{24}$$

$$= 119 \text{ in}^2$$

This quantity will increase slightly when the thermal inputs from the lunar surface are also included. The vehicle is injected in such a fashion that no direct solar radiation will strike this area. The final value for $A_{CA}\,\epsilon_{CA}$ will then probably be around 150 square inches. This value can easily be obtained by using a high-$\epsilon$, low-$\alpha$ paint on this area.

Phase 3, the spin-up phase, will start after 30 or 40 days of picture taking. At this time, all equipment except for the tracking transponder will be turned off and the vehicle will be space-stabilized by causing it to spin about its axis normal to the ecliptic plane. With the reduced power load, it will again be necessary to create an additional source of heat. Because of the exposure of the control area, which was covered by the retro-rocket during transit, it will be necessary to add more heat during this phase than during the transit phase. It is not practical to use the resistor which supplied the additional heat during the transit trajectory. Because of the time decay of the amount of power available from the RTG unit, it will be necessary to conserve as much power as possible in the latter part of the mission in order to extend the tracking portion as much as possible. Therefore, the area of the outer skin surrounding the camera optics will be used to supply the required input. It was mentioned at the beginning of this section that this area would not be covered with an insulating shroud like the rest of the vehicle. Instead, a skin with a high $\alpha/\epsilon$ ratio will be used. The low $\epsilon$ will keep down the heat loss by radiation during transit. Because of the small sun angle during transit, there will still be no appreciable sun input to this area even with a high $\alpha$. Also, while the vehicle is in its picture-taking mode, this area will always face the moon's surface; hence, there will be only a very small input directly from the sun shortly after sunrise and just before sunset. However, once the vehicle begins to spin, the sun will illuminate this area on every rotation. It is then a matter of determining just how much area is required to gain sufficient sun input into the vehicle to maintain the proper temperature level during this time. The actual amount needed will depend upon the results of the computer program, which will give the moon's IR and albedo inputs to the control surface on the bottom of the vehicle and which will also give the moon's albedo input to the side with the high $\alpha$. The program has not been run at this time; hence, any further calculations would be only approximations.

## H. QUALITY CONTROL

### 1. INTRODUCTION

The quality control plan has been prepared in conformance with existing Department of Defense quality assurance policies, particularly Specification MIL-Q-9858 and NASA Quality Publication NPC 200-2. The provisions of this plan would be fully implemented, and in the event of conflict between portions of this plan and any contractual requirements, the latter would control.

Two areas of quality control are not discussed in this section due to contract termination, but they are covered in the general policies of RCA. These areas are:

(1) Quality control participation during the design and development phase, and

(2) Change control for drawings, procedures, documents, and related material.

### 2. OBJECTIVES AND APPROACH

Complex space equipments must be produced under regulated conditions if adequate assurance of quality is to be realized. Production of such equipments requires a systems approach to the control of quality. The objectives of this plan are to establish a systems approach in order to determine those areas where controls are needed to assure a reliable end-product, and to define what these controls must be. In order to be effective, such an approach must include the following:

(a) The establishment and implementation of adequate controls,

(b) Objective evidence that the controls are effective, and

(c) Sufficient inspection and test data to insure that the control of quality is being maintained, and that the product complies with contractual requirements.

A quality control system is most effective when it is planned and developed in conjunction with other functions, such as production, engineering, and subcontracting. This is essential to assure that the development and implementation of quality control procedures and techniques are in phase with production planning and the purchase of subcontract material. This quality control plan has been developed in compliance with this principle.

### 3. SUBCONTRACTED MATERIAL

RCA will assume full responsibility for the adequacy and quality of all subcontracted materials and services, unless otherwise required contractually. Cognizant of this responsibility, RCA will:

(a) Select qualified sources,

(b) Require subcontractors to maintain an effective Quality Control System subject to RCA's approval,

(c) Conduct a survey of the subcontractor Quality Control System before production starts, or at any time thereafter to determine the extent of compliance with contractual requirements, and

(d) Provide surveillance, as deemed appropriate, and reserve the right to inspect at any time procedures, products, processes, and records to determine compliance with contractual requirements.

a. Selection of Subcontractors

Selection of subcontractors will be based on their previous quality history, as indicated by the RCA Vendor Rating System. If no previous quality history exists, selection will be based on a survey of the subcontractor's facilities and Quality Control System. It will be incumbent on the subcontractor to provide objective evidence to the satisfaction of RCA that he is capable of supplying items of a quality equal to or exceeding that contractually required.

b. Procurement Documents

Quality Control will review all procurement documents such as drawings, specifications, engineering orders, test procedures, and purchase orders, prior to release to a subcontractor, to assure that these documents contain and contractually impose on the subcontractor characteristics determined to influence quality. Specifically, these reviews will ascertain that:

(1) Drawings are complete in all details such as dimensions, tolerances, proper values of electrical components, explanatory notes, reference to process procedures, and marking of parts,

(2) Test procedures are adequate and contain all details of test performance including specific test equipment, environmental conditions, and conformance limits, and

(3) Any other documents, as applicable, include conditions, criteria, and methods or characteristics in conformance to contractual requirements.

Results of these reviews will be documented and kept in the Quality Control files along with document copies available for JPL review.

c. Source Inspection

RCA will either provide for source inspection or require objective evidence of compliance with contractual requirements where, in the opinion of RCA's Product Assurance management, the quality of the produced item cannot be solely determined by receiving inspection.

d. Receiving Inspection

Receiving inspections will be performed on all parts, components, and subassemblies in accordance with RCA-DEP Procedure No. 3413. Detailed inspection instructions will be prepared and submitted to JPL for review. Such inspection procedures will cover all aspects of testing, conformance verification, etc. as may be contractually required and/or in accord with best practices of the art.

e. Identification

Parts, components, assemblies, and raw materials received by RCA will be clearly identified and marked as may be required by contract, applicable drawings, or specifications. Receiving inspection personnel will indicate conformance or rejection by tag, stamp, color code or other medium. The integrity of lots will be maintained in bins which will indicate parts that:

(1) are awaiting test,

(2) have been accepted,

(3) have been rejected, or

(4) have been referred to the MRB for review

f. Failure and Deficiency Feedback

A closed-loop system of failure reporting and deficiency feedback will be instituted with all subcontractors and co-ordinated through RCA's purchasing function. Critical failures or malfunctions will be analyzed by RCA's Reliability Engineering function prior to transmittal of the information to a subcontractor to:

(1) Determine cause of failure,

(2) Properly assess the effect of such failures to mission objectives, safety, or delivery schedules, and

(3) Indicate solution to the problem, and request corrective action to correct existing deficiencies and to eliminate or minimize future occurrences.

Copies of all failure analyses and reports will be made available to JPL for information and review. Workmanship deficiencies will be analyzed, documented, and monitored by Quality Control.

## 4. RCA FABRICATED ARTICLES

This portion of the report outlines a quality control program to ensure that during the manufacturing phase the quality inherent in the design of the article is maintained.

a. Inspections and Tests

Inspections and tests will be performed in accordance with a prepared set of manufacturing and assembly flow charts and appropriate test procedures, respectively.

(1) Manufacturing and Assembly Flow Charts. Flow charts will be prepared for each subassembly, assembly, subsystem, and final system. Preparation of these flow charts will be based on a comprehensive study of:

(a) the articles to be manufactured,

(b) the fabrication and processing operations,

(c) system and hardware requirements, and

(d) special assembly or integration technique as may be required by the peculiarities of the system.

These flow charts will show a step-by-step manufacturing and test flow program, such as wiring, mounting of components, assembling of boards into "black boxes", electrical bench tests, environmental tests, and performance tests, along with the required quality control stations and surveillance points. These charts will be prepared in conjunction with engineering, manufacturing, and other appropriate functions to assure their adequacy and completeness. Distribution of these charts will be under the cognizance of Quality Control to insure timely implementation of all quality provisions.

(2) Inspection Procedures. Detailed inspection procedures will be prepared by the Quality Control activity and distributed to all inspection personnel. These procedures will include such information as:

(a) identification of the article,

(b) objective of the inspection,

(c) any measuring device needed to perform the inspection,

(d) detailed operations to be performed by the inspector,

(e) exact method of inspecting or measuring,

(f) conditions to be maintained during inspection and precautions to be observed,

(g) criteria for determining conformance or rejection of the article,

(h) values or characteristics to be observed, and

(i) tolerances and limits under which the characteristics or values being examined may be considered acceptable.

(3) Test Procedures. Test procedures will be prepared by responsible engineering activities and contain information similar to those listed in (a) through (i) above. All tests performed will be under the surveillance of Quality Control to assure proper performance. Data and results of these tests will be analyzed and certified by Quality Control.

(4) Inspection Performance. Inspections, as indicated on the manufacturing flow charts, will be performed by qualified inspectors or other appropriate Quality Control personnel and will insure that all articles are manufactured and assembled in conformance to designated workmanship standards.

(5) End-Item Test Plan. An End-Item Test Plan will be prepared and submitted to JPL for approval. Such a plan will provide:

(a) a technical description of the system and its components,

(b) the parameters to be inspected and tested on each unit and final system,

(c) the values and tolerances of these parameters, and

(d) the sequence of tests.

Final tests will be designed to verify performance under conditions which will simulate end-use to the highest practicable degree. The severity, duration, and number of such tests will be dictated by the conditions and environments under which the system will be required to perform.

(6) Final Inspections. Final inspections will be performed in accordance with a prepared set of procedures, and will provide sufficient assurance that quality characteristics have been incorporated in the design and manufacture of the article to assure reliable operation. Prior to implementation, final inspection procedures will be submitted to JPL for approval.

(7) Data. Data and results of final tests and inspection will be documented and certified by Quality Control regarding accuracy and completeness.

(8) Modifications After Final Tests and Inspection. Any modifications or repairs after final tests and inspection will be re-inspected and re-tested, as may be required, to a degree jointly determined by JPL and RCA.

b. Fabrication Controls

(1) Tooling and Fabrication Equipment. Any tooling or fixtures used in fabrication processes will be checked for initial accuracy, and such accuracy will be periodically verified, as deemed necessary, by critical tolerance requirements.

(2) Material [illegible]. Throughout the manufacturing cycle, the identity of materials and articles will be maintained by both marking of the items and appropriate records.

(3) Clean Areas. Articles whose performance may be degraded by contamination will be fabricated in controlled clean areas.

## 5. NON-CONFORMING MATERIAL

### a. Control

Non-conforming material will be clearly marked, removed from production operations, and subjected to review by competent, authorized personnel for evaluation, disposition, and corrective action.

### b. Material Review Board

A Material Review Board will be set up, consisting of the Quality Control Manager, Engineering Project Manager, and the JPL Representative. This board will be vested with authority to accept or reject discrepant material, and to prescribe any other intermediate course of action.

### c. Disposition

Generally, non-conforming material will be disposed of in one of the following ways:

(1) Material Containing Deviations. Material containing deviations will not be delivered unless specifically authorized by JPL. If for any reason RCA believes that material containing deviations can be utilized, request for approval of its use will be made to JPL.

(2) Material Containing Variations. By means of the review system, RCA will be responsible for control of all variations found during the inspection or test of parts, components, subassemblies, or completed equipment. Material containing variations will be disposed of in one of the following ways:

  (a) Reject Control. If the MRB determines that the material is unacceptable for use and is not economically repairable, this material will be clearly marked as such, diverted from normal channels, and not offered for acceptance or delivered for acceptable material.

  (b) Completed or Repaired Material. Where feasible, and with MRB concurrence, material may be completed or repaired, re-inspected and, if the required sanction has been granted, thereafter handled as acceptable material.

  (c) Use "As Is". If the variation, as originally discovered or resulting from repair, is of such a nature that in the board's unanimous opinion it cannot have a detrimental effect on the performance, reliability, safety, or mission of the equipment, the board may authorize further processing and shipment of the material with the variation present. In such cases, a report of the review action will be prepared and submitted to JPL. This report will contain the following information:

    1) Quantity affected,

    2) Reason for variation,

3) Justification for acceptance,

4) Corrective action taken to prevent recurrence of variation, and

5) Cut-in point of corrective action.

## 6. QUALITY CONTROL DOCUMENTATION

In-plant records will be maintained by Quality Control in five distinct areas:

(1) Purchased Material Inspection,

(2) Fabrication,

(3) Printed board assembly,

(4) Equipment Assembly and Test, and

(5) Packing and Shipping

The forms used for quality documentation of the above listed areas will be briefly described below.

### a. Purchased Material Inspection

(1) Performance Record. The Performance Record contains a complete history of all incoming inspections performed on a specific part number; one is maintained for each part number inspected.

(2) P. M. I. Data Card. A Parts Material Inspection Data Card is completed for each lot of material inspected, and serves as a performance record for each lot.

(3) Receiving Sheet. The reverse side of this sheet is completed, containing sufficient information for material reviews.

(4) Material Discrepancy Report. This is the official form for returning discrepant material to a supplier.

(5) Inferior Quality Report. This report is used to notify a supplier that discrepant material has been delivered to RCA, and, although material is not being returned, corrective action is required to prevent recurrence of discrepancy.

### b. Printed Circuit Assembly and Test

(1) Printed Circuit Inspection Report This report is used to document inspection operations in Printed Circuit Manufacturing.

(2) Printed Circuit Test Card. The PCT card is used by Production and Quality Control to record test results of all printed boards.

### c. Assembly and Test Quality Control

(1) Unit Performance Record - This is a three-part form used to record all defects and failures found during assembly, inspection, and test.

(2) Printed Circuit Analysis Tag - This is a tag attached to every printed board that is replaced due to failure.

(3) Reliability Forms - A total of seven reliability forms are used by Quality Control; they are:

1) Failure Report,

2) Equipment Repair sheet,

3) Log of Failures,

4) Failed Part Summary,

5) Failure Tag,

6) Equipment Longevity Log, and

7) AGREE Tag.

### d. Fabrication

(1) Parts Historical Record - This form is used as a performance record for all parts numbered that are manufactured by the fabrication plant.

(2) Parts Quality Control Daily Record - This record is completed daily by each inspector to indicate what lots have been rejected and what the rejection reasons were.

(3) Final Inspection Report - The FIR form is used to furnish a complete record of all lots that each inspector has checked each day.

(4) In-Process Tag - This is used to move material step-by-step in fabrication or assembly from operation to operation.

(5) First Piece Tag - These tags are used for first pieces coming off machines or from assembly operations.

(6) Approved Tags - These tags verify Quality Control approval for completed, finished good parts or assemblies going in stock, to the customer, or for spare parts.

(7) Quality Control Complaint Report - This form is used to report discrepancies found by Quality Control on material shipped from one department to another.

(8) Quality Action Notice - The QAN form is used to bring to the attention of responsible supervision that some quality characteristic in his area is out of control and requires correction.

(9) Quality Control Hold Notice - This hold notice is used to inform responsible supervision that a quality hold has been placed in his area due to repetitive discrepancies.

### e. Packing and Shipping

(1) Quality Control Inspection Report - The QCIR form is used by Quality Control shipping inspection to record its findings during inspection of items ready for shipment.

## 7. INSPECTION, MEASURING AND TEST EQUIPMENT

RCA presently provides for the maintenance, evaluation, and control of all inspection standards, gages, measuring, and test equipment in order to provide a valid measure of conformance to specification, drawing, and contractual requirements. This work is performed by the Measurement Engineering Laboratory (MEL) and other calibration activities throughout AED which operate in compliance with the calibration and maintenance requirements of Mil-Q-9858 and other applicable Government requirements.

### a. Measurement Engineering Laboratory

The MEL maintains Primary Reference Standards used in the calibration of Transfer Standards from all other calibration activities throughout the AED division.

(1) Calibration Laboratory - The Calibration Laboratory formulates and maintains control of the following:

- (a) Secondary Reference Standards,
- (b) Transfer Standards,
- (c) Measuring and Test Equipment,
- (d) Calibration Frequency,
- (e) Out-of-Service Equipment,
- (f) Equipment Status form,
- (g) Interim Calibration, and
- (h) Gages, Tools, and Fixtures of special design.

### b. Procedure

The individual calibration laboratories of the various activities of AED act in accordance with:

- (1) Quality Control Manual procedures
- (2) Calibration Laboratory procedures

(3) Government procedures

(4) Approved Manufacturer's procedures

(5) Documented specifications for gages, tools, and fixtures of special design.

c. Reference Standards

Reference Standards will be used for calibration of transfer standards and for cross-check purposes only. These standards will be maintained in good condition and periodically certified or calibrated by an approved Government laboratory. Calibration and certification reports will be kept on file. A history card will be maintained in the master file.

(1) Transfer Standards - Transfer Standards will be maintained and calibrated by MEL, with the use of certified Reference Standards. A periodic cycle of calibration will be based on Government specifications, monthly schedule and/or amount of usage. Records of calibration data will be kept on file in the MEL. Transfer standards will be labeled with decals, indicating date of calibration, next calibration due date, and transfer standard identification. A history card will be maintained in the master file for recall purposes.

(2) Measuring Equipment - Periodic calibration of measuring and test equipments will be performed according to calibration procedures and against properly calibrated transfer standards. History cards indicating initial and subsequent calibration results, inspector's initials, and date of calibration will be maintained in the master files. These equipments will also be labeled with decals, showing date of calibration and next calibration due date.

(3) Out-of-Service Equipment - Obsolete or out-of-service equipment will be properly identified by a "Warning" tag and stored in appropriate areas to prevent unauthorized or accidental use.

(4) Equipment Status Forms - The following forms will be used to control various phases of the calibration effort:

(a) Gage Control Record - used to record all the pertinent data of mechanical equipments, for initial and subsequent submittals.

(b) Color Code System - used to indicate the year, month, week and day of recalibration.

(c) Recall Notice Form - used to notify cognizant groups that specific items are due for calibration. Copies of this notice will be forwarded to the Quality Control activity so that adherence of the cognizant groups to calibration schedules can be monitored.

(d) Rejection Notice Form - used to notify cognizant groups that the rejected items should be repaired or replaced.

(e) Label Identification System - used to indicate date calibration performed and/ or calibration due date, and Transfer Standard identification.

(f) Warning Tag - used to inactivate delinquent equipment and to segregate infrequently used equipment with notification of calibration before use.

## I. MASTER PROGRAM PLAN

Effort on the Master Program Plan was preliminary and conceptual in nature. Development of an actual plan requires final definition of the overall design configuration and had just been started at the time of contract termination.

The concept of the Master Program Plan centered around two basic techniques: the work structure breakdown, and the PERT network. This concept provides the benefits of PERT planning, and also insures a systematic breakdown of work. The work breakdown defines assignments and responsibilities clearly, and provides the work structure required for subsequent application of a PERT/COST program.

The first step in generating a Master Program Plan is to develop the work structure breakdown and, having done this, use it as the framework for PERT network analysis and shop order cost-collection and control system. At the time of contract termination, preparation of the work structure breakdown was in process. The over-all Lunar Orbiter Capsule program structure at RCA was broken down into organizational "black boxes", such as the Capsule, Program Management, Support Equipment, and Support Personnel. Each of these was further broken down. Program Management, for instance, was subdivided into system analysis and design, reliability documentation, and program control. The Capsule was broken down into the TV subsystem, telecommunication, attitude control, structure, power supply, system integration, and retro-propulsion. This breakdown continued down to the level of modulators, multiplexers, amplifiers, etc. As the particular breakdowns were agreed upon, responsibility was to be assigned, by name, to each listing or box on the chart.

Upon completion of the work structure breakdown, a state never attained, PERT networks were to be prepared for each subsystem and for the system integration. The networks were to be prepared under the direction of the engineer responsible for the subsystem, with each activity assigned to a specific person. Integration of the individual networks and any resultant re-planning, using a computer and the PERT program, would have yielded the over-all plan for the Lunar Orbiter Capsule.

# Section 4
# FAILURE MODE AND RELIABILITY ANALYSIS

## A. SCOPE OF ANALYSIS

The reliability analysis for the Lunar Orbiter Capsule Study Phase II, comprised the following major tasks.

(1). Development of a Mathematical Model

(2) Reliability Analysis and Prediction

(3) Failure Effects Analysis

(4) Development of a Reliability Program for the Design, Development, and Fabrication Phases.

## B. MATHEMATICAL MODEL

A reliability mathematical model, from which the probability of a successful mission may be determined, was developed for those systems for which sufficient information was available. Reliability block diagrams have been prepared for the TV Camera and Transmitter, Tape Recorder, Transponder, and Attitude Control systems. Insufficient data was available to prepare the reliability diagrams of the Power Supply, Telemetry, and Control systems.

The block diagrams of the Reliability Mathematical Model for each subsystem can not be interpreted as signal flow diagrams. They show those component assemblies or subsystems which must operate properly during the mission to provide the required information at the subsystem interface or to the earth. For example, the transmitter power supply is not in the signal flow path. It is, however, a required element for proper continuous operation of the transmitter. Hence, it is properly considered a series element in the subsystem model. The same reasoning applies to the Solar or Nuclear Power Supplies as series items in the overall system.

A detailed analysis of all subsystems will not be given here. An analysis of the TV System will be presented as a representative example.

The TV system may be operated in either of two modes, remote or direct mapping. The direct mapping mode does not utilize the Tape Recorder unit. This mode would be used infrequently because mapping and transmission of the video information in this mode must be accomplished simultaneously. It cannot, therefore, be considered an alternate or redundant method because of orbital and transmission considerations.

Ignoring the camera reliability for the moment, it is seen from Figure I. 4. B-1 that the probability of survival ($P_{TV}$) of the TV system in the remote mapping mode may be written as:

$$P_{TV} = P_p \, P_{TR} \, P_{XM}$$

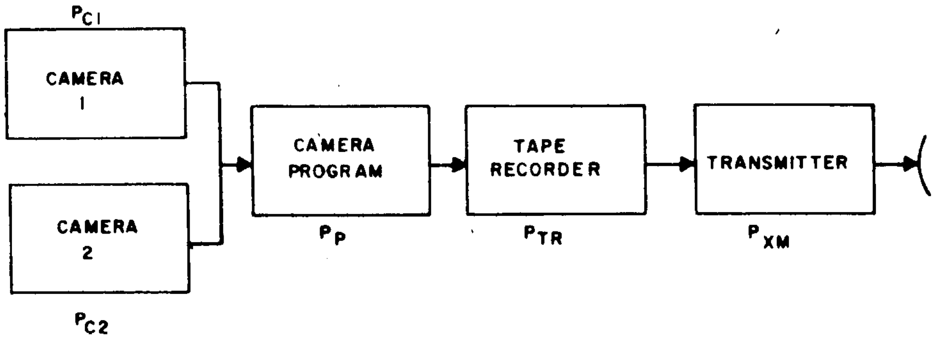

$$P_{TV_2} = (P_{C1} + P_{C2} - P_{C1} P_{C2}) \, P_P \, P_{TR} \, P_{XM}$$

$$= (2P_C - P_C^2) \, P_P \, P_{TR} \, P_{XM} \qquad \text{(IDENTICAL CAMERA)}$$

Figure I. 4. B-1. TV Subsystem Reliability Diagram (Remote Mapping)

Cameras 1 and 2 are not redundant because their fields of view differ in extent. There are four possible operating conditions for the two identical cameras.

$P_{c_1}$ = Probability that camera 1 operates for the entire mission

$P_{c_2}$ = Probability that camera 2 operates for the entire mission

$P_{c_1} \, P_{c_2}$ = Probability that both cameras operate for the entire mission.

$(P_{c_1} + P_{c_2} - P_{c_1} \, P_{c_2})$ = Probability that at least one camera will operate for the entire mission.

The mission can be considered partially successful if one camera survives. Utilizing the above relations, the probability of survival of the TV system with one surviving camera may be expressed as:

$$P_{TV_r} = (2P_c - P_c^2) \, P_{TV} = (2P_c - P_c^2) \, P_p \, P_{TR} \, P_{XM}$$

Similar analyses for the Tape Recorder, TV Transmitter and the Attitude Control System have been performed with the results indicated in Figures I. 4. B-3 through I. 4. B-6. An analysis of the TV system in the direct mapping mode has been included (Figure I. 4. B-2) to complete the set.

The probability of survival of the entire system is the combined product of the probabilities of survival of the individual sybsystems. The prime mission of the LOC is the TV Mapping; the ranging mission is secondary. The final probability of survival, therefore, could have been expressed in several forms, such as

(1) Survival of the TV system and the necessary auxiliary subsystems,

(2) Survival of the TV and Ranging systems together with the auxiliary subsystems, and

(3) Survival of the Ranging and auxiliary subsystems. Together, these would allow better system analysis and comparison.

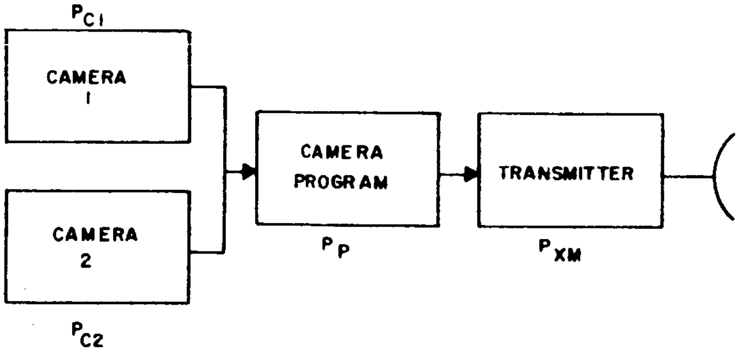
$P_{C1}$
CAMERA 1
CAMERA 2
$P_{C2}$
CAMERA PROGRAM
$P_P$
TRANSMITTER
$P_{XM}$

$$P_{TV_2} = (P_{C1} + P_{C2} - P_{C1}P_{C2})\ P_P\ P_{XM}$$

$$= (2P_C - P_C^2)\ P_P\ P_{XM} \qquad \text{(IDENTICAL CAMERAS)}$$

Figure I. 4. B-2. TV Subsystem Reliability Diagram (Direct Mapping)

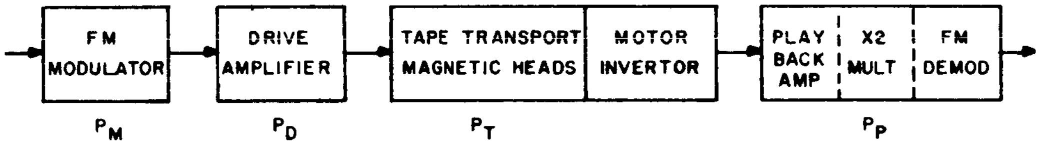
FM MODULATOR
$P_M$
DRIVE AMPLIFIER
$P_D$
TAPE TRANSPORT MAGNETIC HEADS
MOTOR INVERTOR
$P_T$
PLAY BACK AMP
X2 MULT
FM DEMOD
$P_P$

$$P_{TR} = P_M\ P_D\ P_T\ P_P$$

Figure I. 4. B-3. Tape Recorder Reliability Diagram

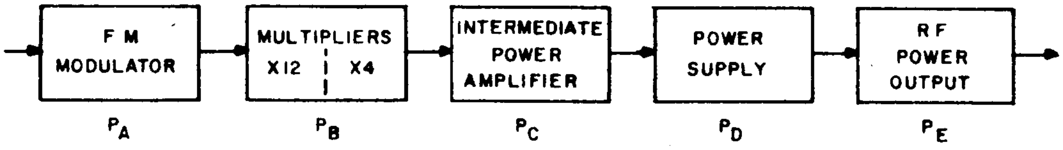
F M MODULATOR
$P_A$
MULTIPLIERS X12 X4
$P_B$
INTERMEDIATE POWER AMPLIFIER
$P_C$
POWER SUPPLY
$P_D$
R F POWER OUTPUT
$P_E$

$$P_{XM} = P_A\ P_B\ P_C\ P_D\ P_E$$

Figure I. 4. B-4. TV Transmitter Reliability Diagram

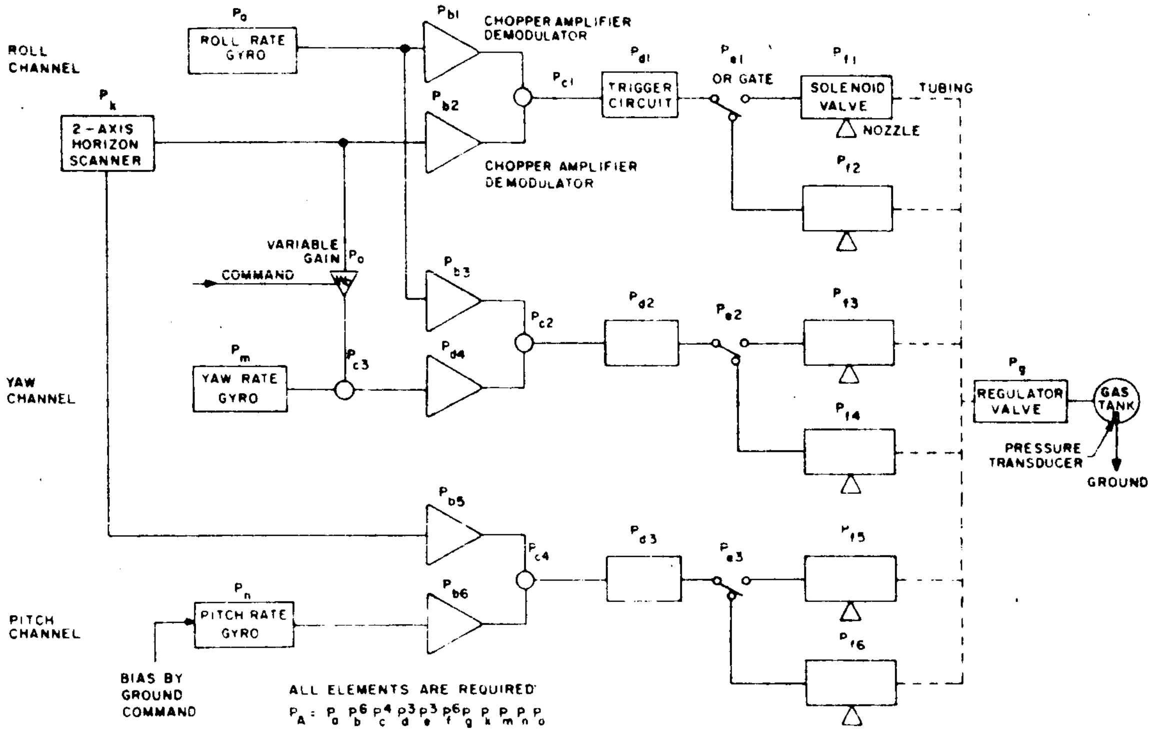
ROLL CHANNEL
$P_a$
ROLL RATE GYRO
$P_k$
2-AXIS HORIZON SCANNER
$P_{b1}$
CHOPPER AMPLIFIER DEMODULATOR
$P_{b2}$
CHOPPER AMPLIFIER DEMODULATOR
$P_{c1}$
$P_{d1}$
TRIGGER CIRCUIT
$P_{e1}$
OR GATE
$P_{f1}$
SOLENOID VALVE
NOZZLE
TUBING
$P_{f2}$
VARIABLE GAIN $P_o$
COMMAND
$P_{b3}$
$P_{c2}$
$P_{d2}$
$P_{e2}$
$P_{f3}$
YAW CHANNEL
$P_m$
YAW RATE GYRO
$P_{c3}$
$P_{d4}$
$P_{f4}$
$P_g$
REGULATOR VALVE
GAS TANK
PRESSURE TRANSDUCER
GROUND
$P_{b5}$
$P_{c4}$
$P_{d3}$
$P_{e3}$
$P_{f5}$
PITCH CHANNEL
$P_n$
PITCH RATE GYRO
$P_{b6}$
$P_{f6}$
BIAS BY GROUND COMMAND
ALL ELEMENTS ARE REQUIRED
$P_A = P_a \, P_b^6 \, P_c^4 \, P_d^3 \, P_e^3 \, P_f^6 \, P_g \, P_k \, P_m \, P_n \, P_o$

Figure I.4.B-5. Attitude Stabilization Reliability Diagram (Mapping Phase)

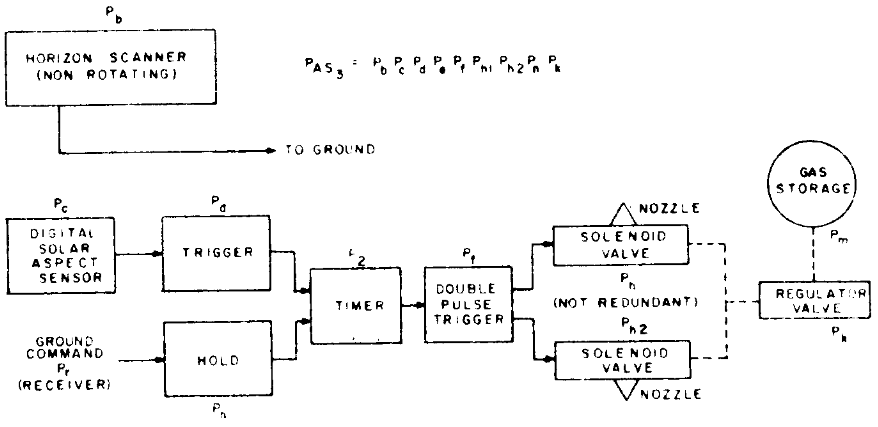
$P_b$
HORIZON SCANNER (NON ROTATING)
TO GROUND
$P_{AS_3} = P_b \, P_c \, P_d \, P_e \, P_f \, P_{h1} \, P_{h2} \, P_n \, P_k$
$P_c$
DIGITAL SOLAR ASPECT SENSOR
$P_d$
TRIGGER
$P_e$
TIMER
$P_f$
DOUBLE PULSE TRIGGER
NOZZLE
SOLENOID VALVE
$P_h$
(NOT REDUNDANT)
$P_{h2}$
SOLENOID VALVE
NOZZLE
GAS STORAGE
$P_m$
REGULATOR VALVE
$P_k$
GROUND COMMAND
$P_r$
(RECEIVER)
HOLD
$P_n$

Figure I.4.B-6. Attitude Stabilization Reliability Diagram (Post-Mapping Phase, Erection of Spin Axis)

## C. RELIABILITY ANALYSIS AND PREDICTION

The camera, TV transmitter, transponder, and tape recorder units for the Lunar Orbiter Capsule were expected to be modified versions of existing equipments. A parts complexity analysis was carried out for the camera, transponder, and tape recorder as information became available. Because the parts analysis data was readily available for the modified TV transmitter, the probability of its survival was calculated. The reliability of this component is 0.988 for an operating time of 50 hours for the first 30 days in orbit.

The balance of the subsystems elements were not completely defined. Therefore, the parts complexity analysis could only have given an estimate based on similar systems, components, and circuits. This was considered inadequate for this report.

The reliability analysis and prediction, when completed, would indicate which subsystems and components required the greatest design effort within the established time limits.

No definite reliability goal was established for this study and, therefore, no allocation of reliability was made for the various subsystems.

## D. FAILURE EFFECTS ANALYSIS

Failure effects analysis is a procedure for systematically examining all the modes of failure of an equipment. This procedure is designed to uncover any reliability problem areas and to direct attention to them. The analysis is performed at the system, subsystem, and circuit levels as the work progresses through the various phases of study, design, and development.

The failure effects analysis of this study was performed at the black box level, assuming a catastrophic failure of some element such as Vidicon open filament, jammed shutter, major component degradation or failure, and loss of signal. Because of the nature of the failure modes considered, the consequences of the failure were catastrophic in the majority of the cases. The results of the failure effects analyses on the subsystems of the TV cameras, Tape Recorder, TV Transmitter and the Attitude Control System are tabulated in Table I. 4. D-1.

The results shown in Table I. 4. D-1 may be misleading unless the probability of occurrence of each failure mode is considered. The probability of occurrence (column 6 of the tables) was not tabulated during this period. The relative reliability risk is the product of the probability of occurrence and the degree of degradation resulting from the failure mode. A comparison of the relative reliability risks quickly reveals the failure modes requiring further design effort to minimize the possibility of failure.

This method of analysis is very effective, although the degree of degradation and probability of occurrence of the failure mode may be a rough estimate. When concientiously applied within the framework of the program design limitations, the maximum design reliability may be achieved at the system and circuit levels.

RE-ORDER No. 62-489

## TABLE I. 4. D-1
## FAILURE EFFECTS ANALYSIS

## TV SUBSYSTEM

| Failure | Cause | Consequences | Classification | Compensation | Probability * of Occurrence |
|---|---|---|---|---|---|
| Camera | | | | | |
| Vidicon | Vibration, shock, filament open | No picture | Catastrophic | Provide 2nd Camera | |
| Yoke | Open, shorted turns | No deflection<br>Out of Focus | Catastrophic | Provide 2nd Camera | |
| Shutter | Open circuit, jams | No picture | Castastrophic | Provide 2nd Camera | |
| Iris Control | Any Failure in operation | Contrast degradation | 50% Capability | Provide 2nd Camera | |
| Lens | 1. Damage or coating of Objective from Rocket Flashback.<br>2. Failure to remove protective covering upon orbital injection. | Minor to very poor picture | ~50% Capability | Provide 2nd Camera | |
| Pre-Amplifier | Component Failure (Major) | No picture | Catastrophic | Provide 2nd Camera | |
| Camera Electronics | | | | | |
| Programmer | Loss of Control Signals | No picture | Catastrophic | Provide Alternate Unit | |

*Not computed

RE-ORDER No. 62-489

## TABLE I. 4. D-1 (Continued)
## FAILURE EFFECTS ANALYSIS (Continued)

### TV SUBSYSTEM

| Failure | Cause | Consequences | Classification | Compensation | Probability of Occurrence |
|---|---|---|---|---|---|
| Beam and Focus Regulators | Loss of Regulation,<br>No Current | Poor picture<br>No picture | 50% Capability<br>Castastrophic | Provide Alternate Unit | |
| Power Supply & Voltage Regulator | Voltage Loss | No picture | Castastrophic | Provide Alternate Unit | |
| Video Amplifier | Degraded Component<br>Major Component Failure | Poor picture<br>No picture | 50% Capability<br>Catastrophic | Provide Alternate Unit | |
| Sequencer | | | | | |
| Master Clock | Major Component Failure | No Timing | Catastrophic | Provide Alternate Unit | |
| Timer Chain | Failure | Loss of Sync | Catastrophic | Provide Alternate Unit | |
| Sequence Timer | Failure | Loss of Control | Catastrophic | Provide Alternate Unit | |

## TABLE I. 4. D-1 (Continued)

## FAILURE EFFECTS ANALYSIS (Continued)

### TV SUBSYSTEM

| Failure | Cause | Consequences | Classification | Compensation | Probability of Occurrence |
|---|---|---|---|---|---|
| Combiner<br>Gates | Major Component | Loss of Video and/or Sync | Catastrophic | Provide Alternate Unit | |
| Summing Amplifier | Failure | No picture | Catastrophic | Provide Alternate Unit | |
| Direct-Remote | Switch-motor Failure | Only one mode possible | 75% capability in remote, only 25% in direct | | |
| | Switch open | No Video output | Catastrophic | | |
| Attitude Control System | Jet Control Failure | Slow drift or optical axis -- degraded picture until axis drifts beyond moon | 50% capability | None | |

## TABLE I.4.D-2
## FAILURE EFFECTS ANALYSIS
## TAPE RECORDER

| Failure | Cause | Consequences | Failure Classification | Compensation | Probability * of Occurrence |
|---|---|---|---|---|---|
| FM Modulator | Active Component Failure | No Video Recording | Catastrophic | Use Direct Transmission | |
| Head Drive Amplifier | Active Component Failure | No Video Recording | Catastrophic | Use Direct Transmission | |
| Magnetic Head | Open or Short | No Video Recording | Catastrophic | Use Direct Transmission | |
| Tape Transport | Mechanical Failure | No Recording or Playback | Catastrophic | Use Direct Transmission | |
| Playback Head | Open or Short | No Playback | Catastrophic | Use Direct Transmission | |
| Playback Amplifier | Active Component Failure | No Recorded Video | Catastrophic | Use Direct Transmission | |
| Frequency Doubler | Active Component Failure | No Recorded Video | Catastrophic | Use Direct Transmission | |
| FM Demodulator | Active Component Failure | No Recorded Video | Catastrophic | Use Direct Transmission | |
| Motor | Electrical Failure | No Recording or Playback | Catastrophic | Use Direct Transmission | |
| Inverter Power Supply | Active Component Failure | No Recording or Playback | Catastrophic | Use Direct Transmission | |

*Not computed

TABLE I. 4. D-3

FAILURE EFFECTS ANALYSIS

TV TRANSMITTER

| Failure | Cause | Consequences | Failure Classification | Compensation | Probability of Occurrence * |
|---|---|---|---|---|---|
| Modulator | Active Component Failure | No Video Transmission | Catastrophic | None | |
| Frequency Multipliers | Active Component Failure | No Video Transmission | Catastrophic | None | |
| Power Supply | Regulator or Active Component Failure | No Video Transmission | Catastrophic | None | |
| Intermediate Power Amplifier | Vacuum Tube Failure | No Video Transmission | Catastrophic | None | |
| RF Power Output Amplifier | Vacuum Tube Failure | No Video Transmission | Catastrophic | None | |
| Antenna Positioner | Motor Failure | Poor Antenna Positioning, Weak Ground Signal | ~50% Capability for mission | None | |
| Attitude Control | Jet Control Failure | Slow drift of axis beyond antenna beam adjustment range | 75% capability | None | |

*Not computed

RE-ORDER No. 62-489

## TABLE I. 4. D-4

## FAILURE EFFECTS ANALYSIS

## ATTITUDE STABILIZATION SYSTEM A - PURE JET CONTROL

| Failure | Cause | Consequences | Failure Classification | Possible Compensation | Probability of Occurrence* |
|---|---|---|---|---|---|
| Roll Channel | | | | | |
| Roll Gyro | Motor Failure | 1. Loss of Roll & Yaw Information | Catastrophic | None | |
| | Torquer Failure | 2. Roll Axis Offset Signal Present | Catastrophic | Ground Command Offset Reference | |
| Roll Horizon Scanner | Active Component Failure | Loss of Roll Reference | Catastrophic | Ground Command Offset Reference | |
| Chopper Amplifiers | Active Component Failure | Loss of Reference or Error Signal | Catastrophic | None | |
| Modulator or Demodulator | Chopper Failure (non-operative) | Roll axis offset | Catastrophic | None | |
| Trigger Circuit | Active Component Failure | No Roll Correction | Catastrophic | None | |
| OR Gate | Component Failure | No Roll Correction | Catastrophic | None | |

*Not computed

TABLE I. 4. D-4 (Continued)

FAILURE EFFECTS ANALYSIS (Continued)

ATTITUDE STABILIZATION SYSTEM A - PURE JET CONTROL

| Failure | Cause | Consequences | Failure Classification | Possible Compensation | Probability of Occurrence |
|---|---|---|---|---|---|
| Solenoid Valve | Sticking valve | No Roll Correction or Overcorrection | Catastrophic | None | |
| | | Loss of gas | Catastrophic | None | |
| | Open coil in solenoid | No Roll Correction Possible | Catastrophic | None | |
| Yaw Channel | | | | | |
| Yaw Gyro | Motor Failure | Loss of Yaw Info & Roll Cross-Coupling | Catastrophic | None | |
| | Torquer Failure | Yaw Axis Offset Signal Always Present | Catastrophic | Ground Command Offset Reference | |
| Roll Horizon Scanner | Active Component Failure | Loss of Roll Reference for Roll Cross-Coupling Correction | Catastrophic | Ground Command offset Reference | |

RE ORDER No. 62-4F9

## TABLE I. 4. D-4 (Continued)

## FAILURE EFFECTS ANALYSIS (Continued)

## ATTITUDE STABILIZATION SYSTEM A - PURE JET CONTROL

| Failure | Cause | Consequences | Failure Classification | Possible Compensation | Probability of Occurrence |
|---|---|---|---|---|---|
| Chopper Amplifier | Active Component Failure | Loss of Reference or Error Signal | Catastrophic | None | |
| | | Permanent Offset | Catastrophic | None | |
| Chopper Modulator and Demodulator | Chopper Failure | Loss of Reference or Error Signal | Catastrophic | None | |
| | | Permanent Offset | Catastrophic | None | |
| Trigger Circuit | Active Component Failure | No Yaw Correction | Catastrophic | None | |
| OR Gate | Component Failure | No Yaw Correction | Catastrophic | None | |
| Solenoid Valve | Open Circuit | No Yaw Correction | Catastrophic | None | |
| | Sticky Valve | No Correction or Overcorrection, Loss of Gas | | | |

### TABLE I. 4. D-4 (Continued)

### FAILURE EFFECTS ANALYSIS (Continued)

### ATTITUDE STABILIZATION SYSTEM A - PURE JET CONTROL

| Failure | Cause | Consequences | Failure Classification | Possible Compensation | Probability of Occurrence |
|---|---|---|---|---|---|
| Pitch-Channel | | | | | |
| Pitch Rate Gyro | Motor Failure | Loss of Pitch Error Signal | Catastrophic | None | |
| | Torquer Failure | Pitch Axis Offset Signal Always Present | Catastrophic | None | |
| Pitch Horizon Scanner | Active Component Failure | Loss of Pitch Reference | Catastrophic | Ground Command Offset Reference | |
| Chopper Amplifier | Active Component Failure | Loss of Reference or Error Signal | Catastrophic | None | |
| Chopper Modulator or Demodulator | Chopper Failure | Loss of Reference or Error Signal | Catastrophic | None | |
| Trigger Circuit | Active Component Failure | No Pitch Error Correction | Catastrophic | None | |
| OR Gate | Component Failure | No Pitch Error Correction | Catastrophic | None | |
| Solenoid Valve | Open Solenoid | No Pitch Correction | Catastrophic | None | |
| | Sticky Valve | No Correction or Overcorrection, Loss of Gas | Catastrophic | None | |

## TABLE I.4.D-5

## FAILURE EFFECTS ANALYSIS

## ATTITUDE STABILIZATION - POST - MAPPING PHASE SYSTEM A - PURE JET CONTROL

| Failure | Cause | Consequences | Failure Classification | Possible Compensation | Probability of Occurrence |
|---|---|---|---|---|---|
| Erection of Spin-Axis | | | | | |
| Horizon Scanner | Active Component Failure | Loss of Horizon-Data Telemetry | Catastrophic | None | |
| Digital Solar Aspect Sensor | Active Component Failure | Incorrect solar Reference Information | 75% capability | Ground Command Correction | |
| Trigger Circuit | Active Component Failure | No Solar Reference Correction | Catastrophic | Ground Command Correction | |
| Timer | Active Component Failure | No Attitude Correction | Catastrophic | None | |
| Pulse Trigger Circuit | Active Component Failure | No Attitude Correction | Catastrophic | None | |
| Solenoid | Open Solenoid Coil | No Attitude Correction | Catastrophic | None | |
| | Sticky Valve | No Attitude Correction | Catastrophic | None | |
| | | Overcorrection | Catastrohpic | None | |

RE-ORDER No. 62-489

## E. RELIABILITY PROGRAM FOR LOC DESIGN AND DEVELOPMENT

### 1. INTRODUCTION

The degree of reliability is an inherent characteristic of an electronic system acquired at the time of concept formulation and design commitment. Because the reliability is established by the equipment design, it can be improved only by design changes. After the design is established it can only be degraded by poor quality control, parts selection, and fabrication techniques. To minimize and eliminate this degradation, a continuous reliability analysis program must run concurrent with system planning, development and fabrication. Through constant monitoring and analysis, immediate corrective action can and must be instituted, when design and component defects are indicated, to minimize all designed-in or fabricated reliability risks.

The following paragraphs outline a reliability program for the Lunar Orbit Capsule design and development phases.

### 2. MISSION ANALYSIS

The mission goals will be established to determine the reliability requirements for a successful mission. The establishment of these goals is necessary so as to permit differentiating between items essential to the mission success and those ancillary items which have various degrees of effect on the mission quality. For example, in the LOC mission the transmission of the TV pictures is of prime importance, the ranging experiment and telemetry are secondary. The essential items, therefore, are the TV system, power supplies, attitude control, and command systems.

A study of the mission profile will be made to analyze the environmental and operational conditions encountered by each subsystem during each phase of the equipment life. These phases shall include manufacturing and acceptance testing, storage, and testing prior to and after mating with the launch vehicle, launching into orbit, orbital flight, and thermal environments. The effects of the various inputs, outputs, and duty cycles in the various environments to be encountered will be investigated.

### 3. DESIGN REVIEWS AND ANALYSES

The purpose of the design review is to bring to bear on each design the cumulative knowledge of personnel having extensive prior experience on all facets of the design. This procedure serves to minimize error, to assure a more reliable and producible end product, to determine that the best approaches are being used in meeting design objective, and, by evaluation, to assure that the design objectives are truly being realized.

The design review board notes and records all deficiencies and needed improvements in the equipment design. The recommendations of the design review board become action items, notices of which together with the minutes of the design review are circulated promptly (within 5 days) to all cognizant personnel. The

Engineering Product Assurance office is responsible for follow-up on the action items to see that they are implemented as soon as possible. These actions are followed for all design reviews.

For LOC, a minimum of three design reviews for each system will be held. They will be as follows:

a. Preliminary Review

The preliminary review will be held during the planning stage before any extensive breadboarding is started. (Breadboarding for feasibility studies may be performed.) This design review will be held to evaluate the design approach(es) required to meet the applicable specifications. The results of the feasibility studies will also be considered at this time. An outline of the design review plan for the subsequent design program will be developed at this time and distributed to all cognizant personnel. The extent of required redundancy and a preliminary analysis of weight, performance, and configuration will result from this review.

b. Major Review

This review will be conducted at the completion of the breadboard testing stage and prior to fabrication. This is the most important review. It presents the best opportunity to initiate any required major rework and specification revisions before the fabrication of the prototype or engineering proof test models. The use of standard and approved components, and specification and test data for special components, together with other circuit details, such as specifications for inputs and outputs, will be reviewed. Emphasis will be placed on meeting all reliability objectives. Consideration will also be given to weight, power, configuration control, installation, operation and testing, producibility, interchange ability of similar units, and like attributes.

Additional design reviews will be held as required or requested by the design and reliability personnel.

c. Final Review

The final review will be held after the completion of the engineering model, or prototype system or subsystem testing as applicable. Any difficulties encountered when using the equipment in the system will be highlighted. It will review all circuit (including mechanical and thermal) changes or problems introduced or encountered subsequent to the Major design review, and any required revisions of the test and performance specifications for successful system operation. This review will also consider weight, power, configuration, etc. The primary goal will be to obtain an overall view of the performance expected during the production cycle, preflight testing, and mission performance.

## 4. RELIABILITY AND QUALITY CONTROL

### a. Parts Selection, Evaluation, and Control

The starting point for incorporating reliability into system design is at the component parts level. The selected parts should be capable of meeting electrical and environmental requirements, and have reliability characteristics consistent with the design goals. Parts will be selected on the basis of performance data from use in prior systems with similar characteristics, or as a result of laboratory evaluations to establish the failure rate.

In the LOC program there may be a need for component parts of a new design for which little or no performance data will be available within the time limitations of the program. The application of such parts will be carefully evaluated and, if of a special design, the specifications for the part will be carefully detailed to avoid reliability risks. Detailed specifications for aging, preconditioning, and stabilization of components will be provided.

Improper application of a "good" part degrades equipment reliability as much as the proper application of a "poor" part. An adequate reliability effort, therefore, includes the study and control of part selection and application, parts specification, and verfication of standard electrical parts and approved non-standard parts.

### b. Subcontractor and Vendor Control

A subcontractor and vendor survey team composed of line personnel from the Purchasing, Engineering, Reliability, and Quality Control groups will select suppliers and determine the reliability and quality control capabilities and the suitability of the supplier prior to the award of any purchase order. The reliability and quality control requirements will be delineated in detailed specifications such as the RCA-AED Specifications 1171810 and 1171811.

### c. Inspection and Testing

All incoming material will be 100 percent inspected to satisfy the extremely critical requirements of a satellite system. Electrical as well as physical inspection standards will be established. The vendors and subcontractors will be required to institute programs similar to those of RCA.

The screening of aged or stabilized components to remove potential early failure will be performed by the inspection group in accord with established specifications for each part type.

Quality Control will establish material flow charts which indicate the assembly, inspection, and testing sequence of operations. The testing will be performed in accordance with detailed test specifications devised by Engineering. Records of inspection and tests results will be maintained in a log book.

## 5. MONITORING AND FAILURE REPORTING

The purpose of monitoring and failure reporting is to uncover failure patterns, parts weaknesses, poor vendor quality control, and ineffectual inspection or test procedures. From an analysis of such deficiencies, Engineering Product Assurance is enabled to make recommendations for improvement.

To furnish a strong basis for continuing reliability improvement throughout all fabrication phases, all tests will be monitored and all malfunctions recorded in equipment logs. The failure reporting program will include evaluation and analysis of all malfunctions and associated failed parts. The failures will be categorized and the necessary corrective action instituted.

The Failure Analysis Report will provide a complete and readily accessible summary of the evaluation of the malfunction. It will make possible the determination of "trouble" areas and the necessary corrective action.

The Engineering Product Assurance office will be responsible for completing the reports and having the associated failed part(s) analyzed by the vendor if an analysis is deemed necessary. Recommendations for corrective action based on the results of the analysis will be made and implemented through the cognizant project area to remove the reliability risk.

## 6. RELIABILITY ANALYSIS AND PREDICTION

### a. Development of a Mathematical Model

During the study and design phases of a subsystem, close contact will be maintained between the reliability engineer and the responsible engineering groups in order to develop a reliability block diagram as soon as possible. The block diagram will be updated as changes are made. As the reliability diagrams are defined, a set of equations will be formulated into the system and subsystem mathematical model. The mathematical model together with the reliability analysis and failure effects analysis will enable the system effectiveness to be evaluated for all possible mission profiles.

The reliability diagrams will be functional diagrams identifying all system components and indicating the flow of operational information. Operational modes and system functions will be described. Redundant components and/or channels will be identified and all series and parallel paths described. The diagrams and corresponding mathematical equations constitute essentially a dynamic model of the system. If the system is changed the mathematical model is no longer valid.

### b. Reliability Prediction

A preliminary reliability estimate based on parts complexity will be performed as a parallel effort with the development of the Reliability Block Diagram. Where the parts complexity is known or can be estimated with reasonable accuracy, the reliability estimate reveals trouble areas and becomes a basis for reliability allocations and trade-off requirements. A detailed Reliability Stress Analysis and Prediction will be performed on the basis of the prototype and flight model design configurations. This analysis will consider the operating parameters and stresses (electrical, thermal, mechanical and operating modes) of each component in the determination of its failure rate. The resultant reliability figures are thus direct functions of the operating conditions to which the prototype and flight models will be subjected.

c. Reliability Demonstration

Reliability evaluation and demonstration is the collection of data from operating equipment for the purpose of measuring reliability. The data collected during all phases of testing permit conclusions to be made regarding reliability and constitute a measure of the performance reliability.

A failure analysis program will be carried on simultaneously with the reliability demonstration and life tests. The total test time for analysis purposes includes both acceptance and operating life test phases. In the evaluation of the observed tests, a comparison may be made between the observed and calculated mean time between failures (MTBF). It should be noted, however, that sufficient life data is not normally available to make a satisfactory statistical comparison concerning the overall reliability of the system.

# PART II.

[illegible] 62-4f9

# TABLE OF CONTENTS

| Section | | Page |
|---|---|---|
| 1 | INTRODUCTION | II. 1-1 |
| 2 | SELENODETIC EXPERIMENT STUDIES | II. 2-1 |
| | A. Introduction | II. 2-1 |
| | B. Objectives | II. 2-1 |
| | C. The Physical Model | II. 2-2 |
| | D. Coordinate Systems and Representation of Solution | II. 2-4 |
| | E. Program Description | II. 2-9 |
| | | II. 2-15 |
| 3 | LUNAR SURFACE SIMULATION STUDIES | II. 3-1 |
| | A. Objectives | II. 3-1 |
| | B. Mission Reliability Versus Lunar Roughness | II. 3-1 |
| | C. Lunar Crater Size Distributions | II. 3-3 |
| | D. Improved Models and Model Photograph | II. 3-12 |
| | E. Photometric Functions of Moon and Models | II. 3-15 |
| 4 | GROWTH POTENTIAL | II. 4-1 |
| | A. Advanced Sensors | II. 4-1 |

# LIST OF ILLUSTRATIONS

| Figure | | Page |
|---|---|---|
| II.2.C-1 | Cartesian Coordinate System Geometry | II.2-6 |
| II.3.C-1 | Suggested Distribution of "Primary" Crater Size | II.3-5 |
| II.3.C-2 | Suggested Distribution of all Lunar Craters | II.3-6 |
| II.3.C-3 | False Droop Inherent in Distribution Counts | II.3-8 |
| II.3.C-4 | Variations in Lunar Crater Size Distributions with Type of Terrain | II.3-10 |
| II.3.E-1 | Photometry of Lunar Model, Light 8.6 Degrees Above Horizon | II.3-16 |
| II.3.E-2 | Photometry of Lunar Model, Light 31.2 Degrees Above Horizon | II.3-17 |
| II.3.E-3 | Photometry of Lunar Model, Light 40.4 Degrees Above Horizon | II.3-17 |
| II.3.E-4 | Photometry of Lunar Model, Light 63.6 Degrees Above Horizon | II.3-18 |
| II.3.E-5 | Photometry of Lunar Model, Light 74.8 Degrees Above Horizon | II.3-18 |
| II.3.E-6 | Influence of Resolutions on Lunar Photometry | II.3-19 |
| II.4.A-1 | Typical Characteristic Curve for RCA Type 4431 Vidicon | II.4-2 |
| II.4.A-2 | Typical Aperture Characteristic Curve for RCA Type 4431 Vidicon | II.4-2 |
| II.4.A-3 | Typical Characteristic Curve for RCA Type 7513 Image Orthicon | II.4-7 |
| II.4.A-4 | Typical Characteristic Curve for RCA Type 7198 Image Orthicon | II.4-7 |
| II.4.A-5 | Typical Aperture Characteristic Curve for RCA Type 7198 Image Orthicon | II.4-9 |
| II.4.A-6 | Dielectric Tape Cross-Sectional View | II.4-12 |
| II.4.A-7 | Photo Dielectric Tape Camera | II.4-13 |

# LIST OF TABLES

Table ... Page

II. 2. E - 1 Table of Input Variables ... II. 2-16

II. 3. B-1 Landing Probability of Success for Upper and Lower Bounds on Crater Size (X) ... II. 3-2
II. 3. C-1 Localized Crater Distribution Counts ... II. 3-11
II. 3. E-1 Photometry of Lunar Model ... II. 3-20

II. 4. A-1 Signal-to-Noise Ratios for Type 4431 Vidicon ... II. 4-3
II. 4. A-2 Vidicon Type 4431 Characteristics (with f/1.5 Lens and 1.67 MSEC Exposure Time) ... II. 4-5
II. 4. A-3 Comparative Sensitivities of Image Orthicons ... II. 4-6
II. 4. A-4 Image Orthicon Type 7198 Characteristics (with f/5 Lens and 1.67 MSEC Exposure Time) ... II. 4-11
II. 4. A-5 Dielectric Tape Camera Parameters for Lunar Orbiter Capsule ... II. 4-15
II. 4. A-6 Typical Signal-to-Noise Characteristics of Dielectric Tape Camera (with f/1.5 Lens and 30 MSEC Exposure Time) ... II. 4-16

# SECTION 1

# INTRODUCTION

Part II of this report presents results of those portions of the LOCS effort that are not directly concerned with the system integration of a specific LOC configuration. In general, the items discussed here represent studies of ground data-interpretation techniques and deal with the growth potential capability of the LOC. In the tracking-data and surface-simulation studies, when the effort was halted, the formative stages of study were in the process of completion. In the case of the surface-simulation studies, effort has continued under RCA funding, and the results are included herein for completeness.

In the section on advanced sensors, an over-all increase in system capability has been assumed. A second mid-course correction for the Ranger bus has been assumed, thereby permitting the selection of a lower orbital altitude (100 km). An increase in communication bandwidth (based upon nominal advances in the state-of-the-art) also is assumed. For this report, a 120-kc bandwidth is used.

One parameter for advanced capability has not been fully explored with regard to LOC growth potential. The injected weight for lunar payloads with an increased Agena capability is approximately 900 pounds (as opposed to 825 pounds assumed in Part I of this report). Unfortunately, an evaluation of the effects of increased payload weight on system performance capabilities were not investigated. It is anticipated that the RCA photo-dielectric sensor system described in Part II could take advantage of this increase in weight to permit more flexible system performance than described in the present report.

[illegible] 62-489

# Section 2

# SELENODETIC EXPERIMENT STUDIES

## A. INTRODUCTION

The success of both the television and geodetic missions of the lunar orbiter depends upon the extraction of information from range-rate data. There is some difference of opinion in the literature with regard to how much information is actually contained in a range-rate time history of doppler tracking. From the purely theoretical point of view, range rate is a one-valued function of the orbital parameters, such that a unique orbit is defined by a time history. One method of processing doppler data uses the information which can be obtained from portions of the doppler curve; accuracy would be achieved by using a sufficiently large number of doppler curves. On the other hand, another point of view claims that the doppler method is inherently capable of such accuracy that even a single doppler curve, if all of it is used, contains implicitly not only the orbital parameters but also the effects of the various perturbations (e.g., earth oblateness, or even triaxiality, and lunar-solar perturbations) when applied to earth satellites. There is the clear implication that similar statements would be applicable to a lunar satellite. Moreover, if this latter view is the correct one, the reduction of doppler data by a method which does not explicitly take into account these perturbations would lead to errors of larger magnitude than those inherent in the doppler method of tracking. The correctness of one view or the other has not been demonstrated. It still remains to examine the kind of data to be received from the practical point of view of effectively obtaining from the doppler curve the data which the theory tells us it contains.

The development of satisfactory data reduction techniques for the range-rate data to be received from the lunar orbiter evidently requires a suitable source of simulated data. Such simulated data has now become available in the form of a digital computer program (described in Section 2.E) which is capable of simulating all the perturbative effects which seem likely to produce a significant influence upon the data, including arbitrary modifications of them. The program also permits inclusion of simulated motion of the observer, or arbitrary modifications of it. Consequently, it is now possible to make reasonably trustworthy estimates of the effects of these various influences upon the range-rate histories and to provide the means of making realistic tests of the extent to which the information may be extracted from the time histories by the methods available. The motive for preparing this computer program was precisely this need for suitable data simulation.

It may be recalled that the computational method used in the program is the method of variation of parameters. This method was selected because of the direct manner in which it reflects the effects of the various physical factors involved in the determination of the actual trajectory. Moreover, the system of parameters chosen to represent the osculating orbits was one which would be free of the singularities which would impair computations with the traditional parameters and which would be valid for any motion of the widely aberrant orbits. Since most orbits will actually be nearly circular, a modification of the variation-of-parameters portion of the program was to be introduced which was to make the integration more rapid and use longer integration intervals.

It should be remarked that the program has been checked against results furnished by the Jet Propulsion Laboratory. The entire set of planned checks had not yet been completed at the termination of the study. So far, it has been found that the values of the orbital parameters and their variations as obtained from the two programs with the same, or nearly the same, initial conditions are comparable, with comparable, or perhaps somewhat longer, integration intervals for the RCA program (one which is not definitively settled). On the other hand, it is reasonable to expect that, when the indicated modifications are introduced into the program, appreciably longer integration intervals should become feasible. Another check of the program was also planned; namely, to use the program to integrate a path which can be obtained analytically and which would not be seriously unlike the actual trajectory of interest in the lunar orbiter project.

Because one of the study objectives was to predict the long-term behavior of lunar orbits of a specified range, consideration was given to computing such results. Neither the JPL nor the RCA program was entirely suitable, since both compute all short-period effects and require many relatively short integration steps. On the other hand, this application requires a method of computation which gives the evolution of the orbit over relatively long periods of time, without special regard for the position of the orbiter within the orbit at any specific time. A scheme which averages out the short-period oscillations is therefore indicated, and two such schemes were contemplated, the methods of Krylov-Bogoliubov and Halphen-Goriachev. Of the two, the latter seems to be the more promising and would allow the longer integration intervals. A selection between the two had not been made by the termination of the study period, but one of the methods would have to be embodied in the RCA program to provide the essential long-term estimates.

The final question to be discussed in this context is that of determination of the coefficients in the potential function of the moon. Two classes of approach to this problem are available. One method would be to predict the evolution of orbits over extended periods. The data from actual orbits would be compared with the predicted simulated data for those orbits, the discrepancies being assumed to be assignable to the errors in assumed values for the coefficients J and L, and thus furnishing corrections. Naturally, this approach is contingent upon the possession of methods of determining individual orbits from the data obtained from single (or very few) passes of the lunar satelite. The alternative method is to attempt to determine these constants from the doppler curve of a single pass and then, having done so separately for many passes, to combine the results to arrive at some sort of best estimate. This is the phase of the work which had just begun at the time of project termination.

## B. OBJECTIVES

The lunar-satellite trajectory program for the IBM 7090 computer was written as part of a study of the motion of a satellite of the moon, and its structure and procedures must be interpreted only in terms of the requirements which caused it to be written. The emphasis was never upon maximum speed or efficiency, but rather upon the greatest possible degree of flexibility and adaptability, as well as ease of programming and debugging. Even though the envisaged study program did not run its anticipated course, the computer program nevertheless reached the stage where it has become an adequate tool for much of the study originally planned. It is so readily modifiable that it is rather widely applicable to satellite studies; in addition, its speed of computation is satisfactory, requiring on the average about 0.5 second per integration step.

The lunar satellite study imposed a number of rather unrelated requirements. It seemed desirable, especially during the earlier stages of the study, to be able to make relatively long-term estimates of orbital changes under a considerable range of injection conditions in order to estimate times of useful TV coverage, vehicle lifetimes, and orbital stability. The possibility of some sort of propulsive capability was discussed at that time, with the corollary requirements upon the computer program. The question of orbital stability under extreme but possible injection conditions would have to be answered. An investigation was required to determine which orbits would be most or least favorable for providing data from which the coefficients in the moon's gravitational potential function could be determined. Finally, it was necessary to be able to produce simulated radar data for use in the development of the most effective methods of orbit determination from doppler data. This last requirement contained an internal conflict because of the possible different approaches to the problem of determining the moon's gravitational potential from doppler observations.

The implications of the various requirements for the program are discussed in the section on the integration of the equations of motion. At this point, it may be sufficient to note that the present program uses a method of variation of parameters, with a nonstandard set of orbital parameters which was adopted in order that the program would be capable of dealing with any orbit that could conceivably arise and be useful in the lunar orbiter project. This is what was needed by the project as first conceived, and therefore was the first method to be written for the program. Nevertheless, it was appreciated from the beginning that the most important class of trajectories to be flown by the vehicle would be nearly circular and close to the moon, because of the TV aspect of the mission. For such trajectories, the most convenient orbital parameters are not those actually used in the present program, but the abbreviation of the project prevented the inclusion of a method employing a better set.

In its present form, therefore, the program uses a set of orbital parameters which will remain nonsingular for all useful orbits of the satellite vehicle, and computes by a method which gives all details of both short-term and long-term perturbative effects, and consequently requires short integration steps. Comparison with the JPL program shows that the lunar orbiter program continues to give results even for integration steps that are so long that the JPL program becomes unstable. However to achieve close agreement with "good" JPL calculations, integration steps of approximately the same length have to be taken. These are only tentative conclusions; checks and comparisons are as yet incomplete. The preliminary checks indicate that, even with relatively unfavorable orbital parameters, the variation-of-parameters method compares extremely well with the Encke method in the cases that have been tried, while retaining much broader applicability.

## C. THE PHYSICAL MODEL

### 1. REMARKS ON NOTATION

Because of the many coordinate transformations required, it was convenient to carry out the complete analysis in terms of matrices. The computer program reflects this approach by employing macro-instructions corresponding to the matrix operations. The following notational conventions have been adopted:

(a) Underlined symbols always represent matrices, and symbols that are not underlined are always scalars. Underlined lower-case Greek or Roman letters denote column matrices or vectors. Underlined capitals denote square matrices. All matrices are three-dimensional, and an asterisk (*) denotes the transpose of the indicated matrix. The symbol for a row vector, therefore, is the indicated transpose of a column vector.

(b) The following special matrices occur so frequently that it is convenient to have special symbols for them:

$$\underline{A}_1(\alpha) = \begin{bmatrix} 1 & 0 & 0 \\ 0 & \cos\alpha & -\sin\alpha \\ 0 & \sin\alpha & \cos\alpha \end{bmatrix} ;$$

$$\underline{A}_2(\alpha) = \begin{bmatrix} \cos\alpha & 0 & \sin\alpha \\ 0 & 1 & 0 \\ -\sin\alpha & 0 & \cos\alpha \end{bmatrix} ;$$

$$\underline{A}_3(\alpha) = \begin{bmatrix} \cos\alpha & -\sin\alpha & 0 \\ \sin\alpha & \cos\alpha & 0 \\ 0 & 0 & 1 \end{bmatrix} ;$$

$$\underline{I} = \begin{bmatrix} 1 & 0 & 0 \\ 0 & 1 & 0 \\ 0 & 0 & 1 \end{bmatrix} \quad ;$$

$$\underline{I}_1 = \begin{bmatrix} 1 \\ 0 \\ 0 \end{bmatrix} \quad ; \quad \underline{I}_2 = \begin{bmatrix} 0 \\ 1 \\ 0 \end{bmatrix} \quad ; \quad \underline{I}_3 = \begin{bmatrix} 0 \\ 0 \\ 1 \end{bmatrix} \quad .$$

If $\underline{u}$ is any vector, $\begin{bmatrix} u_1 \\ u_2 \\ u_3 \end{bmatrix}$, define the matrix

$$[\underline{u}] = \begin{bmatrix} 0 & u_3 & -u_2 \\ -u_3 & 0 & u_1 \\ u_2 & -u_1 & 0 \end{bmatrix}$$

An important special case is:

$$|\underline{I}_3| = \begin{bmatrix} 0 & 1 & 0 \\ -1 & 0 & 0 \\ 0 & 0 & 0 \end{bmatrix}$$

Finally, if $\underline{u}$ is any vector, its magnitude is $|\underline{u}| = \underline{(\underline{u} * \underline{u})^{1/2}}$.

## 2. EQUATIONS OF MOTION

Assume a right-hand orthogonal Cartesian coordinate system having its origin at the center of mass of the sun, positive "1" axis directed toward the first of Aries, and the positive "3" axis in the same sense and direction as the angular momentum vector of the earth with respect to the sun. See Figure II.2.C-1. The space spanned by this coordinate system may be considered an inertial system. The program is now written to include in the physical model only the sun, earth, and orbiter (regarded as mass particles), and the moon (regarded as a rigid body with triaxial mass distribution). The vectors and symbols used in the formulation are shown in Figure II.2.C-1.

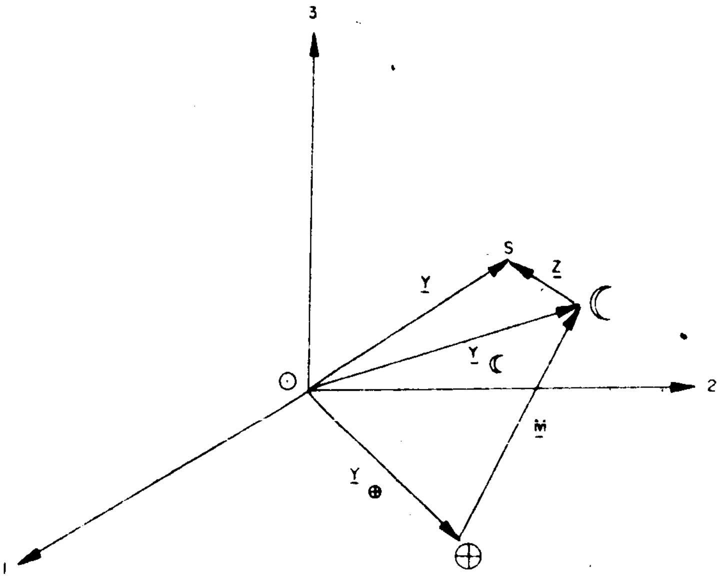

Figure II.2.C-1. Cartesian Coordinate System Geometry

If m is the mass of a particle and k the gaussian constant, then the gravitational attraction of that particle is conveniently expressed in terms of $\mu = k^2 m$.

In this report, the symbols $\odot$, $\oplus$, and $\leftmoon$, used as subscripts, denote the sun, earth, and moon respectively. With respect to the inertial system (also called the ecliptic coordinate system),

$\underline{y}$ = position vector of the lunar satellite S,

$\underline{y}_{\leftmoon}$ = position vector of the moon, and

$\underline{y}_{\oplus}$ = position vector of the earth.

Definition of the following vectors is also convenient:

$\underline{x} = \underline{y} - \underline{y}_{\oplus}$ = position of the lunar satellite relative to the earth,

$\underline{x}_{\odot} = - \underline{y}_{\oplus}$ ,

$\underline{m} = \underline{y}_{\leftmoon} - \underline{y}_{\oplus}$ , and

$\underline{z} = \underline{x} - \underline{m} = \underline{y} - \underline{y}_{☾}$ = position of the lunar satellite relative to the moon.

All vectors above have been considered to be represented with respect to the ecliptic (inertial) coordinate system. Additional coordinate systems must be defined later in the formulations.

The equation of motion of the lunar satellite (per unit mass) may be written immediately as follows:

$$\ddot{\underline{y}} = - \frac{\mu_{\odot}}{||\underline{y}||^3} \underline{y} + \frac{\mu_{\oplus}}{||\underline{x}||^3} (\underline{y}_{\oplus} - \underline{y}) + \underline{f}_{JL} +$$

$$+ \frac{\mu_{☾}}{||\underline{y}_{☾} - \underline{y}||^3} (\underline{y}_{☾} - \underline{y}) ,$$

where dots over a symbol denote differentiation with respect to the time t, and $\underline{f}_{JL}$ is that part of the moon's gravitational effect that can be attributed to the triaxiality of the moon's mass distribution.

Substitute

$$\underline{y} = \underline{z} + \underline{y}_{☾}$$

and

$$\ddot{\underline{y}}_{☾} = - \frac{\mu_{\odot}}{||\underline{y}_{☾}||^3} \underline{y}_{☾} - \frac{\mu}{||\underline{m}||^3} \underline{m} ,$$

assuming that the mass of the lunar satellite is negligible in its effect upon the motions of the other bodies. The equation then becomes

$$\ddot{\underline{z}} + \frac{\mu_{☾}}{||\underline{z}||^3} \underline{z} = \underline{f}_{JL} - \frac{\mu_{\oplus}}{||\underline{x}||^3} \underline{x} + \frac{\mu_{\oplus}}{||\underline{m}||^3} \underline{m} + \frac{\mu_{\odot}}{||\underline{m} - \underline{x}_{\odot}||^3} (\underline{m} - \underline{x}_{\odot})$$

$$- \frac{\mu_{\odot}}{||\underline{x} - \underline{x}_{\odot}||^3} (\underline{x} - \underline{x}_{\odot}),$$

and this is the equation of motion to be integrated. If the right-hand side is denoted by f, the equation assumes the abbreviated form

$$\ddot{\underline{z}} + \frac{\mu_{☾}}{||\underline{z}||^3} \underline{z} = \underline{f} .$$

For a satellite close to the moon, the dominant force is the gravitational attraction of the moon, and all the remaining forces combined in $\underline{f}$ are relatively small. It is reasonable to expect the orbit of a lunar satellite, therefore, to differ only relatively little from a Kepler ellipse.

Write

$$\underline{f} = \underline{f}_{JL} + \underline{f}_{\odot} + \underline{f}_{\oplus} \, ,$$

where:

$\underline{f}_{JL}$ = perturbing force resulting from the non-central gravity field of the moon,

$\underline{f}_{\odot}$ = perturbing force of the sun, and

$\underline{f}_{\oplus}$ = perturbing force of the earth.

To make the physical model more precise, it is only necessary to find the appropriate additional components of the perturbing force $\underline{f}$.

## 3. TYPES OF SOLUTION

The object of the program is to obtain a purely numerical solution of the equations of motion, since a useful closed-form solution is not available. The numerical aspect of the problem (i.e., integration of the differential equations) can be performed by either the Runge-Kutta method or Milne's predictor-corrector method, at the operator's option. The Runge-Kutta option has hitherto been preferred in the checkout runs, but it is anticipated that the greater speed of the Milne method will often render it preferable.

The more important decision to be made concerned the choice of system of equations to be integrated. The three systems which present themselves constitute the methods associated with the names: variation of constants, Cowell, and Encke, respectively. The method of variation of constants was selected for the following reasons.

The lunar orbiter problem imposed the following requirements. It would be necessary to be able to compute orbits for a period of a month or more. Orbits of various types would have to be considered, ranging from nearly circular orbits through elliptical orbits of large eccentricity up to possible hyperbolic escape orbits. At one time, it appeared that orbits of small inclination might be required. Finally, the program would have to serve as a simulator of doppler data such as would be received at earth ground stations from the lunar orbiter.

The Cowell method could have been used, but would have the usual disadvantage of requiring more integration steps, and it would be uncertain through how long a time the integration could meaningfully be carried. This would be the more serious problem in light of the fact that results of the longer calculations were to be used as simulations of doppler data from which to make inferences about the moon's mass distribution.

The Encke method computes not the trajectory itself, but its departure from a reference trajectory, thus retaining more significance in the numbers. This offers advantages for trajectories in gravitational fields dominated by the field of a single body. In terms of the lunar orbiter capsule project, these advantages would be more than overbalanced by two facts. First, some of the trajectories considered probable would deviate so appreciably from a reference trajectory that frequent 'rectification' would be required, thereby nullifying much of the advantage of speed of computation. Secondly, the doppler curve contains a great deal of information about the orbit, and, therefore, about the orbital elements. Encke's method, which may be regarded as a method of variation of coordinates, would be less likely to provide a sufficiently veridical simulation of the doppler data to the capability of the data processing techniques adopted for determining the variations in orbital parameters resulting from the triaxial mass distribution of the moon.

The method of variation of constants, therefore, appeared to be indicated as the best method for the lunar orbiter application. The details of the method may be found in Section 2. D. 3.

## D. COORDINATE SYSTEMS AND REPRESENTATION OF SOLUTION

### 1. COORDINATE SYSTEMS

All vectors in the ecliptic (inertial) coordinate system described in the previous section were considered to be represented in terms of the ecliptic coordinate system. A description of the motions of the bodies in the physical model and of the perturbing forces, however, is most expeditiously done for each of the bodies by other suitable coordinate systems. The systems all can be obtained from the ecliptic coordinate system by a rigid rotation. The various coordinate systems which were required will be described, with the appropriate notational conventions. The same letter is always used to denote the same vector, and the number of primes indicates the coordinate system with respect to which it is represented. Unprimed letters refer to the ecliptic coordinate system.

A moving coordinate system, in which two of the axes lie within the instantaneous orbit plane and the third is the normal to the orbit plane, is the most convenient for describing the motion of a lunar satellite. A precise description of this coordinate system becomes involved as the result of the role it plays in the scheme of variation of parameters. Details of the parameter variation problem are provided in the following section. A single prime denotes that the elements in the matrix representation of the indicated vector are components with respect to this orbit-fixed coordinate system; in some cases, it is convenient to use a lower-case Greek letter.

Let $\underline{T}$ be the orthogonal matrix whose columns contain the components relative to the ecliptic coordinate system of the unit basis vectors of the orbit-fixed coordinate system. The computation of $\underline{T}$ involves the integration of a system of ordinary differential equations (for which see Section 2. 5). Then, if $\underline{x}$ is a vector represented in terms of the ecliptic coordinate system and if $\underline{x}'$ or $\underline{\xi}$ is the representation of the same vector with respect to the orbit-fixed coordinate system, then $\underline{x} = \underline{T}\,\underline{x}'$ or $\underline{x} = \underline{T}\,\underline{\xi}$.

RE-ORDER No. 62-459

The motion of the earth about the sun and the direction of the gravitational attraction of the sun upon the lunar satellite are most easily described in ecliptic coordinates. To obtain the respective components of these perturbing forces with respect to the orbit-fixed coordinate system, as required by the differential equations to be integrated, it is sufficient to pre-multiply the ecliptic representations by $\underline{T}^*$, the inverse of $\underline{T}$.

In order to determine the attractive force of the earth upon the lunar satellite, it is easiest to use a coordinate system in which the moon's orbit with respect to the earth lies in one of the coordinate planes. Reference to this earth-moon coordinate system is indicated by '' or the symbol $\oplus ☾$. The mutual orientation of the earth-moon system and the ecliptic system is done in terms of the Euler angles,

$\Omega_{\oplus ☾}$ = angle between the 1-axis of the ecliptic coordinate system and the intersection of the ecliptic plane with the moon-orbit plane;

$I_{\oplus ☾}$ = angle between the 3-axis of the ecliptic coordinate system and the 3''-axis of the earth-moon orbit plane;

$\omega_{\oplus ☾}$ = angle between the line of intersection of the ecliptic plane and the earth-moon orbit plane and the 1''-axis.

For the actual numerical values, reference may be made to the report by Kalensher on Selenocentric Coordinates and to the Nautical Almanac and Ephemeris. Let A denote the transformation matrix between the ecliptic coordinate system and the earth-moon orbit-fixed coordinate system so that, if $\underline{x}$ and $\underline{x}''$ represent the same vector with respect to the two coordinate systems, the relation between their components is $\underline{x} = \underline{A}\,\underline{x}''$. Then (using the notation of the previous section),

$$\underline{A} = \underline{A}_3(\Omega_{\oplus ☾})\,\underline{A}_1(I_{\oplus ☾})\,\underline{A}_3(\omega_{\oplus ☾}) .$$

The potential function of the moon's mass distribution is readily expressible in terms of a moon-fixed coordinate system, which is also convenient for prescribing the initial conditions for a lunar orbit. An equatorial coordinate system is rigidly fixed in the moon, with the transformation matrix $\underline{M}$, and vectors referred to this moon-fixed coordinate system are denoted by triple primes. Thus, if $\underline{x}$ and $\underline{x}^{III}$ represent the same vector with respect to the ecliptic and moon-fixed coordinate systems respectively, then the relations among the components are given by the equation $\underline{x} = \underline{M}\;\underline{x}^{III}$. Incidentally, we remark that $\underline{M}$ is chosen to be the matrix of the principal directions of the moon's mass distribution. The computation of $\underline{M}$ is made to depend upon Euler angles, now denoted by the subscript $☾$ ; thus,

$$\underline{M} = \underline{A}_3(\Omega_{☾})\,\underline{A}_1(I_{☾})\,\underline{A}_3(\dot{\omega}_{☾}t + \omega^{0}_{☾}) ,$$

where $\dot{\omega}_{☾}$ is the angular velocity of the moon about its own axis.

Finally, in the simulation of doppler signals received by an earth observer, it is evidently necessary to take into account the diurnal rotation of the earth and the consequent motion of the observer. For this purpose, it is convenient to have an equatorial coordinate system rigidly fixed in the earth. It has the transformation matrix $\underline{E}$, and

RE-ORDER No. 62-4A9

vectors referred to this earth-fixed coordinate system are indicated by quadruple primes. Thus, if $\underline{x}$ and $\underline{x}^{IV}$ represent the same vector with respect to the ecliptic and earth-fixed coordinate systems respectively, the relations among their components are contained in the equation $\underline{x} = \underline{E}\, \underline{x}^{IV}$. The transformation matrix $\underline{E}$ is computed in terms of Euler angles, this time distinguished by the subscript $\oplus$ ; thus,

$$\underline{E} = \underline{A}_3 (\Omega_\oplus)\, \underline{A}_1 (I_\oplus)\, \underline{A}_3 (\dot{\omega}_\oplus t + \omega^\circ_\oplus),$$

where $\omega_\oplus$ is the angular velocity of the earth around its own axis.

The transformation matrices are all orthogonal matrices, for which inverses are computed by simply transposing. The representation of a vector in any of the coordinate systems described, given the components of that vector with respect to any of the coordinate systems described, may be obtained by a sequence of matrix multiplications.

## 2. REPRESENTATION OF SOLUTIONS

The motions of natural or artificial celestial bodies (i.e., the solutions of the equations of motion) are too complicated for mathematics in its present state to be able to provide perspicuous analytical representations, or even, as a matter of fact, to provide a complete and useful classification of types of solutions. The precise and detailed prediction of motion demands numerical approximation. The method of variation of parameters, as used in the present program, employs a representation of the solution of the equations of motion (supposed to include all significant perturbative forces) as the envelope of a one-parameter family of the solutions of the equations obtained by setting $\underline{f} = 0$. Thus, the solution is in the form of the envelope of a family of Keplerian trajectories which have the property that, at the point of tangency, the velocities on the envelope and on the tangent Kepler trajectory (osculating trajectory) are the same and equal to the actual velocity. The reasons for preferring such a representation, even at the cost of possible additional computations, have already been presented.

A solution of the equations of motion has the form of three functions of time which depend upon six parameters, integration constants or equivalent. The same is true of the osculating Kepler trajectories. These orbital parameters may be chosen in various ways, and many mathematically equivalent systems of parameters have been proposed and used. Despite mathematical equivalence, however, alternate sets of parameters may differ widely in expediency. This difference may be such that certain systems of parameters, including the best known, impose considerable hardship upon computation, or sometimes even become entirely unworkable in particular applications, whereas the computations may proceed without any particular difficulty with another set of parameters. Furthermore, in the method of variation of parameters, the systems of differential equations (often called the 'planetary equations') governing the variation of the orbital parameters as we proceed through the sequence of osculating orbits may differ widely in complexity and ease of solution.

The system of parameters actually chosen is described in the next section, and the reasons leading to the particular choice are outlined in Section 2.B. It was realized that, although this system of parameters would lead to a reasonable computation for any combination of conditions that might be envisaged, some other set could be significantly superior for any particular class of trajectories, such as the family of nearly circular close orbits about the moon. Consequently, the program was constructed such that another set of orbital parameters could be substituted with very little difficulty.

## 3. PERTURBATION SOLUTION BY THE METHOD OF VARIATION OF PARAMETERS

This section begins with a description of the orbital parameters to be used in describing a Keplerian trajectory, then displays and discusses the system of differential equations governing the changes in these parameters with time in response to the perturbing forces. Matrix notation is used, corresponding to the procedures embodied in the computer program, as described in detail in Section 2. E of Part II. The derivation of the equations offers no particular difficulty and may be found (in vector notation) in Appendix A-III of the RCA Phase I report, "Lunar Orbiter Capsule Study."

The need for a set of orbital parameters which would not lead to singularities was discussed in Section 2. B of Part II. The set chosen is a combination of parameters, all of which have been used by others but not, apparently, all at the same time. The following parameters are used.

A vector first integral of the equations of motion of a mass point in an attracting inverse square central force field is $\underline{h}$, with magnitude equal to the angular momentum per unit mass of the orbiting body with respect to the attracting center and directed normally to the orbital plane. With respect to the inertial Cartesian orthogonal coordinate system, called the ecliptic system, let $\underline{z}$ and $\underline{\dot{z}}$ be, respectively, the vectors of position and velocity. Then, $[\underline{z}]^{*}\underline{\dot{z}} = \underline{h}$ = constant. (For notation, see Section 2. C. of Part II). The magnitude h of this vector is the first of the orbital parameters. The direction of this vector is also involved in the definition of more of the parameters, as will be seen in a moment. It is evidently essential to impose the restriction $h \neq 0$; otherwise, the direction of $\underline{h}$ would have no meaning. This is the only restriction to be imposed and is harmless in the problem of the lunar orbiter.

Next, we specify a preferred coordinate system to which to refer the motion. Take an orthogonal Cartesian coordinate system with origin at the attracting center, its 1-axis directed toward the initial position $\underline{z}_0$ of the orbiting body, and its 3-axis in the direction of $\underline{h}$. This coordinate system will evidently remain invariant for a Keplerian motion, since it has been defined in terms of invariants of that motion. It is always uniquely determinable (provided that $h \neq 0$), no matter what the form of the orbit may be or how it is oriented with respect to the ecliptic coordinate system. Quantities represented with respect to this coordinate system are denoted by primed or Greek letters, consistent with the notation introduced in Section 2. C. The symbol $\underline{T}$ denotes the orthogonal transformation matrix from the ecliptic coordinate system to the orbit-fixed coordinate system just defined. Since there are only three independent components in the matrix $\underline{T}$, it is seen that three more orbital parameters have been introduced. It is analytically and numerically much more convenient to use the entire matrix $\underline{T}$ (with nine components) than to try to obtain a minimal set of three parameters. Consequently, these three orbital parameters are defined only implicitly through the matrix $\underline{T}$, the effective reduction from nine to three being obtained implicitly through the requirement that the matrix be orthogonal.

The last two orbital parameters are obtained from another first integral of the equations of motion, the so-called Laplacian integral,

$$\underline{a} = [\underline{h}]^{*}\dot{\underline{z}} - \frac{\mu}{r}\underline{z},$$

where $r = |\underline{z}|$ and, for the lunar orbiter problem, $\mu = \mu_{\ell}$

Define

$$\underline{b} = \frac{1}{h^2}\underline{a},$$

so that $\underline{b}$ is also a first integral of the motion. The quantity $\underline{b}$ is evidently a vector constrained to lie in the orbit plane; consequently, it involves only two independent components, thus supplying the remaining two orbital parameters. It may be noted that $\underline{b}$ is a vector directed from the attracting center to the perifocus and that its magnitude is $\mu e/h^2$, where e is the eccentricity of the orbit.

In terms of $\underline{b}$, we may write

$$\dot{\underline{z}} = [\underline{h}]^{*}(\underline{b} + \frac{\mu}{h^2 r}\underline{z}),$$

the so-called Hamiltonian integral of motion, which provides a convenient expression for the velocity of the orbiting body as a function of its position and the orbital parameters. From either form of this first integral, we readily obtain a form of the polar equation of a conic section:

$$\frac{1}{r} = \frac{\mu}{h^2} + \frac{1}{r}\underline{b}^{*}\underline{z}.$$

If we express all quantities with respect to the primed coordinate system (i.e., transformation with the matrix $\underline{T}$), the vectors $\underline{z}$, $\dot{\underline{z}}$, $\underline{h}$, and b become, respectively, $\underline{\xi}$, $\dot{\xi}$, $\underline{hI_3} = [\underline{\xi}]^{*}\dot{\underline{\xi}}$, and $\beta$. It is also convenient to introduce the unit vector $\rho = \frac{1}{r}\underline{\xi}$. The Hamiltonian integral may now be written

$$\frac{1}{r} = \frac{\mu}{h^2} + \underline{\beta}^{*}\underline{\rho}.$$

Define $\Theta(t)$ as the angle between the initial position vector $\underline{z}_0$ and the present position vector z(t). Then we have

$$\underline{\rho}(t) = \begin{bmatrix} \cos\Theta \\ \sin\Theta \\ 0 \end{bmatrix},$$

and the Kepler principle of areas gives the relation

$$\dot{\theta} = h/r^2.$$

To this point, it has been assumed that $\underline{f} = 0$; i.e., that there is no perturbing force. As soon as perturbation is allowed to act, the invariants of the motion cease being invariant, so that the orbital parameters become functions of time. Their values at the initial time are readily obtained from a knowledge of initial position and velocity $\underline{z}_o$, $\dot{\underline{z}}_o$. Thus, at $t = t_o$, $\Theta = 0$, $r = r_o = |\underline{z}_o|$, $\underline{h}_o = [\underline{z}_o]^* \dot{\underline{z}}_o$, and $\underline{T} = \underline{T}_o$ = a matrix whose columns are respectively

$$\frac{1}{r_o}\underline{z}_o, \quad \frac{1}{r_o h_o} [\underline{h}_o]^* \underline{z}_o, \quad \frac{1}{h_o}\underline{h}_o; \quad \underline{b}_o = \frac{-1}{h_o{}^2} [\underline{h}_o]^* \dot{\underline{z}}_o - \frac{\mu}{r_o h_o{}^2} \underline{z}_o.$$

The differential equations satisfied by these quantities remain to be written. There are, in all, 13 unknowns; namely, the nine components of $\underline{T}$, the components of h and $\Theta$, and the two components of $\underline{b}$ (after transformation to the primed coordinates).

Let $\gamma$ be the representation with respect to the primed coordinate system of the perturbing force; i.e., $\underline{f} = \underline{T}\gamma$. It can be shown that the angular velocity of the primed coordinate system with respect to the ecliptic coordinate system is $\underline{w}' = \frac{\gamma_3}{h} \underline{\xi}$ and that, therefore,

$$\dot{\underline{T}} = \underline{T} \, [\underline{w}']^* \underline{\xi},$$

a set of nine linear ordinary differential equations for the components of $\underline{T}$. One of the reasons for using the entire matrix rather than attempting to reduce it to three independent elements is the greater simplicity of the differential equations when the entire matrix is retained.

Two more easily obtained equations are

$$\dot{\Theta} = \frac{h}{r^2}$$

$$\dot{h} = r\,(\gamma_2 \cos\Theta - \gamma_1 \sin\Theta),$$

and with a little more trouble, the final vector equation,

$$\dot{\underline{\beta}} = \frac{\dot{h}}{h} \left[ \left(\frac{2\mu}{h^2} - \frac{1}{r}\right) \underline{\rho} + \frac{\dot{r}}{h} [\underline{I}_3]^* \underline{\rho} \right] - \frac{1}{h} [\underline{I}_3]^* \underline{\gamma}.$$

Note that this vector equation has only two non-zero components, so that it is equivalent to a set of two equations for the two non-zero components of $\underline{\beta}$. The system of differential equations is thus complete and well-defined and obviously well-behaved for any flight of a lunar orbiter. Consequently, these equations may be integrated step-by-step, providing a time-history for each of the orbital parameters, and a numerical solution of the equations of motion is obtained.

## E. PROGRAM DESCRIPTION

The programming system used is S.O.S., including SCAT, INTRAN, OUTRAN, and the debugging macros. The program consists of four main sections:

1) Pre-Initialization - The purpose of the pre-initialization phase is to facilitate the modification of physical constants, if required, by reducing manual calculations and the quantity of changes to a minimum. For instance, all angular constants are initially in degree units, but are scaled to radian units for internal processing. Pre-initialization is done once.

2) Initialization - For each run under consideration, the program scales and generates the required problem parameters. Initialization is done once for each run.

3) Central Processing - The program obtains the required solutions of the differential equations and, at predetermined time intervals, transfers control to the output processing program section.

4) Output Processing - Using the results obtained by the central processing section of the program, the program generates, scales, and writes on output tapes all the required variables.

Units used internally are kilometers for linear distance, radians for angular distance, ephemeris days for time, and the mass of the sun as the unit of mass. Units used for input/output purposes are specified in another section below.

In order to prevent certain losses of significance, the internal computations assume a zero-starting-time reference. The coefficients of the polynomials used to determine the position of the moon and the sun are adjusted to account for a zero-time reference from start of the run, rather than from January 1, 1950. The use of such a time reference results in some reduction of calculations.

The use of subroutines to represent certain functions is made in order to simplify as much as possible future program modifications. It should be noted that the present version of this program is not considered to be a final product, since it is often being amended.

### 1. INPUT FORMATS

Input data is read by the program from cards read in from the card reader. INTRAN, as found on the S.O.S. system tape, is used as the input system.

The input program allows for variable-length words to be stored on cards. Each word is separated by a comma. Since the cards are read by the card reader rather than by tape units, column 72 is the last column that can be used.

The first word of each card is a two-digit integer representing the number of words punched on that card which are to be stored in memory. The exception to the above rule is the last card of a group representing one run. The first word of the last card is the two-digit integer 00, followed by a comma, then followed by a binary word described below. The last card can be followed by one or more sets of cards, each of which represents a run. The last card of the deck is completely blank.

The sequence of variables listed below must be that which is used in key-punching the cards.

### TABLE II. 2. E. -1

### TABLE OF INPUT VARIABLES

| Word Number | Format | Identification And Description |
|---|---|---|
| 1 | Integer | Run number, 1 to 6 numeric characters |
| 2 | Integer | Frequency of output. (That is, a 2 means that every other set of output values will be generated for output purposes.) |
| 3 | Integer | 1. Selenocentric equatorial Cartesian input<br>2. Selenocentric ecliptic Cartesian input<br>3. Selenocentric equatorial orbit element input<br>4. Selenocentric ecliptic orbit element input |
| 4 | Integer | 0. Do not generate binary output tape.<br>1. Generate binary output tape. |
| 5 | Integer | 0. Do not generate special printer output.<br>1. Generate special printer output. |
| 6 | Integer | 0. (Not used at the present time.) |
| 7 | Floating point | Latitude of observer on earth (degrees) |
| 8 | Floating point | Longitude of observer earth (degrees) |
| 9 | Floating point | The initial position and velocity as defined by word 3. above. If Cartesian vectors, position and velocity units are km and km/sec and are punched in that sequence. If the input is orbital elements, the units are km, degrees, and ephemeris day and are stored in the following sequence: Semi-major axis, eccentricity, inclination, longitude of ascending node, argument of perigee, time of perigee passage with respect to initial starting time. |
| 10 | Floating point | |
| 11 | Floating point | |
| 12 | Floating point | |
| 13 | Floating point | |
| 14 | Floating point | |

RE-ORDER No. 62-4F9

### TABLE II. 2. E. -1 (Cont.)

### TABLE OF INPUT VARIABLES

| Word Number | Format | Identification And Description |
|---|---|---|
| 15 | Floating point | Starting time, in ephemeris days from January 1, 1950. |
| 16 | Floating point | End of problem time, in ephemeris days from January 1, 1950. |
| 17 | Floating point | Integrating internal, in ephemeris days |

As was indicated previously, the last card of each set is one with a zero word count, followed by a comma, then followed by a binary word. The binary word has four bit positions. The presence of a one in a bit position indicates the use of the option of a corresponding perturbing force. A zero in that bit position indicates that the corresponding perturbing force is disregarded. The word definition is, for left to right:

1. Perturbation resulting from the presence of the sun.
2. Effect of the earth on the orbiter.
3. The moon's acceleration about the earth.
4. The perturbing force caused by the non-spherical shape of the moon.

## 2. OUTPUT

Two output tapes are generated for off-line printing. On an optional basis, a binary tape can also be generated. The content of the printer output tapes is as follows:

(1) Part A.

a. A header page describing the input data as read from cards and the values of $\mu_{\odot}$, $\mu_{\oplus}$, and $\mu_{☾}$ .

b. The following variables:

I Time from start of run, ephemeris days.

II Inclination, degrees

III Longitude of ascending node, degrees

IV Argument of perigee, degrees

V Argument of perigee rate, degrees per ephemeris day

VI Semi-major axis, kilometers

VII Eccentricity

VIII Range between moving observer on earth and orbiter, kilometers.

IX Range rate of orbiter as measured by moving observer on earth, kilometers per second.

X Time from January 1, 1950, ephemeris days

XI Period, minutes

XII Period rate, minutes per ephemeris days

XIII Inclination rate, degrees per ephemeris day

XIV Longitude of ascending node rate, degrees per ephemeris day

XV Time of last perigee passage with respect to start of run, ephemeris days.

XVI Selenocentric position and velocity vectors: The orientation of the reference plane is the same as that used in the input data, kilometers and kilometers per second, respectively.

XVII Distance and velocity from the center of the moon, kilometers and kilometers per second.

(2) Part B.

a. A header page describing the input data as read from cards and the values of $\mu_{\odot}$, $\mu_{\oplus}$, and $\mu_{☾}$.

b. The following variables:

I Time from start of run, ephemeris days.

II The vector $\vec{\beta}$ (kilometers)$^{-1}$

III Angular momentum, (kilometers)$^{2}$ per second.

IV Angular position of the orbiter in its instantaneous orbital plane with respect to its starting point, degrees.

V Angular rate of change of the orbiter's position vector in the instantaneous orbital plane, degrees per second.

VI The matrix T.

VII On an option basis, $T^*T$, and $T^*(x-m)$, the latter vector being in kilometers per second.

NOTE: All orbital elements and their rates are moon-centered and oriented in a plane parallel to the ecliptic plane. The vector $\beta$ is oriented in the instantaneous plane of the orbiter.

(3) Binary Output Tape

a. A block of data containing all the input data.

b. The following variables (in that order):

I Time from start of run, ephemeris days

II Inclination, degrees

III Longitude of ascending node, degrees

IV Argument of perigee, degrees

V Argument of perigee rate, degrees per ephemeris day.

VI Semi-major axis, kilometers.

VII Eccentricity

VIII The two non-zero components of the vector $\beta$, $(\text{kilometers})^{-1}$

IX Angular momentum, $(\text{kilometers})^2$ per second

X Angular position of the orbiter in its instantaneous orbital plane with respect to its starting point, degrees

XI Angular rate of change of the orbiter's position vector in the instantaneous orbital plane, degrees per second.

XII Range between an observer on earth and the orbiter, kilometers.

XIII Range rate of the orbiter as measured by an observer on earth, kilometers per second.

XIV Period, minutes

XV Period rate, minutes per ephemeris day

XVI Inclination rate, degrees per ephemeris day

XVII Longitude of ascending node rate, degrees per ephemeris day.

XVIII Time of last perigee passage with respect to start of run, ephemeris days.

XIX $\overline{x}-\overline{m}$, kilometers.

XX $\dot{\overline{x}}-\dot{\overline{m}}$, kilometers per second.

XXI Radial distance from center of the moon to the orbiter, kilometers.

XXII Speed of the orbiter, kilometers per second.

XXIII $\overline{T}$.

XXIV $\dot{\overline{T}}$.

## 3. OPERATING INSTRUCTIONS

(1) Program tape (SQUOZE) on $A_3$.

(2) Scratch tapes on $A_2$, $B_1$, $B_2$, and $B_5$; in addition, on $A_6$ if binary tape option is exercised.

(3) Data deck in card reader.

(4) S.O.S. systems tape on $A_1$.

(5) Push CLEAR, then LOAD TAPE buttons.

(6) At S.O.S.'s "STOP" location, end of job.

Output tapes:

(1) $A_2$; print off-line P.C., two files (second file is a symbolic core dump)

(2) $B_5$; print off-line, P.C.

(3) $A_6$; save if special option exercised.

NOTE: In case of recompilation, the LBR tape is required.

## 4. DATA FLOW

(1) Pre-Initialization

a. The gravitational constants are scaled to kilometers, mass of the sun, and ephemeris days.

b. Compute variables that remain constant throughout the program. For example, the moon's angular momentum, semi-major axis, and semi-minor axis, $\overline{A}_1 (I_{☾})$, $A_1 (I_{☾\oplus})$, $A_1 (I_{\oplus})$, $\overline{W}^{1V}$, and $\overline{s}^{1V}$ remain constant.

c. Scale all angle arguments to radian units. This includes the coefficients of the polynomials used in determining angular variables.

d. Call in INTRAN and OUTRAN.

(2) Initialization

a. Read in cards representing input data for a single run.

b. Set switches to allow for the use of any combination of perturbing forces. In addition, set all other optional switches.

c. If the initial position and velocity are in the form of orbital elements, compute the equivalent Cartesian position and velocity vectors.

d. Write a header page on both output printer tapes.

e. If a binary tape is to be generated, write a header block on the tape. The block is made up of the content of the cards.

f. Scale the input to the required internal units.

g. Reset the coefficients of the polynomials used to calculate the ephemerides of the moon and sun so that the time variable is referenced to the start of the run.

h. If the initial position and velocity vectors are oriented to the moon's equator, compute M, then transform the two vectors to an ecliptic moon-centered orientation.

i. Compute the initial values of $\overline{T}$, h, and $\overline{\beta}$ and set $\Theta$ to zero. These values are used as starting points in the solution of the differential equations of the above variables.

(3) Central Processing - This phase involves the solution of the differential equations of the problem. Below is an outline of the computations used to define the derivatives. It should be noted that certain intermediate variables are used in the computation of output variables.

a. Computer:

$$\frac{1}{r} = \frac{\mu_{☾}}{h^2} + \overline{\beta} \cdot \overline{\rho}$$

where

$$\overline{\rho} = \begin{bmatrix} \text{Cos } \Theta \\ \text{Sin } \Theta \\ 0 \end{bmatrix}$$

r = distance from the center of the moon to the orbiter.

b. Compute the position of the moon and sun.

c. Compute $\overline{M}$ and $\overline{A}^*$.

d. Compute $\overline{\xi}$

e. Compute $\overline{x-m}$, $\overline{m}$, and x

f. Compute $\gamma$

g. Compute $\overline{W}^1$

h. Compute $\dot{\overline{T}}$

i. Compute h, $\dot{\Theta}$, and $\dot{\overline{\beta}}$

(4) Output Processing

a. Compute $\dot{\overline{Y}}$

b. Compute $\dot{\overline{\xi}}$ from $\overline{\xi}$, $\dot{Y}$, and $\dot{\Theta}$

c. Compute a and e from $||\beta||$ h, $\dot{\overline{\xi}}$, $\gamma$ and $\mu_{☾}$

d. From the elements of $\overline{T}$, compute $\Omega$ and I.

e. From $\Omega$, $\overline{T}$, and $\overline{\beta}$, compute $\omega$

f. Compute R and $\dot{R}$ as outlined in CRRD, below.

g. Compute $\dot{\Omega}$, $\dot{\omega}$, $\dot{I}$, and $\dot{P}$.

h. Scale all required data and write on printer tapes.

i. Write on tapes all optional output.

5. PROGRAMMED MACRO-INSTRUCTIONS

Note: If the variables in the address field of a macro-instruction represent one or more blocks, each of which consisting of more than one memory location, the symbolic designation of the first word of the block is used; for example, if A represents a matrix, the location A specifies the matrix element in the first row and first column. All elements in a matrix are sequentially stored by rows.

(1) QEXIT A - Stores the content of index registers 1, 2, and 4 in the address part of location A, A+1, and A+2, respectively.

(2) QRET - Used in conjunction with QEXIT to restore the content of the three index registers. The address field of QEXIT should be the location field of QRET.

(3) QROT x, A, y

$$\bar{x} = \bar{A}\ \bar{y},$$

where $\bar{x}$ and $\bar{y}$ are vectors and A represents a transformation matrix.

(4) QROTT x, A, y

$$\bar{x} = \bar{A}^{*}\ \bar{y},$$

where $\bar{x}$ and $\bar{y}$ are vectors and $\bar{A}^{*}$ represents the transpose of the transformation matrix $\bar{A}$.

(5) QVADD z, x, y

$$\bar{z} = \bar{x} + \bar{y},$$

where $\bar{x}$, $\bar{y}$, and $\bar{z}$ are vectors.

(6) QVSUB z, x, and y

$$\bar{z} = \bar{x} - \bar{y},$$

where $\bar{x}$, $\bar{y}$, and $\bar{z}$ are vectors.

(7) QVDV z, x, y

$$z = \bar{x} \cdot \bar{y}$$

where z represents the result of the scalar product of the vectors $\bar{x}$ and $\bar{y}$.

(8) QVCRV z, x, y

$$\bar{z} = \bar{x} \times \bar{y},$$

where the vector $\bar{z}$ represents the result of the cross-product of the vectors $\bar{x}$ and $\bar{y}$.

(9) QMATM A, B, C

$$\bar{C} = \bar{A}\ \bar{B},$$

where $\bar{A}$, $\bar{B}$, and $\bar{C}$ are matrices.

(10) QMTTM A, B, C

$$\bar{C} = \bar{A}^* \bar{B},$$

where $\bar{A}^*$ is the transpose of matrix A, and B and C are matrices.

## 6. PROGRAMMED SUBROUTINES

### a. MA1

This subroutine generates $\bar{A}_1 (\alpha)$, where

$$\bar{A}_1 (\alpha) = \begin{bmatrix} 1 & 0 & 0 \\ 0 & \cos \alpha & -\sin \alpha \\ 0 & \sin \alpha & \cos \alpha \end{bmatrix}$$

The calling sequence is TSX MA1, 4; where $\alpha$ is the MQ and the first location of $\bar{A}_1 (\alpha)$ is in the address part of the AC.

The following subroutines and macro-instructions are used:

(a) Library

I. SIN1 and COS1

(b) Programmed

I. QEXIT and QRET

### b. MA2

This subroutine generates $\bar{A}_2 (\alpha)$ and is the same as MA1, except that

$$\bar{A}_2 (\alpha) = \begin{bmatrix} \cos \alpha & 0 & \sin \alpha \\ 0 & 1 & 0 \\ -\sin \alpha & 0 & \cos \alpha \end{bmatrix}$$

Note: MA2 has not been used thus far in the program. It was written for purposes of completeness and to be available for future requirements.

c. MA3

This subroutine generates $\bar{A}_3$ $(\alpha)$ and is the same as MA1 and MA2, except that

$$\bar{A}_3\ (\alpha) = \begin{bmatrix} \cos\alpha & -\sin\alpha & 0 \\ \sin\alpha & \cos\alpha & 0 \\ 0 & 0 & 1 \end{bmatrix}$$

d. MATRE

This subroutine generates the matrix $\bar{E}$, where

$$\bar{E} = \bar{A}_3\ (\Omega_\oplus)\ \bar{A}_1\ (I_\oplus)\ \bar{A}_3\ (\omega_\oplus t + \omega_{\oplus_o})$$

$$= \bar{A}_1\ (I_\oplus)\ \bar{A}_3\ (\dot{\omega}_\oplus t + \omega_{\oplus_o})$$

Since $\Omega_0$ is zero and

$I_\oplus$ = inclination of the earth's equator to the ecliptic plane,

$t$ = time measured in days from start of computation,

$\dot{\omega}_\oplus$ = angular rate of rotation of the earth in radians per day,

$\Omega_\oplus$ = longitude of ascending node of the earth's equator with respect to the ecliptic plane, and

$\omega_{\oplus_o}$ = the Greenwich hour angle, in radians, of the vernal equinox at time $t + t_o$, where $t_o$ is the time at start of computation from January 1, 1950, in days;

$E$ = $(100.0754260 + 0.985647346\ [t + t_o] + 2.9015 \times 10^{-13}\ [t + t_o]^2$ $/57.2957795 + \dot{\omega}_\oplus\ \Delta t.$

The quantity $[t + t_o]$ is the nearest lower integer of $t + t_o$, and $\Delta t$ is the difference between $t + t_o$ and $[t + t_o]$.

The calling sequence is TSX MATRE, 4, where t has previously been placed in EDAY, $\omega_{\oplus_o}$ in OEO, and $\bar{A}_1$ $(I_\oplus)$ has been precomputed and placed in memory locations starting at TEMP + 31. (The quantities $\bar{A}_1$ $(I_\oplus)$ and $\omega_{\oplus_o}$ are computed during the initialization phase of the program.) The matrix is placed in locations starting at E.

The following subroutines and macro-instructions are used:

(a) Library -- none

(b) Programmed

- I. QEXIT and QRET
- II. REDUC
- III. MA3
- IV. QMATM

e. MATRM

This subroutine generates the matrix $\overline{M}$, where

$$\overline{M} = \overline{A}_3 (\Omega_{\leftmoon}) \overline{A}_1 (I_{\leftmoon}) \overline{A}_3 (\omega_{\leftmoon} t + \omega_{\leftmoon_o})$$

and

$\Omega_{\leftmoon}$ = longitude of ascending node of the moon's equator on a plane parallel with and referenced to the ecliptic plane,

$I_{\leftmoon}$ = inclination of the moon's equator to the ecliptic plane,

$\dot{\omega}_{\leftmoon}$ = angular rate of rotation of the moon in radians per day,

t = time measured in days from start of computations, and

$\omega_{\leftmoon_o}$ = angular position of the moon's x-axis from a plane parallel to the ecliptic plane (computed during the initialization phase by multiplying $\dot{\omega}_{\leftmoon}$ by the time taken for the moon to move from the line of ascending node to the initial position of the moon at the start of computation),

The calling sequence is TSX MATRM, 4, where t has been previously placed in EDAY, $\omega_{\leftmoon_o}$ in OMO, and $\Omega_{\leftmoon_\bullet}$ and $\overline{A}_1$ $(I_{\leftmoon})$ have been previously computed and placed in TEMP + 41 and starting in TEMP + 40, respectively. $\Omega_{\leftmoon_0} = \Omega_{\leftmoon_\bullet} + 180$ degrees, and $\Omega_{\leftmoon_\bullet}$ is the longitude of the ascending node of the moon's orbital plane with respect to the ecliptic plane. The quantity $\Omega_{\leftmoon_\bullet}$ is a partial output of MOON. $\overline{A}_1$ $(I_{\leftmoon})$ is computed during the initialization phase of the program.

The subroutine output is: The matrix is placed in locations starting at M.

The following subroutines and macro-instructions are used:

(a) Library -- none

(b) Programmed

I. QEXIT and QRET

II. REDUC

III. MA3

IV. QMATM

f. MATMA

This subroutine generates the transpose of the matrix $\bar{A}$, where

$$\bar{A} = \bar{A}_3\,(\Omega_{\text{☾}})\ \bar{A}_1\,(I_{\text{☾}})\ \bar{A}_3\,(\omega_{\text{☾}}).$$

Hence, the transpose of $\bar{A}$ is

$$\bar{A}^* = \bar{A}_3\,(-\omega_{\text{☾}})\ \bar{A}_1\,(-I_{\text{☾}})\ \bar{A}_3\,(-\Omega_{\text{☾}}),$$

since

$$A_1^*\,(\alpha) = A_1\,(-\alpha)$$

and, with respect to the ecliptic plane,

$\omega_{\text{☾}}$ = argument of perigee of the moon's orbit,

$I_{\text{☾}}$ = inclination of the moon's orbit, and

$\Omega_{\text{☾}}$ = longitude of ascending node of the moon's orbit.

The calling sequence is TSX MATMA, 4, where $\omega_{\text{☾}}$, $\Omega_{\text{☾}}$, and $\bar{A}_1\,(-I_{\text{☾}})$ have been previously computed and are stored in locations TEMP + 8, TEMP + 4, and starting at TEMP + 85, respectively. ($\bar{A}_1\,(-I_{\text{☾}})$ is computed during the initialization phase of the program, and $\omega_{\text{☾}0}$ and $\Omega_{\text{☾}0}$ are partial outputs of MOON.)

The output of this subroutine is: The matrix is placed in locations starting at AT.

The following subroutines and macro-instructions are used:

(a) Library -- none

(b) Programmed

I. QEXIT

II. QMATM

III. MA3

g. MATRN

This subroutine computes a matrix $\bar{N}$, where

$$\bar{N} = \bar{A}_3\ (\Omega)\ \bar{A}_1\ (I)\ \bar{A}_3\ (\omega)$$

and $\Omega$, I, and $\omega$ are any generalized set of values of longitude of ascending node, inclination, and argument of perigee, respectively. $\bar{N}$ is used at the input stage, when orbital elements are the input option, to convert initial conditions to the corresponding equatorial and ecliptic plane-oriented Cartesian vectors. In addition, it is used in the reverse direction to compute time of perigee from a Cartesian position vector for output purposes.

The calling sequence is TSX MATRN, 4, where I, $\Omega$, and $\omega$ are previously placed in locations TEMPA + 36 to TEMPA + 38, respectively.

The output of this subroutine is: The matrix is placed in locations starting at TEMPA + 39.

The following subroutines and macro-instructions are used:

(a) Library -- none

(b) Programmed

I. QEXIT and QRET

II. QMATM

III. MA1

IV. MA3

h. MOON

This subroutine generates the Cartesian position and velocity vectors of the moon with respect to the earth-moon plane. The required equations are:

$$\Omega_{\text{☾}\oplus} = [\,12.1127902 - 0.0529539222\ (t_o + t) + 20.795 \times 10^{-4}\ (T_o + T)$$
$$+ 20.81 \times 10^{-4}\ (T_o + T)^2 + 0.02 \times 10^{-4}\ (T_o + T)^3\,]$$
$$/57.2957795 \text{ radians}$$

$$\omega_{☾\oplus} = [64.37545167 + 13.1763965268\,(t_o + t) - 11.31575 \times 10^{-4}\,(T_o + T)$$

$$-11.3015 \times 10^{-4}\,(T_o + T)^2 + 0.019 \times 10^{-4}\,(T_o + T)^3]$$

$$/57.2957795 \text{ radians}$$

$$\Gamma' = [208.8439877 + 0.1114040803\,(t_o + t) - 0.010334\,(T_o + T)$$

$$-0.010343\,(T_o + T)^2 - 0.12 \times 10^{-4}\,(T_o + T)^3]$$

$$/57.2957798 \text{ radians}$$

where

$\theta_{☾\oplus}$ = $☾ - \Gamma'$ = mean anomaly of the moon,

$\omega_{☾\oplus}$ = $\Gamma' - \Omega$ = argument of perigee of the moon,

$t_o$ = time of start of program with respect to 0 hours, January 1, 1950, in days,

$t$ = number of days past start of program, and

$T$ and $T_o$ have definitions corresponding to $t$ and $t_o$ in centuries of 36,525 days.

Then,

$$E_{☾\oplus} - e_{☾\oplus} \sin E_{☾\oplus} = \theta_{☾\oplus}$$

is solved for $E_{☾\oplus}$, where

$E_{☾\oplus}$ = eccentric anomaly of the moon and

$e_{☾\oplus}$ = eccentricity of the moon's orbit.

Therefore,

$$\bar{x}_{☾\oplus} = \begin{bmatrix} a_{☾\oplus}\,(\cos E_{☾\oplus} - e_{☾\oplus}) \\ b_{☾\oplus}\,\sin E_{☾\oplus} \\ 0 \end{bmatrix}$$

where

$\bar{x}_{\leftmoon\bullet}$ = Cartesian position vector of the moon in the earth-moon plane,

$a_{\leftmoon\bullet}$ = semi-major axis of the moon's path, and

$b_{\leftmoon\bullet}$ = semi-minor axis of the moon's path

$= a_{\leftmoon} \sqrt{1 - e^2_{\leftmoon\bullet}}$ .

In addition,

$$\dot{\bar{x}} = \begin{bmatrix} -a_{\leftmoon\bullet} \dot{E}_{\leftmoon\bullet} \sin E_{\leftmoon\bullet} \\ b_{\leftmoon\bullet} \dot{E}_{\leftmoon\bullet} \cos E_{\leftmoon\bullet} \\ 0 \end{bmatrix}$$

where

$$\dot{E}_{\leftmoon\bullet} = 1 \Big/ \left[ \frac{P_{\leftmoon\bullet}}{2\pi} \left(1 - e_{\leftmoon\bullet} \cos E_{\leftmoon\bullet}\right) \right]$$

= rate of change of eccentric anomaly,

$\dot{\bar{x}}_{\leftmoon\bullet}$ = rate of change of Cartesian position vector, and

$P_{\leftmoon\bullet}$ = orbital period of the moon

The calling sequence is TSX MOON, 4, where T, t, $a_{\leftmoon\bullet}$, $b_{\leftmoon\bullet}$, $e_{\leftmoon\bullet}$, and $P_{\leftmoon\bullet}$ have previously been placed in locations JCENT, EDAY, AM, TEMP + 137, EMOON, and TEMP, respectively. (The latter four parameters are preset as a part of the loading of the program or the pre-initialization phase of the program.)

The primary output of this subroutine is:

(a) $\bar{x}_{\leftmoon\bullet}$ starting at TEMP + 19

(b) $\dot{\bar{x}}_{\leftmoon\bullet}$ starting at TEMP + 10

The following subroutines and macro-instructions are used:

(a) Library

I. SIN1 and COS1

(b) Programmed

I. QEXIT and QRET

II. REDUC

III. CMPE

This subroutine generates the Cartesian position vector of the sun with respect to the ecliptic plane. The required equations are:

$$L = [280.08121009 + 0.9856473354\ (t_o + t) + 3.03 \times 10^{-4}\ (T_o + T) + 3.03 \times 10^{-4}\ (T_o + T)^2]\ /57.2957795 \text{ radians}$$

$$\Gamma = [282.08053028 + 0.470684 \times 10^{-4}\ (t_o + t) + 4.5525 \times 10^{-4}\ (T_o + T) + 4.575 \times 10^{-4}\ (T_o + T)^2 + 0.03 \times 10^{-4}\ (T_o + T)^3]\ /57.2957795 \text{ radians}$$

$$e_{\theta\boldsymbol{\theta}} = 0.016730109 - 0.4192 \times 10^{-4}\ (T_o + T) - 0.126 \times 10^{-6}\ (T_o + T)^2$$

where

$\theta_{\theta\boldsymbol{\theta}}$ = L - Γ = mean anomaly of the sun,

$t_o$, t, $T_o$, and T are as defined in MOON,

$e_{\theta\boldsymbol{\theta}}$ = eccentricity of the sun's orbit about the earth, and

$\bar{x}_{\theta\boldsymbol{\theta}}$, the position vector of the sun with respect to the ecliptic plane, is computed by equations similar to those used to calculate $\bar{x}_{(\boldsymbol{\theta}}$ in MOON.

The calling sequence is TSX SUN, 4, where T, t, and $a_{\theta\boldsymbol{\theta}}$ have been previously placed in JCENT, EDAY, and AS, respectively. ($a_{\theta\boldsymbol{\theta}}$ is stored as a program constant.)

The primary output is: $\bar{x}$ starting at XSUN.

The following subroutines and macro-instructions are used:

(a) Library

- I. SIN1 and COS1
- II. SQRT

(b) Programmed

- I. QEXIT and QRET
- II. REDUC
- III. CMPE

### j. REDUC

This subroutine reduces an input angle, in radian argument, to a positive angle, module 2π.

The calling sequence is TSX REDUC, 4, where the input angle, positive or negative, is previously placed in the accumulator.

The output of this subroutine is: A positive angle, reduced module 2π, is left in the accumulator.

No subroutines or macro-instructions are used.

### k. ROTA

This subroutine generates a position vector of the orbiter with respect to the ecliptic plane. The equations are:

$$\bar{m} = (\bar{A}^*)^*\bar{x}_{\leftmoon}$$

$$(\bar{x} - \bar{m}) = \bar{T}\ \bar{\xi}$$

$$\bar{x} = (\bar{x} - \bar{m}) + \bar{m}$$

where

$\bar{m}$ = position vector of the moon with respect to the ecliptic plane,

$\bar{A}$ = matrix used to transform a position vector from the earth-moon plane into the ecliptic plane,

$\bar{x}_{\leftmoon}$ = position vector of the moon with respect to the earth-moon plane,

$\bar{\xi}$ = position of the orbiter with respect to its instantaneous orbital plane,

$\bar{T}$ = matrix used to transform the position vector of the orbiter from its instantaneous orbital plane to a moon-centered plane parallel to the ecliptic plane, and

$\bar{x}$ = position vector of the orbiter with respect to the ecliptic plane.

The calling sequence is TSX ROTA, 4, where $\bar{A}^*$, $\bar{x}'_{\oplus}$, $\bar{T}$, and $\bar{\xi}$ are previously stored in locations starting at AT, MX2, T, and X1, respectively. ($\bar{A}^*$ is computed in MATMA, $\bar{x}'_{\oplus}$ in MOON, and $\bar{T}$ and $\bar{\xi}$ as partial results in solving the differential equations.)

The output of this subroutine is:

(a) $\bar{m}$ starting at MX

(b) $\bar{x} - \bar{m}$ starting at TEMP + 115

(c) $\bar{x}$ starting at x

The following subroutines and macro-instructions are used:

(a) Library -- none

(b) Programmed

I. QEXIT and QRET

II. QROTT

III. QROT

IV. QVADD

1. CRRD

This subroutine generates, for output purposes, the range and range rate of the orbiter as measured by an observer on a moving spherical earth. The equations are:

$$\bar{s} = \overline{Es}^{1V}$$

$$s = \overline{EW}^{1V}\bar{s}^{1V}$$

$$\dot{\bar{m}} = (A^*)^*\bar{x}'_{\oplus}$$

$$\dot{\bar{x}} - \dot{\bar{m}} = \bar{T}^* \dot{\bar{\xi}}$$

$$R = \|\bar{x} - \bar{s}\|$$

$$\dot{R} = (\bar{x} - \bar{s}) \cdot (\dot{\bar{x}} - \dot{\bar{s}})/R$$

where

$\bar{s}^{IV}$ = position vector of the observer with respect to a fixed earth equatorial orientation

$$= r_{\oplus} \begin{bmatrix} \cos\delta & \cos\phi \\ \cos\delta & \sin\phi \\ \sin\delta & \end{bmatrix} ;$$

$r_{\oplus}$ = radius of the earth;

$\delta$, $\phi$ = latitude and longitude, respectively, of the observer;

$\bar{E}$ = matrix used to transform a position vector from the earth equatorial plane to the ecliptic plane;

$\bar{W}^{IV}$ = matrix used to determine the rate of change of a position vector fixed on the earth with respect to the earth's equatorial plane;

$$= \omega_{\oplus} \begin{bmatrix} 0 & -1 & 0 \\ 1 & 0 & 0 \\ 0 & 0 & 0 \end{bmatrix} ;$$

$\dot{\omega}_{\oplus}$ = earth's angular rate of rotation in radians;

$\bar{s}$ = position vector of the observer with respect to the ecliptic plane;

$\dot{\bar{s}}$ = rate of change of the position vector of the observer with respect to the ecliptic plane;

$\bar{A}^*$ = as defined in ROTA;

$\dot{\bar{m}}$ = rate of change of the moon's position vector with respect to the ecliptic plane;

$\mathring{\bar{\xi}}$ = rate of change of position vector of the orbiter with respect to the orbiter's instantaneous plane;

$\dot{\bar{x}}$ = rate of change of position vector of the orbiter with respect to the ecliptic plane;

$\dot{\bar{x}}_{\text{☾}\oplus}$ = rate of change of the moon's position vector with respect to the earth-moon plane;

$R, \dot{R}$ = range and range rate, respectively, of the orbiter as measured by an observer on a moving earth; and

$\bar{T}$ = matrix as defined in ROTA.

The calling sequence is TSX CRRD, 4, where $\bar{x}$, $\bar{s}^{1V}$, $\dot{\bar{x}}_{\text{☾}\oplus}$, $\dot{\bar{\xi}}$, $\bar{W}^{1V}$, $\bar{T}$, and $\bar{A}^*$ are previously placed in locations starting at TEMP +115, S4, TEMP + 10, XID, W4, T, and AT, respectively. ($\bar{s}^{1V}$ and $\bar{W}^{1V}$ are preset during the pre-initialization and initialization phases; $\bar{x}$ is computed in ROTA, $\dot{\bar{x}}_{\text{☾}\oplus}$ in MOON, $\bar{A}^*$ in MATMA, $\dot{\bar{\xi}}$, and $\bar{T}$ as partial results in solving the differential equations.)

The primary output of this subroutine is: R in MAGR and $\dot{R}$ in MAGRD

The following subroutines and macro-instructions are used:

(a) Library

I. SQRT

(b) Programmed

I. QEXIT and QRET

II. MATRE

III. QROT

IV. QROTT

V. QVADD AND QVSUB

VI. QVDV

m. GAMM

This subroutine generates $\bar{\gamma}$, a vector representing the perturbing forces acting upon the orbiter. Through input options, the presence or absence of three types of perturbing forces are controlled. The three sources of these perturbing forces are as follows:

(a) The presence of the earth.

(b) The presence of the sun.

(c) The non-spherical shape of the moon.

In terms of the ecliptic-plane coordinate system, the required equations are:

$$\overline{T}\overline{\gamma} = \frac{\mu_\theta}{\|\overline{x}_{\theta\bullet} - \overline{x}\|^3}(\overline{x}_{\theta\bullet} - \overline{x}) - \frac{\mu_\theta}{\|\overline{x}_{\theta\bullet} - \overline{m}\|^3}(\overline{x}_{\theta\bullet} - \overline{m}) + \frac{\mu_\bullet}{\|\overline{m}\|^3}\overline{m} - \frac{\mu_\bullet}{\|\overline{x}\|^3}\overline{x} + \overline{f}_{(}$$

where

$\overline{T}, \overline{\gamma}$ = total perturbing force with respect to the ecliptic plane,

$\mu_0$ = gravitation constant of the sun,

$\mu_\bullet$ = gravitation constant of the earth,

$\overline{x}_{\theta\bullet}$ = position vector of the sun with respect to the ecliptic plane,

$\overline{x}$ = position vector of the orbiter with respect to the ecliptic plane,

$\overline{m}$ = position vector of the moon with respect to the ecliptic plane, and

$\overline{f}_{(}$ = perturbing force resulting from the moon's shape, where

$$\overline{M}^*\overline{f}_{(} = \frac{3k^2}{2r^5}\begin{bmatrix} x_1' \\ x_2' \\ x_3' \end{bmatrix}\left\{ -(A + B + C) + 5I - 3\begin{bmatrix} A \\ B \\ C \end{bmatrix} \right\}$$

$$\begin{bmatrix} x_1' \\ x_2' \\ x_3' \end{bmatrix} = \overline{x}' = \overline{M}^*(\overline{x} - \overline{m})$$

A, B, C = the moments of inertia about the principal axes of the moon,

k = Gauss' constant,

r = $\|\overline{x} - \overline{m}\| = \|\overline{x}'\|$, and

I = $\frac{1}{r^2}(Ax_1^2 + Bx_2^2 + Cx_3^2)$.

[illegible] No. 62-489

The calling sequence is TSX GAMM, 4, where $\overline{T}$, $\overline{M}$, $\bar{x} - \bar{m}$, r, $\bar{x}_{\theta\oplus}$, $\bar{x}$, and $\overline{m}$ are previously stored in locations starting at T, M, TEMP + 115, TEMP + 125, XSUN, X, and MX, respectively (i.e., the subroutines MOON, SUN, MATRM, and ROTA must be used before entry into GAMM).

The output of this subroutine is: $\bar{\gamma}$, starting at location TEMP + 172

The following subroutines and macro-instructions are used:

(a) Library

- I. SQRT

(b) Programmed

- I. QEXIT and QRET
- II. QROT
- III. QROTT

## n. ORBIT

This subroutine converts orbital elements, as read as part of the input data, into the corresponding Cartesian position and velocity vectors. The required equations are; using

$$E - e \sin E. = \frac{2\pi}{P} (t - \tau),$$

the Cartesian position vector with respect to the particular frame of reference used;

$$x'' = \overline{N} \begin{bmatrix} a(\cos E - e) \\ b \sin E \\ 0 \end{bmatrix} .$$

where

$$N = A_3(\Omega) A_1(I) A_3(\omega).$$

Also, the velocity vector is

$$x'' = \overline{N} \begin{bmatrix} -a \dot{E} \sin E \\ b \dot{E} \cos E \\ 0 \end{bmatrix}$$

where

$$\dot{E} = \frac{2\pi}{P(1 - \cos E)}$$

and

$P = 2\pi \left(\frac{a^3}{\mu}\right)^{1/2}$ = period of orbiter,

$\tau$ = time of perigee passage,

$e$ = eccentricity,

$E$ = eccentric anomaly,

$a$ = semi-major axis,

$b = a\sqrt{1 - e^2}$ = semi-minor axis,

$I$ = inclination of orbital plane,

$\omega$ = argument of perigee, and

$\Omega$ = longitude of ascending node.

If the orbital elements are referenced to a plane parallel to the ecliptic plane,

$$\bar{x}'' = \bar{x} - \bar{m}\,;$$

if the elements refer to the moon's equatorial plane,

$$\bar{x}'' = M^*(\bar{x} - \bar{m}) = \bar{x}^{1}.$$

The calling sequence is TSX ORBIT, 4, where a, e, I, $\omega$, $\Omega$, $\tau$, and t are previously stored in locations starting at TEMPA + 18 and t at EDAY. The angles are stored in units of degrees.

The outputs of this subroutine are:

(a) $\bar{x}''$ starting at TEMPA + 18

(b) $\dot{\bar{x}}''$ starting at TEMPA + 21

The following subroutines and macro-instructions are used:

(a) Library

I. SQRT

II. SIN1, COS1

(b) Programmed

- I. QEXIT and QRET
- II. QROT
- III. CMPE
- IV. REDUC
- V. MATRN

o. CMPE

This subroutine solves for the eccentric anomaly, E, from

$$E - e \sin E = \frac{2\pi}{P} (t - \tau)$$

(Note that M or E is not to be confused with the transformation matrices $\overline{M}$ or $\overline{E}$, respectively.) The solution for E involves a Newton-Raphson type of iterative procedure; namely,

$$E_{j+1} = E_j - C_j ,$$

$$C_j = (E_j - e \sin E_j - M)/(1 - \cos E_j),$$

$$E_o = M + (e + e^2 \cos M + e^3) \sin M - 1.5\ e^3 \sin^3 M,$$

where the process is halted when $C_j$ is less than some predetermined value.

The calling sequence is TSX CMPE, 4, where M and e are previously placed in the accumulator and the MQ, respectively.

The output of this subroutine is: E is placed in the accumulator.

The following subroutines and macro-instructions are used:

(a) Library

- I. SIN1 and COS1

(b) Programmed

- I. QEXIT and QRET

[illegible] 62-489

# Section 3

# LUNAR SURFACE SIMULATION STUDIES

## A. OBJECTIVES

The primary objectives of the lunar surface simulation studies are:

(1) To establish a reliability criterion for a lunar mission based on certain assumed surface roughnesses for the average moon, and based on an assumed ability of a surface mechanism to tolerate the presence of obstructions of a stated size and those that are smaller;

(2) To extend our knowledge of distribution of crater sizes by actual count from available atlases;

(3) To extend the range of crater sizes that can be analyzed in pictures of table-top models;

(4) To compare the photometric function of a table-top model, containing superposed and juxtaposed craterlets, with that of the moon.

## B. MISSION RELIABILITY VERSUS LUNAR ROUGHNESS

Based on C. Allen's book,* let it be assumed that there are about 320 craters on the lunar hemisphere that are larger than 30 kilometers in rim-to-rim diameter, and that the largest crater is something between 250 and 550 kilometers, depending on whether or not certain walled plains and maria are classed in the family of craters for statistical purposes. Then let it be supposed that the equation:

$$N = \frac{k}{x^n}$$

can describe the entire family of craters for values of crater diameter x kilometers, far too small to be seen from earth telescopes, and even in a range of crater diameters of vital concern in the lunar landing and surface movements of men and machines. N is the number of craters per hemisphere with diameters larger than x; k and n are presumed constant.

The smoothest moon would then be described by:

$$N = 300{,}000/x^2 \,, \qquad (1)$$

---

* Astrophysical Quantities, C. W. Allen, Univ. of London, The Athlone Press, 1955, p. 163.

and the roughest moon by:

$$N = 3,000,000/x^{2.7} \tag{2}$$

Finally, let the adequacy of the design of a landing mission be based on the assumption that an area $D^2$ of the lunar surface can be found which will contain no crater centers larger than X and smaller than D, and no steep inner rim slopes of craters larger than D. Two cases are considered. First, assume D = 30 meters, and that a landing, selected at random, is to be effected on a roughly square or circular area 30 meters in diameter. Next, assume that an area 300 meters in diameter is selected at random, but that a landing operation includes a hovering capability sufficient to search this larger area and select the required spot, 30 meters in diameter, free of the specified roughness.

It is interesting to note that if X is given a range of 0.5 to 20 meters, the "smooth moon" of equation (1) would contain enough craters in this size range to cover almost 10 percent of the lunar surface with no overlap. Equation (2), for the rougher moon, suggests a sufficiency of craters in this size range to cover the moon some eighty times over, yet a flat-random distribution would still leave a calculable probability of landing on a "clear" area 30 meters in diameter, with or without hovering. If landing equipment is made capable of tolerating craterlets larger than 0.5 meter in diameter, the probabilities of success are increased. The nature of the mathematical approach to such a study inherently provides upper and lower bounds, but not explicit results. For a fixed value of X, the range from upper to lower bounds on probability of success (P) is very great; this is so because small variations in X produce very great changes in P. Therefore, a much more interpretable set of results is obtained by tabulating the upper and lower bounds on X at a stated value of P, as is listed in Table II.3.B-1 below.

TABLE II.3.B-1

LANDING PROBABILITY OF SUCCESS FOR UPPER AND LOWER BOUNDS ON CRATER SIZE (X)

| Probability of Success (P) | Smooth Moon Equation 1 | | Rough Moon Equation 2 | |
|---|---|---|---|---|
| | Random Landing | Hover and Search | Random Landing | Hover and Search |
| | (Meters) | | (Meters) | |
| 0.999 | 40-120 | 1.7-5.0 | 200-400 | 23-56 |
| 0.99 | 16-44 | 1.5-4.6 | 80-160 | 21-52 |
| 0.9 | 9.0-17 | 1.3-4.0 | 40-80 | 20-50 |
| 0.5 | 4.0-8.0 | 1.2-3.2 | 25-45 | 19-47 |
| 0.1 | 2.5-5.0 | 1.1-2.9 | 22-40 | 17-42 |
| 0.01 | 1.6-3.2 | 1.0-2.8 | 20-36 | 16-36 |
| 0.001 | 1.3-2.7 | 0.9-2.6 | 18-32 | 14-32 |

It is to be noted that the spread between upper and lower bounds is far too large to justify the number of significant figures. These have been given only to show the extreme advantages of even very small increases in the tolerable roughness permitted by a given mechanism design. The results are preliminary, and it is planned not to write up the intricate mathematical basis by which both small holes and the 40-degree inner slopes of larger craters were included until the whole subject can be put on a firmer basis; first, by reducing the spread between boundary equations, if possible; and second, by using improved crater-distribution equations discussed elsewhere in this report.

One other implication from this study should be noted. For both the smooth-moon and the rough-moon assumptions, the mission plan which allows the hover and search capability goes from 0.001 chance of success to 0.999 chance of success by roughly doubling the size of roughness feature which can be tolerated. This improvement stems largely from the drastic reduction in the number of craters of concern, since the crater size which can be neglected is increased by more adequate design. If rims of large craters were ignored (and their effect is small when considering the hovering type mission), then the values of X in Table II.3.B-1 could be replaced by equivalent number values of craterlets per hemisphere area. For either rough or smooth moon, the number per hemisphere is increased by only a factor of four to cut the mission success probability of a given design from 0.999 to 0.001. In other words, a mission design having a 0.999 chance on any particular moon whose roughness was caused only by craterlets, boulders, cracks, or domes would deteriorate to a 0.001 chance of success if like distributions of all four kinds of roughness were encountered. On the other hand, the high probability of success could be restored by approximately doubling the tolerable obstruction sizes given in Table II.3.B-1. Unfortunately, there is a vast disparity between the types of landing equipment design needed for the "smooth" and "rough" moons assumed in this study, ranging perhaps from stilts with moderate sized feet all the way to very large inflated spheres which could bounce and roll, and then be erected after vigorous use of pick and shovel. It would appear that a great deal of effort to extend our knowledge of the roughness of the real moon is justifiable. Of course, those who believe in no roughness at a scale beyond that of present knowledge will find even the "smooth" moon of this study far too rough. Yet, it would be remarkable if N should increase as X decreases right to the threshold of present knowledge, and cut off just at that threshold. Every advance in telescopy since Galileo has demonstrated the opposite.

## C. LUNAR CRATER SIZE DISTRIBUTIONS

This part of the study program was intended (1) to extend our knowledge of crater size distributions "per lunar hemisphere" to smaller crater diameters than have been previously classified, (2) to consider the statistical handling of other forms of roughness, and (3) to attempt to make separate distribution evaluations for specific areas or types of terrain smaller than the lunar hemisphere.

As a result of the study, it is suggested that the lunar craters properly belong in two family groups. In a paper by V. P. Head(1), a logarithmico-normal distribution, and an alternate distribution of the form $N = K/X^n$ were considered.

---

(1) A Lunary Surface Model for Engineering Purposes, ARS Paper No. 2475-62, by V. P. Head.

It now appears that the actual distribution, as extended with the aid of the U.S.A.F. lunar charts and the Photographic Lunar Atlas, may best be represented by N (the number of craters larger than diameter x) as the sum of $N_p$ (or number of primary craters larger than x, and $N_s$), the number of secondary craters larger than x.

For the counts obtained, it appears that the number of primary craters, $N_p$, is about 4,000, half of which are larger than 11 kilometers, with the standard deviations of the normal distribution of log x fixed by x = 33 km, and x = 3.67 km. This distribution is shown on standard probability co-ordinates in Figure II.3.C-1. While conforming to the known distributions of large craters, walled plains, and maria treated as a family, this primary distribution accounts for far fewer small craters than have been observed. The suggested distribution for secondary craters is:

$$N_s = 500{,}000/x^{2.75},$$

as is shown by the straight line on Figure II.3.C-2. On this figure, the logarithmico-normal values of $N_p$ have also been replotted from Figure II.3.C-1. The heavy S-shaped curve in Figure II.3.C-2 gives the sum of the assumed primary and secondary craters combined, while the points show actual counts as obtained at RCA during September, 1962 for sample areas of maria and continents that were converted to a "per lunar hemisphere" basis by assuming that the moon's face, as seen from earth, is equally divided between maria and continents.

Six points are perhaps insufficient to establish with any accuracy the five constants needed to write the complete equation for N, even if the validity of the two-family assumption be granted. A single straight line would fit the points of Figure II.3.C-2 fairly well, defined by $N = 100{,}000/x^{1.4}$. However, such a line would fall far short of the total number of craters exceeding one or two kilometers (as estimated by many astronomers), and would also predict far more walled plains and maria above 500 km than exist. The two-family equation is valid when extrapolated to both these extremes.

More important, the point scatter implied by such a straight line could be accepted only if more extreme and random scatter existed in the six regions of the lunar hemisphere analyzed. However, this is not the case. The bulge or knee in the curve through the range of 6 to 30 kilometers and the sudden upswing below six kilometers is a thoroughly repeatable phenomenon from one lunar area to another.

It is interesting to speculate that the family we have called primary may be explosion craters of possibly volcanic, or more probably impact, origin. With a minimum set on the impact velocity necessary to produce an explosion might there not be a lower limit on the size at which explosion primaries could be formed in any significant number? Moreover, might not this explain the limited number of rayed craters?

It has been shown by V.P. Head's experiment that a very large number of secondary craters, forming scatter patterns very like those on the moon, can be formed by the flying debris from a single, dynamically modeled explosion crater in the laboratory.

RE-ORDER No. 62-489

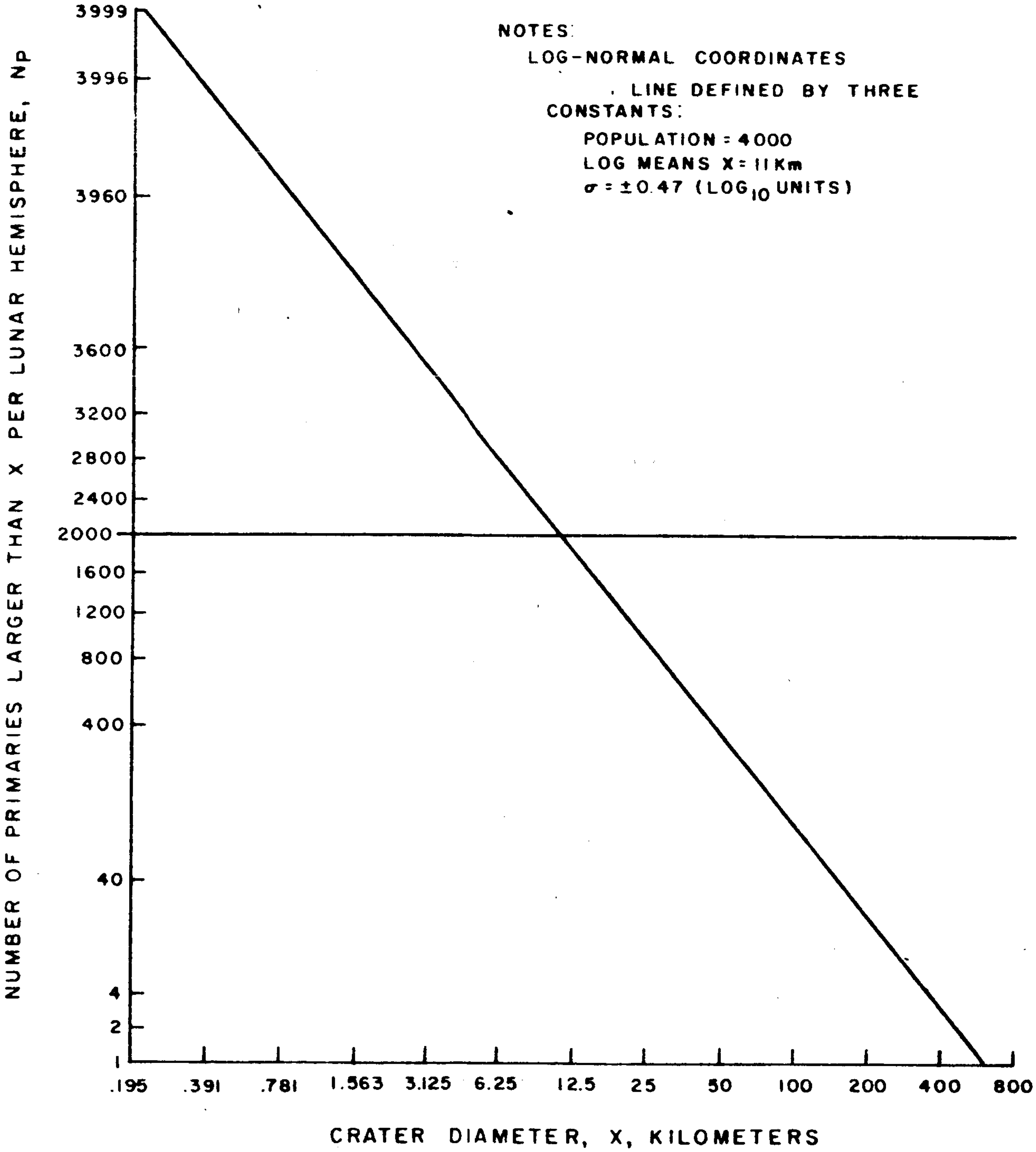

Figure II.3.C-1. Suggested Distribution of "Primary" Crater Size

RE-ORDER No. 62-489

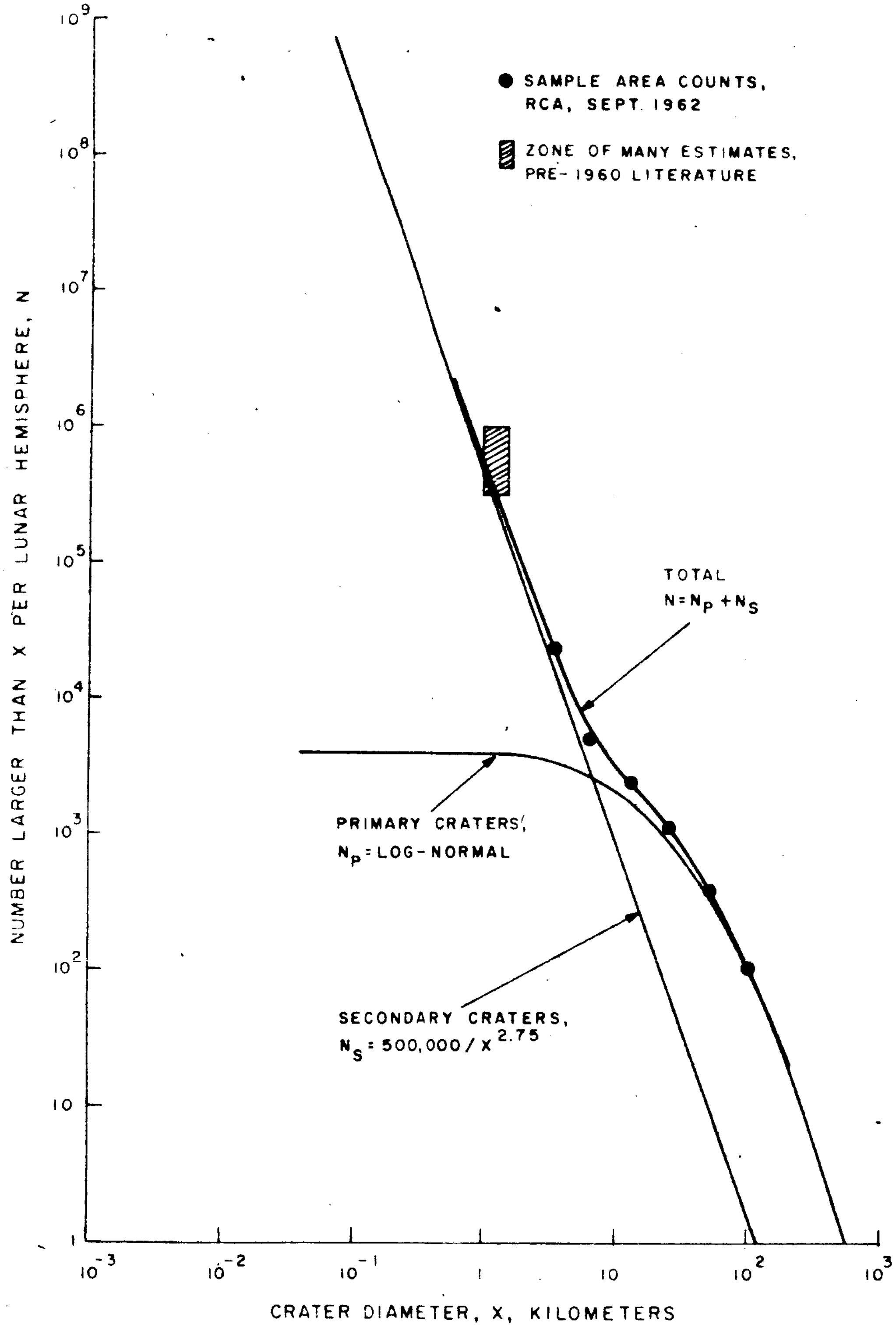

Figure II.3.C-2. Suggested Distribution of all Lunar Craters

RE-ORDER No. 62-489

Moreover, Shoemaker and others (ref. 2) have shown that a single hypervelocity impact of a small pellet on any of many rock targets will produce fragments, the size distributions of which are of the log-log type suggested here for secondary craters, and with exponents often exceeding 2.5. It can be demonstrated mathematically that a finite mass can not be shattered in such a way as to yield an exponent of 3 or more. Thus a slope of 2.75 is not unreasonable for the distribution of secondary craters, though this exact value can hardly be accepted from work of such limited scope. The true slope for lunar craterlets, in the size range from a fraction of a meter to a kilometer, can only be established when many close-up pictures of the moon become available.

It should be noted and explained here that two crater count observations were deliberately withheld from Figure II.3.C-2. Likewise, it should be explained why similar observations should be ignored whenever a counting process has resulted in a published distribution of crater sizes, star magnitudes, or the like. Whether from sheer fatigue, from an approach to the resolution limit, or because of overlap, counting always stops at a finite number, and a curve of log N versus log x must approach a horizontal asymptote or value of N as x decreases. This fact is well known to investigators who have studied photomicrographs of wood fibers, crushed rock, or the like. A finite population approximated by the log-normal distribution always results. However, when magnification is increased, total population always increases, and the supposed logarithmic mean value of x always decreases. Recent literature concerning the moon has ignored this fact, and statements have been made to the effect that the combined area of "all" craters on the moon would cover less than ten percent of the moon's area without overlap. Actually, about one-half of the moon's visible side is covered with large craters which do overlap, considering the "continents" alone.

Figure II.3.C-3 shows the integration of three histograms, primarily for the purpose of emphasizing the false droop that must accompany any distribution count, however painstaking the observer. Not only is the count finite as limited by resolution, but the count is always too low for the last size bracket which should be visible. The lowest curve labeled "Ancient History" portrays a faked set of observations such as might have been obtained by the naked eye before Galileo, had the more circular maria been classified as craters. The curve based on Young's data stemmed from our integration of the histogram as found in Fielder's publication (ref. 3). For the purpose of this study, this curve has been extended toward x = 0; the droop is evident in the original curve between 30 kilometers and 16 kilometers. The RCA curve is identical to that of Figure II.3.C-2 except for the inclusion of the two points which must be regarded as meaningless droop. The estimated brackets on the findings of a future orbiter have been drawn so as to portray an uncertainty of plus and minus one order of magnitude in extrapolating present knowledge to x = 100 meters. The true curve may or may not fall between the two x (droop) curve points shown at the top of Figure II.3.C-3. Wherever it falls, a finite count and false droop will be inevitable.

---

(2) "Astrogeological Studies", Semiannual Progress Report (Feb. 26, 1961 to August 24, 1961), U.S. Department of the Interior, Geological Survey; (a) Shoemaker and Moore, pp. 93-105; and (b) Moore and Gault, pp. 106-112.

(3) The Structure of the Moon's Surface, by Gilbert Fielder, Pergamom Press, New York, 1961, page 219.

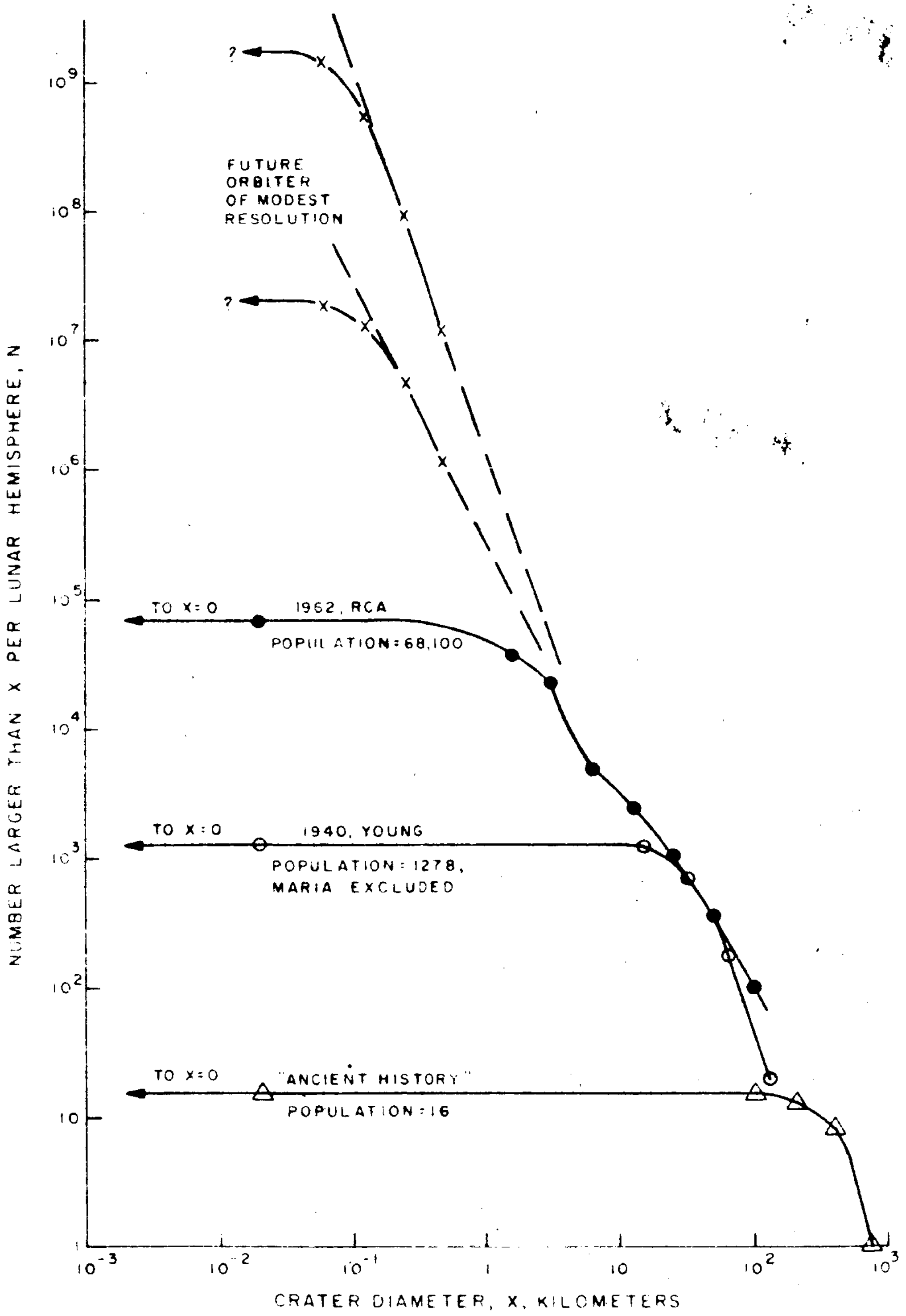

Figure II.3.C-3. False Droop Inherent in Distribution Counts

It is hoped that the subject of false droop has been belabored sufficiently in this report, and that statistical information from an orbiter will be used together with present knowledge of crater diameters in the range of 3 to 6 kilometers, to establish a straight line for secondary crater distributions that is comparable to one of the suggestive dashed lines in Figure II.3.C-3.

Distribution counts extended to sizes much less than four times the optical resolution must be discounted, and are shown by observation points without curves through them in Figure II.3.C-4.

Six distribution counts for specified portions of the lunar surface were studied in a search for variations with type of terrain. Five of these were counts made at RCA using the Photographic Lunar Atlas (ref. 4) and, where available, the U.S.A.F. Lunar Charts. Fearful that the increased steepness of the log N - log x curves below $x = 6$ km, on which all of the above discussion has been based, might prove to be an exception, a further search for confirmation was made. It was found in observations by Opik (ref. 5), published in 1960. Table II.3.C-1 provides the results of these studies by RCA and E.J. Öpik.

The data in Table II.3.C-1 may be best compared by converting to a "per lunar hemisphere" basis. Zone I was taken to be representative of lunar "continents", so the first column was multiplied by $1.89 \times 10^7 \div 2.8 \times 10^5$ to obtain the points plotted on the curve for "continents" (Figure II.3.C-4). While more information is needed, the pain of counting from the Photographic Lunar Atlas with loss of contrast and significant droop at $x = 1$ mile suggests that any extension of data for continents should await the availability of the LAC charts for such regions.

Zones II, III, IV and V were added to give distribution counts representative of the maria from a total area of $1.16 \times 10^6$ km$^2$, and again corrected to a "lunar hemisphere" area of $1.89 \times 10^7$ km$^2$. As might be expected, the table shows the Copernicus region to be much richer in small craterlets than the three adjoining regions studied. However, Öpik's data, similarly prorated, shows that the average of a very different location is quite comparable to that from the combined data of all five lunar continents. The curves labeled "maria" and "continents" in Figure II.3.C-4 are to be understood as representing a hypothetical hemisphere containing either maria or continents only. The curve for the visible "real hemisphere" assumes a 50-50 split between these types of terrain, as estimated from a full-moon view. Using only the data for $x = 3$ km or more, trial and error methods were employed to deduce from this average curve the five constants necessary to explain the curve shape in terms of the "primary" and "secondary" populations of Figures II.3.C-1 and II.3.C-2.

---

(4) Photographic Lunar Atlas, ed. by G. P. Kuiper, University of Chicago Press, Chicago, 1960.

(5) Opik, E.J., The Lunar Surface as an Impact Counter, Monthly Notices of the Royal Astronomical Society, 120, pp. 404-411.

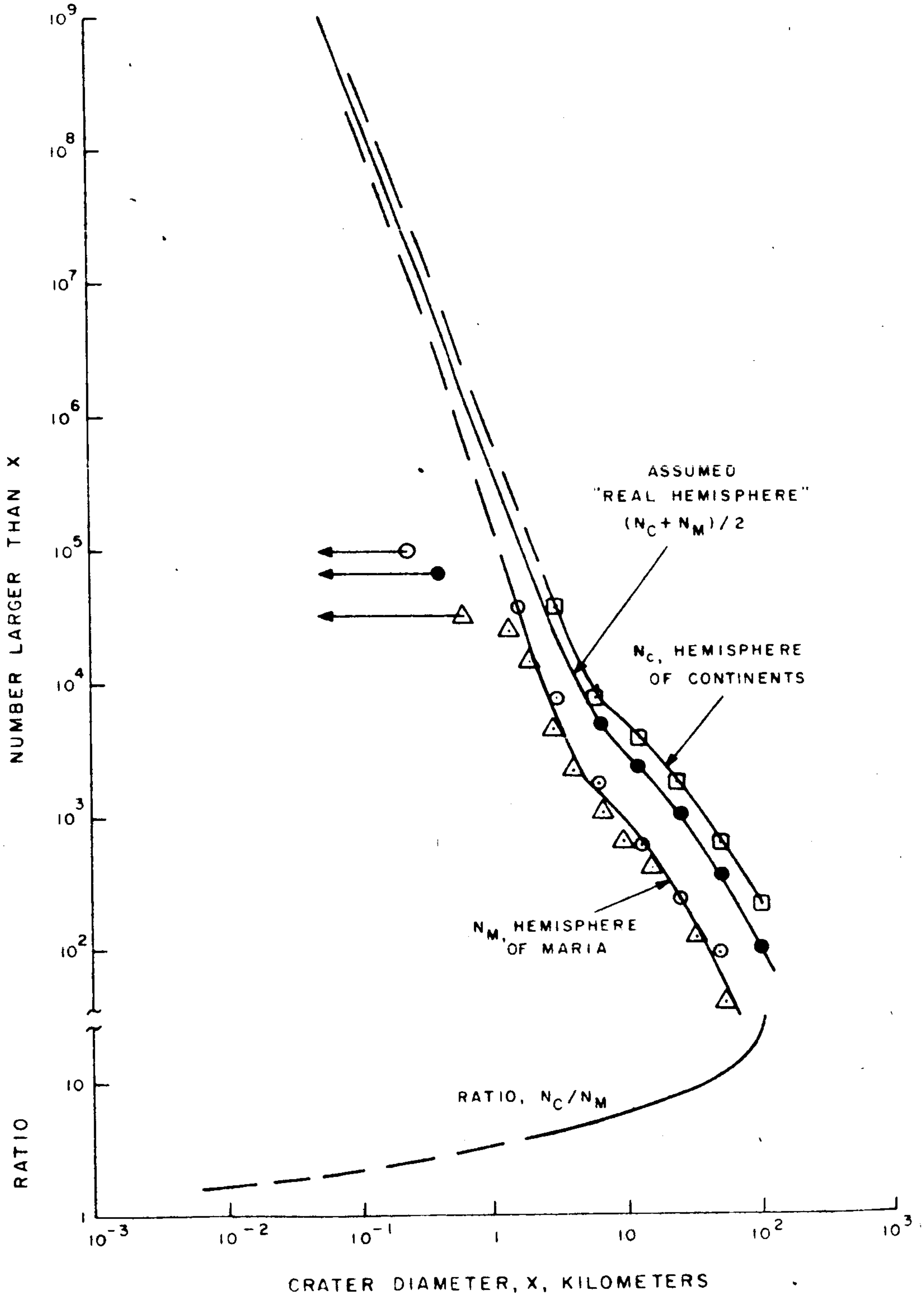

Figure II.3.C-4. Variations in Lunar Crater Size Distributions with Type of Terrain

RE-ORDER No. 62-489

# TABLE II.3.C-1

# LOCALIZED CRATER DISTRIBUTION COUNTS

| RCA-AED, 1962 | | | | | |
|---|---|---|---|---|---|
| | I | II | III | IV | V |
| Zone | Tycho | Kepler | Copernicus | Letronne | Riphaeus |
| Source | PLA D7-a | LAC-57 | LAC-58 | LAC-75 | LAC-76 |
| Area km$^2$ | $2.8 \times 10^5$ | $2.9 \times 10^5$ | $2.9 \times 10^5$ | $2.9 \times 10^5$ | $2.9 \times 10^5$ |
| x (km) | Cumulative Count per Zone Area, N | | | | |
| 0 | 533 | 644 | 3,842 | 693 | 989 |
| 1.61 | 533 | 231 | 1,252 | 261 | 389 |
| 3.22 | 533 | 63 | 192 | 84 | 144 |
| 6.44 | 114 | 31 | 27 | 24 | 29 |
| 12.9 | 58 | 4 | 16 | 7 | 11 |
| 25.8 | 27 | 2 | 6 | 2 | 5 |
| 51.5 | 9 | 0 | 3 | 0 | 3 |
| 103 | 3 | 0 | 0 | 0 | 0 |
| 206 | 0 | 0 | 0 | 0 | 0 |

| Opik, 1960 | |
|---|---|
| $4.65 \times 10^5$ km$^2$ Trapezoidal Zone on Mare Imbrium | |
| x (km) | N |
| 0 | 812 |
| 0.64 | 812 |
| 1.40 | 615 |
| 2.05 | 343 |
| 2.92 | 111 |
| 4.1 | 54 |
| 6.7 | 26 |
| 9.7 | 16 |
| 16 | 10 |
| 34 | 3 |
| 55 | 1 |

A vital problem in the Apollo mission concerns itself with the possible variations in roughness from place to place on the lunar surface. If such variations are large, for example, in the range of 1 to 100-meters in crater diameter, a search for a "smooth" area would then be a useful part of an orbiter mission. If such variations are small, then the determination of a single "per hemisphere" distribution by sampling methods would become a primary goal to provide a guide to design. A very tentative trend is found in the ratio $N_C/N_M$, at the bottom of Figure II.3.C-4. The density of craters larger than 50 kilometers is greater by eleven to one in the continental areas as compared to the maria. For a crater diameter of 3 kilometers, this ratio drops to about four to one. Should this trend continue, as suggested by the dashed lines of Figure II.3.C-4, the differences in small-scale roughness as a function of the broad terrain types seen from earth would vanish. To whatever extent the "photometric functions" of various parts of the moon are explainable by shadow content of sub-resolution craterlets, this trend would appear to be supported by the great similarities reported to exist between the marial and the continental photometric functions.

No work has been attempted, as yet, in the determination of size distributions for objects other than craters which may also contribute to small-scale roughness.

## D. IMPROVED MODELS AND MODEL PHOTOGRAPH

Models of the lunar surface were made at AED in 1961 (see ref. 1).* The ratio of maximum-primary to minimum-secondary crater and dome sizes which were dynamically meaningful were about 180 to 1. False droop appears to have cut the valid-count size ratio to about 50 to 1. In the same reference, it was seriously suggested that an increase in lunar rock strength in proportion to depth could account for known trends in crater proportions. It was also suggested that the subterfuge of a shallow layer of model "rock" material, backed-up by a hard container bottom, might be avoided if such a gradient could be duplicated in the model material. The goal of the present work in this area was to achieve larger model explosion craters having the proportions of a 35-km diameter lunar crater, hopefully increasing in size from about 3 centimeters to about 10 centimeters diameter, while employing a strength gradient such that the model depth from crater bottom to container bottom would be two or more times the crater depth. At the opposite extreme, it was hoped that model secondary craters and domes down to about 30 microns in diameter could be given dynamic meaning by decreasing the particle size of model material. Such a decrease is required if the higher model "rock" strength is to be achieved, as required by the parameters $S/g\rho d$, as the model primary diameter d is increased. Thus, an overall size ratio of dynamically-modeled features of 3000 to 1 might be achieved and, if an adequate camera were available, distribution counts, free of false droop, might cover a 700-to-1 size ratio or better.

Success in making a model crater 10.2 centimeters in diameter and 0.95 centimeters deep in a bed of model material about 3.5 centimeters deep was achieved. The crater bed was prepared by depositing 2 or 3 millimeters gradient depth at a time with a sifter and compacting it with a weighted roller, decreasing the roller weight in successive steps to the vanishing point for successive layers. No evaluation of the contact areas of the curved roller was attempted, but at least qualitative assurance of the significance of rock strength proportional to depth is indicated. The "explosion" energy was provided by bombarding the surface with a lightly compacted ball of the same material as the bed, about 3 centimeters in diameter, with a fall height of 2.5 meters. The material used was 5-micron aluminum oxide, and the bed was roughly square, 30 centimeters on a side. In addition to a central peak and well-proportioned rim, considerable debris was ejected, most of which struck the floor and walls of the room far outside the limits of the prepared model bed. Thus, the loss of potential secondary craters has been accentuated by the increase in modeled crater size. It is now clear why Wegener and Ley failed to attach significance to secondary formation in their experiments for generating models about this size. It would appear that the modeled trajectories of some of the flying fragments were dynamically equivalent to lunar ballistic trajectories almost circling the moon, if not actually escaping from it. Such far-flying debris from many such primary craters should produce a surface scattering of secondary craters at a concentration having less and less geographic variation for smaller and smaller craterlets. A very small amount of the model material became air-borne dust, lingering visibly for several seconds after the bombardment, and indicating that further reduction in grit size would be undesirable. A higher-density material might permit smaller grain size without floating dust, but only if tensile strength were also higher. Another minor disadvantage in generating larger and larger models is that the size of the pellet must increase more rapidly than the increase in size of the resulting crater. The exponent is about four to three.

---

* See page II.3-3.

One crude attempt to explode a paper cap resulted in a slow "fizz" and no disturbance of the bed. This should be kept in mind as a reminder that the two parameters, $S/g\rho d$ and $E/g\rho d^4$, cannot completely characterize the dynamics of crater modeling. The pulse shape of power versus time, characterizing the energy release, requires consideration.

Some skepticism regarding the evaluation of E as the air energy, rather than the KE of the pellet itself have been voiced; it is likely that a small part of KE contributes. If this were as much as one percent, it would increase E by an order of magnitude. As a further check, small craters were made in a shallow bed of SiC, using about 0.2-gram pellets of compacted SIC, of rubber, and of wood, at equal fall heights. The resulting craters were of the same size and shape, except for the central peak and for grooves cut by the bounce and roll of the stronger materials. This demonstrates that the contribution of the re-directed velocity of the crushed pellet after impact is not an essential element in the excavation of the model crater.

A major problem in making a complete and realistic model scene at this increased scale of about 10 cm = 35 km is the loss of potential secondary craters described earlier. At this scale, the diameter of a spherical moon would be ten meters, and the crude approximation of even a hemisphere of lunar area with radial gravity by a flat circular area 5000 km across, modeled in the laboratory scene by a circle of seven meter radius, would be a costly and questionable venture. . To account for the concentration of secondary craters, at even the center of such an area would require a concentration of primary craters matching those on the moon (several thousand within the seven-meter circle) plus additional primary craters of like concentration extending outside the circle to a greater and greater radius until no further debris were observed to fall near the center. The result might be a realistic distribution over one square meter at the center of such a fantastic model. Without such excess area, the number of dynamically meaningful secondary craters available for size classification would be too low by several orders of magnitude.

Thus, the goal of trying to extend valid concentrations of craterlets for size-distribution evaluation below several hundred meters is defeated unless the degree of interest is increased sufficiently to justify the considerable costs required to construct such a model. Furthermore there is no assurance that the results would be valid in view of the failure to duplicate a spherical gravitational field. It can only be hoped that the qualitative findings from smaller models and the observed concentrations of small lunar craters, augmented by the U.S.A.F. chart data, will prove sufficiently convincing that possibilities, other than the popular notion of smooth rolling maria, will be seriously considered.

If a revised goal of duplicating a prescribed distribution of primary and secondary craters can replace the former goal of establishing such a distribution by dynamically meaningful model work, then very simple techniques will suffice. One objective would be to study the photometric function for such a prescribed surface. Another would be to provide slides for studying the performance of TV systems such that the detail in the slides would provide a size spectrum extending from well above to well below the resolution limits. Automatic classification of the roughness features derived from thousands of future moon pictures, taken from an orbiter, could be developed well in advance of launch date. This could be done by correlating brightness versus percent area of video images and their equivalents made with differentiated video signals, by video brightness contours, or by the autocorrelations of video signals against scenes of known distributions of craterlets, boulders, domes, and cracks at various illumination angles, using materials of known normal albedo.

A subterfuge for making such models was found by using a sifter to lay down successive layers for the simulated strength gradient described above. After sifting new material onto the surface and before rolling, the surface was found to be very rough on a small scale. It was also found that when the sifter was held a few inches above the surface a pattern of overlapping "domes" of random size was produced. When the fall distance was increased to a foot or two, a pattern of overlapping craterlets resulted. A wide variety of surfaces could be produced with low or high concentrations of of domes, craters, or both, depending on fall height and amount of material deposited by the sifter. Continued deposition would soon saturate the surface so that earlier formations were destroyed or buried at a rate equal to that at which new surface formations appeared. When such a rain of particle aggregates was allowed to fall on a fresh three-inch, primary crater of sharp outline, the appearance quickly softened to produce a startling likeness to an old, eroded lunar crater such as Albategnius. It would appear that such a rain from the sifter can simulate the ejecta from many widely dispersed primaries, except that all impacts have zero-incidence angle. While incidence angle is unimportant in the formation of impact explosion craters on the moon, it would be of some importance in secondary crater formation. Even grooves can be seen on many parts of the moon, presumably from nearly horizontal incidence of such ejecta.

Photographs were taken of one such scene, described in detail in paragraph E of this section. The slope of a log N versus log x graph was found to be minus 2.7, and the appearance was again reminiscent of Minnaert's superimposed and juxtaposed holes of all sizes.

## E. PHOTOMETRIC FUNCTIONS OF MOON AND MODELS

Preliminary experiments sufficient to clarify procedures that might be employed in photometric studies of table-top models were just getting under way at the termination of the LOC Phase II contract. This included crude determinations of the luminance of flattened surfaces of various powders by photographing them together with a crude reflecting grey scale of nine steps. These steps consisted of mat surface cards darkened to match the nine steps of a reflectance scale, published in high gloss by Eastman Kodak. It was later learned that the "reflectance densities" of the Eastman scale are based on normal observation and 45° illumination which approximates average conditions under which photographic prints are viewed. Consequently, the "normal albedo" values determined for the materials tested could be too low by as much as 29 percent. The uniformity of the illumination was poor, with one eccentric hot-spot bright enough to produce a similar error in the opposite direction. The camera used was the same as that for the early models, so that statistical descriptions of the surfaces were still resolution-limited and could not take advantage of the fine surface structure made possible by the use of 5-micron $Al_2O_3$. This material was far too bright, and attempts to cut the "normal albedo" of the flattened material, by blending it with powdered charcoal, were accompanied by loss of material density and strength properties, necessary to form four-inch diameter primary craters. The mixture proved so dusty that microstructure was destroyed as the dust settled.

Portland cement powder, much darker than $Al_2O_3$, was then tried again; it was found that a "normal albedo" of about 0.07 was obtained when 80 percent by volume of cement and 20 percent by volume of charcoal were blended, with fair mechanical properties retained. A "normal albedo" of about 0.11 was found for the 20-micron SiC used in the 1961 model experiments. This material might be useful in superimposing "bright rays" on a marial scene of the darker mixed material. These albedo estimates are still subject to the uncertainties given above. Moreover, no such thing as a combination of $i = 0$ and $\epsilon = 0$ (that is, both normal incidence and normal camera axis) could be achieved without an "eclipse" of lamp by camera or vice versa. Actually, a value of $\epsilon = 0$ for the camera axis, and $i = 15°$ for the cone of light axis was the closest approach to the condition defining normal albedo. One-third of the scene was eclipsed at this condition. This could be reduced to about 4° with a camera of sufficient resolution to justify an altitude of six or eight feet.

It was decided that reflectance standards could be improved by comparing cards at various angles of illumination and observing them with a magnesia block. One large card could then be used to establish the variations in illumination by recording on films, first, the illuminated card, and then the scene, with no change in position of lamp and camera. A "Spectra" photometer already available was found excellent for comparing the magnesia block with various cards. The following purchases were recommended (but never purchased) for the continuance of the photometry of lunar models:

(1) A 4 x 4" Linhof Super Technika IV Camera with anatomic grip, Xenotar 150 mm f/2.8 lens

(2) A 2-1/4 x 3-1/4 ground-glass, spring-back adapter

(3) A polarizing slip-on filter, 80 mm suitable for Xenotar 150 mm lens

(4) A 240 mm f/5.6 lens

(5) A junior Solarspot, Mole-Richardson Type 412, with low pedestal, Type 1411

Without such equipment available, and fearing that the whole point of this work might be lost, an attempt was made to estimate the values of $\phi$ for five simulated elevations of the sun, (90° - i), at camera axis $\epsilon = 0$, using the available camera and crude spotlight. This brief effort included the taking of five pictures and measuring the integrated transmittances of the negatives for various spot sizes. A compromise was chosen between the published D-log E curve for the film and its processing, and the homemade gray-scale cards, all but the three brightest of which were placed adjacent to the model scene before shooting. It was established by counting that the distribution of craterlets was essentially that of the real moon, including the extrapolation given in Figure II.3.C-2. Of the sun-angles simulated, the optimum condition for counting was the "sun elevation" angle of 31.2 degrees. At higher angles, the shadow content of craterlet bottoms decreased rapidly, while at lower sun elevations many of the smallest craterlets were lost in shadow below the rims of larger craterlets. Brightnesses were normalized with respect to the values for the scene materials in flattened piles at highest sun elevation, assuming that the "ray" material dominated less than 2 percent of the area where transmittances were measured. The smallest spot size was approximately 0.1 mm in diameter on the negative or 0.25 mm on the scene, simulating an 80-meter circle on a lunar surface of comparable roughness. At this spot-size, the calibration of the photometer was seriously upset by the small homemade aperture characteristics, and a special

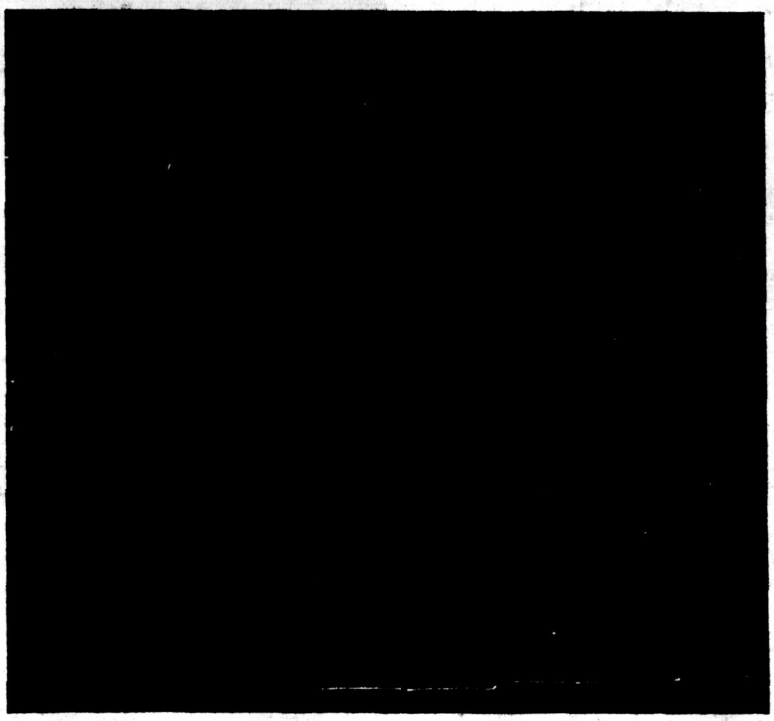

Figure II.3.E-1. Photometry of Lunar Model, Light 8.6 Degrees Above Horizon

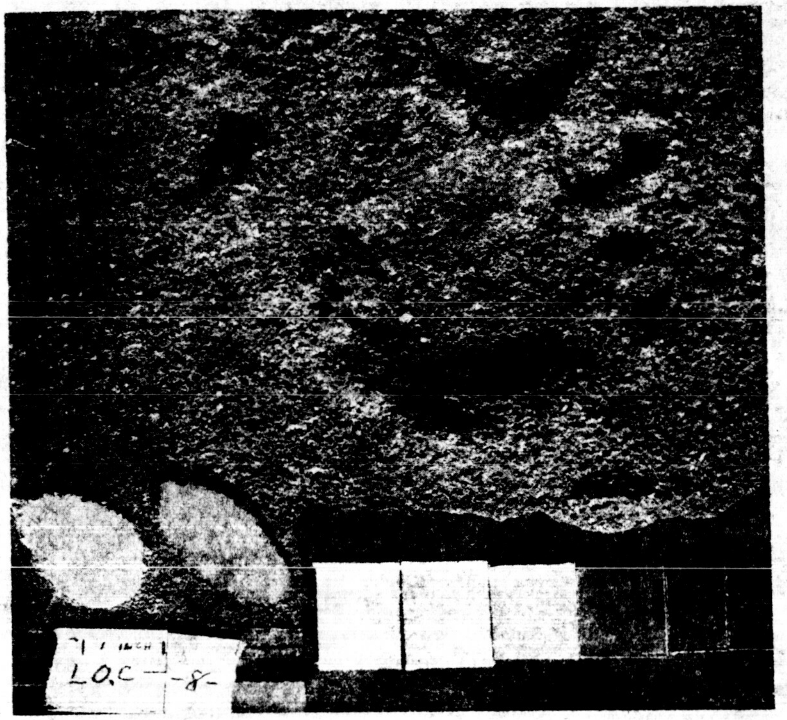

Figure II.3.E-2. Photometry of Lunar Model, Light 31.2 Degrees Above Horizon

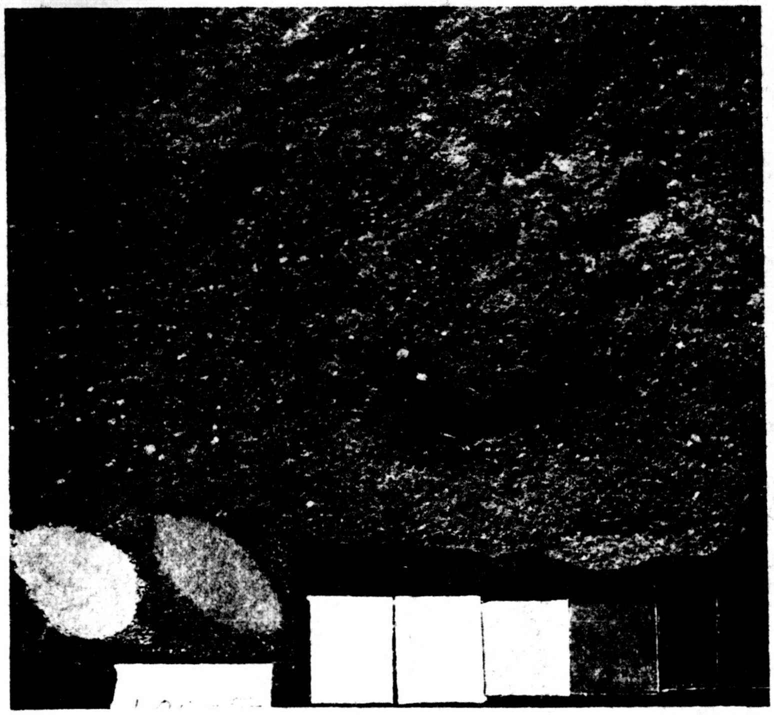

Figure II.3.E-3. Photometry of Lunar Model, Light 40.4 Degrees Above Horizon

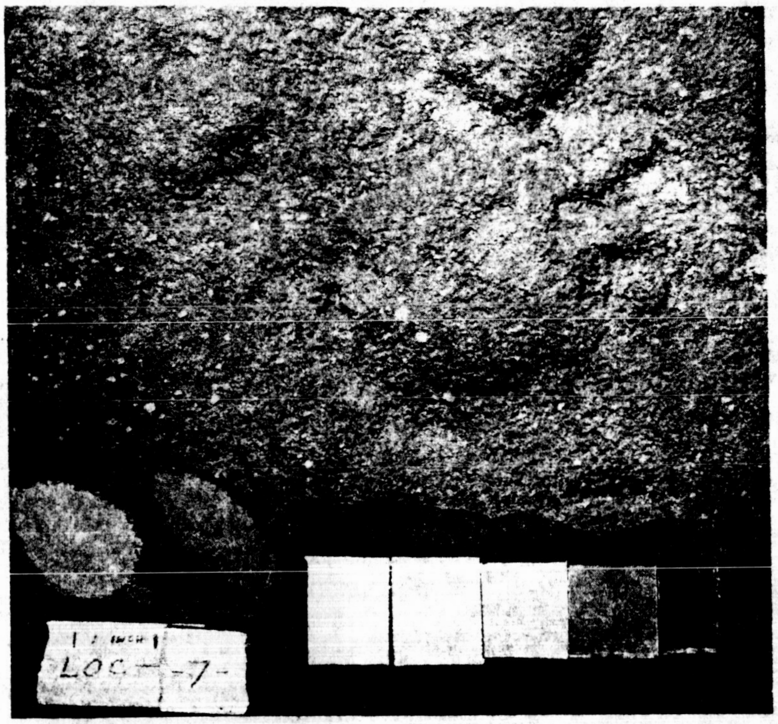

Figure II.3.E-4. Photometry of Lunar Model, Light 63.6 Degrees Above Horizon

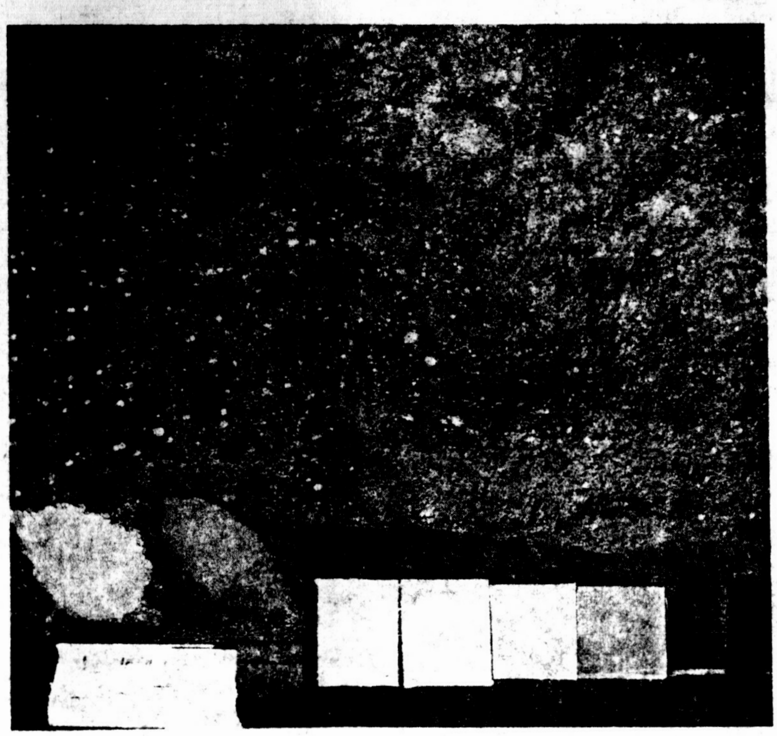

Figure II.3.E-5. Photometry of Lunar Model, Light 74.8 Degrees Above Horizon

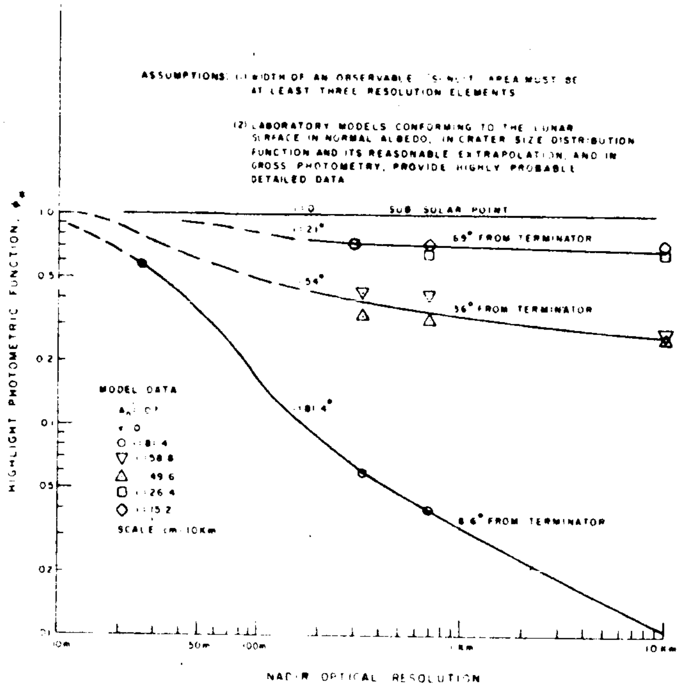

Figure II.3.E-6. Influence of Resolutions on Lunar Photometry

correction curve was applied, based on a calibration of the transmittance readings of the photometer with this orifice against a set of Wratten neutral density filters.

All five pictures were made with identical camera aperture, exposure time, and processing. According to the photometric function of this scene at coarsest resolution, Figure II.3.E-1 should have required, by "smooth moon" design standards, 175 times the exposure actually used. Yet it is obvious that the variations in grey levels contained within the small illuminated portions of this scene would have been totally washed out by such exposure.

It is suggested that a TV system designed to measure lunar roughness from an orbiter or impacter should be based on not less than 500 foot-lamberts average scene luminance whether the accent is on maria near the terminator or not, though further tests with refined equipment and with several values of the observation angle $\epsilon$ other than zero are badly needed.

Table II.3.E-1 shows the values of $\phi$ derived from these negatives as a function of sun elevation and optical resolution, assumed to be one-third the diameter of the integrated photometry spot. This value was converted to lunar equivalent meters by assigning to the model a scale which harmonized the crater distributions of moon and model. The results show clearly that the use of the lunar photometric function, as observed from earth, in designing a camera system for a spacecraft close to the moon, will lead to extreme overexposure, except for the unlikely condition that the real histogram of the lunar crater distribution is truncated precisely at the place where optical resolution

Table II.3.E-1. PHOTOMETRY OF LUNAR MODEL

| Sun Elevation (degrees) | Average $\phi$ (light and shadow in 10 km diameter spot) | Sunlit $\phi$ (areas containing no black shadow which would be discernible at stated R = one-third simulated spot diameter, meters) | | |
|---|---|---|---|---|
| | | R = 700 meters | R = 330 meters | R = 27 meters |
| 74.8 | 0.72 | 0.72 | 0.72 | - |
| 63.6 | 0.65 | 0.65 | 0.72 | - |
| 40.4 | 0.26 | 0.32 | 0.33 | - |
| 31.2 | 0.27 | 0.42 | 0.43 | - |
| 8.6 | 0.01 | 0.04 | 0.06 | 0.59 |

must truncate the observed histogram. Such over-exposure at low sun elevations will not completely destroy the value of pictures, but will produce over-size, washed-out, white-sun-lit areas against shrunken jet-black shadows. Exposures reduced by an order of magnitude would reveal variations in gray within the small sunlit areas. Such over-exposure can cause resolution deterioration by aggravating the lateral leakage of both light and charge in the vidicon's photoconductive layer.

The value $\phi = 0.59$ at highest resolution, and lowest sun elevation of 8.6° (or $i = 81.4°$) is higher by far than for a flat Lambertian surface; this suggests an approximate Lambertian reflector at $i = 53.8$ degrees, having an average brightness slope of about 27.6 degrees. This is not unreasonable as representing an average, for a nadir view, of the brow of a hill sloping away from the sun by 8.6 degrees at the edge of one shadow, decreasing to zero slope at highest elevation, and then plunging to a slope of 55 degrees on the sunny side of the hill at the point where the next shadow begins. Slopes of 50 to 60 degrees are common in sections of the model and on the real moon as well. It may be significant that Minnaert still clings to the view that the photometric function of the moon will ultimately be accounted for by the slopes and shadow content in scenes of essentially Lambertian materials (Ref. 6).

Figure II.3.E-6 shows a plot portraying smoothed estimates of the influence of resolution on the photometric function of the lunar surface highlights. It must be remembered that, for a lunar impacter, such as RA6-9, the high contrast between sunlit highlights and shadow areas at ever decreasing sun elevation is offset by the increasing odds that the last few pictures may see only a field in full shadow. Thus, an impacter destined for a point less than 30 degrees from the terminator has a risk of wasting the last

---

(6) Planets and Satellites, ed. by G.P. Kuiper and B.M. Middlehurst, Chapter 6, Photometry of the Moon, by M. Minnaert.

RE-ORDER No. 62-489

two or three frames, even in a purely marial zone, if the continuum of craterlets found in the models is a faithful portrayal of real maria. For an orbiter mission, this danger is readily eliminated by choosing an inclined orbit.

Because of the point scatter in Table II.3.E-1, the combined data for solar elevations of 74.8 and 63.6 degrees (Figure II.3.E-6) have been lumped together on one line labeled i = 21 degrees. Similarly, combined data for solar elevations of 40.4° and 31.2° are averaged as 36 degrees, labeled i = 54 degrees.

# Section 4
# GROWTH POTENTIAL

## A. ADVANCED SENSORS

### 1. VIDICON SENSOR PERFORMANCE

In considering advanced sensors, the performance of the standard vidicon sensor will be discussed first. This will enable the performance level, obtained from the advanced sensors studied, to be compared with that of the vidicon.

The characteristic curve of a typical RCA 4431 vidicon is shown in Figure II.4.A-1. A tabulation of signal-to-noise ratios is given in Table II.4.A-1, for various values of exposure. The aperture characteristic is given in Figure II.4.A-2. The response at 650 lines is -17 db, and this number will be used for determining the resolution element.

For a picture height of 11 mm, the resolution element will be

$$\frac{11}{650} = 0.0173, \text{ which is } 17 \times 10^{-6} \text{ meters.} \qquad (1)$$

The magnification for a 5-meter object will then be:

$$\frac{17}{5} \times 10^{-6} = 3.40 \times 10^{-6} \qquad (2)$$

The focal length required to give this magnification at 100 km altitude will be given by:

$$\begin{aligned} f &= 100 \times 3.40 \times 10^{-6} \text{ km} \qquad (3) \\ &= 340 \times 10^{-6} \text{ km} \\ &= 340 \text{ mm} \\ &= 13.4 \text{ inches} \end{aligned}$$

A lens aperture of f/1.5 is considered to be practical; the diameter of its aperture would be nine inches approximately. The transmittance will be assumed to be 0.6.

The photometry of the vidicon system can now be calculated.

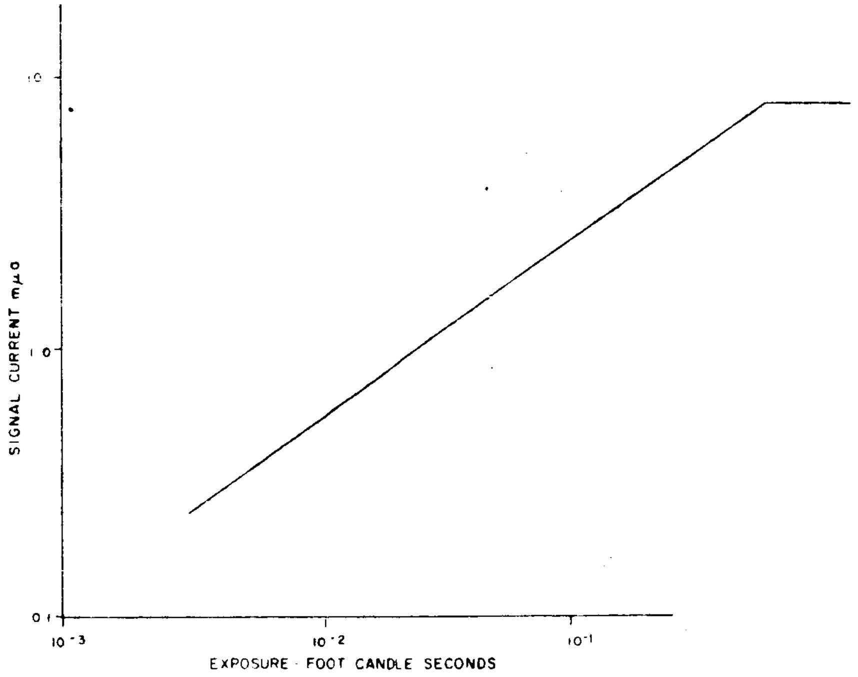

Figure II. 4. A-1. Typical Characteristic Curve for RCA Type 4431 Vidicon

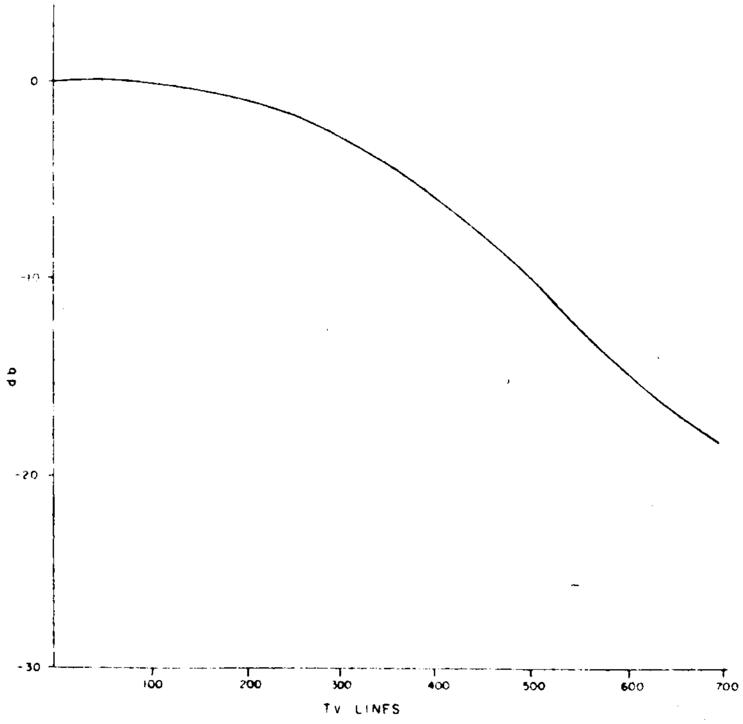

Figure II. 4. A-2. Typical Aperture Characteristic Curve for RCA Type 4431 Vidicon

## TABLE II. 4. A-1

## SIGNAL-TO-NOISE RATIOS FOR TYPE 4431 VIDICON

| Exposure ft-candle/sec | Signal $m\mu a$ (peak) | Noise $m\mu a$ (rms) | Signal-to-Noise Ratio db |
|---|---|---|---|
| 0.003 | 0.24 | 0.04 | 16 |
| 0.0075 | 0.43 | 0.04 | 20.5 |
| 0.01 | 0.55 | 0.04 | 23 |
| 0.02 | 0.83 | 0.04 | 26 |
| 0.03 | 1.10 | 0.04 | 29 |
| 0.04 | 1.40 | 0.04 | 31 |
| 0.05 | 1.70 | 0.04 | 32.5 |
| 0.06 | 1.80 | 0.04 | 33 |
| 0.07 | 2.0 | 0.04 | 34 |
| 0.08 | 2.2 | 0.04 | 34.9 |
| 0.09 | 2.4 | 0.04 | 35.5 |
| 0.10 | 2.5 | 0.04 | 35.5 |
| 0.20 | 4.0 | 0.04 | 40 |
| 0.30 | 5.4 | 0.04 | 42.5 |
| 0.40 | 6.8 | 0.04 | 44.5 |

The illuminance on the target will be:

$$E = \frac{0.6\,B}{4\,(f\#)^2} = \frac{0.6\,B}{4\,(1.5)^2} = \frac{2}{3} \times 10^{-1}\,B \tag{4}$$

where: B is the luminance of the object in foot-lamberts.

The exposure time T is determined from the relation

$$\frac{1}{2}\,\Delta = VT \tag{5}$$

where: $\Delta$ is the dimension of the resolution element referred to as the lunar surface, and V is the spacecraft velocity. The equation expresses the fact that the motion smear is half the element size.

Substituting $\Delta = 5$ m and $V = 1500$ m/sec ,

then: $$T = \frac{\Delta}{2\ V} = \frac{5}{3} \times 10^{-3} \text{ sec} = 1.67 \text{ msec} \tag{6}$$

The exposure is then given by:

$$Ex = 1.67 \times 10^{-3} \tag{7}$$

$$E = \frac{1}{9} \times 10^{-3}\ B \text{ ft-candles/sec} \tag{8}$$

The average luminance of the lunar surface is given by:

$$B = I_s\ a_n\ \phi_g \tag{9}$$

where: $I_s$ (= 14,000 lumens/ft$^2$) is the solar constant, $a_n$ is the normal albedo, and $\phi_g$ is the photometric functions.

Table II.4.A-2 shows a tabulation of scene luminance, exposure, signal-to-noise ratio, the product $a_n\ \phi_g$, and the values of $\phi_g$ for two values of albedo. These quantities are tabulated for several values of scene luminance. The values of $\phi_g$ in the last two columns represent how close to the terminator a picture of the given S/N ratio can be obtained. The conversion to terminator angle can be made based on the fact that $\phi_g = 8 \times 10^{-2}$ at 10° from the terminator, and decreases approximately linearly with angle as the terminator is approached. Thus, for example, a 20.5 db picture can be obtained at an albedo of 0.06, 10° from the terminator; or a 16 db picture, 4° from the terminator at 0.06 albedo.

The vidicon performs marginally within 10° of the terminator, except for the higher albedos. It has the advantage of simplicity and proven operation in space environment. If its limitations can be accepted, it would provide a reliable system with ready availability. Some preliminary studies of other sensors (or sensor assemblies), which are either of the vidicon type, or which include an image intensifier, have been made. These studies have included the selenium surface vidicon, the standard vidicon with image intensifier, and the multiple vidicon. These studies have indicated that (1) the selenium vidicon has more sensitivity (by a factor of about 4) but has a short shelf and operating life as the amorphous selenium surface changes spontaneously to crystalline form in a period of about one month; (2) the loss of resolution due to the intensifier seriously curtails the performance of the overall system; and (3) the multiple vidicon, still in development, which has problems with multiplier surfaces that do not work well in the absence of cesium (whose presence is poisonous to the photoconductor). Based upon a more favorable result with further development, this latter approach would seem, potentially, to offer many advantages.

## TABLE II. 4. A-2

### VIDICON TYPE 4431 CHARACTERISTICS (WITH F/1.5 LENS AND 1.67 MSEC EXPOSURE TIME)

| Scene Luminance B ft.- lamb. | Exposure $E_x$ ft-candles/sec | SNR DB | $a_n \phi_g$ B/14000 | $\phi_g$ for Albedo of | |
|---|---|---|---|---|---|
| | | | | 0.06 | 0.18 |
| 27 | $3.0 \times 10^{-3}$ | 16 | $1.92 \times 10^{-3}$ | $3.2 \times 10^{-2}$ | $1.1 \times 10^{-2}$ |
| 67 | $7.5 \times 10^{-3}$ | 20.5 | $4.78 \times 10^{-3}$ | *$8.0 \times 10^{-2}$ | $2.7 \times 10^{-2}$ |
| 90 | $10.0 \times 10^{-3}$ | 23 | $6.42 \times 10^{-3}$ | $10.7 \times 10^{-2}$ | $3.6 \times 10^{-2}$ |
| 180 | $20.0 \times 10^{-3}$ | 26 | $12.8 \times 10^{-3}$ | $21.3 \times 10^{-2}$ | $7.1 \times 10^{-2}$ |
| 270 | $30.0 \times 10^{-3}$ | 29 | $19.3 \times 10^{-3}$ | $32.2 \times 10^{-2}$ | $10.7 \times 10^{-2}$ |
| 360 | $40.0 \times 10^{-3}$ | 31 | $25.7 \times 10^{-3}$ | $42.8 \times 10^{-2}$ | $14.2 \times 10^{-2}$ |
| 450 | $50.0 \times 10^{-3}$ | 32.5 | $32.1 \times 10^{-3}$ | $53.4 \times 10^{-2}$ | $17.8 \times 10^{-2}$ |
| 900 | $100.0 \times 10^{-3}$ | 35.5 | $64.3 \times 10^{-3}$ | - | $35.7 \times 10^{-2}$ |
| 1800 | $200.0 \times 10^{-3}$ | 40 | $128 \times 10^{-3}$ | - | $71.0 \times 10^{-2}$ |

*Permits working within 10° of the terminator at a SNR of 20.5 db

## 2. IMAGE ORTHICON

The image orthicon is widely used for television studio equipment. At high scene luminance, it is surpassed by the vidicon in signal-to-noise ratio. However, if the scene illumination is reduced to a level for the vidicon that will make its signal-to-noise ratio equal to the value obtained at a given illumination with the image orthicon, the scene illumination required for the vidicon is about 100 to 200 times the value required for the image orthicon. In other words, the image orthicon is more sensitive than the vidicon.

The sensitivities of typical image orthicons are shown in Table II. 4. A-3, which also shows, for comparison, the sensitivity of a type 4401 vidicon at two values of signal-to-noise ratio. The figures on image orthicons are taken from available tube manual and application note sources. It must be emphasized that the sensitivities quoted from these sources are in foot-candles, upon the assumption that the tube will be used in circuits operated on EIA standards as used in TV broadcasting. These standards provide for 525-line interlaced scanning, with a 30-cps field rate. The sensitivities shown in the column "Sensitivity ft-candles/sec" of Table II. 4. A-3 are derived on the assumption that the frame interval of $\frac{1}{30}$ second is the integration period.

Signal-to-noise ratios shown are the best which can be obtained with the tube, and correspond to the illuminance or exposure shown under the column headed "Sensitivity", which in turn represents operation in the vicinity of the knee of the characteristic curve of illuminance versus signal current output. Typical characteristic curves are shown in Figures II. 4. A-3 and II. 4. A-4, which correspond to RCA image orthicon types 7513 and 7198, respectively. It will be noted that the former tube exhibits a sharp knee at an illuminance of 3 x $10^{-2}$ ft-candles; the latter has no well defined knee, but rather a gradual curvature.

TABLE II. 4. A-3

COMPARATIVE SENSITIVITIES OF IMAGE ORTHICONS

| Tube Type | Sensitivity<br>Illuminance (ft-candles) | <br>Exposure ft-candles/sec | Highlight SNR (db) |
|---|---|---|---|
| RCA 4401 | 1.0 x $10^{-2}$ | 3.3 x $10^{-4}$ | 33 |
| 5820 | 2.0 x $10^{-2}$ | 6.7 x $10^{-4}$ | 32 |
| 7198 | .4 x $10^{-2}$ | 1.3 x $10^{-4}$ | 26 |
| 7295A | 1.5 x $10^{-2}$ | 5.0 x $10^{-4}$ | 36 |
| 7389 | 2.0 x $10^{-2}$ | 6.7 x $10^{-4}$ | 39 |
| 7513 | 3.0 x $10^{-2}$ | 10.0 x $10^{-4}$ | 35 |
| For comparison the type 4431 vidicon has the following sensitivity | | | |
| RCA 4431 | | 6.0 x $10^{-2}$ | 33 |
| | | 2.0 x $10^{-2}$ | 26 |

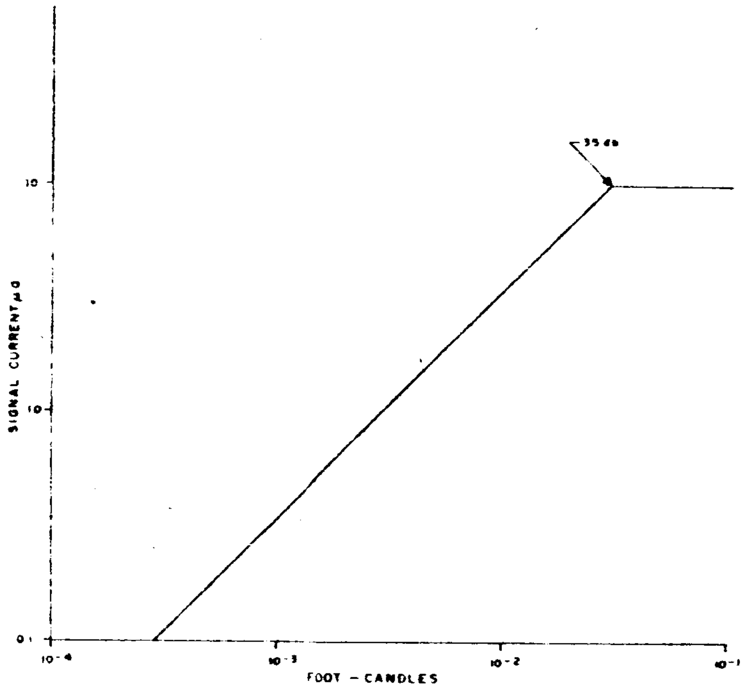

Figure II. 4. A-3. Typical Characteristic Curve for RCA Type 7513 Image Orthicon

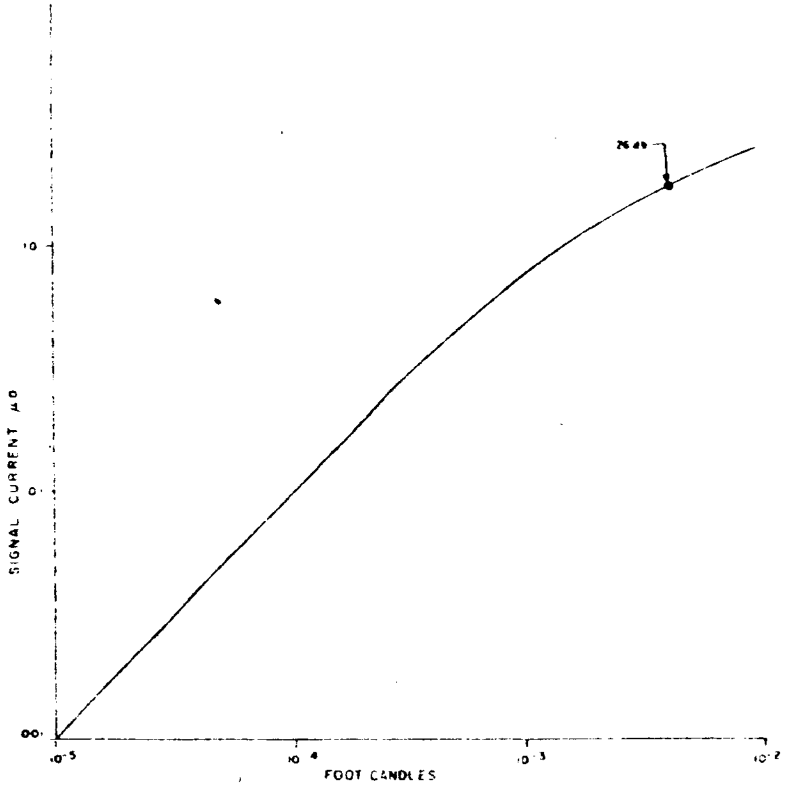

Figure II. 4. A-4. Typical Characteristic Curve for RCA Type 7198 Image Orthicon

Type 7198 image orthicon has been ruggedized so that it is suitable for use under adverse environmental conditions. Sample lots of these tubes are tested under conditions similar to those described in MIL-E-5272A for vibration, shock, and temperature-humidity. This tube will, therefore, represent a suitable choice for the service under consideration. The aperture characteristic for the type 7198 tube is shown in Figure II. 4. A-5. Since in previous consideration of vidicon selection it has been considered that the -17db point on the aperture characteristic represented the line number corresponding to element size, the same assumption will be made for the image orthicon. This would put the element size at the corresponding number of 540 lines, as can be seen in Figure II. 4. A-5.

For a square aspect ratio the picture height on the photo-cathode is 32 mm. Thus, the resolvable element is:

$$\frac{32}{540}\ \text{mm} = 59.2 \times 10^{-6}\ \text{meters.} \qquad (10)$$

Accordingly, the magnification required for a 5-meter object will be:

$$\frac{59.2}{5} \times 10^{-6} = 11.8 \times 10^{-6} \qquad (11)$$

Thus, at 100 km altitude, the required focal length will be

$$\begin{aligned} f &= 100 \times 11.8 \times 10^{-6} \qquad (12) \\ &= 1180\ \text{mm} \\ &= 46\ \text{inches} \end{aligned}$$

It will be considered that a 9-inch aperture will be the largest that is practical to install; thus the lens aperture will be approximately f/5. It will be assumed that the lens has a transmission of 0.6.

It is now possible to calculate the photometry of the image orthicon system. The illuminance on the photocathode will be given by

$$E = \frac{0.6\ B}{4\ (f\#)^2} = \frac{0.6\ B}{4\ (5)^2} = 6 \times 10^{-3}\ B, \qquad (13)$$

where B is the illuminance of the object in foot-lamberts.

The exposure time T is determined by the consideration that the spacecraft shall not travel a sufficient distance to smear the resolution element objectionably. For purposes of this analysis, it will be assumed, as before, that it will be satisfactory to travel $\frac{1}{2}$ a resolution unit during the exposure time. This leads to the relation

$$\frac{1}{2}\,\Delta = VT, \qquad (14)$$

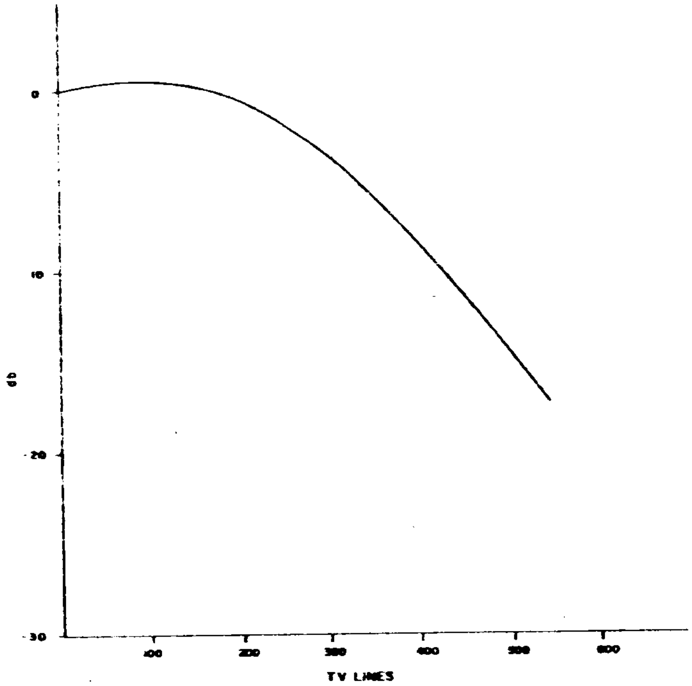

Figure II. 4. A–5. Typical Aperture Characteristic Curve for RCA Type 7198 Image Orthicon

where: $\Delta$ is the resolution element and V is the satellite velocity. Substituting: $\Delta$ = 5 meters and $\bar{V}$ = 1500 meters/sec

$$T = \frac{\Delta}{2\bar{V}} = \frac{5}{3} \times 10^{-3} \text{ sec} = 1.67 \text{ milliseconds} \tag{15}$$

The exposure is given by:

$$E_x = 1.67 \times 10^{-3} \; E = 10^{-5} \; B \text{ foot-candle-seconds} \tag{16}$$

The average luminance of the lunar surface is given by:

$$B = I_s \, a_n \, \phi_g \, , \tag{17}$$

where: $I_s$ is the solar constant (or illuminance provided by the sun at the lunar surface) measured in lumens per square foot; $a_n$ is the normal albedo; and $\phi_g$ is the photometric function.

RE-ORDER No. 62-459

Table II.4.A-4 shows the results of calculating the exposure for several values of scene luminance. The corresponding values of signal-to-noise ratio, obtained from published data for the type 7198 image orthicon, are listed in this table. Values of the product $a_n \phi_g$ are also listed in Table II.4.A-4, based on the equation:

$$a_n \phi_g = \frac{B}{I_s} = \frac{B}{14000} \tag{18}$$

For two values of $a_n$, the corresponding values of $\phi_g$ are derived. In effect, these values represent how close to the terminator the camera can give pictures of the indicated signal-to-noise ratio. The angular distance from the terminator can be estimated by using the fact that $\phi_g = 8 \times 10^{-2}$ at 10° from the terminator, and decreases linearly with the angle.

It can be seen that the image orthicon will provide a 26 db signal-to-noise ratio at about 2° from the terminator, with an albedo of 0.06. Lower signal-to-noise ratio values, or higher albedo values, will permit working even closer to the terminator. So far as performance is concerned, it would appear to be satisfactory, covering a field of 2.7 x 2.7 km with each frame.

The image orthicon tube has some disadvantages. It is more complex than a vidicon, and requires more controls, some of which are critical if best performance is to be obtained. However, RCA has built large numbers of this tube type, and considerable quantities of camera equipment using it. The tube is large (3" diameter and 15-1/2 inches long) and requires a large and heavy focus-deflection coil assembly, weighing about 15 pounds. This weight could be reduced, perhaps by five pounds or more, by using aluminum wire. The photocathode is large, requiring a picture of 1.8 inches diagonal (46 mm) to fill it, and the resolution in TV lines per picture height is somewhat lower than that of a vidicon. These two factors cause the focal length of the lens to be increased by a factor of about 3.5 times over that required for the vidicon, so that the lens may be larger and heavier. In the analysis given, the lens aperture was kept small (f/5) to keep the dimensions within reasonable bounds, and some of the sensitivity of the tube was sacrificed to permit this. The tube has a critical requirement on both temperatures and temperature gradients for satisfactory operation. In ground service, this is taken care of by blowers and heaters operating in conjunction with thermostats. With no air available in lunar service, maintaining the proper temperature may present a problem. Finally, there are restrictions in the operating attitude to prevent loose particles (which cannot be completely eliminated in manufacture) from falling on the target. This may be a problem, though the tube will be weightless while in orbit and this may alleviate the problem somewhat. When operated on the ground, it is recommended that the axis, when the base is up, should never be less than 20° from the vertical.

It would appear that, though this tube will provide high performance, there will be some packaging and operational problems to be solved. It is not thought that the problems posed are insurmountable, but it is essential to recognize their existence.

## TABLE II. 4. A-4

## IMAGE ORTHICON TYPE 7198 CHARACTERISTICS
(With f/5 Lens and 1.67 msec Exposure Time)

| Scene Luminance B (ft-lamb.) | Exposure $E_x$ (ft-candles/sec) | SNR (db) | $a_n \phi_g$ (B/14,000) | $\phi_g$ for Albedo of | |
|---|---|---|---|---|---|
| | | | | 0.06 | 0.18 |
| 3.3 | $33 \times 10^{-6}$ | 16 | $2.35 \times 10^{-4}$ | $0.39 \times 10^{-2}$ | $0.13 \times 10^{-2}$ |
| 10 | $100 \times 10^{-6}$ | 20 | $7.14 \times 10^{-4}$ | $1.19 \times 10^{-2}$ | $0.40 \times 10^{-2}$ |
| 13 | $130 \times 10^{-6}$ | 26 | $9.28 \times 10^{-4}$ | [*]$1.54 \times 10^{-2}$ | $0.52 \times 10^{-2}$ |

[*] Permits working within 2° of the terminator at SNR of 26 db

### 3. DIELECTRIC TAPE CAMERA

### a. General Description

RCA has developed a television camera based upon the principle of storing the visual image produced by a lens on a thin dielectric film by means of electrostatic charges whose amounts represent, at each image element, the corresponding illumination intensity incident upon the dielectric film. This film, together with a photoconductive film and a conductive gold film, is supported by a base material such as Cronar. The assembly comprises a tape which, upon exposure to an image in a suitable camera, is charged electrostatically as desired. The tape bears similarity to photographic film, except that the image is stored by electrostatic charges rather than by chemical changes. It may be manufactured in widths such as are used for photographic motion picture film. A cross-section of the tape is shown in Figure II. 4. A-6.

The image stored on the tape can only be recreated by electronic means, specifically by scanning with an electronic beam to produce a television signal. In this respect, it acts like the storage target of a television camera tube, only differing basically in that it is not an integral part of the tube. The quality of the stored image has been found to be equivalent to that of good photographic film, namely 80 lines per millimeter or better[*]. The image does not fade appreciably with time[**], and is not erased by the scanning process.

---

[*] This refers to the quality obtained in the readout process. Tests have shown that the quality of the charge image exceed 200 TV lines per millimeter.

[**] Exposed tape has been stored for a week without appreciable loss of image charge or degradation of image quality. Sealed-off tubes, containing the equivalent of dielectric tape, have been stored for a month without loss of image quality.

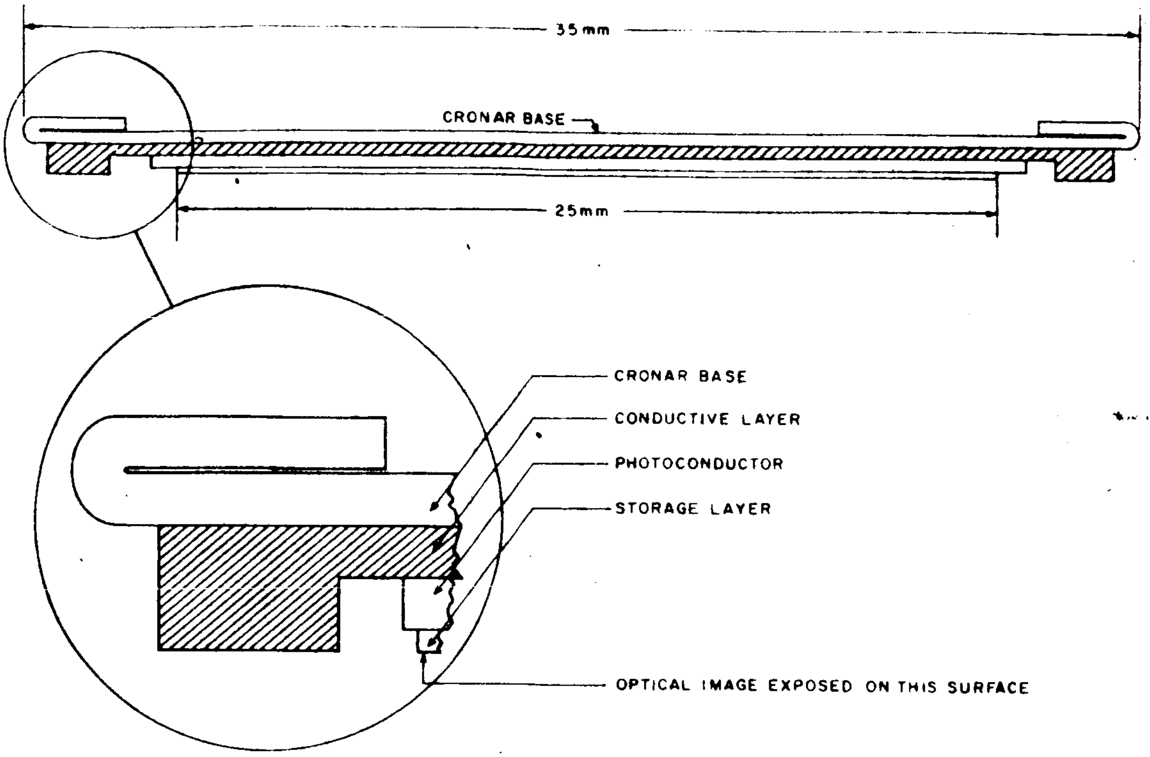

Figure II. 4. A-6. Dielectric Tape Cross-Sectional View

The dielectric tape must be prepared before exposure by placing a charge across the dielectric film. This operation will also erase any charges remaining from a previous exposure. During exposure, the outer surface of the dielectric film must be held at a fixed potential, while the charge on the dielectric film is dissipated through the conductivity induced in the photoconduction layer by exposure to image light. Naturally, the extent of discharge depends upon the exposure time and the image intensity at a given point.

The surface preparation is accomplished by flooding it with electrons from an electron gun called the "erase-prepare gun" (or "prepare gun" for brevity); simultaneously, it is illuminated from a suitable light source to place the photoconductor in a conducting condition. During the exposure phase, the outer surface is held at a constant potential by similarly bombarding it with electrons from an electron gun called the "write gun". These two guns, the prepare gun and the write gun, are flood guns, each producing a relatively broad beam of electrons, rather than a focused beam. Also, because of the fact that the beams are broad enough to cover the width of the tape, no scanning is required.

The dielectric tape now carries an array of charges representing the image. If the tape is scanned by a focused beam obtained from a third electron gun, called the "read gun", a television signal can be produced. The beam provided by this gun may be scanned along a single line by a single pair of deflection coils, in which case the scanning in the other direction is provided by moving the tape at a uniform rate. Alternatively, the tape may be held stationary in a gate (as in a movie camera) while it is scanned in the usual fashion, by the use of two pairs of orthogonally-arranged deflection coils.

Because all of the tape operations described require the use of electron beams, it is obvious that the tape and the guns must be under vacuum. To this end, the tape reels, tape transport mechanism, prepare gun, write gun, and the read gun are all enclosed in a vacuum chamber. The image is projected onto the tape by means of a lens placed internal to the chamber, the light rays passing through a vacuum-tight window. The general arrangement is shown in Figure II. 4. A-7. The drive motor for the tape transport (or at least its stator) may be placed outside the chamber if desired. The deflection coils and all supply voltages, suitably time-sequenced, are fed from an external electronic unit.

### b. Description of Proposed Camera

So far as the recording section of the camera is concerned, the tape will move continuously past a recording slit which is placed perpendicular to the tape. The tape is moved along its length at a velocity equivalent in direction and magnitude to the motion of the image formed by the camera lens. The image of a given point on the lunar surface moves in the plane determined instantaneously by the velocity vector and the point in question. This plane intersects the focal plane of the lens in a line which

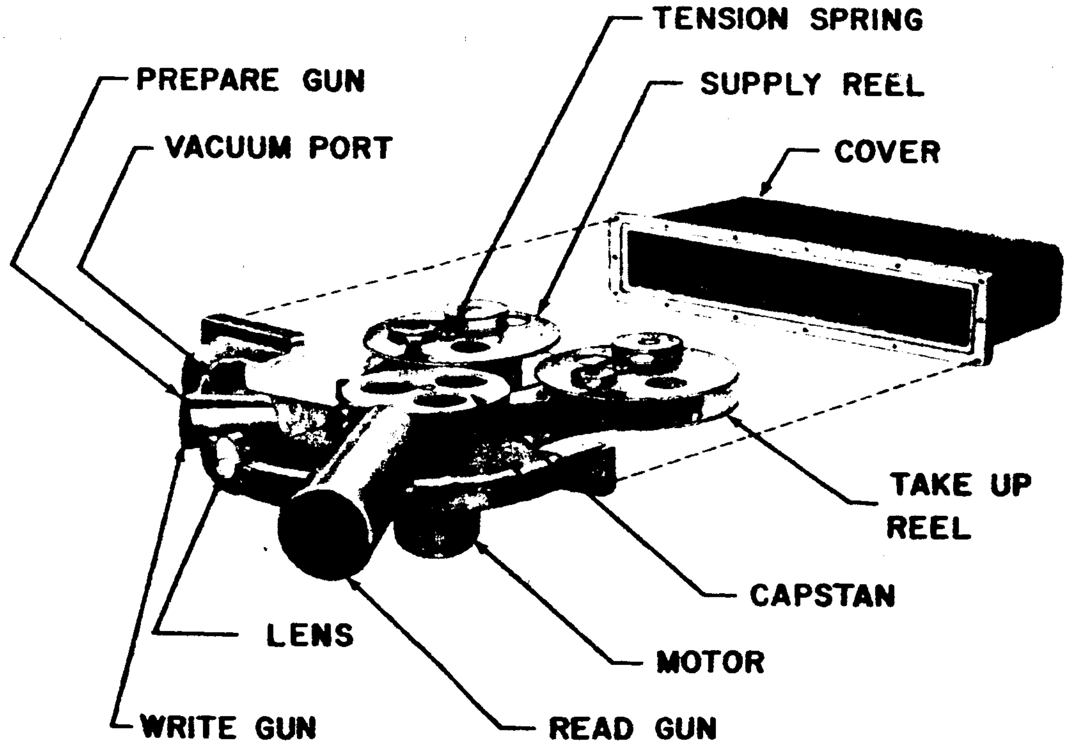

Figure II. 4. A-7. Photo Dielectric Tape Camera represents the motion of the point image. It follows that the tape must be moved parallel to the velocity vector. The tape velocity required to immobilize the image with respect to the tape may be calculated from the satellite velocity and the magnification of the optical system. The magnification required of the optical system, is, in turn, set by the size, inverse ratio of the desired lunar resolvable element, and the resolution element size of the dielectric tape camera.

Using 35 mm tape, which has a useful recording area per frame of 25 mm x 25 mm, and a resolution capability of at least 80 elements per millimeter, the lens magnification (m) required is the ratio of:

$$\frac{1}{80} \text{ mm to } 5,000 \text{ mm}, \quad \text{or } m = 2.5 \times 10^{-6} \qquad (19)$$

The lens focal length required, based on 100 km altitude, is then:

$$f = 100 \text{ m} \times 10^{6} \text{ millimeters} = 250 \text{ millimeters} \qquad (20)$$

The tape velocity required for immobilization is given by:

$$v = m\overline{V}, \qquad (21)$$

where: $\overline{V}$ is the satellite velocity.

For an orbital altitude of 100 km, $\overline{V} \doteq 1.5$ km/sec, leading to:

$$\begin{aligned} v &= m\overline{V} \\ &= 2.5 \times 10^{-6} \times 1.5 \times 10^{+6} \qquad (22) \\ &= 3.75 \text{ mm/sec} \end{aligned}$$

Table II.4.A-5 shows these and other system parameters which form the essential system specification.

Exposure is accomplished by using continuously moving tape (the velocity of the tape being such as to immobilize the image with respect to the tape) within a fraction of a resolution element of displacement within the exposure time of 30 msec. The exposure time is chosen to be short enough that attitude perturbations produce small image displacements compared with the resolution element.

While the exposure or "write" operation is accomplished with continuously moving tape, the image may be read out in frames. Because of the limitation on bit-rate, imposed by the transmission channel, it is not possible to transmit bits as fast as they are recorded on the tape. This can be seen by observing that the tape is capable of reading 2000 resolution elements of 5-meter dimension on the lunar surface, while the velocity of the spacecraft ($1.5 \times 10^3$ m/sec) causes it to sweep 300 elements per second. Thus, the bit recording rate on tape is $6 \times 10^5$ bits per second. The transmission channel can only transmit $2.4 \times 10^5$ bits per second, in view of the fact that a

## TABLE II. 4. A-5

## DIELECTRIC TAPE CAMERA PARAMETERS FOR LUNAR ORBITER CAPSULE

| Parameters | Performance Characteristics |
|---|---|
| Satellite: | |
| Altitude | 100 km |
| Velocity | 1.5 km/sec |
| Stability | $0.85 \times 10^{-3}$ radians/sec |
| Orbit Period | 2.5 hours |
| Communication System: | |
| Earth Contact Time | 10 min (max) |
| Bandwidth | 120 kc |
| Camera: | |
| Surface Resolution | 5 meters |
| Tape Width | 35 mm |
| Useful Tape Width | 25 mm |
| TV Resolution Elements: | |
| per mm | 80 |
| per picture width | 2000 |
| Lens: | |
| focal length | 250 mm |
| aperture | f/1.5 |
| transmission | 0.6 |
| Frame Size | 25 x 25 mm |
| Scanning Rate Readout: | |
| line | 110 cps |
| frame | 0.037 cps |
| Scanning Lines per Frame | 3000 |
| Scanning Lines per Frame - active | 2500 |
| Kill Factor | 0.08 |
| Sensitivity at 26 db S/N | 9 ft-lamberts |
| Dynamic Range | 37 db |
| Exposure Time | 30 m/sec |
| Tape Velocity (record) | 3.75 mm/sec |
| Tape Velocity (record) Accuracy | ±1% |
| Slit Width | 0.113 mm |
| Field Angle | 5.7° |
| Surface Area Covered per Frame | 10 x 10 km |
| Total Number of Frames (for 10 mm contact time) | 22 |
| Total Area Covered (per orbit) | 2200 $\text{km}^2$ |
| Tape Length for Above Coverage | 3 ft |
| Camera Weight (less lens) | 38 lbs |
| Power Requirements: | |
| Record | 9 watts |
| Read | 15 watts |

bandwidth of 120 kc is assumed. By providing frame scanning, it becomes possible, without altering the tape transport speed, to adjust the number of bits read out to fit the time available for readout; this could be done conveniently by adjusting the scanning rate. The rates shown in Table II. 4. A-5 will transmit, within a period of 10 minutes and through a communication channel of 120 kc bandwidth, all the elements in a lunar surface area of 10 Km x 220 Km dimensions. The number of picture elements obtained from the tape camera will exceed that of the vidicon because the effective target width is 25 mm, as compared with 11 mm on the vidicon. With scanning spots of equal size in each device, there are more resolution elements in the tape camera, in the ratio of $\left(\frac{25}{11}\right)^2 = 5.2$ times. This advantage results in a correspondingly larger field of view for the tape camera, with a resolution element of a given size. Actually, the advantage may be somewhat greater than this, since the aperture response of a tape camera has been measured to be 25 percent at 2,000 TV lines, whereas a typical vidicon response at 900 lines (which represents the equivalent line density on its smaller target) would be only about 10 percent.

Table II. 4. A-6 shows typical signal-to-noise characteristics of the dielectric tape camera. The signal-to-noise ratio for various values of scene luminance is shown, as well as corresponding values of photometric function for two values of albedo. The values in these columns are related to the angular distance from the terminator at which the indicated S/N ratio is obtained. Based on a value of $\phi_g = 8 \times 10^{-2}$ at 10° from the terminator, it is seen that a 26 db picture can be obtained much closer to the terminator than this. If the assumption is made that $\phi_g$ is directly proportional to the angle from the terminator for angles less than 10°, it is seen that even with an albedo of 0.06, a 26 db picture will be obtained 1.3° from the terminator.

TABLE II. 4. A-6

TYPICAL SIGNAL-TO-NOISE CHARACTERISTICS OF DIELECTRIC TAPE CAMERA (With f/1.5 Lens and 30 msec Exposure Time)

| Scene Luminance B (ft-lamb.) | Exposure $E_x$ (ft-candles/sec) | SNR (db) | $a_n \phi_g$ (B/14,000) | $\phi_g$ for Albedo of | |
|---|---|---|---|---|---|
| | | | | 0.06 | 0.18 |
| 1.3 | $0.24 \times 10^{-3}$ | 16 | $0.93 \times 10^{-4}$ | $0.155 \times 10^{-2}$ | $0.052 \times 10^{-2}$ |
| 9 | $1.6 \times 10^{-3}$ | 26 | $6.43 \times 10^{-4}$ | *$1.07 \times 10^{-2}$ | $0.36 \times 10^{-2}$ |
| 24 | $4.3 \times 10^{-3}$ | 32 | $17.0 \times 10^{-4}$ | $2.83 \times 10^{-2}$ | $0.94 \times 10^{-2}$ |

*Permits working at 1.3° from the terminator at SNR of 26 db

c. Conclusion

It is believed that the tape camera represents a good approach to the problem of high-resolution lunar surveillance. For a given signal-to-noise ratio, it can work closer to the terminator than either the type 7198 image orthicon or the type 4431 vidicon.

RE-ORDER No. 62-489

# PART III.

# TABLE OF CONTENTS

| Appendix | | Page |
|---|---|---|
| A | PROPOSED STATEMENT OF WORK FOR PROCUREMENT OF SOLID ROCKET MOTOR | III.A-1 |
| | A. Scope | III.A-1 |
| | B. General Design Criteria of Rocket Motor | III.A-1 |
| | C. Detailed Requirements of Rocket Motor | III.A-1 |
| | D. Operational Testing | III.A-2 |
| | E. Data Required | III.A-2 |
| B | DERIVATION OF THERMAL DESIGN LIMITS OF INTEGRATION | III.B-1 |
| | A. Introduction | III.B-1 |
| | B. Limits of Integration | III.B-2 |
| | C. Effect of Emission Characteristic | III.B-10 |
| C | ANALYSIS OF A PINNED SYSTEM FOR ATTITUDE CONTROL | III.C-2 |
| | A. Conditions for Stability | III.C-2 |
| | B. Effects of Stator Asymmetry on Precessional Motion | III.C-6 |
| | C. Gyro Precession Damping | III.C-9 |
| D | PHOTO-COVERAGE GEOMETRY ANALYSIS AND PROGRAMMING | III.D-1 |
| | A. General | III.D-1 |
| | B. The Coordinate System and its Transformation | III.D-1 |
| | C. Determination of the Right Ascension and Declination of the Moon | III.D-3 |
| | D. Subsatellite and Solar Contour Circle Intersection | III.D-3 |
| | E. Vector Transformation to a Moon Equatorial Coordinate System | III.D-5 |
| E | TV MISSION DESIGN FOR VERTICAL RESOLUTION BY SHADOW MEASUREMENT NEAR THE LUNAR TERMINATION | III.E-1 |
| | A. Problem Definition and Delineation | III.E-1 |
| | B. The Vidicon as Sensor | III.E-2 |
| | C. The Image Orthicon as Sensor | III.E-9 |

# LIST OF ILLUSTRATIONS

| Figure | | Page |
|---|---|---|
| A-1 | Rocket Motor Installation Data | III. A-2 |
| B-1 | Geometry for Obtaining Thermal Radiative Power from the Lunar Surface | III. B-2 |
| B-2 | Determining the Field of View | III. B-3 |
| C-1 | Geometry of System B Inertia | III. C-3 |
| C-2 | Coordinate System Geometry | III. C-7 |
| C-3 | Single-Gyro System Configuration | III. C-10 |
| C-4 | Two-Gyro System Configuration | III. C-14 |

RE-ORDER No. 62-459

# LIST OF TABLES

Tables                                                                 Page

B-1 Boundaries for Equation (B-1) . . . . . . . . . . . . . . . . . . . . . . . III. B-5
B-2 Boundaries for Equation (B-4) . . . . . . . . . . . . . . . . . . . . . . . III. B-8
B-3 Boundaries for Equation (B-3) . . . . . . . . . . . . . . . . . . . . . . . III. B-9
B-4 Boundaries for Equation (B-2) . . . . . . . . . . . . . . . . . . . . . . . III. B-10
B-5 Values of B (R/ρ) for Various Orbital Altitudes . . . . . . . . . . III. B-12
D-1 Matrix-C Elements . . . . . . . . . . . . . . . . . . . . . . . . . . . . . . III. D-2
D-2 Matrix-B Elements . . . . . . . . . . . . . . . . . . . . . . . . . . . . . . III. D-3
E-1 Samples of $\ell$, the Horizontal Object Resolution Per Line . . . . III. E-1
E-2 Typical Vidicon Focal Lengths (In Meters) . . . . . . . . . . . . . . III. E-3
E-3 Comparison of Fitted and Original $\phi$ Data . . . . . . . . . . . . . . III. E-3
E-4 Specifications for Vidicon Type #4431†. . . . . . . . . . . . . . . . . III. E-4
E-5 Values of f for $\epsilon = 1.0$ and 0.1, Using the Vidicon . . . . . . . . III. E-7
E-6 Exposure Time (In Milliseconds) for $\epsilon = 1.0$ . . . . . . . . . . . . . III. E-8
E-7 Comparison of y and $\ell$ . . . . . . . . . . . . . . . . . . . . . . . . . . . III. E-9
E-8 Typical Image-Orthicon Focal Lengths (In Meters). . . . . . . . . III. E-10
E-9 Values of f for $\epsilon = 1.0$, Using the Image Orthicon . . . . . . . . . III. E-11

RE-ORDER No. 62-489

# APPENDIX A
# PROPOSED STATEMENT OF WORK FOR PROCUREMENT OF SOLID ROCKET MOTOR

## A. SCOPE

This statement of work defines the configuration, performance, and operational requirements of a solid-fuel rocket motor, the purpose of which is to provide the retro thrust necessary for the injection, from the transient trajectory, of a payload into an orbit about the moon. To meet the end-trajectory conditions the motor must be of sufficient size to provide a nominal velocity change of 1250 meters per second to a vehicle having an initial weight of 450 pounds with a usable payload weight greater than 262 pounds.

## B. GENERAL DESIGN CRITERIA OF ROCKET MOTOR

1. The design shall be based upon the integration of developed design concepts.

2. The rocket-motor case shall be used to transmit the static and dynamic loads from the payload to the launching vehicle.

3. The test program shall be of sufficient scope to establish "Preliminary Flight Rating Test" (PFRT) status for the intended mission and not full qualification status to military specifications.

4. The reliability shall be estimated and based upon previous experience, with only sufficient testing to lend credence to the estimate.

5. The critical items listed in the order of priority are reliability, weight, schedule, and cost. This listing assumes that the desired performance and physical characteristics are within the state-of-the-art.

## C. DETAILED REQUIREMENTS OF ROCKET MOTOR

1. Thrust Level - the desired thrust level is 3000 pounds. The deviation from this nominal level should not exceed ± 10 percent over the burn time.

2. Total Impulse - the total impulse delivered at a given temperature shall be within ± 0.5 percent of the design value.

3. Weight - the total and burnout weights shall not exceed 188 and 20 pounds, respectively. All the items necessary for the motor to operate satisfactorily for the intended mission must be included within these weights.

4. Loads - the rocket motor housing will be capable of transmitting the static and dynamic loads of launch and injection to the payload. These loads are defined on Figure A-1.

NOTES.

(1) All dimensions in inches

(2) Maximum motor case outside diameter permissible is 18.3 inches.

(3) Maximum motor diameter at the mounting plane is 20 inches

(4) Spin RPM during burning and at ignition is 300 RPM (max)

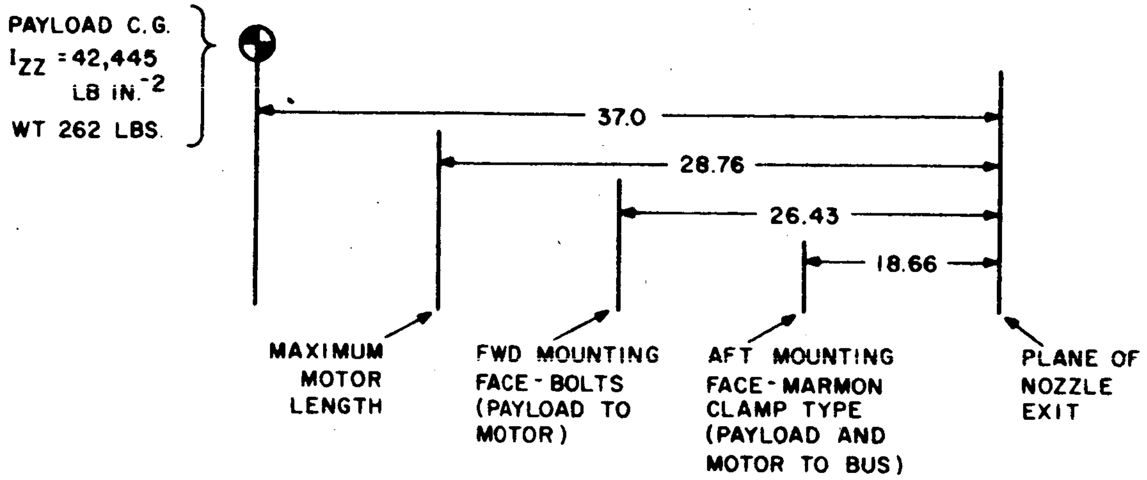
PAYLOAD C.G.
$I_{ZZ}$ = 42,445 LB IN.$^{-2}$
WT 262 LBS.
37.0
28.76
26.43
18.66
MAXIMUM MOTOR LENGTH
FWD MOUNTING FACE - BOLTS (PAYLOAD TO MOTOR)
AFT MOUNTING FACE - MARMON CLAMP TYPE (PAYLOAD AND MOTOR TO BUS)
PLANE OF NOZZLE EXIT

DEFINITION OF AXES

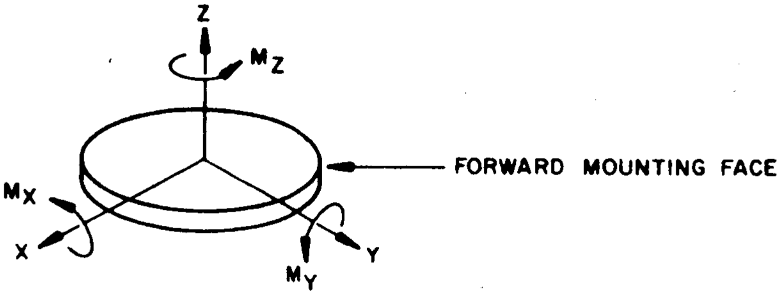
Z
$M_Z$
FORWARD MOUNTING FACE
$M_X$
X
$M_Y$
Y

Rocket Case Loading

| Load Condition | $F_X$ | $F_Y$ | $F_Z$ | $M_X$ | $M_Y$ | $M_Z$ |
|---|---|---|---|---|---|---|
| Vibratory | 7.56 | 7.56 | 11.80 | 79.6 | 79.6 | - |
| Acceleration | 2.85 | 2.85 | 5.70 | 30.1 | 30.1 | - |
| Spin | - | - | - | - | - | 137 |

Forces in 1000-lb., Moments in In. 1000-lb.

| Accelerations | X | Y | Z |
|---|---|---|---|
| Vibratory | 26.5g | 26.5 g | 41.40 g |
| Acceleration | 10 g | 10 g | 20 g |
| Spin | - | - | 254 rad/sec$^2$ |

Figure A-1. Rocket Motor Installation Data

5. Size - the available installation envelope is shown by Figure A-1. These dimensions are maximum, and the maximum motor dimension including manufacturing tolerances must not exceed this envelope.

6. Temperature

a. Storage - the desired storage temperature range is 0° to 125°F.

b. Operational - the required operational temperature range is 40° to 90°F.

c. Operating - the temperature of the case or nozzle shall not exceed 200° and 400°F, respectively, during or after burning under hard vacuum conditions when exposed to a sink temperature of 60°F.

7. Environmental - the following is a list of the types of environmental tests that will be required. (The significant parameters have not been specified at this time. To obtain preliminary cost and schedule it may be assumed that standard Military Specifications will be adequate.)

a. Vibration

b. Humidity

c. Sterilization - the equipment shall be exposed to a sterilization gas composed of 12% ethylene oxide and 88% Freon-12 for a period of 24 hours at 104°F.

d. Temperature and Humidity Cycling

e. Shock

f. Acoustics

g. Salt Spray

h. Environmental Atmosphere - applicable to electrical components only

i. Radiation

j. Acceleration

k. Altitude

(1) Static - three days at 12 micron 70°F.

(2) Firing - motors will be tested with facilities available at Arnold Engineering Development Center (AEDC). These firings will be made with the motor mounted to a vehicle structure (to be supplied by RCA) for determination of the amount of metal particles that may be deposited on the solar cells.

8. Ignition - provisions will be required for the determination of the average motor temperature during flight so that the firing point can be varied to compensate for the performance changes.

9. Thrust Misalignment - the thrust misalignment shall not exceed 0.010 inch at the nozzle throat, including combustion and installation items.

10. Balance - the motor mass unbalance shall not exceed 5 inch-ounces before loading and 15 inch-ounces after loading and during firing.

11. Chuffing - this characteristic must be eliminated.

12. Outgassing - the thrust level and duration must be defined by test.

13. Weight Control - weight must be controlled to within 0.1%.

14. Electrical Power - the electrical power supply will have a 24- to 32-volt output.

15. Acceleration - the acceleration applied by the rocket motor to the 450-pound gross-weight vehicle should be less than 40 g's at ignition.

16. Reliability - a reliability of 0.9998 at 90% confidence level is desired.

## D. OPERATIONAL TESTING

1. Flight Proof - these tests will be conducted on prototype motors to prove conformance with the requirements noted above.

2. Acceptance - these tests will be conducted on all or part of a group of motors, and shall include vacuum storage, temperature cycling, vibration, and the firing of motors exposed to the previous conditions at a low, medium, and high temperature level.

3. Motors which have undergone operational testing shall not be delivered as flight articles.

## E. DATA REQUIRED

In answer to this statement of work, the following data should be supplied.

1. Performance and Physical Characteristics

| Items | Remarks |
|---|---|
| Thrust | Thrust time trace showing the ignition peak, deviation, and stability. |
| Propellant Composition | |
| Total Impulse | |
| Burning Time | |
| Specific Impulse | |
| Thrust Coefficient | |
| Chamber Pressure | |
| Nozzle Expansion Ratio | |
| Nozzle Half-Angle | |

| Items | Remarks |
|---|---|
| Ignition g's | Include rate of g on-set |
| Structural Factor | Include all inerts of the motor assembly. |
| Weight Breakdown | Include sliver* loss |
| Thrust Misalignment | |
| Center of Gravity | As a function of burning time |
| Moment of Inertia | As a function of burning time |
| Mass Unbalance | As a function of burning time |
| Reliability | At 90% confidence level |
| Electrical Power | Requirement vs. time |
| Motor Temperature | Case and nozzle temperatures vs. time, until outgassing stops. |
| Sketch | Showing grain design, materials, installation dimensions, and component arrangement. |
| Interfaces | Define the commands and operational interfaces with the payload. |
| Specific Heat Ratio | |

2. Cost - total program cost must be broken down into Development, Design, Testing, Production, Tooling, Facilities, Support, Models, and Documentation. Costs should be quoted on the basis of no overtime, and on the basis of 20 percent overtime if major schedule improvements can be obtained. The following are some of the cost items that must be included under models, documentation and support.

a. Monthly Progress Letter Reports
b. Quarterly Progress Reports
c. Test Reports
d. Design Report
e. Operational Manual
f. Flight data evaluation and reports
g. Weekly meeting at RCA
h. Two man-months of support at RCA during test phase

---

* "Sliver" - Residual Propellant

i. Special handling and test equipment

j. Four man-months AMR launch support

k. Models

1) Wooden mock-up kept up to date with respect to installation arrangements

(2) Mechanical models which duplicate the initial and burnt-mass, and center of gravity.

(3) Thermal model - actual components non-PFRT

l. Hardware

(1) One prototype - PFRT

(2) Six flight articles

m. Inputs for a Program Evaluation Review Technique (PERT) Program

3. Schedule - indicate the schedule date from go-ahead for the following milestones based upon the two cost bases - no overtime and 20% overtime.

a. Design Freeze

b. Development Test Start and Complete

c. All drawings applicable

d. Fabrication start

e. PFRT - Start and Complete

f. Delivery date for all the models

g. Delivery of first flight item and delivery of subsequent items

4. Improvements - indicate the improvement (reduction in motor weight) that could be obtained if delivery of the first flight article were 18 and 24 months from date of go-ahead. Provide a list of the possible improvements and estimated development time and cost.

# APPENDIX B

# DERIVATION OF THERMAL DESIGN LIMITS OF INTEGRATION

## A. INTRODUCTION

In Section I.3.G, Thermal Control, two equations were developed, from the geometry shown in Figure B-1, to give the thermal inputs to an area at an altitude $\rho$ from the moon's center. These were:

$$I_{th} = \frac{B^2}{\pi} \int_{\phi_{min}}^{\phi_{max}} \int_{\delta_{min}}^{\delta_{max}} f(\delta, \phi) \cos \delta \frac{\cos \delta \cos \delta_s \cos \phi + \sin \delta \sin \delta_s - B}{\left[1 + B^2 - 2B \left(\cos \delta \cos \delta_s \cos \phi + \sin \delta \sin \delta_s\right)\right]^2}$$

$$\frac{\cos(\delta_s - \alpha)}{\cos \delta_s} \left[\frac{\cos^2 \delta_s - \sin^2 \alpha}{\cos^2 (\delta_s - \alpha)} + 1 - 2B \left(\cos \delta \cos \delta_s \cos \phi + \sin \delta \sin \delta_s + \ldots \right.\right.$$

$$\left.\left. - \frac{\sin \delta \sin \alpha}{\cos(\delta_s - \alpha)}\right)\right] d\delta \, d\phi \qquad \text{(B-1)}$$

and:

$$I_{th} = \frac{B^2}{\pi} \int_{\phi_{min}}^{\phi_{max}} \int_{\delta_{min}}^{\delta_{max}} f(\delta, \phi) \cos \delta \frac{\cos \delta \cos \delta_s \cos \phi + \sin \delta \sin \delta_s - B}{\left[1 + B^2 - 2B \left(\cos \delta \cos \delta_s \cos \phi + \sin \delta \sin \delta_s\right)\right]^2}$$

$$\left[\cos \beta - B \left(\cos \delta \cos \delta_s \cos \phi \cos \beta + \cos \beta \sin \delta \sin \delta_s + \ldots \right.\right.$$

$$\left.\left. - \cos \delta \sin \beta \sin \phi\right)\right] d\delta \, d\phi \qquad \text{(B-2)}$$

Equation (B-1) was derived for the case where $\beta$ is zero; Equation (B-2) for the case where $\alpha$ is zero and $f(\delta, \phi)$ is equal to $\epsilon_M \sigma T_M^4$. Before determining the limits of integration, it must first be noted that Equation (B-1) cannot be used for certain regions of integration (e.g, when $\delta_s$ is equal to $\pi/2$ and when $(\delta_s - \alpha)$ is equal to $\pi/2$). In the case where $\delta_s$ is equal to $\pi/2$, the second line to Equation (B-1) can be changed, by geometrical reasoning, to:

$$2 \left[\cos \alpha - B \left(\sin \delta \cos \alpha - \cos \delta \cos \phi \sin \alpha\right)\right] d\delta \, d\phi \qquad \text{(B-3)}$$

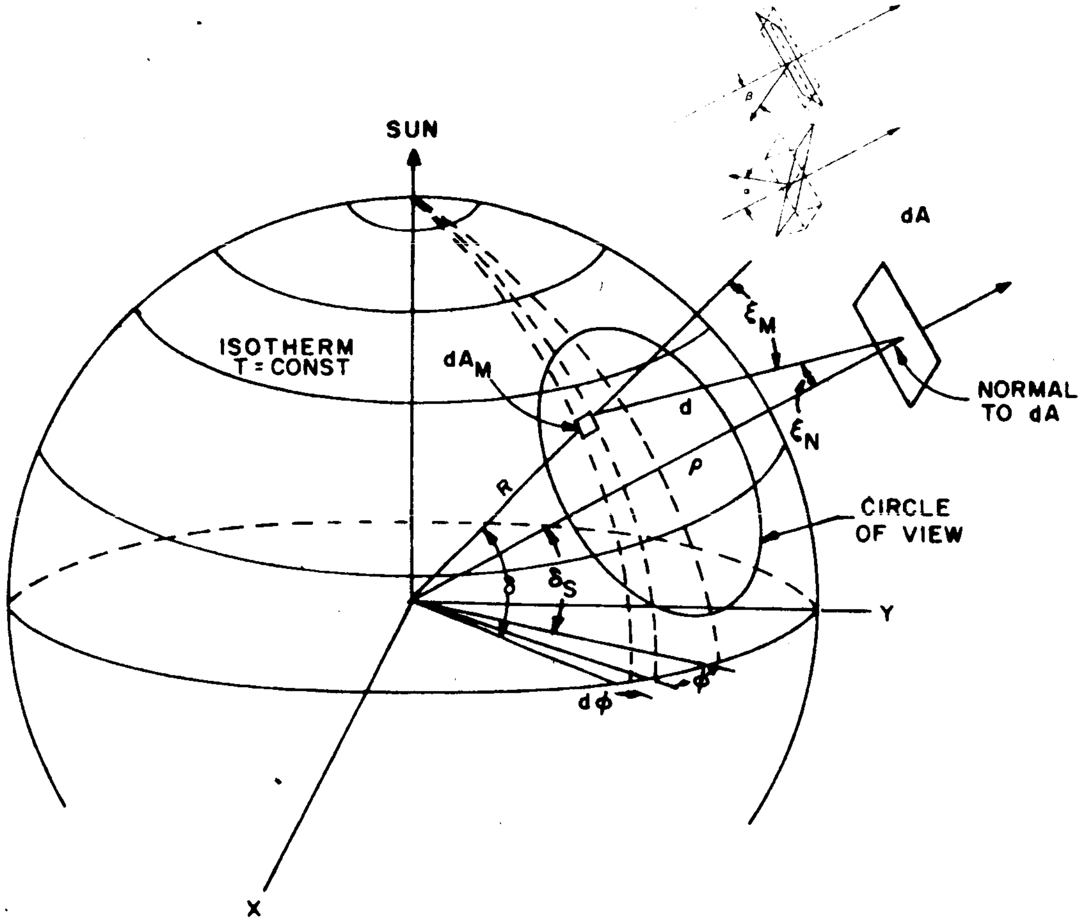
SUN
ISOTHERM
T = CONST
$dA_M$
dA
$\varepsilon_M$
$\varepsilon_N$
NORMAL TO dA
d
R
$\rho$
CIRCLE OF VIEW
$\delta$
$\delta_S$
Y
$d\phi$
$\phi$
X

Figure B-1. Geometry for Obtaining Thermal Radiative Power from the Lunar Surface

In the second case, for which ($\delta_s$ - $\alpha$) is equal to $\pi/2$, takes the limit of $I_{th}$ as $\delta_s$ approaches ($\pi/2 + \alpha$) gives, for the second line of Equation (B-1):

$$\frac{1}{\cos \delta_s} \left[ - \sin 2\alpha - \sin \delta \ \sin \alpha \right] d\delta \, d\phi \qquad \text{(B-4)}$$

It now remains to determine the limits of integration for Equations (B-1) through (B-4).

## B. LIMITS OF INTEGRATION

A plate which is perpendicular to the position vector ($\alpha = 0,\ \beta = 0$) can "see" the maximum surface area of the moon. The limit on the field of view is determined only by the condition that, once d and R become normal to each other, no more of the moon's surface can be seen. This area is known as the "circle of view" (shown in Figure B-1). However, as $\alpha$ (or $\beta$) increases from zero, a point will be reached beyond which any further increase in the angle will result in the plate cutting off part of the circle of view (see Figure B-2). From Part b of Figure B-2, the angle at which the plate begins to cut off some of the moon's surface is given by:

$$\left.\begin{matrix}\alpha\\ \beta\end{matrix}\right\} \leq \text{arc cos B} \qquad \text{(B-5)}$$

The limits of integration can now be determined for the case in which the complete circle of view is in sight of the plate. $\delta_{\text{min}}$ and $\delta_{\text{max}}$ are merely the lower and higher extremes of the circle of view. $\phi_{\text{min}}$ and $\phi_{\text{max}}$ are found from the right extreme ($\phi_{\text{max}}$) and the center of the circle of view ($\phi_{\text{min}} = 0$).

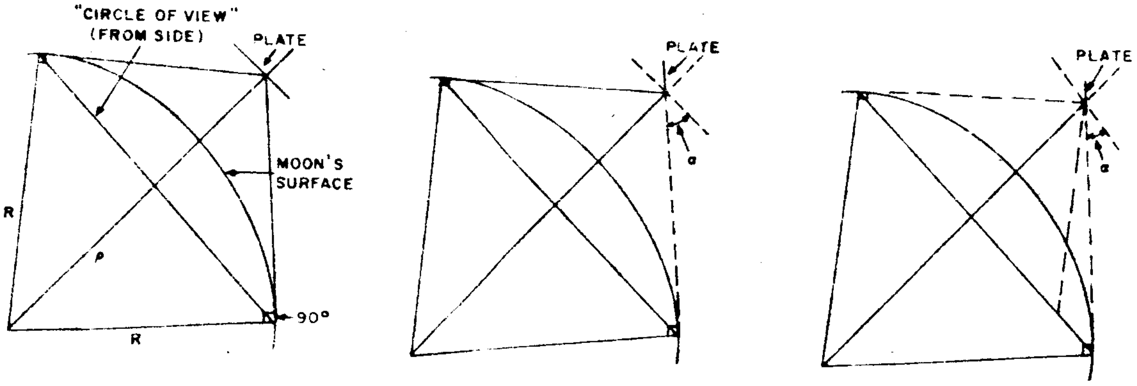

(a) PLATE NORMAL TO ρ

(b) PLATE AT ANGLE α STILL SEEING COMPLETE CIRCLE OF VIEW

(c) PLATE AT ANGLE α CUTTING OFF PART OF MOON'S SURFACE (SHADED AREA)

Figure B-2. Determining the Field of View

In the case for which part of the circle of view is cut off by the plate, the limits are found by solving simultaneously the two condition equations:

$$\cos \xi_m = 0 \qquad \text{(B-6)}$$

$$\cos \xi_n = 0 \qquad \text{(B-7)}$$

Tables B-1 through B-4 summarize the results of these calculations. Also shown in these tables are the shapes of the visible area of the moon's surface as seen from the plate.

RE-ORDER No. 62-489

## TABLE B-1

## BOUNDARIES FOR EQUATION (B-1)

I. $\alpha \geqq 0$

$$\delta_{\max} = \delta_s + \text{arc cos } B \qquad \text{B-I-1}$$

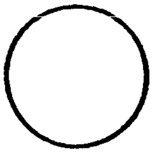

$$0 \leqq \alpha \leq \text{arc cos } B$$

$$\delta_{\min} = \delta_s - \text{arc cos } B \qquad \text{B-I-2}$$

$$0 \leq \alpha \geq \text{arc cos } B$$

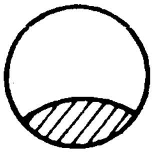

$$\delta_{\min} = \text{arc sin} \left[ \frac{\cos(\delta_s - \alpha)}{\sin \alpha} \left( B - \frac{\cos^2 \delta_s + \cos^2 (\delta_s - \alpha) - \sin^2 \alpha}{2 B \cos^2 (\delta_s - \alpha)} \right) \right] \qquad \text{B-I-3}$$

$$\phi_{\max} = \text{arc cos} \left[ \frac{B - \sin \delta \sin \delta_s}{\cos \delta \cos \delta_s} \right] \qquad \text{B-I-4}$$

The visible region must now be broken up into two separate regions as shown in the diagrams.

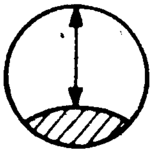

$$\delta_{\max}(\text{B-I-1}) \geq \delta \geq \delta_s - \alpha + \text{arc cos } \frac{\cos \alpha}{B} \qquad \text{B-I-5}$$

$$\phi_{\min} = 0 \qquad \text{B-I-6}$$

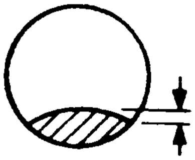

$$\delta_{\min}(\text{B-I-3}) \leq \delta < \delta_s - \alpha + \text{arc cos } \frac{\cos \alpha}{B} \qquad \text{B-I-7}$$

$$\phi_{\min} = \text{arc cos} \left[ \frac{1}{\cos \delta \cos \delta_s} \left( \frac{\cos^2 \delta_s + \cos^2 (\delta_s - \alpha) - \sin^2 \alpha}{2 B \cos^2 (\delta_s - \alpha)} + \ldots - \sin \delta \sin \delta_s + \frac{\sin \delta \sin \alpha}{\cos (\delta_s - \alpha)} \right) \right] \qquad \text{B-I-8}$$

In B-I-8 $\phi_{\min}$ is defined along the arc of intersection.

## TABLE B-1

## BOUNDARIES FOR EQUATION (B-1) (Continued)

II. $\alpha \leq 0,\ \delta_s - \alpha < \frac{\pi}{2}$

$$\delta_{min} = \delta_s - \text{arc cos } B \qquad \text{B-I-2}$$

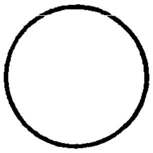

$$|\alpha| \leq \text{arc cos } B$$

$$\delta_{max} = \delta_s + \text{arc cos } B \qquad \text{B-I-1}$$

$$|\alpha| \geq \text{arc cos } B$$

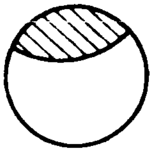

$$\delta_{max} = \text{arc sin}\left[\frac{\cos(\delta_s - \alpha)}{\sin \alpha}\left(B - \frac{\cos^2 \delta_s + \cos^2(\delta_s - \alpha) - \sin^2 \alpha}{2 B \cos^2(\delta_s - \alpha)}\right)\right] \qquad \text{B-II-1}$$

$$\phi_{max} = \text{arc cos}\left[\frac{B - \sin \delta \ \sin \delta_s}{\cos \delta \ \cos \delta_s}\right] \qquad \text{B-I-4}$$

Again the region must be broken up into two parts.

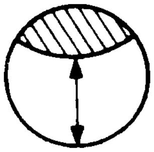

$$\delta_{min}\,(\text{B-I-2}) \leq \delta \leq \delta_s - \alpha - \text{arc cos}\left(\frac{\cos \alpha}{B}\right) \qquad \text{B-II-2}$$

$$\phi_{min} = 0 \qquad \text{B-I-6}$$

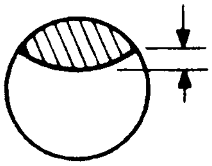

$$\delta_{max}\,(\text{B-II-1}) \geq \delta > \delta_s - \alpha - \text{arc cos}\left(\frac{\cos \alpha}{B}\right) \qquad \text{B-II-3}$$

$$\phi_{min} = \text{arc cos}\left[\frac{1}{\cos \delta \ \cos \delta_s}\left(\frac{\cos^2 \delta_s + \cos^2(\delta_s - \alpha) - \sin^2 \alpha}{2 B \cos^2(\delta_s - \alpha)} + \ldots - \sin \delta \ \sin \delta_s + \frac{\sin \delta \ \sin \alpha}{\cos(\delta_s - \alpha)}\right)\right] \qquad \text{B-II-4}$$

## TABLE B-1

## BOUNDARIES FOR EQUATION (B-1) (Continued)

III. $\alpha \le 0,\ \delta_s - \alpha > \frac{\pi}{2}$

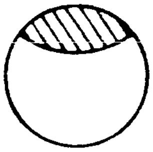

$$\delta_{\max} = \delta_s - \alpha - \text{arc cos}\left(\frac{\cos\alpha}{B}\right) \qquad \text{B-III-1}$$

$$\delta_{\min} = \delta_s - \text{arc cos } B \qquad \text{B-III-2}$$

$$\phi_{\min} = 0 \qquad \text{B-I-6}$$

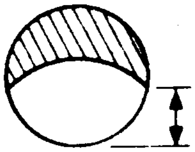

$$\delta_{\min}\,(\text{B-III-2}) \le \delta \le \text{arc sin}\left[\frac{\cos(\delta_s - \alpha)}{\sin\alpha}\left(B - \frac{\cos^2\delta_s + \cos^2(\delta_s - \alpha) - \sin^2\alpha}{2B\cos^2(\delta_s - \alpha)}\right)\right] \qquad \text{B-III-3}$$

$$\phi_{\max} = \text{arc cos}\left[\frac{B - \sin\delta\ \sin\delta_s}{\cos\delta\ \cos\delta_s}\right] \qquad \text{B-III-3}$$

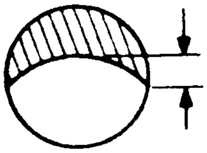

$$\text{arc sin}\left[\frac{\cos(\delta_s - \alpha)}{\sin\alpha}\left(B - \frac{\cos^2\delta_s + \cos^2(\delta_s - \alpha) - \sin^2\alpha}{2B\cos^2(\delta_s - \alpha)}\right)\right] < \delta \le \delta_{\max}\ (\text{B-III-1}) \qquad \text{B-III-4}$$

$$\phi_{\max} = \text{arc cos}\left[\frac{1}{\cos\delta\ \cos\delta_s}\left(\frac{\cos^2\delta_s + \cos^2(\delta_s - \alpha) - \sin^2\alpha}{2B\cos^2(\delta_s - \alpha)} + \cdots - \sin\delta\ \sin\delta_s + \frac{\sin\delta\ \sin\alpha}{\cos(\delta_s - \alpha)}\right)\right] \qquad \text{B-III-5}$$

RE-ORDER No. 62-489

TABLE B-2

BOUNDARIES FOR EQUATION (B-4)

IV. $\delta_s - \alpha = \frac{\pi}{2}, \quad \alpha \geq 0$

$$\delta_{min} = \text{arc sin} \left( \frac{\cos \alpha}{B} \right) \qquad \text{B-IV-1}$$

Other limits are same as I.

$\alpha \leq 0$

$$\delta_{max} = \delta_s - \alpha - \text{arc cos} \left( \frac{\cos \alpha}{B} \right) \qquad \text{B-III-1}$$

$$\delta_{min} = \delta_s - \text{arc cos B} \qquad \text{B-I-2}$$

$$\phi_{max} = \text{arc cos} \left[ \frac{B - \sin \delta \ \sin \delta_s}{\cos \delta \ \cos \delta_s} \right] \qquad \text{B-I-4}$$

$$\phi_{min} = 0 \qquad \text{B-I-6}$$

## TABLE B-3
## BOUNDARIES FOR EQUATION (B-3)

V. $\delta_s = \frac{\pi}{2}$

$$\delta_{max} = \frac{\pi}{2} + \text{arc cos B} \tag{B-V-1}$$

$$\delta_{min} = \frac{\pi}{2} - \text{arc cos B} \tag{B-V-2}$$

$$\phi_{max} = \frac{\pi}{2} \tag{B-V-3}$$

$\alpha \leq$ arc cos B

$$\phi_{min} = 0 \tag{B-I-6}$$

$\alpha \geq$ arc cos B

$\phi_{min} = 0$, when

$$\delta_{max}\ (\text{B-V-1}) \geq \delta \geq \frac{\pi}{2} - \alpha + \text{arc cos} \left( \frac{\cos \alpha}{B} \right) \tag{B-V-4}$$

$\phi_{min} = \text{arc cos} \left[ \dfrac{\sin \delta - \frac{1}{B}}{\cos \delta \ \tan \alpha} \right]$, when

$$\delta_{min}\ (\text{B-V-2}) \leq \delta \leq \frac{\pi}{2} - \alpha + \text{arc cos} \left( \frac{\cos \delta}{B} \right) \tag{B-V-5}$$

## TABLE B-4

## BOUNDARIES FOR EQUATION (B-2)

VI. Because of the symmetry of the temperature distribution with respect to the angle $\beta$, limits are needed only for $\beta \geq 0$.

$$\delta_{max} = \delta_s + \text{arc cos } B \qquad \text{B-VI-1}$$

$$\delta_{min} = \delta_s - \text{arc cos } B \qquad \text{B-VI-2}$$

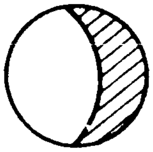

$$\phi_{max} = \text{arc cos} \left[ \frac{B - \sin \delta \sin \delta_s}{\cos \delta \cos \delta_s} \right] \qquad \text{B-VI-3}$$

$$\phi_{min} = - \text{arc cos} \left[ \frac{-A \cos \delta_s + \sqrt{A^2 \cos^2 \delta_s - (\tan^2 \beta + \cos^2 \delta_s)(A^2 - \tan^2 \beta)}}{\tan^2 \beta + \cos^2 \delta_s} \right] \qquad \text{B-VI-4}$$

$$\text{where} \quad A = \tan \delta \sin \delta_s - \frac{1}{B \cos \delta}$$

## C. EFFECT OF EMISSION CHARACTERISTIC

As indicated in Section I. 3. G. 7, the emission characteristic affects the results. Calculations for several different values of $f(\delta, \phi)$ were made, and are summarized below.

First, two forms of $f(\delta, \phi)$ were considered:

$$f_1 (\delta, \phi) = 0.8 \sin^{2/3} \delta \qquad \text{(B-8)}$$

$$f_2 (\delta, \phi) = F (\xi_M) K \sin^{2/3} \delta \qquad \text{(B-9)}$$

Values of Equation (B-8) were taken as:

$$f_1 \ (\delta, \phi) \geq 0.008 \ \text{watt/in}^2 \quad \text{(at sunrise*)}$$

$$f_1 \ (\delta, \phi) \geq 0.014 \ \text{watt/in}^2 \quad \text{(at sunset*)}$$

Two different computer runs were made, one with each of these two values.

The second form of $f(\delta, \phi)$, given by Equation (B-9), accounts for a variation in the emission characteristic. Values of 0.8, 0.83, and 0.85 were used for K, and $f(\delta, \phi)$ was again taken as greater than or equal to 0.008 watt per square inch at sunrise and greater than or equal to 0.014 watt per square inch at sunset. The factor $\xi_M$ is given by:

$$\xi_M = \text{arc cos} \left[ \frac{\cos \delta \cos \delta_s \cos \phi + \sin \delta \sin \delta_s - B}{\left(1 + B^2 - 2B \left\{ \cos \delta \cos \delta_s \cos \phi + \sin \delta \sin \delta_s \right\} \right)^{1/2}} \right] \quad \text{(B-10)}$$

The value of $F(\xi_M)$ is given below for various values of $\xi_M$.

| $\xi_M$ | 0 | 10 | 20 | 30 | 40 | 50 | 60 | 70 | 80 | 90 |
|---|---|---|---|---|---|---|---|---|---|---|
| $F(\xi_M)$ | 1.0 | 1.0 | 1.0 | 0.999 | 0.9909 | 0.9775 | 0.9437 | 0.8582 | 0.6445 | 0 |

The limits on $\delta_s$ are given by:

$$\frac{\pi}{2} \geq \delta_s \geq - \text{arc cos } B$$

Table B-5 lists the values of B, where B is equal to $R/\rho$, for various orbital altitudes.

---

*For $\delta_s \leq$ arc cos B.

62-489

## TABLE B-5

## VALUES OF B (R/ρ) FOR VARIOUS ORBITAL ALTITUDES

| Orbit Altitude H (km) | B |
|---|---|
| 50 | 0.9720 |
| 100 | 0.9456 |
| 150 | 0.9205 |
| 200 | 0.8968 |
| 250 | 0.8742 |
| 300 | 0.8528 |
| 400 | 0.8129 |
| 500 | 0.7766 |
| 750 | 0.6986 |
| 1000 | 0.6348 |
| 1500 | 0.5367 |
| 2000 | 0.4649 |
| 5000 | 0.2579 |

# APPENDIX C

# ANALYSIS OF A PINNED SYSTEM FOR ATTITUDE CONTROL

This appendix summarizes the work on System B — the pinned system — during and subsequent to Phase II, that was concerned directly with stabilization. As started in Section III. B, Part I, of this report, the major effort was directed to optimizing the configuration, layout etc. and any report on this work would be essentially descriptive.

It was considered, at this stage, that the most important problems associated with System B concerned the minimum attainable residual error rates of this system, because this parameter was critical in comparing the merits of Systems A and B. Therefore, the effort was directed towards determining the maximum tolerable dynamic unbalance, the shift of the principal axis resulting from antenna rotation, and the minimum precession cone angles achievable. The design of the pitch servo itself was not given particular attention because the residual rates arising from this source could be reduced to any specified value by including a rate gyro in the loop. Moreover, the uncertainty concerning the level of coulomb and viscous friction torques rendered any detailed analysis of the loop questionable; hence, it was proposed to examine the subsystem characteristics by building a bench-test model if System B was selected for development.

This appendix is purely analytical; however, some conclusions can be drawn:

1) A shift of the principal axis of the stator is in no way critical.

2) If a damper is mounted on the stator, no condition is imposed on the inertia ratios.

3) If a damper is rotor mounted, the conditions given in the Phase I Final Report apply.

4) Satisfactory damping time constants can be obtained using a stator-mounted gyro. However, every attempt was made to satisfy the conditions for rotor damping (an AED passive "TEAM" damper device could then be employed).

5) No analysis of dynamic balance is included because the results would be questionable as a result of vehicle flexure. Although it is not unreasonable to specify an uncertainty of less than 0.1 degree in the principal axis as a result of balancing machine errors, the realizable uncertainty may, in some cases, be as much as 0.25 degree. This was the value taken in determining 4 milliradians per second as the minimum achievable rate with the system.

However, AED now feels that this figure can be somewhat improved by careful design of the structure. It is now expected that a residual rate of less than 1 milliradian per second can be achieved.

## A. CONDITIONS FOR STABILITY

The total kinetic energy of the body shown in Figure C-1 is given by:

$$2E = A\omega_{12}^2 + C\omega_3^2 + R\omega_R^2 \qquad \text{(C-1)}$$

also

$$H \sin \theta = A\omega_{12} \qquad \text{(C-2)}$$

$$H \cos \theta = C\omega_3 + R\omega_R \qquad \text{(C-3)}$$

where

$A$ = total transverse inertia of rotor and "stator" (the slowly rotating component is called the "stator")

$C$ = polar inertia of the "stator"

$R$ = polar inertia of the rotor

$\omega_{12}$ = transverse angular momentum

$\omega_3$ = polar angular velocity of "stator"

$\omega_R$ = polar angular velocity of rotor

$H$ = total angular momentum

### 1. MOTOR ABSENT (CASE 1)

First, consider the case of perfectly smooth bearings between rotor and stator where no motor is required to sustain the relative angular velocity. Further, assume that the damper is mounted on the rotor. In this case, the stator, being a rigid body, must obey Euler's equations of motion. In the absence of external torques the equation for motion about OP of the stator is simply:

$$C\dot{\omega}_3 = 0$$

$$\omega_3 = \text{const.}$$

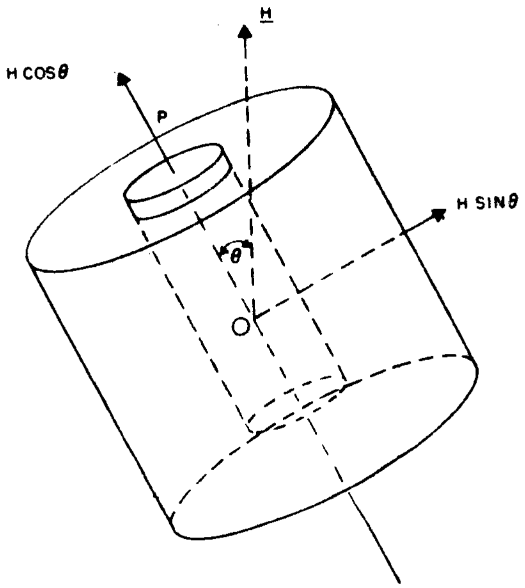

Figure C-1. Geometry of System B Inertia

From Equations (C-1), (C-2), and (C-3):

$$2E = \frac{H^2 \sin^2 \theta}{A} + C\omega_3{}^2 + \frac{(H \cos \theta - C\omega_3)^2}{R}$$

$$\frac{2\,dE}{d\theta} = \frac{2H^2 \sin \theta \cos \theta}{A} + \frac{2}{R}(H \cos \theta - C\omega_3)(- H \sin \theta)$$

For stability:

$$\frac{dE}{d\theta} > 0$$

Therefore:

$$\frac{H \cos \theta}{A} - \frac{(H \cos \theta - C\omega_3)}{R} > 0 \qquad \left[\text{as } \theta > 0\right]$$

$$H \cos \theta \left(\frac{1}{A} - \frac{1}{R}\right) + \frac{C\omega_3}{R} > 0$$

$$(C\omega_3 + R\omega_R)\left(\frac{1}{A} - \frac{1}{R}\right) + \frac{C\omega_3}{R} > 0$$

$$\frac{C\omega_3 + R\omega_R}{A} - \omega_R > 0$$

$$(R - A)\omega_R + C\omega_3 > 0 \qquad \text{(C-4)}$$

By similar reasoning, if the damper is mounted on the stator, $\omega_R$ is constant, and:

$$2E = \frac{H^2 \sin^2 \theta}{A} + R\omega_R^{\ 2} + \frac{(H\cos\theta - R\omega_R)^2}{C}$$

and the condition

$$dE/d\theta > 0$$

reduces to

$$(C - A)\omega_3 + R\omega_R > 0 \qquad \text{(C-5)}$$

## 2. MOTOR PRESENT (CASE 2)

In the previous case, as $\theta$ varies, the spin angular momentum of the component containing the damper increases at the expense of the transverse angular momentum, the spin angular momentum of the other component remaining constant. However, by adding a motor, it is possible to change the spin angular momentum of both components. In particular, it is possible to maintain the angular velocity of either component constant. It would appear from the previous analysis, therefore, that the conditions for stability depend, in this case, on which component, if either, has constant angular velocity and not on the location of the damper. However, this is not the case. In Case (1), the kinetic energy, E, is the total energy of the system. Therefore, the condition that $dE/d\theta$ be greater than zero is a sufficient condition for stability. In Case 2, however, the motor is supplying energy which is being used in two ways — to overcome bearing friction, and to transfer spin angular momentum from one component to the other. The energy required for this case must, therefore, be added to the kinetic energy, E, for the previous analysis to be valid.

In fact, four cases arise here:

a) Damper on stator, stator angular velocity constant;

b) Damper on stator, rotor angular velocity constant;

c) Damper on rotor, stator angular velocity constant; and

d) Damper on rotor, rotor angular velocity constant.

Neglecting the motor and gear inertia:

$$H \sin \theta = A\omega_{12} \qquad \text{(C-6)}$$

$$H \cos \theta = C\omega_3 + R\omega_R \qquad \text{(C-7)}$$

$$2E_K = A\omega_{12}^{\,2} + C\omega_3^{\,2} + R\omega_R^{\,2} \qquad \text{(C-8)}$$

where the suffix indicates that the right-hand side of Equation (C-8) represents the kinetic energy alone.

If the component whose angular velocity is held constant does not contain the damper (cases b and c), the energy supplied by the motor is dissipated solely as friction in the bearings and the previous analysis still applies. This is not so for cases a and d. In case a, for which the stator angular velocity, $\omega_3$, is constant, Equation (C-8) gives:

$$\frac{dE_K}{dt} = A\omega_{12}\frac{d\omega_{12}}{dt} + R\omega_R\frac{d\omega_R}{dt} \qquad \text{(C-9)}$$

There is no damper on the rotor; hence, a change in its spin angular momentum must be caused by a torque applied by the motor. The rate of input of energy from the motor, $E_M$, is equal to the product of this torque and the motor speed. Thus:

$$\dot{E}_M = -R\frac{d\omega_R}{dt}(\omega_R - \omega_3) \qquad \text{(C-10)}$$

The total rate of change of energy of the system, $\frac{dE}{dt}$ is given by:

$$\begin{aligned}\frac{dE}{dt} &= \dot{E}_K + \dot{E}_M \\ &= A\omega_{12}\,\dot{\omega}_{12} + R\dot{\omega}_R\,\omega_3 \\ &= H \sin \theta \left(\frac{H \cos \theta}{A}\right)\dot{\theta} - H \sin \theta\,\dot{\theta}\omega_3 \qquad \text{(C-11)}\end{aligned}$$

Again, for stability:

$$\frac{dE}{dt} > 0$$

$$\frac{H \cos \theta}{A} - \omega_3 > 0$$

$$(C - A)\,\omega_3 + R\omega_R > 0 \qquad \text{(C-12)}$$

which is the condition obtained before for the case where the damper is mounted on the stator.

Similarly it can be shown that, for case d, the condition is:

$$(R - A)\,\omega_R + C\omega_3 > 0 \qquad \text{(C-13)}$$

3. CONCLUSION

For the LOC, the "stator" angular velocity is held constant and equal to the orbital angular velocity. Therefore, either cases a or c apply, depending on the damper location. The value of $\omega_3$ is approximately zero; therefore, with the damper mounted on the stator, there is virtually no restriction on the vehicle inertias. However, if the damper is mounted on the rotor, the condition for stability is that the polar moment of inertia of the rotor alone must exceed the total transverse inertia.

## B. EFFECTS OF STATOR ASYMMETRY ON PRECESSIONAL MOTION

Because of the presence of the tape recorder and rotatable antenna on the stationary component of System B (the pinned system), it will be extremely difficult to maintain the polar principal axis of this component coincident with the bearing axis. Any shift in the center of gravity will also affect the dynamics of the system; however, this parameter will be far easier to control (by careful design). Therefore, no analysis of the latter effect was performed during the Phase II study. Because of the severe constraints that could be imposed on the design by the former effect, however, an approximate analysis of the dynamical behavior of a body containing an asymmetric stator was made.

For a small residual "stator" spin (of the order of the orbital angular velocity), the tolerances on any displacement of the principal axes are sufficiently large to present essentially no design problems.

Consider the two sets of orthogonal axes shown in Figure C-2. Axes $(\hat{i}, \hat{j}, \hat{k})$ are taken to be fixed in the stator and axes (i, j, k) fixed in the rotor. Axis OK is the bearing axis and, for no optical axis "wobble" in the steady state, the total vehicle angular velocity vector should be parallel to this axis. Assume that the center of gravity of each component is conicident with the others at the origin, O, and let:

(a) the direction cosines of k with respect to $(\hat{i}, \hat{j}, \hat{k})$ be $(\rho, m, n)$;

(b) $\omega_1\ \omega_2\ \omega_3$ be components of the stator angular velocity;

(c) $\omega_x\ \omega_y\ \omega_z$ be components of the rotor angular velocity; and

(d) A', B', C' and a, a, c be the inertias of stator and rotor respectively.

The total angular momentum of the vehicle, $\underline{H}$ is given by:

$$\underline{H} = A'\omega_1 \hat{i} + B'\omega_2 \hat{j} + C'\omega_3 \hat{k} + a(\omega_x i + \omega_y j) + C\omega_2 k \qquad \text{(C-14)}$$

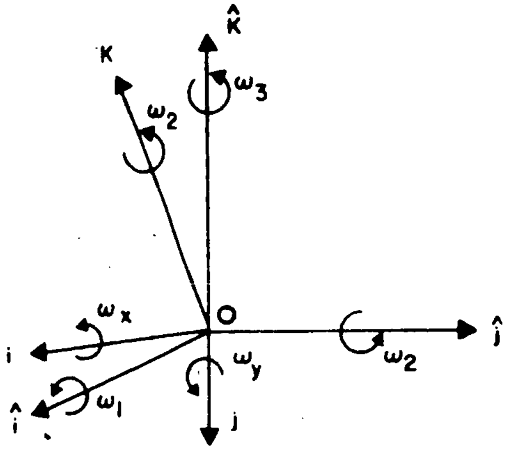

Figure C-2. Coordinate System Geometry

The angular velocities of stator and rotor differ in the k component only; thus:

$$\omega_x i + \omega_y j + (\omega_z - \Delta\omega_z) k = \omega_1 \hat{i} + \omega_2 \hat{j} + \omega_3 \hat{k} \tag{C-15}$$

where $\Delta\omega_z$ is the relative spin rate. From Equations (C-14) and (C-15):

$$\begin{aligned} \underline{H} &= (A'+a)\omega_1 \hat{i} + (B'+a)\omega_2 \hat{j} + (C'+a)\omega_3 \hat{k} - [a\omega_z - a\Delta\dot{\omega}_z - C\omega_z] \\ &= A\omega_1 \hat{i} + B\omega_2 \hat{j} + C\omega_3 \hat{k} - p(\rho \hat{i} + m\hat{j} + n\hat{k}) \end{aligned} \tag{C-16}$$

where $A = A' + a$, etc.

$$p = a\omega_z - a\Delta\omega_z - c\omega_z.$$

In the absence of external forces:

$$\dot{\underline{H}} + \underline{\omega} \times \underline{H} = 0 \tag{C-17}$$

where

$$\omega = \omega_1 \hat{i} + \omega_2 \hat{j} + \omega_3 \hat{k}$$

If the motor maintains the angular velocity of the stator constant at $\Omega$, then:

$$\omega_z - \Delta\omega_z = \Omega \tag{C-18}$$

and

$$p = a\Omega - c\omega_z \tag{C-19}$$

In this case, using Equation (C-16), Equation (C-17), in component form, becomes:

$$A\dot{\omega}_1 + c\rho\dot{\omega}_2 + (C-B)\omega_2\omega_3 - (a\Omega - c\omega_2)\,(n\omega_2 - m\omega_3) = 0 \qquad \text{(C-20)}$$

$$B\dot{\omega}_2 + cm\dot{\omega}_2 + (A-C)\omega_1\omega_3 - (a\Omega - c\omega_2)\,(\omega_3\rho - \omega_1 n) = 0 \qquad \text{(C-21)}$$

$$C\dot{\omega}_3 + cn\dot{\omega}_2 + (B-A)\omega_1\omega_2 - (a\Omega - c\omega_2)\,(\omega_1 m - \rho\omega_2) = 0 \qquad \text{(C-22)}$$

Moreover:

$$\rho\omega_1 + m\omega_2 + n\omega_3 = \Omega \qquad \text{(C-23)}$$

In an exact analysis, these four equations would be solved for $\omega_1$, $\omega_2$, and $\omega_3$. Then, using Equation (C-15), $\sqrt{\omega_x^2 + \omega_y^2}$ would be determined. This quantity is a measure of the precession of axis OK. By adding a damper (i.e., a rate gyro as in Appendix B of the Phase I Final Report), and modifying the equations accordingly, the residual precession, if any, can be determined. A numerical analysis of the exact equations would, of course, be carried out if the pinned system were selected. A few simplifications, however, provide an approximate estimate of the magnitude of the residual precession. If $\rho$ and m are small, and if $\dot{\omega}_2$ and $\omega_1\,\omega_2$ are neglected, the equations reduce to:

$$\omega_3 = \text{const.} \approx \Omega$$

$$B\dot{\omega}_2 + (A-C)\Omega\omega_1 + (a\Omega - c\omega_2)\,(\omega_1 n - \rho\Omega) = 0$$

$$A\dot{\omega}_1 + (C-B)\Omega\omega_2 + (a\Omega - c\omega_2)\,(m\Omega - n\omega_2) = 0$$

or:

$$B\dot{\omega}_2 + \left[(A-C)\Omega - hn\right]\omega_1 + h\Omega\rho = 0 \qquad \text{(C-24)}$$

$$A\dot{\omega}_1 + \left[(C-B)\Omega + hn\right]\omega_2 - hm\Omega = 0 \qquad \text{(C-25)}$$

where:

$$h = c\omega_z$$

$$\omega_z >> \Omega$$

Without introducing a damper, the effect can be deduced from the form of these equations. If $\rho$ and m are zero and n is one, the equations reduce to the well-known equations of motion for a satellite containing a rotor whose axis is coincident with the

No. 62-489

satellite "C" axis. In this case, $\omega_1$ and $\omega_2$ approach zero. (See Appendix B of the Phase I Final Report.) The third term in each equation does, however, give rise to non-zero steady-state values of $\omega_1$ and $\omega_2$:

$$\omega_2 = -\frac{h\Omega\rho}{(A-C)\Omega - hn} \approx \frac{\rho}{n}\Omega \tag{C-26}$$

and

$$\omega_1 \approx \frac{m\Omega}{n} \tag{C-27}$$

From Equation (C-15):

$$\omega_x^2 + \omega_y^2 \approx \omega_1^2 + \omega_2^2 = \frac{\Omega^2}{h^2}(\rho^2 + m^2) \tag{C-28}$$

Hence, the residual precession angle is approximately equal to:

$$\tan^{-1} \frac{a\Omega}{cn\omega_z} (\rho^2 + m^2)^{\frac{1}{2}}$$

For example, if $\Omega$ is 10 milliradians per second, $\omega_2$ is 1.0 radian per second, and c is approximately equal to a, the precession angle '$\theta$' is approximately given by:

$$\theta = 0.573 \sqrt{\rho^2 + m^2} \tag{C-29}$$

If $\theta$ must be less than 0.1 degree:

$$\sqrt{\rho^2 + m^2} < \frac{1}{5.73}$$

which should not be difficult to satisfy.

## C. GYRO PRECESSION DAMPING

The rotation of the platform of System B would be controlled by a motor/gyro speed servo loop; thus, the question arises as to whether the gyro can also be employed as a precession damper. It is shown below that the decay rates achievable with this system are unsatisfactory for most purposes. Much better response can be obtained by introducing a second gyro whose input axis is set normal to the input axis of the rate control gyro. Furthermore, the damper can be mounted on the platform, in which case the conditions for stability impose no restriction on the vehicle inertias.

## 1. SINGLE-GYRO CONFIGURATION

Consider the system shown in Figure C-3, in which the stator-mounted gyro is used for de-spin control and thus has its input axis aligned with the spin axis. An integrating gyro is used in the rate mode, and the Torque Generator feedback current, being proportional to the input rate, is used to control the despin motor. The gimbal will tend to oscillate (at precession frequency) as a result of residual precession. If a low-pass filter is introduced into the feedback loop to block signals at the precession frequency, the torquer will not follow this oscillation, and the gyro might act as a damper.

In Figure C-3:

$\phi$ is the angular movement of the gimbal relative to the case;

$\beta$ is the viscous coefficient of the gimbal;

x, y, z, $(\hat{i}, \hat{j}, \hat{k})$ and 1, 2, 3 (i, j, k) are axes fixed in the stator and rotor respectively;

$\underline{H}$ is the total angular momentum of the vehicle; and

$A_1$, C, $A_1$ and $A_1'$, C', $A_1'$ as the inertias of stator and rotor, respectively.

The angle $\phi$ is assumed to be small; thus:

$$\cos \phi \approx 1$$
$$\sin \phi \approx \phi$$

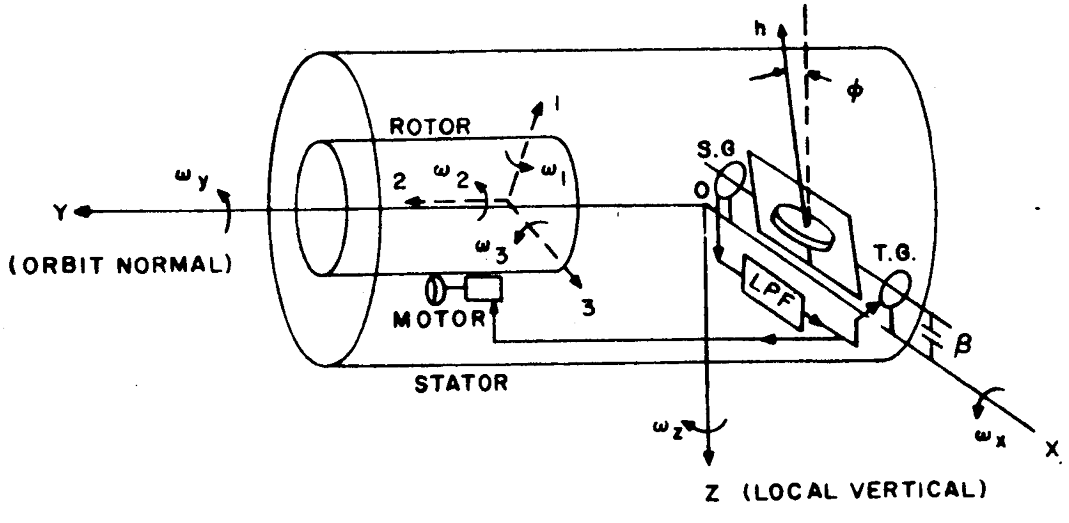

Figure C-3. Single-Gyro System Configuration

Then:

$$\underline{H} = A_1(\omega_x\hat{i} + \omega_z\hat{k}) + C\omega_y\hat{j} + A_1'(\omega_1 i + \omega_3 k) + C'\omega_2\hat{j} - h\hat{k} + h\phi\hat{j} \qquad \text{(C-30)}$$

and

$$\omega_x\hat{i} + \omega_z\hat{k} = \omega_1 i + \omega_3 k \qquad \text{(C-31)}$$

Therefore:

$$\underline{H} = A(\omega_x\hat{i} + \omega_z\hat{k}) + (C\omega_y + C'\omega_2)\hat{j} + h\phi\hat{j} - h\hat{k} \qquad \text{(C-32)}$$

where:

$$A = A_1 + A_1'$$

Therefore:

$$\underline{H} = A\omega_x\hat{i} + (C'\omega_2 + C\omega_y + h\phi)\hat{j} + (A\omega_z - h)\hat{k} \qquad \text{(C-33)}$$

If:

$$\underline{\omega} = \omega_x\hat{i} + \omega_y\hat{j} + \omega_z\hat{k} \qquad \text{(C-34)}$$

Then:

$$\dot{\underline{H}} + \underline{\omega} \times \underline{H} = 0 \qquad \text{(C-35)}$$

from which:

$$A\dot{\omega}_x + (A-C)\,\omega_y\omega_z - C'\omega_2\omega_z - h\omega_y - h\omega_z\phi = 0 \qquad \text{(C-36)}$$

$$C'\dot{\omega}_2 + C\dot{\omega}_y + h\dot{\phi} + h\omega_x = 0 \qquad \text{(C-37)}$$

$$A\dot{\omega}_z - (A-C)\,\omega_x\omega_y + C'\omega_2\omega_x + h\omega_x\phi = 0 \qquad \text{(C-38)}$$

$$\beta\dot{\phi} = h\phi\,\omega_z \qquad \text{(C-39)}$$

Note that no gyro inertial terms have been included thus far. Nominally, $\omega_y$ is zero, since it is held by the motor. In this event, Equations (C-36) and (C-38) reduce to:

$$A\dot{\omega}_x - \omega_z\,(C'\omega_2 + h\phi) = 0 \qquad \text{(C-40)}$$

$$A\dot{\omega}_z + \omega_x\,(C'\omega_2 + h\phi) = 0 \qquad \text{(C-41)}$$

and $\omega_z$ x equation (C-40) + $\omega_z$ x equation (C-41) gives $\omega_{xz}$ equal a constant (i. e., no damping takes place).

The angular momentum along the spin axis must remain constant; therefore, a change in $\phi$ (i. e., a change in the resolute of h along the spin axis) must be accompanied by either a change in the rotor spin or a change in the stator 'spin' or both. How this change in momentum is distributed between the two depends on the motor response. If the input to the motor is filtered so that it will not respond to inputs at the precession frequency, then it will not respond to this excitation at the frequency of $\phi$ (the precession frequency). In this case, the relative spins of rotor and stator will remain constant, and both $\omega_y$ and $\omega_2$ will vary. If the motor has a fast response (e.g., $\omega_y \equiv 0$), damping will not take place.

For a given motor and filter characteristic, $\omega_2$ can be related to $\omega_y$. For example, if:

$$f\,(\omega_2,\ \omega_y) = 0, \tag{C-42}$$

there are 5 equations in the 5 unknowns $\omega_x$, $\omega_y$, $\omega_z$, $\phi$ and $\omega_2$, from which $\omega_x$ and $\omega_z$ can be determined as functions of time. These equations would require numerical solution. However, from Equations (C-36) and (C-38):

$$\frac{d}{dt}\left(\omega_x^2 + \omega_z^2\right) = 2h\omega_y\omega_x,$$

and it does not seem likely from the form of this equation that there is any inherent damping in the system.

Equations (C-36) through (C-39) do not include terms arising from the inertia of the gyro rotor plus the float itself.

These terms can be included and the other small terms in the equations which do not appear to contribute to the damping can be dropped. If $\omega_y$ is zero:

$$A\dot{\omega}_x + J\ddot{\phi} - H\omega_z = 0 \tag{C-43}$$

$$A\dot{\omega}_z + H\omega_x = 0 \tag{C-44}$$

$$\beta\dot{\phi} = -J\,(\ddot{\phi} + \dot{\omega}_x) \tag{C-45}$$

where J is the float inertia and H (equal to $C'\omega_2$) is the angular momentum of the vehicle. Eliminating $\phi$ and $\omega_z$, gives, in Laplace notation:

$$\left\{AJ\,(A-J)S^3 + \beta A^2S^2 + JH^2S + H^2\beta\right\}\omega_x = 0 \tag{C-46}$$

It is certain that only light damping can be obtained by this technique. Therefore:

$$S = i\,\frac{H}{A} + \epsilon$$

where terms of order $\epsilon^2$ can be neglected. Substituting in Equation (C-46) yields:

$$\epsilon = \frac{-J^2 H^2}{2A^2 (JHi + \beta A)} \tag{C-47}$$

Hence, the real part of S is given by:

$$S = \frac{-\beta J^2 H^2}{2A (J^2 H^2 + \beta^2 A^2,} = R_{(s)} \tag{C-48}$$

The decay time constant $(\tau)$ is given by:

$$\tau = -\frac{1}{R_{(s)}} = \frac{2A}{\beta} \left(1 + \left[\frac{\beta A}{JH}\right]^2\right) \tag{C-49}$$

This is minimum for:

$$\beta = \frac{JH}{A} \tag{C-50}$$

In this case:

$$\tau_{min} = \frac{4A^2}{JH} \tag{C-51}$$

If:

$J = 200$ gm cm$^2$

$A = 10^8$ gm cm$^2$

$H = 10^8$ gm cm$^2$/sec

Values for LOC at the present time

Then:

$\tau_{min} = 550$ hours

It is clear that such a damper would be unsatisfactory. This result is not unexpected, because the damping in this case depends only on the inertia of the rotor plus the float and not on the gyroscopic stiffness of the device.

## 2. TWO-GYRO SYSTEM

A considerable improvement in damping can be obtained if a second gyro is added and aligned such that the gyroscopic stiffness is effective in removing the transverse angular velocity. (In other words, the gyro should be oriented such that its input axis lies in a plane normal to the spin axis.) One possible orientation (shown in Figure C-4), in which the rotor axis is maintained parallel to the axis of symmetry of the stator by a light spring restraint, provides satisfactory damping characteristics. Furthermore, by mounting the damper on the stator, no restriction is imposed on the vehicle moments of inertia. (The damping characteristics of a rigid-body-mounted gyro were investigated during the Phase I of the LOC Study and are discussed in the Phase I Final Report.) For this second unit, no signal or torque generators are required. (The conclusion in the Phase I Final Report that the condition C > A no longer holds, is incorrect.)

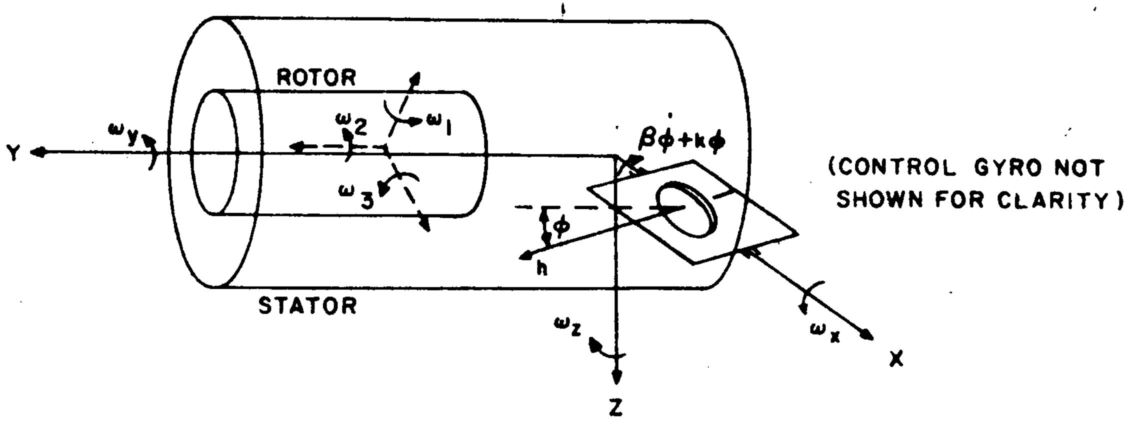

Figure C-4. Two-Gyro System Configuration

Again, in this figure:

x, y, z $(\hat{i}, \hat{j}, \hat{k})$ are fixed in the stator;

1, 2, 3 (i, j, k) are fixed in the rotor;

C'C, are the polar inertias of stator and motor, respectively; and

A is the total transverse inertia.

$$\underline{H} = A\omega_x \hat{i} + (C'\omega_2 + C\omega_y + h)\hat{j} + (A\omega_z + h\phi)\hat{k} \qquad \text{(C-52)}$$

for small values of $\phi$. Also:

$$\dot{\underline{H}} + \underline{\omega} \times \underline{H} = 0 \qquad \text{(C-53)}$$

$$\underline{\omega} = (\omega_x, \omega_y, \omega_z) \qquad \text{(C-54)}$$

Substituting for H yields:

$$A\dot{\omega}_x + (A-C)\,\omega_y\omega_z - C'\omega_2\omega_z + h\phi\omega_y - h\omega_z = 0 \tag{C-55}$$

$$C'\dot{\omega}_2 + C\dot{\omega}_y - h\omega_x\phi = 0 \tag{C-56}$$

$$A\dot{\omega}_z + h\dot{\phi} - (A-C)\,\omega_x\omega_y + C'\omega_2\omega_x + h\omega_x = 0 \tag{C-57}$$

Assuming that $\phi$, $\omega_x$, and $\omega_z$ are small, and setting $\omega_y$ equal to zero, these equations reduce to:

$$A\dot{\omega}_x - \omega_z\,(C'\omega_2 + h) = 0 \tag{C-58}$$

$$A\dot{\omega}_z + \omega_x\,(C'\omega_2 + h) + h\dot{\phi} = 0 \tag{C-59}$$

These equations should be compared with Equations (C-40) and (C-41).

Also, equating roll torques acting on the gimbal yields:

$$h\omega_z - h\phi\omega_y = \beta\dot{\phi} + \kappa\phi \tag{C-60}$$

or, since $\omega_y$ is zero:

$$\phi = \frac{h\omega_z}{\beta_S + \kappa} \tag{C-61}$$

From Equations (C-58), (C-59), and (C-61):

$$\left\{ A^2\beta S^3 + A\,(A\kappa + h^2)\,S^2 + H^2\beta S + \kappa H^2 \right\}\omega_z = 0 \tag{C-62}$$

where:

$$H = C'\omega_2 + h$$

Note that this equation represents a stable system for all values of the inertias.

The existence of two parameters ($\beta$ and $\kappa$) in Equation (C-62) which can be varied (for a given gyro rotor) allows a wide choice of response characteristics. In particular, the roots of Equation (C-62) can be made equal to give the maximum possible decay rate.

For example, if A is equal to H in CGS units as before, take:

$$\kappa = \frac{h^2}{8A}$$

$$\beta = \frac{3\sqrt{3}}{8} \quad \frac{h^2}{H}$$

thus, Equation (C-62) reduces to

$$(\sqrt{3}S + 1)^3 = 0 \tag{C-63}$$

giving a time constant of 1.7 seconds.

These values of $\beta$, $\kappa$ would be too small to realize in practice. The values:

$$h = 10^5 \text{ gm cm}^2/\text{sec}$$

$$H = 10^8 \text{ gm cm}^2/\text{sec.}$$

would yield:

$$\kappa = \frac{10^{10}}{8 \times 10^8} = 12.5 \text{ dyne cm/radian}$$

and:

$$\beta = \frac{3\sqrt{3}}{8} \times \frac{10^{10}}{10^8} = 65 \text{ gm cm}^2/\text{sec.}$$

For reasonable values of the parameters, the time constant will be large and we can proceed as before, that is:

$$S = \frac{iH}{A} + \epsilon \tag{C-64}$$

where $\epsilon$ is small.

Substituting in Equation (C-62) yields:

$$R_{(s)} = \frac{-\beta h^2 H^2}{2A\left[(A\kappa + h^2)^2 + \beta^2 H^2\right]} \tag{C-65}$$

This is a maximum for

$$\beta = (A\kappa + h^2)/_H \qquad \text{(C-66)}$$

A reasonable figure for $\beta$ in an inertial grade gyro is one-tenth of the rotor momentum (i.e. $\beta = h/_{10}$). From Equation (C-66):

$$\frac{hH}{10} - h^2 = A\kappa \qquad \text{(C-67)}$$

Solving for $\kappa$ gives:

$$\kappa \approx \frac{hH}{10A} \qquad \text{(C-68)}$$

from which:

$$R_{(s)_{max}} = {}^{10}/_{4}\ {}^{h}/_{A} \qquad \text{(C-69)}$$

Therefore, the time constant, $\tau$, is given by:

$$\tau = 0.4\ \frac{A}{h} \qquad \text{(C-70)}$$

Again taking:

$$h = 10^5 \text{ gm cm}^2/\text{sec},$$

$$A = H = 10^8 \text{ gm cm}^2/\text{sec}$$

gives:

$$\beta = 10,000 \text{ gm cm}^2/\text{sec.}$$

$$\kappa = 10,000 \text{ dyne cm/radian}$$

$$\tau = 400 \text{ seconds}$$

Reducing $\kappa$ and $\beta$ by a factor of 10 gives (approximately):

$$\kappa = 1000 \text{ dyne cm/radian}$$

$$\beta = 1000 \text{ gm cm}^2/\text{sec}$$

$$\tau = 40 \text{ seconds}$$

The advantages of the second configuration over the first are quite apparent from the example. The time constants derived would be suitable for most applications.

From Equation (C-60)

$$\beta\dot{\phi} + \kappa\phi = h\omega_z \qquad \text{(C-71)}$$

For values of $\tau$ greater than 40 seconds, $\omega_z$ is given by:

$$\omega_z = \alpha \cos \frac{Ht}{A} \qquad \text{(C-72)}$$

with $\alpha$ constant over one cycle.

The solution of Equation (C-71) is:

$$\phi = \left( \frac{h\alpha\kappa}{\beta^2 \left( \frac{\kappa^2}{\beta^2} + \frac{H^2}{A^2} \right)} \right) \left[ \cos \frac{Ht}{A} + \frac{H\beta}{A\kappa} \sin \frac{Ht}{A} - e^{\frac{-\kappa}{\beta} t} \right] \qquad \text{(C-73)}$$

For most examples, $\kappa/\beta$ is approximately equal to 1 in CGS units. Therefore, the last (transient) term in this expression can be assumed to have vanished before $\alpha$ has changed appreciably. Consequently:

$$\phi_{max} \approx \frac{h\alpha_i}{\sqrt{\kappa^2 + \beta^2 \frac{H^2}{A^2}}} \qquad \text{(C-74)}$$

where:

$\alpha_i$ = initial (max) value of $\alpha$

In our example:

$\kappa = \beta = 10^3$

$H = A$

$$\phi_{max} = \frac{h\alpha_i}{\sqrt{2}\,\beta} = 71\,\alpha_i$$

where $\alpha_i$ is in degrees/sec, $\phi_{max}$ in degrees

Assume an initial precession angle of 0.5 degree and a spin rate of 2 radians per second. Then:

$$\alpha_i = 0.5 \text{ degrees/sec.}$$

and:

$$\phi_{max} = 35.5 \text{ degrees}$$

This is obviously much too large. It can be remedied in practice by incorporating resilient stops to limit gyro float rotation or by making $\kappa$ increase with $\phi$ (non-linear system). The merits of the latter approach require further analysis. If stops are introduced, the decay time-constant will be greater than that calculated above. Two further alternatives are; first, to reduce the magnitude of the initial precession by other means or second, to increase the viscous coefficient, $\beta$, at the expense of response time. From Equation (C-73) for large $\beta$ ($\beta >> \kappa$):

$$\phi_{max} = \frac{H h \alpha_i}{A \beta H^2 / A^2} = \frac{A h}{H \beta} \alpha_i \qquad \text{(C-75)}$$

Setting:

$$A = H$$

$$h = 10\beta$$

gives:

$$\phi_{max} \text{ (degrees)} = 10 \; \alpha_i \text{ (degrees/sec)}$$

In this event, an initial precession angle of 0.5 degree results in a float travel of ± 5 degrees, which is probably tolerable. However, the response is seriously degraded. For large $\beta$:

$$R_{(s)} \approx \frac{-h^2}{2 A \beta} \qquad \text{(C-76)}$$

In this case:

$$R_{(s)} \approx \frac{10 h}{2 A} = \tau^{-1} \qquad \text{(C-77)}$$

Therefore:

$$\tau = \frac{2 A}{10 h} = \frac{2 \times 10^8}{10 \times 10^5} = 200 \text{ secs. (3.3 minutes)}$$

The damping characteristics of a gyro mounted as in Figure C-3 are certain to be unacceptable for most satellite applications. Much better response can be obtained from the configuration shown in Figure C-4. However, a compromise would, in general, have to be made between the conflicting requirements of maximum response time and limited gimbal travel. The merits of the various alternatives given would depend to some extent on the particular application.

# APPENDIX D
# PHOTO-COVERAGE GEOMETRY ANALYSIS AND PROGRAMMING

## A. GENERAL

If, for a moon satellite, i represents the inclination of the orbital plane and $\bar{\Omega}$ the right ascension of the ascending node, then the Cartesian coordinates of the orbit normal pierce point with a moon-centered unit sphere are given by:

$$\left.\begin{aligned} N_X &= -\sin\bar{\Omega}\,\sin i \\ N_Y &= \cos\bar{\Omega}\,\sin i \\ N_Z &= \cos i \end{aligned}\right\} \qquad \text{(D-1)}$$

Transforming the Equations of (D-1) into spherical coordinates is a relatively simple process which yields the declination and right ascension of the center of the orbital projection circle. The radius of this circle is exactly $\pi/2$ at all times.

## B. THE COORDINATE SYSTEM AND ITS TRANSFORMATION

In order to determine the coordinates of the center of a solar contour circle, the components of a unit vector in the moon-to-sun direction must be known. This unit vector can be found by normalizing the vector

$$\vec{L'} = |\vec{d'}|\,\hat{d'} + |L|\,T\,(\hat{L}) \qquad \text{(D-2)}$$

where:

$\hat{d'} = \dfrac{\vec{d'}}{|\vec{d'}|}$ is a unit vector (origin at the moon) directed towards the earth and relative to a selenographic coordinate system;

$\hat{L} = \dfrac{\vec{L}}{|\vec{L}|}$ is a unit vector (origin at the earth's center) directed towards the sun and relative to a true ecliptic coordinate system of date*; and

$T$ represents a rotation operator transforming true ecliptic vector components into selenographic vector components.

---

*i.e., date of solution of the problem.

The unit vector L has components (cos $\theta$, sin $\theta$, 0) where $\theta$, the solar longitude of date along the true ecliptic, can be evaluated with an existing solar model accurate to 10 seconds of arc. The operator T to be applied to this vector is

$$T = [t_{ij}] = [C_{ik}]\,[b_{kj}]. \qquad \text{(D-3)}$$

The matrices $C = [C_{ik}]$ and $B = [b_{kj}]$ are those formulated by Kalensher in Reference 1; each element of both C and B is defined below.

The components of the unit vector d' are $\cos \mu_e \cos \lambda_e$, $\cos \mu_e \sin \lambda_e$, and $\sin \lambda_e$ where $\mu_e$ and $\lambda_e$ are the earth's selenographic latitude and longitude, respectively. Reference 1 contains a complete description of these quantities and their relationship to the moon's orbital elements referred to the earth. For convenience, these quantities are further defined below.

The distances between earth and sun, $|\vec{L}|$, and between moon and earth, $|\vec{d'}|$, can be established as functions of calendar data by a least-square fitting process to data in the "American Ephemeris and Nautical Almanac".

The transformation T which will rotate a vector located in a true ecliptic coordinate system of date into a vector in a moon-fixed equatorial coordinate system is given as:

$$T = [t_{ij}] = [C_{ik}]\,[b_{kj}]. \qquad \text{(D-4)}$$

Table D-1 lists the elements of matrix C, which transforms from true earth equatorial of date to moon equatorial.

TABLE D-1

MATRIX-C ELEMENTS

$C_{11} = \cos \Omega' \cos \Lambda - \sin \Omega' \sin \Lambda \cos i$

$C_{12} = \sin \Omega' \cos \Lambda + \cos \Omega' \sin \Lambda \cos i$

$C_{13} = \sin \Lambda \sin i$

$C_{21} = -\cos \Omega' \sin \Lambda - \sin \Omega' \cos \Lambda \cos i$

$C_{22} = \sin \Omega' \sin \Lambda + \cos \Omega' \cos \Lambda \cos i$

$C_{23} = \cos \Lambda \sin i$

$C_{31} = \sin \Omega' \sin i$

$C_{32} = -\cos \Omega' \sin i$

$C_{33} = \cos i$

Table D-2 lists the elements of matrix B, which transforms from true ecliptic of date to true earth equatorial of date.

TABLE D-2

MATRIX-B ELEMENTS

| | | |
|---|---|---|
| $b_{11} = 1$ | $b_{12} = 0$ | $b_{13} = 0$ |
| $b_{21} = 0$ | $b_{22} = \cos\tilde{\epsilon}$ | $b_{23} = -\sin\tilde{\epsilon}$ |
| $b_{31} = 0$ | $b_{32} = \sin\tilde{\epsilon}$ | $b_{33} = \cos\tilde{\epsilon}$ |

Appendix B contains the equations required in the determination of the quantities $\Omega'$, $\Lambda$, i and $\tilde{\epsilon}$.

## C. DETERMINATION OF THE RIGHT ASCENSION AND DECLINATION OF THE MOON

The earth's selenographic latitude ($\mu_e$) and longitude ($\lambda_e$), as referenced to an equatorial coordinate system fixed at the center of the moon, is given by the following equations:

$$\sin\mu_e = \sin i \sin (A - \Omega') \cos\phi - \cos i \sin\phi \tag{D-5}$$

$$\lambda_e = \sin^{-1}\left[\frac{-\sin\ A - \Omega')}{\sin\Psi}\right] + \sin^{-1}\left[\frac{\tan\mu_e}{\tan\Psi}\right] - \Lambda. \tag{D-6}$$

In Equations (D-5) and (D-6), A and $\phi$ are the right ascension and declination, respectively, of the moon, and i, $\Lambda$, $\Omega'$ are Eulerian angles describing the orientation of the moon-fixed system relative to a true ecliptic-of-date system. The angle $\Psi$ is given by

$$\cos\Psi = -\sin i \cos (A - \Omega'). \tag{D-7}$$

## D. SUBSATELLITE AND SOLAR CONTOUR CIRCLE INTERSECTION

Determination of the points of intersection (if any) of a subsatellite great circle with a solar contour circle of radius $\gamma$ is performed in the following manner. If $(\delta_N, \alpha_N)$ and $(\delta_H, \alpha_H)$ are the coordinates of the center of the subsatellite and solar contour circles, respectively, then the spherical distance between centers (C) is given by

$$\cos C = \sin\delta_N \sin\delta_H + \cos\delta_N \cos\delta_H \cos(\alpha_H - \alpha_N). \tag{D-8}$$

No62-489

To guarantee the existence of an intersection configuration, the following tests are executed:

(1)

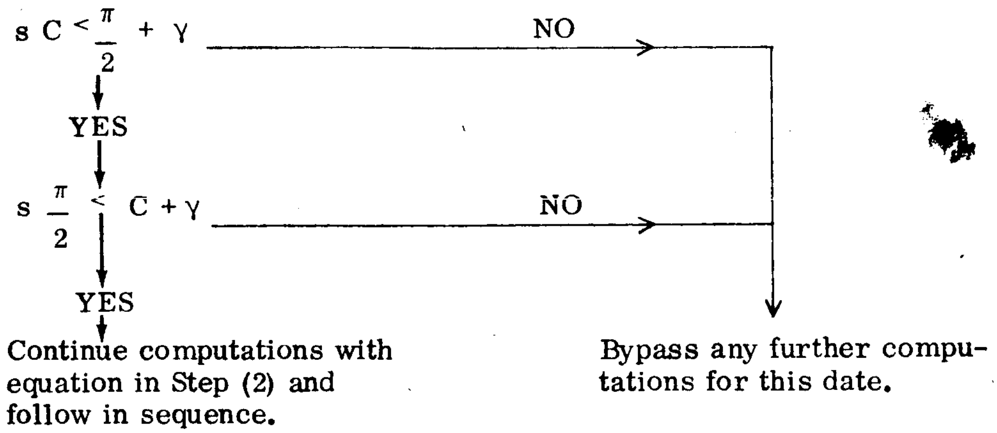

s C < π/2 + γ
NO
YES
s π/2 ≤ C + γ
NO
YES
Continue computations with equation in Step (2) and follow in sequence.
Bypass any further computations for this date.

(2) $$S_1 = \frac{1}{2}\left(\gamma + C + \frac{\pi}{2}\right)$$

(3) $$r_1 = \sqrt{\frac{-\cos S_1 \sin\left(S_1 - \gamma\right) \sin\left(S_1 - C\right)}{\sin S_1}}$$

(4) $$\theta = 2 \arctan\left[\frac{r_1}{-\cos S_1}\right]$$

(5) $$S_2 = \frac{1}{2}\left(\pi - \delta_N - \delta_H + C\right)$$

(6) $$r_2 = \sqrt{\frac{\cos\left(S_2 + \delta_N\right) \cos\left(S_2 + \delta_H\right) \sin\left(S_2 - C\right)}{\sin S_2}}$$

(7) $$\beta = 2 \arctan\left[\frac{r_2}{-\cos\left(S_2 + \delta_N\right)}\right]$$

(8) $$\sin \delta_1 = \cos \gamma \sin \delta_H + \sin \gamma \cos \delta_H \cos\left(\beta + \theta\right)$$

(9) $$\sin \delta_2 = \cos \gamma \sin \delta_H + \sin \gamma \cos \delta_H \cos\left(\beta - \theta\right)$$

(10) $$S_3 = \frac{1}{2}\left(\pi - \delta_H - \delta_1 + \gamma\right)$$

(11) $$r_3 = \sqrt{\frac{\cos\left(S_3 + \delta_1\right)\cos\left(S_3 + \delta_{II}\right)\sin\left(S_3 - \gamma\right)}{\sin S_3}}$$

(12) $$\alpha_1 = \alpha_H - 2\arctan\left[\frac{r_3}{\sin\left(S_3 - \gamma\right)}\right]$$

(13) Repeat steps (10) to (12) using $\delta_2$ in place of $\delta_1$.

(14) $(\delta_1, \alpha_1)$ and $(\delta_2, \alpha_2)$ are the coordinates of the two points of intersection.

## E. VECTOR TRANSFORMATION TO A MOON EQUATORIAL COORDINATE SYSTEM

The transformation of a vector located in a true ecliptic coordinate system into a vector in a moon equatorial coordinate system depends on the knowledge of the quantities * $\Omega'$, $\Lambda$, i and $\hat{\epsilon}$. If d and t represent the number of Julian days and centuries, respectively, since January 10, 1950, at midnight, then the following sequence can be utilized:

(1) ☾ $= 64.^\circ37545167 + 13.^\circ1763965268 \text{ x } d$

(2) $\Omega = 12.^\circ1127902 - 0.^\circ0529539222 \text{ x } d$

(3) $\bar{\epsilon} = 23.^\circ4457874$

(4) $\Gamma' = 208.^\circ8439877 + 0.^\circ1114040803 \text{ x } d - 0.^\circ010334 \text{ x } t$

(5) $\Gamma = 282.^\circ08121009 + 0.^\circ9856473354 \text{ x } d$

(6) $L = 280.^\circ08121009 + 0.^\circ9856473354 \text{ x } d$

(7) $g = 215.^\circ54013 + 13.^\circ064992 \text{ x } d$

(8) $g' = 358.^\circ009067 + 0.^\circ9856005 \text{ x } d$

(9) $\omega = 196.^\circ745632 + 0.^\circ9856005 \text{ x } d$

(10) $\tau = -0.^\circ3333(10^{-2}) \sin g + 0.^\circ0163888 \sin g' + 0.^\circ5\,(10^{-2}) \sin 2$

(11) $\sigma = 37.3692077\,[-0.^\circ0302777 \sin g + 0.^\circ0102777 \sin (g + 2\omega) - 0.^\circ305555\,(10^{-2}) \sin (2g + 2\omega)]$

(12) $\rho = -0.^\circ0297222 \cos g + 0.^\circ0102777 \cos (g + 2\omega) - 0.^\circ305555\,(10^{-2}) \cos (2g\ 2\omega)$

(13) $\Delta\epsilon = 0.^\circ255833\,(10^{-2}) \cos \Omega$

(14) $d\epsilon = 0.^\circ24444\,(10^{-4}) \cos 2$☾

(15) $E = \Delta\epsilon + d\epsilon$

(16) $\tilde{\epsilon} = E + \bar{\epsilon}$

---

* i, $\Lambda$, $\Omega'$ are the set of Eulerian angles; $\hat{\epsilon}$ is the true obliquity of date.

$$(17)\qquad \Psi = -0.^\circ 47895611\,(10^{-2})\,\sin\Omega - 0.^\circ 35333\,(10^{-3})\,\sin 2\,L$$

$$(18)\qquad \cos i = \cos(I+\rho)\cos\tilde{\epsilon} + \sin(I+\rho)\sin\tilde{\epsilon}\,\cos(\Omega+\sigma+\Psi)$$

$$I = 1^\circ 32.'1$$

$$(19)\qquad \sin\Omega' = -\sin(\Omega+\sigma+\Psi)\csc i\,\sin(I+\rho)$$

$$(20)\qquad \sin\Delta = -\sin(\Omega+\sigma+\Psi)\csc i\,\sin\tilde{\epsilon}$$

$$(21)\qquad \cos\Delta = \cos(\Omega+\sigma+\Psi)\cos\Omega' - \sin(\Omega+\sigma+\Psi)\,\sin\Omega'\cos\tilde{\epsilon}$$

$$(22)\qquad \Delta = \arctan\left[\frac{\sin}{\cos}\right]$$

$$(23)\qquad \Lambda = \Delta + \text{☾} + \tau - \Omega - \sigma.$$

# APPENDIX E

# TV MISSION DESIGN FOR VERTICAL RESOLUTION BY SHADOW MEASUREMENT NEAR THE LUNAR TERMINATOR

## A. PROBLEM DEFINITION AND DELINEATION

The problem is the resolution and recognition of an arbitrary vertical distance y on the lunar surface by examining the length of its shadow at low solar elevation angles, by means of TV-link sensor systems from a lunar orbiter.

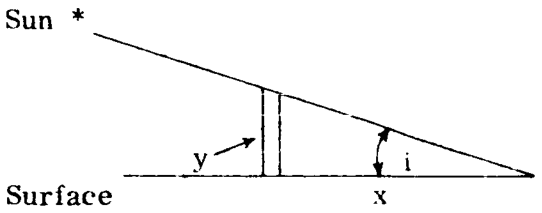

y = the vertical distance
x = shadow length
i = solar elevation angle

$$y = x \tan i \qquad \text{(E-1)}$$

For adequate recognition, it is required to cover the shadow of the object with three optical line pairs or six TV resolution lines. Let $x = n\,\ell$, where n is the number of TV lines within the shadow, and $\ell$ is the horizontal object resolution per line.

Then $y = n\,\ell \tan i$ (E-2)

or

$$\ell = \frac{y \cot i}{n} \qquad \text{(E-3)}$$

Table E-1 lists some examples of $\ell$ for the situation where y = 2 meters and n = 6 TV resolution lines.

TABLE E-1

SAMPLES OF $\ell$, THE HORIZONTAL OBJECT RESOLUTION PER LINE

| i (degrees) | cot i | $\ell$ (meters) |
|---|---|---|
| 0 | ∞ | ∞ |
| 1 | 57.29 | 19.10 |
| 2 | 28.64 | 9.55 |
| 3 | 19.08 | 6.36 |
| 4 | 14.30 | 4.77 |
| 5 | 11.43 | 3.81 |
| 10 | 5.671 | 1.89 |
| 15 | 3.732 | 1.24 |
| 20 | 2.748 | 0.916 |
| 30 | 1.7321 | 0.577 |
| 45 | 1.000 | 0.333 |
| 60 | 0.5774 | 0.192 |

By similar triangles, the focal length of the optical system can be defined as:

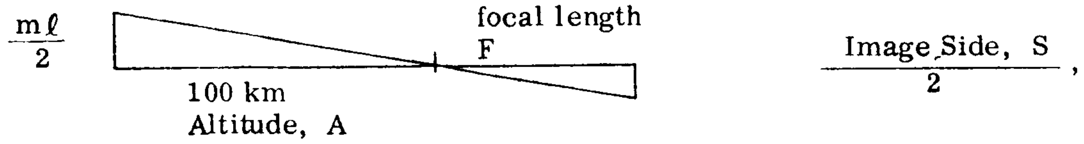

where

m = number of TV resolution lines in the field of view, and

S = image size.

$$\frac{m\,\ell}{A} = \frac{S}{F} \tag{E-4}$$

$$f = \frac{SA}{m\,\ell} = \frac{n\,SA\tan i}{m\,y} \tag{E-5}$$

## B. THE VIDICON AS SENSOR

For a 1-inch vidicon, such as the type #4431,

S = 11.125 mm, and

m = 650 resolution lines.

Let

A = 100 km orbit altitude, and

n = 6 TV lines per shadow

$$\text{focal length} = \frac{6\,(11.125)\,(100)\tan i}{650\,y}$$

$$= \frac{10.2692\tan i}{y}\,\text{(meters)}$$

$$\begin{aligned} F &= 5.134\tan i && \text{for } y = 2\\ &\phantom{=}\ 2.054\tan i && \text{for } y = 5\\ &\phantom{=}\ 1.027\tan i && \text{for } y = 10 \end{aligned}$$

Typical focal lengths are tabulated for y = 2, 5 and 10 meters in Table E-2.

## TABLE E-2

## TYPICAL VIDICON FOCAL LENGTHS (IN METERS)

| i (degrees) | tan i | Focal Length (Meters | | |
|---|---|---|---|---|
| | | for y = 2 meters | for y = 5 meters | for y = 10 meters |
| 0 | 0 | 0 | 0 | 0 |
| 1 | 0.01746 | 0.0896 | 0.0359 | 0.0179 |
| 2 | 0.03492 | 0.1793 | 0.0717 | 0.0359 |
| 3 | 0.05241 | 0.2691 | 0.1077 | 0.0538 |
| 4 | 0.06993 | 0.3590 | 0.1436 | 0.0718 |
| 5 | 0.08749 | 0.4492 | 0.1797 | 0.0899 |
| 10 | 0.1763 | 0.9051 | 0.3621 | 0.1811 |
| 15 | 0.2679 | 1.3754 | 0.5503 | 0.2751 |
| 20 | 0.3640 | 1.8688 | 0.7477 | 0.3738 |
| 25 | 0.4663 | 2.3940 | 0.9578 | 0.4789 |
| 30 | 0.5774 | 2.9644 | 1.1860 | 0.5930 |

The photometry of the surface, in conjunction with the vidicon sensitivity characteristic and allowable image motion, will determine the exposure time and speed of optics. The following lunar photometric data has been received from JPL:

| i° | $\phi$ |
|---|---|
| 10 | 0.083 |
| 15 | 0.13 |
| 20 | 0.18 |
| 30 | 0.27 |

($\phi$ = photometric function)

If it is assumed that $\varphi(O) = 0$, then $\varphi$ can be fitted adequately by $\phi_c = 0.470 \tan i$ over the range of $0 \le i \le 30°$. This fit is compared in Table E-3 with the original data.

## TABLE E-3

## COMPARISON OF FITTED AND ORIGINAL $\phi$ DATA

| i° | $\varphi$ | $\varphi_c$* |
|---|---|---|
| 0 | | 0 |
| 5 | | 0.0410 |
| 10 | 0.083 | 0.0829 |
| 15 | 0.13 | 0.1260 |
| 20 | 0.18 | 0.1711 |
| 25 | | 0.219 |
| 30 | 0.27 | 0.272 |

* Slide rule accuracy

The total illumination falling on the sensitive target is given by

$$I = \frac{S_c \, a_n \, T \, \phi \, t}{4 f^2} , \qquad \text{(E-6)}$$

where:

$I$ = illumination in f-cd-sec,

$S_c$ = solar constant,

$a_n$ = normal albedo,

$T$ = transmission factor of optics,

$\varphi$ = photometric function,

$t$ = exposure time, and

$f$ = f-number of optics.

The following definitions can be made:

$S_c = 13{,}000$

$a_n = 0.06$*

$T = 0.6$

$\varphi = 0.470 \tan i$*

I for a particular tube type is given as a function of signal-to-noise ratio. Data for the type #4431 vidicon is given in Table E-4.

TABLE E-4

SPECIFICATIONS FOR VIDICON TYPE #4431 †

| f-cd-sec | Large Area S/N | 650 Lines S/N |
|---|---|---|
| 0.01 | 23.0 | 6.0 |
| 0.02 | 26 | 9 |
| 0.03 | 29 | 12 |
| 0.04 | 31 | 14 |
| 0.05 | 32.5 | 15.5 |
| 0.06 | 33 | 16 |
| 0.07 | 34 | 17 |
| 0.08 | 34.5 | 17.5 |
| 0.09 | 35.5 | 18.5 |
| 0.10 | 35.9 | 18.9 |
| 0.20 | 40 | 23 |
| 0.30 | 42.5 | 25.5 |
| 0.40 | 44.5 | 27.5 |

† Source: J. Bingley, Technical Discussion of Proposed Television Subsystem Study for JPL.

---

* The value of normal albedo and photometric function assumed here is for an average condition. There will be highlight areas brighter than this average condition, and the condition used here is very pessimistic.

A signal-to-noise ratio of 30 db for nominal large-area response has been suggested as a reasonable design point. For resolving fine detail, a 17-db loss by the vidicon in responding to the higher spatial frequency must be accepted. In addition, the aim is to resolve at least a 2-to-1 contrast ratio, which is converted by the gamma curve of the vidicon into a 4-db signal variation. The remaining 9 db may be used as protection against loss of signal due to image motion or smear. According to the results derived by R. M. Scott,* image motion causes loss of contrast. The ratio of the final modulation to initial modulation is the transfer function of the process and is given by

$$T = \frac{\sin \pi x}{\pi x} \qquad \text{for } x < 1, \text{ and}$$

$$T = 0, \qquad \text{for } x \geq 1,$$

where

$x$ = fraction of one cycle of the spatial frequency through which the image moves during the exposure.

For small contrast, it can be assumed that the transfer function closely approximates the value of [ final contrast/original contrast ] , and the concern in this study is with signals much smaller than the average incident light.

A linear relationship exists between the log of Illumination Ratio and the log of Electrical Signal Output Ratio. For the Type #4431 vidicon this extends over nearly a 40-db range of input. The relation between optical and electrical db can be shown as follows:

$$\text{db} \left[ \text{Electrical Signal} \right] = \gamma \cdot \text{db} \left[ \text{Optical Signal} \right] ,$$

and, from Table E-4,

$$\gamma = \frac{35.9 - 23.0}{20} .$$

Image smear is an optical degradation, but 9 db of video S/N can be allowed. Therefore, 9/0.645 or 13.95 db of optical degradation can be allowed for smear. A value of -13.95 db yields a T of 0.201 or a smear motion of 1.65 TV lines per exposure.

The orbital motion, non-circularity of the orbit, residual angular rates of the orbiter about its axes, and misalignment of the orbiter axes with their intended directions are factors which contribute to image motion and to the difficulty of image-motion compensation, if used. Presuming that an overall vector-motion error, equal to $V_S \epsilon$, remains after image-motion compensation, exposure time can be calculated to permit only the allowable smear during the exposure. For a 100-km altitude circular orbit, the subsatellite point moves over the lunar surface at a rate of 1.543 km/sec.

---

* Contrast Rendition as a Design Tool, PS&E; Vol. 3, No. 5, 1959.

$$t = \frac{(L/E)\,\ell}{V_s\,\epsilon}\,, \tag{E-7}$$

where:

$t$ = exposure time

$(L/E)$ = TV lines of smear per exposure

$\ell$ = horizontal distance on object per TV resolution line

$V_s$ = object velocity relative to camera

$\epsilon$ = fractional uncompensated object velocity.

$\ell$ may be replaced by:

$$\ell = \frac{y \cot i}{n}$$

and the expression for exposure time becomes:

$$t = \frac{(L/E)\, y \cot i}{V_s\, \epsilon\, n}\,. \tag{E-8}$$

Taking:

$(L/E)$ = 1.65 lines,

$V_s$ = 1.543 km/sec, and

$n$ = 6,

then

$$t\ (\mathrm{ms}) = \frac{1.65\, y \cot i}{1.543\,(6)} = \frac{.1782\, y \cot i}{\epsilon}$$

for $y = 2$: $t = 0.3564 \cot i/\epsilon$ ms

$y = 5$: $t = 0.8910 \cot i/\epsilon$ ms

$y = 10$: $t = 1.782 \cot i/\epsilon$ ms.

The formula for illumination, Equation (E-6), can now be used, rearranging to solve for $f^2$.

$$f^2 = \frac{S_c\, a_n\, T\, \phi\, t}{4\, I} \tag{E-9}$$

From Table E-5, it can be found that illumination of 0.035 ft-cd-sec corresponds to a 30-db S/N ratio.

Since

$$\varphi = 0.470 \tan i$$

and

$$t = \frac{0.1782 \; y \cot i}{\epsilon},$$

substituting to solve for $f^2$ yields

$$f^2 = \frac{(13.1 \times 10^3)\,(.06)\,(.6)\,(0.470 \tan i)\,(0.1787 \cot i)\; y \; 10^{-3}}{4\,(0.035)\;\epsilon}$$

$f^2 = 0.2821 \; y/\epsilon$ for a 30-db S/N ratio.

For f = 1.5, which is probably the fastest optical system which might be considered for focal lengths over 0.150 meter, $y/\epsilon$ can be found to be 7.976.

If no image-motion compensation (IMC) is used, $\epsilon = 1.00$ and y = 7.98 meters vertical distance resolution. If $\epsilon = .10$, then 10 percent of image motion remains and y becomes 0.80 meter.

If the optical system can provide a smaller f-number for the shorter focal lengths (i.e., below 0.150 meters), then even smaller vertical distances can be resolved. For example, for f = 0.75 and $\epsilon = 1.00$, y will be 2.00 meters.

Additional results are listed in Table E-5 for the vidicon at a 100-km altitude.

TABLE E-5

VALUES OF f FOR $\epsilon = 1.0$ AND 0.1, USING THE VIDICON

| f | $\epsilon = 1.0$ y (meters) | $\epsilon = 0.1$ y (meters) |
|---|---|---|
| 4 | 56.72 | 5.67 |
| 3 | 31.91 | 3.19 |
| 2 | 14.18 | 1.42 |
| 1.5 | 7.98 | 0.80 |
| 1.0 | 3.55 | 0.36 |
| 0.75 | 1.99 | 0.20 |

It can be seen from Table E-5 that a standard vidicon without IMC can yield from 2 to 20 meters vertical-distance resolution on the lunar surface, depending on the speed of the optical system, at a S/N of 30 db. Additional S/N ratio will be obtained as greater selected detail is observed, because of the increased response of the vidicon to the lower spatial frequency.

It has been observed that focal length is a function of sun elevation angle when a given vertical-distance resolution is being sought. Focal length will grow proportionally to tan i up to some arbitrary cutoff point, say 5 degrees, after which it will be held constant. Exposure time is proportional to cot i for constant L/E, percent of detail length smeared, and grows as the shadow length grows, to some maximum exposure length.

Table E-6 lists various exposure times for $\epsilon = 1.0$ (with no IMC).

TABLE E-6

EXPOSURE TIME (IN MILLISECONDS) FOR $\epsilon = 1.0$

| i (degrees) | cot i | Exposure Time (milliseconds) | | |
|---|---|---|---|---|
| | | y = 2 (meters) | y = 5 (meters) | y = 10 (meters) |
| 0 | ∞ | ∞ | ∞ | ∞ |
| 0.5 | 114.59 | 40.84 | 102.1 | 204.2 |
| 0.8 | 71.62 | 25.53 | 63.81 | 127.6 |
| 1 | 57.29 | 20.42 | 51.05 | 102.1 |
| 2 | 28.64 | 10.21 | 25.52 | 51.04 |
| 5 | 11.43 | 4.074 | 10.18 | 20.37 |
| 10 | 5.671 | 2.021 | 5.053 | 10.11 |

The values of t listed in Table E-6 can be divided by $\epsilon$ to account for IMC. Exposure times can alternatively be expressed in terms of i and f-number. In fact, y = 2 corresponds to f = 0.75, y = 5 to f = 1.190, and y = 10 to f = 1.68. From this, it is obvious that a selection of optics of different focal lengths and, therefore, possibly different speeds makes possible trade-off between exposure time and resolution as an operational tool during the mission to optimize the matching of the camera to the photometry of the surface.

A mode of operation has been defined for sun angles below, say, a 5-degree cut-off which will yield constant vertical-dimension resolution on the lunar surface. To obtain this, variable focal length is desirable, and variable exposure time is necessary. The f-number can be constant. Above 5 degrees, presuming focal length may not be extended further, constant horizontal-dimension resolution of the lunar surface will be obtained.

For a y specified below 5 degrees, the horizontal distance resolved at 5 degrees and above will be given by

$$\ell = \frac{y \cot i_{co}}{n} .$$

If $i_{co} = 5°$, $\cot 5° = 11.43$, and $n = 6$,

then

$$\ell = 1.905\ y.$$

TABLE E-7

COMPARISON OF $y$ AND $\ell$

| $y$ (meters) | $\ell$ (meters per TV resolution line) |
|---|---|
| 1 | 1.91 |
| 2 | 3.82 |
| 5 | 9.53 |
| 10 | 19.05 |
| 20 | 38.10 |

Smear will be no greater than at 5°, and will be, in general, less for higher sun angles as exposure time is reduced.

## C. THE IMAGE ORTHICON AS SENSOR

The image orthicon is a potential alternate to the vidocon as a TV sensor for this mission. The image orthicon is much more sensitive than the vidicon, but has a somewhat poorer sensor resolution.

The sensitive area for the type-7198 image orthicon is calculated to be 32.3 mm on a side. The total number of TV resolution lines is 540. The S/N ratio is 26 db from an illumination of $1.3 \times 10^{-4}$ ft-cd-sec. At 540 lines the response of the 7198 is down 20.5 db below the large-area response. A 2/1 contrast ratio is the minimum optical signal which might be distinguished; and, since the gamma for the type-7198 at this operating point is approximately .47, this contrast ratio is converted into a 2.82-db S/N ratio.

$$26 \text{ db} - 20.5 - 2.82 = 2.68 \text{ db margin for smear loss.}$$

Since smear is an optical phenomenon, it is necessary to convert to optical db loss by dividing by the gamma of the image orthicon.

$$\frac{2.68}{0.47} = 5.7 \text{ db optical loss.}$$

This corresponds to 1.18 TV lines of smear. Thus

$$\text{focal length} = \frac{n\ SA\ \tan i}{m\ y}$$

where

$S$ = 32.3 mm field side

$m$ = 540 TV resolution lines per field

$A$ = 100 km

$n$ = 6

$$F = \frac{6\ (32.3)\ (100)\ \tan i}{540\ y} = \frac{35.89\ \tan i}{y}\ \text{meters}$$

$F$ = 17.94 tan i; for $y$ = 2 meters

7.178 tan i; for $y$ = 5 meters

3.589 tan i; for $y$ = 10 meters

Table E-8 lists the focal lengths for $y$ = 2, 5 and 10 meters.

TABLE E-8

TYPICAL IMAGE-ORTHICON FOCAL LENGTHS (IN METERS)

| i (degrees) | tan i | Focal Length (meters) | | |
|---|---|---|---|---|
| | | y = 2 meters | y = 5 meters | y = 10 meters |
| 1 | .01746 | 0.313 | 0.125 | 0.063 |
| 2 | .03492 | 0.626 | 0.250 | 0.125 |
| 3 | .05241 | 0.940 | 0.376 | 0.188 |
| 4 | .06993 | 1.256 | 0.502 | 0.251 |
| 5 | .08749 | 1.570 | 0.628 | 0.314 |
| 10 | .1763 | 3.165 | 1.267 | 0.633 |
| 15 | .2679 | 4.805 | 1.923 | 0.961 |
| 20 | .3640 | 6.54 | 2.61 | 1.308 |

The focal length has been extended with the image orthicon by a factor of about 3.50 over the vidicon.

Using the previously derived expressions for illumination, f-number, and photometric function, the required optical f-number can be calculated.

$$I = \frac{S_c \ a n \ T \ \phi \ \ t}{4 f^2} \text{ ; where } I = 1.3 \times 10^{-4} \text{ f-cd-s for 26 db S/N}$$

$$t = \frac{(L/E) \ y \ \cot \ i}{V_s \ \epsilon \ n}$$

$$\phi = 0.470 \ \tan \ i$$

$$f^2 = (54.33) \frac{Y}{\epsilon} \text{ for 26 db S/N}$$

Since no IMC is required to obtain usable f-numbers, let $\epsilon = 1.0$.

Then:

$$f = 7.37 \sqrt{y}$$

Table E-9 lists various values of y and the corresponding f values.

TABLE E-9

VALUES OF f FOR $\epsilon = 1.0$, USING THE IMAGE ORTHICON

| y | f-number |
|---|---|
| 1 | 7.37 |
| 2 | 10.42 |
| 5 | 16.50 |
| 10 | 23.22 |

It is clear that aperture is no problem with this sensor, nor is IMC required. As in the case of the vidicon, exposure is varied to maintain constant percentage line smear and yields a constant f-number below the cut-off sun angle. The essential limitations are probably the practical limit of achievable focal length and the f-number which can be constructed for the optics.

These two factors will determine the region of solar elevation angles which can be covered and the vertical dimension resolution which can be obtained. Above the critical value of i, the system reverts to a constant horizontal-dimension resolution. If y is chosen as 2 meters, $\ell$ will be 3.8 meters per TV line at 5 degrees, as in the case of the vidicon. Alternatively, a focal length set up for a 3-degree critical angle will yield 6.35 meters per TV line above 3 degrees (see Table E-1).

One issue of interest is the rather low smear component which will be possible because of the high sensitivity and short exposure above the critical angles. This may provide distinct benefits in the event that the surface photometry is not essentially smooth; i.e., sparsely populated with large objects throwing conveniently oriented shadows. If the surface is made up of a few very bright areas illuminated by protrusion above a very rough surface principally in shadow, the image orthicon is well equipped to produce very low-smear pictures at the highest resolution.